APPLICATION OF PHOSPHATE AND SURFACTANT-MODIFIED ZEOLITE FOR REMEDIATION/ATTENUATION OF TRACE ELEMENTS IN SOIL AND COAL FLY ASH

by

GHANASHYAM NEUPANE

RONA J. DONAHOE, COMMITTEE CHAIR
CHUNMIAO ZHENG
C. FRED T. ANDRUS
GEOFFREY R. TICK
YUJI ARAI

A DISSERTATION

Submitted in partial fulfillment of the requirements
for the degree of Doctor of Philosophy
in the Department of Geological Sciences
in the Graduate School of
The University of Alabama

TUSCALOOSA, ALABAMA

2012

Copyright Ghanashyam Neupane 2012
ALL RIGHTS RESERVED

ABSTRACT

This dissertation presents results of a research work aimed at understanding and addressing trace element contamination sourced by coal fly ash and arsenic trioxide herbicide. Both alkaline and acidic fly ash samples were found to contain significant concentrations of environmentally available trace elements. The treatment of fly ash leachate with surfactant-modified zeolite (SMZ) decreased the mobility of several trace elements. In general, up to 30% of the As, Mo, and V; up to 80% of the Cr; and up to 20% of the Se and Sr were removed from the leachate after SMZ treatment.

Batch experiments, surface complexation modeling, and X-ray spectroscopic tools were used to elucidate the kinetics and mechanisms of arsenate ($As_{(V)}$) and phosphate (P_i) adsorption on ferric hydroxide. Both oxyanions showed similar adsorptions during single-ion adsorption experiments; however, $As_{(V)}$ was preferentially adsorbed during competitive adsorption experiments. Similarly, more $As_{(V)}$ was adsorbed when it was loaded in sequence in P_i-equilibrated system than *vice versa*. Both oxyanions competed for adsorption on ferric-hydroxide and each of them showed a limited capacity to desorb the other, and relatively, more pre-equilibrated P_i was desorbed by sequentially added $As_{(V)}$ than *vice versa*. The As K-edge EXAFS analysis indicated the presence mononuclear and binuclear bidentate $As_{(V)}$ surface complexes. The Fe coordination numbers (CN) of these complexes increased with increasing time and decreased with addition of P_i into the system.

Finally, an arsenic-contaminated soil collected from an industrial site located in the southeastern United States was amended with P_i and Ca to precipitate the arsenic as As-bearing apatite-like minerals. Phosphoric acid amendment of the soil with simultaneous addition of Ca dramatically decreased the mobility of soil As to near zero at pH > 6. Characterization of precipitate separated from the Ca-P_i treated soil by X-ray diffraction indicated that a carbonate-apatite mineral was formed in the soil and likely incorporated $As_{(V)}$ into its structure. The low solubilities of many of the Ca-P_i-$As_{(V)}$ minerals suggest that Ca-P_i treatment has promise as an effective, long-term method for in situ chemical fixation of As in contaminated soils and wastewaters.

DEDICATION

To My Mother

Maya Davi Neupane

(1951-2008)

LIST OF ABBREVIATIONS AND SYMBOLS

Å	Angstrom
ACAA	American Coal Ash Association
ACS	American Chemical Society
Al	Aluminum
ANL	Argonne National Laboratory
APS	Advanced Photon Source
$As_{(III)}$	Arsenite
$As_{(V)}$	Arsenate
As	Arsenic
B	Boron
Ba	Barium
BET	Brunauer-Emmett-Teller
C	Celsius, concentration, carbon
Ca	Calcium
C_C	Cumulatively leached amount of an element from fly ash
CCP	Coal combustion product
Cd	Cadmium
C_e	Equilibrium concentration of a sorbate
C_{env}	Environmentally available concentration of an element in fly ash

C_i	Initial concentration of a sorbate
Cl	Chlorine
cm	Centimeter
CN	Coordination number
Co	Cobalt
$Cr_{(III)}$	Chromite
$Cr_{(VI)}$	Chromate
Cr	Chromium
Cs	Cesium
Cu	Copper
DDI	Distilled deionized
DGS	Department of Geological Sciences
DOE	Department of Energy
eV	Electron volt
EXAFS	Extended x-ray absorption fine structure
F	Faraday constant
Fe	Iron
FGD	Flue gas desulfurization
FL	Florida
FR	Flow rate
g	gram
GCAGS	Gulf Coast Association of Geological Societies
GeV	Giga electron volt

GSA	Geological Society of America
h	Hour/pseudo-second order constant
H_2O	Water
H_2SO_4	Sulfuric acid
H_3AsO_4	Ortho-arsenic acid
H_3PO_4	Ortho-phosphoric acid
HCl	Hydrochloric acid
HDTMA-Br	Quaternary amine hexadecyltrimethylammonium bromide
HNO_3	Nitric acid
IAP	Ion activity product and
IC	Ion chromatography
ICP-OES	Inductively coupled plasma-optical emission spectroscopy
K	Kelvin, Potassium
K_{sp}	Solubility constant
k	Pseudo-second order constant
kg	Kilo gram
L	Liter
m	Meter
M	Mole
mA	Milliampere
Mg	Magnesium
mg	Milligram
min	Minute

mL	Millileter
mM	Millimole
mmol	Millimole
Mo	Molybdenum
MS	Multiple scattering
MSW	Municipal solid waste
mV	Millivolt
N	Coordination number
n	Power function constant
Na	Sodium
$Na_2HAsO_4 \bullet 7H_2O$	Di-sodium hydrogen $As_{(V)}$ hepta-hydrate
NaCl	Sodium chloride
NaOH	Sodium hydroxide
Ni	Nickel
O	Oxygen
P	Phosphorus, Pressure
P_i	Phosphate
PRB	Permeable reactive barrier
PZPNC	Point of zero net proton charge
q_e	Equilibrium surface coverage
q_t	Surface coverage at any time t
R	Gas constant, Inter-atomic bond distance
R^2	Coefficient of determination

rpm	Revolution per minute
SAR	Synthetic acid rain
SCM	Surface complexation model
$Se_{(IV)}$	Selenite
$Se_{(VI)}$	Selenate
Se	Selenium
SI	Saturation index
Si	Silicone
SMZ	Surfactant modified zeolite
Sr	Strontium
T	Temperature
t	Time
TLM	Triple layer Model
US	United States
USEPA	United States Environmental Protection Agency
V	Vanadium
XAS	X-ray absorption spectroscopy
XRD	X-ray diffraction
Zn	Zinc
α	Elovich constant, power function constant
β	Elovich constant
Γ	Surface coverage
σ^2	Debye-Waller factor

ACKNOWLEDGMENTS

I would like to thank a number of people and institutions for their help to complete my doctoral program at the University of Alabama. I am very thankful to my advisor Dr. Rona J. Donahoe. I greatly appreciate her for accepting me as a graduate student in the Department of Geological Sciences and letting me perform my doctoral research at UA. Moreover, I deeply treasure her time, guidance, and support throughout this endeavor. Similarly, I am very thankful to my dissertation committee members Dr. Geoffrey Tick, Dr. Fred Andrus, Dr. Chunmiao Zheng, and Dr. Yuji Arai for their support and help to complete my projects. I greatly appreciate Dr. Arai for his help during the XAS data analysis. Similarly, I would also like to acknowledge the support and encouragement that I got from Dr. Bhoopesh Mishra during XAS data collection and analysis. I appreciate the occasional discussions with Dr. Rasoul Rahnemaie at Tarbiat Modares University, Iran and Dr. Juan Antelo at University of Santiago de Compostela, Spain about the surface complexation modeling of phosphate and arsenate at the ferric hydroxide-water interface. I also like to thank my MS adviser Dr. Sheila J. Roberts at Bowling Green State University for encouraging me to go for a doctoral program.

I am also grateful to Ms. Betsy Graham and Dr. Sidhartha Bhattacharyya for their support in ICP-OES and IC analysis of aqueous samples in the Geochemical Analytical Laboratory at the University of Alabama. The readily available help from Mr. Jim Donahoe to solve computer problems are greatly appreciated. I would also like to thank him for his assistance in XRD data collection and interpretation. Mr. Prakash Dhakal (University of Kentucky) is appreciated for

his help in BET surface area measurement of ferric-hydroxide. I greatly appreciate my lab mates Sid, Ziming, Erica, and Ted for endless discussions related to research as well as all other topics ranging from Alabama Football to devastating Tornado in our town. I would also like to thank Brittany, Chad, Whitney, and Drew for their hard work to keep our labs and equipment running. I appreciate our department secretary and assistants Ms. Debbie, Ms. Betty, and Ms. Darlene for their help in various ways. I appreciate Ms. Diane Thrower for her help in drafting and printing my posters several occasions.

This research was partially supported by funding from the Electric Power Research Institute and Southern Company Services, Inc. Additionally, this research was partially funded by Hooks Fund (UA Department of Geosciences) and student research grants from Geological Society of America (GSA) and Gulf Coast Association of Geological Societies (GCAGS). Similarly, I also like to appreciate Graduate Student Association at UA and Graduate School for providing small research and travel grants. The timely completion of this research was greatly facilitated by Graduate School at University of Alabama by awarding me a research fellowship for a year. Use of the National Synchrotron Light Source, Brookhaven National Laboratory, was supported by the U.S. Department of Energy, Office of Science, Office of Basic Energy Sciences, under Contract No. DE-AC02-98CH10886. Similarly, use of the Advanced Photon Source, an Office of Science User Facility operated for the U.S. Department of Energy (DOE) Office of Science by Argonne National Laboratory, was supported by the U.S. DOE under Contract No. DE-AC02-06CH11357. I greatly appreciate beam line scientists Dr. Syed Khalid at NSLS and Ms. T. Bolin at APS for assistance during XAS data collection.

Finally, I like to thank my family. Thank you my wife Laxmi. She has been very patient, generous, and supportive in the last 8 years. While working on tedious experiments, I had

intentionally dodged numerous phone calls from you, but you were always in my mind when I was busy in laboratory. I also like to thank my father for his continuous encouragement and being a model of an honest man. I greatly appreciate his support and unwavering belief in education that greatly influenced my academic career. It has been a continuous pleasure for us to live with him after untimely demise of my mother. I also like to thank my sisters, brother, brother-in-laws, and sister-in-law for their continuous support. My two *bhanjee,* a *bhatijee,* and a *bhanja* are constant source of joy for me. Avash was a 4-month baby when I first met him but now he has grown up as a big boy as he always likes to be. And finally, he got his little cousin Anjal last February. I owe thanks to my son Anjal for not being cranky during night after the first month.

CONTENTS

LIST OF TABLES

LIST OF FIGURES

CHAPTER – 1

INTRODUCTION

Elevated levels of trace elements in near-surface environments are major concerns for protecting the health of humans and other organisms. Enrichment of inorganic pollutants in the environment may result from both natural and anthropogenic sources; however, the latter source has greatly enhanced the environmental input of different trace elements. Geo-media such as soil, sediment, aquifers, ground water, and surface water are rarely pristine because of anthropogenic loadings of potentially toxic metal and metalloid elements (e.g., Hernandez et al., 2003; Steinnes and Friedland, 2006). For example, improper disposal of large volumes of coal combustion products has resulted in several environmental disasters in the past. One notable incident occurred on December 22, 2008 in Tennessee, when the rupture of a containment structure spilled over 3.7 million cubic meters of wet coal ash from the Tennessee Valley Authority (TVA) Kingston coal-fired power plant (Ruhl et al., 2010).

The characterization and understanding of the geochemical mobility of As and other trace elements in contaminated soil and coal fly ash are very important in developing suitable physical and chemical treatment methods to reduce the potential risk to the environment. One portion of this study was aimed at studying the leaching behavior of different priority trace elements from alkaline and acidic fly ash samples and testing the ability of surfactant-modified zeolite to control the potential dispersion of several priority

pollutant elements from old fly ash disposal facilities. The geochemical interaction of arsenate ($As_{(V)}$), in the presence/absence of phosphate (P_i), with ferric hydroxide, a common soil constituent known for its As harboring properties, was also investigated as part of the overall study. Finally, a P_i-based treatment method for As-contaminated soil was also evaluated in this dissertation research.

1.1. Fly ash

Millions of tons of coal combustion products (CCPs) are produced every year by coal-fired power plants. CCPs include fly ash, bottom ash, boiler slag, flue gas desulfurization (FGD) materials, and various gases (Kalyoncu, 2000). Fly ash, the most voluminous fraction of CCPs, is fine particulate matter collected on fabric filters and through mechanical and electrostatic methods from flue gas produced by the combustion of pulverized coal in the boiler assembly. . In 2010, 67.7 million short tons of coal fly ash were produced in the US, accounting for 52.0% of the total CCPs (American Coal Ash Association, 2011). Although the beneficial use of fly ash and other CCPs has varied in recent years (37.9% or 27.7 short tons of fly ash were recycled and used in 2010), the majority of the fly ash is buried in impoundment lagoons or dry landfills along with other unused CCPs (American Coal Ash Association, 2011). Because fly ash contains numerous hazardous trace elements, the development of effective techniques to prevent the dispersion of these elements from fly ash disposal facilities is very important.

1.1.1 Composition

Fly ash is an inorganic material with some unburned coal (carbon) content (Tishmack and Burns, 2004; Külaots et al., 2004), and mostly consists of amorphous aluminosilicate spheres

with minor amounts of iron-rich spheres (Kutchko and Kim, 2006). On the basis of chemical compositions, coal fly ash is generally divided into two groups: Class F (lime poor or acidic) and Class C (lime rich or alkaline) (Glasser, 2004; Tismhmack and Burns, 2004). The chemical and mineralogical compositions of fly ash primarily depend on the compositions of the source coal and co-feed materials, as well as the combustion technology, pollution control technology, and fly ash handling technology used (National Research Council, 2006; Mardon et al., 2008).

Coal is composed of organic derivatives, predominantly carbon, some hydrogen, oxygen, nitrogen and sulfur, and a minor amount of inorganic materials. The inorganic materials include primary detrital minerals such as quartz, feldspar, clays, mica, and zircon, and/or secondary minerals such as calcite and sulfides (Miller and Given, 1986; Glasser, 2004). Several hazardous elements, such as Sb, As, Be, Cd, Cr, Co, Pb, Mn, Hg, Ni, and Se, are present in trace quantities in coal (Bool and Helble, 1995). Given and Miller (1987) reported considerably higher concentrations of trace elements (e.g., Be, V, Cu, Y, and Yb) in a coal seam than in the adjacent inorganic layers. Average concentrations of As in world and US bituminous coals are 9 ppm and 24 ppm, respectively (Yudovich and Ketris, 2005), significantly higher values than the world average soil concentration of 5 ppm (Mandal and Suzuki, 2002). Trace elements in coal are associated with different coal fractions. For example, B, Ge, Be, Ti, and V are closely affiliated with the organic fraction of coal (Tishmack and Burns, 2004). Miller and Given (1987) reported that a substantial amount of Ca, Mg, Sr, Ba, Na, and Mn are present as exchangeable ions associated with the organic fraction of lignite coal., Similarly, Be, Sc, Cr, Y, Yb, V, Ni, Cu, and Zn are enriched primarily or partially in organic matter (Miller and Given, 1986). Lithophile elements (e.g., Li, F, B, Cr, Sr, Ba, I, Ti, Br, and Mn) are also associated with silicates and alluminosilicates; siderophile elements (e.g., Ni, Co, Mo, Mn, P, Ge, Pt, Ti, and Sn) are

associated with iron-titanium oxides; and chalcophile elements (e.g., As, Cu, Co, Pb, Hg, Zn, Mo, Cd, and Se) are affiliated with sulfides in coal (Tishmack and Burns, 2004).

During the gas-suspension combustion of pulverized coal, temperatures in the boiler assembly typically reach 1400-1800° C (Glasser, 2004). At these temperatures, most of the carbon and sulfur components of coal are converted into gaseous form, while coal mineral components are exposed to partial or complete thermal transformations (Clarke, 1993). Trace elements associated with organic, sulfide, and carbonate fractions of coal are volatilized more easily than the trace elements associated with silicate minerals (Bool and Helble, 1995). As temperature decreases, the volatilized trace elements in the hot flue gas are re-deposited on the ash particles (Goodarzi et al., 2008; Smith, 1980; Gieré et al., 2003). In general, trace elements tend to enrich in the finer fly ash fraction collected by filter fabric at low temperatures, rather than in the coarser fraction of fly ash collected by mechanical cyclone separator at relatively high temperatures (Mardon et al., 2008). Similarly, these elements are enriched more on the surfaces of fly ash particles than in the interiors (Natusch et al., 1974; Smith, 1980; Lecuyer et al., 1996).

1.1.2. Trace elements in fly ash leachate

Fly ash in disposal facilities undergoes mineralogical and chemical transformations with gain, loss, or redistribution of major, minor, or trace elements, along with alteration of its physical properties (McCarthy et al., 1997; 1999). During these chemical and mineralogical transformations, a significant proportion of the trace elements can be released into the environment. Therefore, fly ash deposited in unlined ponds or dry landfills, or used as filling material such as mine backfill, is a potential long-term source of leachate containing several hazardous elements (Donahoe, 2004). Many studies have been carried out to evaluate the

mechanism of trace element release into the environment from fly ash using various leaching schemes and solutions (e.g., Kim, 2002; Hassett et al., 2005). Sometimes, the results obtained through different leaching methods may present difficulties for interpreting the release mechanism of trace elements from fly ash because of the heterogeneous nature of fly ash and the use of different leaching protocols (Hassett et al., 2005). In general, the nature of trace element leaching from fly ash depends on the concentrations, speciation and distribution of trace elements, the aggressiveness, redox potential and pH of the leaching solution and the duration of leaching,the desorption/sorption and chemical reactions controlling the weathering of fly ash, and the formation of secondary minerals during leaching (Iyer, 2002; Kim, 2002; Donahoe, 2004; Hassett et al., 2005; Otero-Rey et al., 2005; Jankowski et al., 2006).

Fernández-Turiel et al. (1994) reported that 1.5%-36.4% of the total elements in fly ash are extractable under natural conditions. Jankowski et al. (2006) studied acidic and alkaline fly ashes using leaching solutions with various initial pH, and found significant mobilities for As, B, Mo, and Se. Long-term leaching of As, B, and Se from alkaline fly ash showed an initial increase in the leachate concentrations of these elements to their maximum values, followed by gradually decreasing concentrations thereafter due to the formation of ettringite, a secondary sulfate mineral which can sequester oxyanion elements (Hassett et al., 2005; Jankowski et al., 2006). For Class F fly ash, Fe, Pb, and Cr are moderately soluble at acidic pH, while As is very labile at pH <4 (due to dissolution) and at pH >9 (due to desorption) (Jegadeesan et al., 2008).

1.1.3. Treatment of fly ash

Several studies have attempted to treat municipal solid waste (MSW) fly ash to immobilize the associated toxic metals (Auer et al., 1995; Derie, 1996; Crannell et al., 2000;

Bournonville et al., 2004); however, relatively few studies have been aimed at controlling the mobility of trace elements in coal fly ash (Donahoe et al., 2007; Bhattacharya et al., 2009). Auer et al., (1995), while working on MSW fly ash rich in sulfates, alkali chlorides, and heavy metals, noted that the addition of reactive calcium aluminates to fly ash resulted in the formation of ettringite-type minerals capable of partially incorporating Co, Ni, Cu, Zn, and Cd. Therefore, reactive calcium aluminates can be the first treatment step, followed by the addition of other binding materials for solidification and fixation of heavy metals in sulfate-rich fly ash (Auer et. al., 1995). To stabilize the heavy metals in MSW fly ash, Derie (1996) described a four-step method which included pH-controlled washing of soluble salts in fly ash, the addition of phosphoric acid, followed by heating of the solid residue to about 800° C, and hydration along with the addition of Portland cement clinker at the end. Crannell et al. (2000) were able to stabilize Pb, Cu, Zn, and Cd through formation of apatite-like minerals with the addition of soluble phosphate (P_i) to MSW bottom ash. Similarly, Bournnonville et al. (2004) used phosphoric acid to form insoluble calcium phosphates with apatite structures that incorporated heavy metals present in water-washed MSW fly ash. Hunag and Lo (2004) reported a 94.8% decrease in the leachability of Pb in MSW fly ash after treating the ash with a colloidal aluminate oxide. Yang (2005) and Yang et al. (2007) successfully demonstrated the chemical fixation of arsenic in an arsenic trioxide contaminated soil using a ferrous sulfate treatment solution. Donahoe et al. (2007) and Bhattacharyya et al. (2009) extended the ferrous sulfate treatment method to immobilize trace elements in coal fly ash. They reported that ferrous sulfate treatment at a 1:30 ratio of fly ash:treatment solution was most effective in decreasing the synthetic acid rain leachability of several priority trace elements associated with coal fly ash.

1.1.4. Permeable reactive barrier for fly ash leachate treatment

A permeable reactive barrier (PRB) is a simple remediation technology which involves the subsurface installation of reactive materials across the flow path of a groundwater plume to intercept, treat, and prevent the down-gradient dispersion of contaminants (Morrison and Spangler, 2006). PRBs areused for controlling both inorganic (Cantrell et al., 1995; Blowes et al., 2000) and organic (Gillham and O'Hannesin, 1994) contaminants in groundwater. Permeable reactive barriers involve the construction of permanent, semi-permanent, or replaceable reactive units in such a way that most of the plume passes through them, thus yielding an acceptable quality of groundwater in the down-gradient zone (Smyth et al., 1997; Guerin et al., 2002). When contaminated groundwater enters the PRB system passively, the contaminants are removed by ion exchange, adsorption, fixation, precipitation, and degradation reactions (Gillham and O'Hannesin, 1994; Cantrell et al., 1995; Benner et al., 1999; Bowman et al., 1999; Guerin et al., 2002). Besides being reactive to the target contaminants, the materials used for PRBs must also must have sufficient and sustainable permeability, and must be affordable and easily available (Benner et al., 1997; Waybrant et al., 1998). Several different materials, including zero-valent iron (Gillham and O'Hannesin, 1994; Cantrell et al., 1995), zeolites (Ouki et al., 1993; Ouki, 1997), surfactant-modified zeolites (Bowman et al., 1999), and organic-rich matter (Benner et al., 1997; Guerin et al., 2002), are used for PRBs. Some PRBs use mixtures of several components to optimize their functionality. For example, Baker et al. (1998) used crushed high-calcium limestone and silica sand to provide a continuous source of Ca and better permeability, respectively, along with reactive metal oxides.

For the same chemical conditions, trace elements with predominantly cationic aqueous species (Cu, Co, Fe, Mn, Ni, Pb, etc.) show different leaching behaviors than trace elements

having predominantly oxyanionic aqueous species (As, Mo, Se, V, etc). Cationic aqueous species are more soluble under acidic conditions, while oxyanionic aqueous species are more labile under basic conditions (Sposito, 1984). Remediation methods which are useful in controlling the mobility of aqueous cationic trace elements are therefore not effective in controlling the solubility of trace elements existing as oxyanionic aqueous species.

Ready availability, low cost, and high cation exchange capacities make natural zeolites very useful materials in commercial water treatment applications (Bowman, 1996). Zeolites are hydrated aluminosilicate minerals that are characterized by cage-like structures having high internal and external surface areas and high cation exchange capacities (Newsam, 1986; Bowman, 2003). Although natural zeolites have been widely used to remove cationic heavy metals from solution due to their negative surface charge (Leppert, 1990; Ouki et al., 1993; Ouki, 1997), they are not useful for removing inorganic oxyanions such as chromate (CrO_4^{2-}) (Haggerty and Bowman, 1994). However, the outer surface of natural zeolites can be altered to have a positive charge using a surfactant and make it suitable to adsorb oxyanions of arsenic, chromium, and selenium (Haggerty and Bowman, 1994). For example, quaternary amine hexadecyltrimethylammonium (HDTMA), a long-chain cationic surfactant, selectively exchanges with the inorganic cations on the external surfaces of zeolites, up to the external cation exchange capacity, and forms a stable surfactant bilayer with anion-exchange properties (Haggerty and Bowman, 1994; Li et al., 1998; Bowman, 2003). Bowman et al. (1999) showed the ability of surfactant-modified zeolite (SMZ) as a PRB material to remove oxyanionic metals from contaminated groundwater; however, SMZ has not been evaluated as a possible material for preventing the dispersion of hazardous materials from unlined fly ash disposal facilities.

1.2. Arsenic and phosphorus geochemistry

Arsenic is a toxic element. An acute dose of 50 to 300 mg As is considered to be lethal for humans due to gastrointestinal, respiratory, cardiovascular, neurological or other body system failures (ATSDR, 2000). In addition, chronic ingestion of As, either through food or water, has been proven to be responsible for several different types of cancers (Jackson and Grainge, 1975; Bates et al., 1992; Karagas et al., 2002). Elevated concentrations of As in the environment can occur by both natural processes and anthropogenic activities (Smedley and Kinniburgh, 2002). The arsenic in groundwater that affects millions of people in several countries around the world, including Bangaldesh, India, Taiwan, and Argentina, has a natural origin (Nordstrom, 2002; Mandal and Sujuki, 2002; Smedley and Kinniburgh, 2002; Hossain, 2006). Anthropogenic As contamination has occurred through the use of As-based pesticides (Simcox et al., 1995; Robinson et al., 2007)and herbicides (Yang and Donahoe, 2007), wood preservatives (Morrell et al., 2003), and from ore mining and smelting activities (Carbonell-Barrachina et al., 2004). In the environment, As undergoes biogeochemical cycling through water, soil, air, and organisms (Oremland and Stolz, 2003; Islam et al., 2004). In general, inorganic arsenic in soil primarily exists as oxyanions of As(III) or As(V), depending on pH and redox potential (Cullen and Reimer, 1989). The mobility of As in soil depends on redox potential, pH, mineralogy, organic matter content, and concentrations of competing oxyanions (Masscheleyn et al., 1991; Nickson et al., 1998; Kalbitz and Wennrich, 1998; Harvey et al., 2002; Bauer and Blodau, 2006; Smedley et al., 2005).

Phosphorus has similar chemical properties to those of As, but is not toxic to the biosphere. Phosphate (P_i) has the potential to desorb adsorbed $As_{(V)}$ to the environment through ion-exchange reactions (Manning and Goldberg, 1996; Geelhoed et al., 1997; Gao and Mucci,

2001) and co-precipitate it with low solubility P_i minerals (Grisafe and Hummel, 1970; Twidwell et al., 1994). Both $As_{(V)}$ and P_i exhibit a high degree of adsorption on Fe, Mn, and Al hydroxides (Mucci et al., 2000). In natural soils and sediments, these anions are mostly associated with iron hydroxide (Belzile and Tessier, 1990; Slomp et al., 1996). Several studies have indicated that P_i and $As_{(V)}$ adsorb on metal hydroxides as inner-sphere surface complexes (Parfitt and Atkinson, 1976; Waychunas et al., 1993). Similarly, other studies have demonstrated the co-precipitation of arsenic in apatite-like minerals (Twidwell et al., 1994). Both $As_{(V)}$ adsorption on metal oxides and co-precipitation with apatite-like minerals have been used to treat As-contaminated soils and wastewaters (Yang et al., 2007; Twidwell et al., 1994). Therefore, the competitive adsorption/desorption behavior of P_i and $As_{(V)}$ on Fe hydroxide is a very important control on the leachability, mobility, and bioavailability of arsenic in the environment.

1.2.1. Arsenic adsorption on Fe-hydroxide

In contaminated soil, As is mostly adsorbed on Fe and Al oxyhydroxides and clay minerals (Manning and Goldberg, 1997; Dixit and Hering, 2003). Adsorption and desorption of As by Fe-hydroxide are controlled by prevailing chemical conditions and play an important role in determining the mobility and bioavailability of As in soils, groundwater, and surface water (Smedley and Kinniburgh, 2002). The endemic As-contaminated groundwater in Bangladesh is related to either oxidative dissolution of As-bearing sulfide minerals caused by excessive pumping lowering the water table (Das et al., 1996), or to reductive dissolution of iron hydroxide and release of adsorbed As (Nickson et al., 1998; 2000; Stüben et al., 2003). Most recent studies agree that the release of As to groundwater in Bangladesh is primarily due to the reductive dissolution of iron hydroxide coatings on sediment particles (Ahmed et al., 2004). Similarly,

loess deposits in Argentina release adsorbed As from Fe and Mn oxides into groundwater at elevated levels due to the presence of high pH and competitive oxyanions (Smedley et al., 2005). Soil contaminated by the application of arsenic trioxide herbicide during the 1950s has a significant fraction of the total As associated with Fe and Al hydroxides (Yang and Donahoe, 2007). Qi and Donahoe (2008) showed that nearly 55% of the As in these soils is adsorbed irreversibly (i.e., non-leachable by synthetic acid rain under oxic conditions) on iron hydroxides, while 25% of the soil As is reversibly adsorbed on metal hydroxides and/or layer silicates.

Several studies have attempted to understand the nature of As adsorption on iron hydroxide under diverse chemical and physical conditions. Adsorption of As involves ligand exchange for H_2O and OH^- on iron hydroxide surfaces (Jain et al., 1999). Uptake of $As_{(V)}$ and $As_{(III)}$ by ferrihydrite is rapid initially due to adsorption on surface/near-surface sites, but this rapid uptake is then followed by a long period of slow sorption controlled by diffusion into the mineral interior (McGeehan et al., 1992; Fuller et al., 1993; O'Reilly et al., 2001). Grossl et al. (1997) proposed a two-step mechanism for As adsorption on goethite: (1) rapid initial adsorption by ligand exchange reaction of $As_{(V)}$ for OH^- at the goethite surface, forming an inner-sphere monodentate surface complex, and (2) the subsequent slow adsorption of As by a second ligand exchange reaction, forming an inner-sphere bidentate surface complex.

Arsenic adsorption on Fe hydroxide has been found to be strongly dependent on pH and speciation. Adsorption of $As_{(V)}$ (arsenate) on Fe hydroxide increases with decreasing pH from 10 to 4 (Hsia et al., 1994; Raven et al., 1998; Goldberg, 2002), while $As_{(III)}$ (arsenite) shows higher adsorption on the same substrates with increasing pH from 4 to 9 (Raven et al., 1998; Goldberg, 2002). Furthermore, adsorption of $As_{(V)}$ on iron hydroxide is not affected by changes in ionic strength (Hsia et al., 1994, Antelo et al., 2005), but adsorption of $As_{(III)}$ decreases with increasing

ionic strength (Goldberg and Johnston, 2001). Jia et al. (2007) reported that $As_{(V)}$ sorption on ferrihydrite at pH 3 and elevated temperature (75 °C) indicated the formation of crystalline scorodite in addition to surface complexation, but similar experiments at neutral and alkaline pH conditions only provided evidence for the formation of protonated and unprotonated surface complexes. Adsorption experiments for $As_{(III)}$ at pH 4.6, however, indicated the formation of partially protonated surface complexes on ferrihydrite (Jain et al., 1999).

Macroscopic and spectroscopic studies have indicated that $As_{(III)}$ forms both inner- and outer-sphere surface complexes, while $As_{(V)}$ forms only inner-sphere surface complexes on iron hydroxide (Waychunas et al., 1993; Hsia et al., 1994; Sun and Doner, 1996; Fendorf et al., 1997; Goldberg and Johnston, 2001). A consensus exists on the formation of dominant bidentate binuclear $As_{(V)}$ complexes on the surfaces of ferrihydrite and FeOOH polymorphs by sharing apical oxygen of adjacent Fe hydroxyl octahedra (Waychunas et al., 1993; Waychunas et al., 1995; Manceau, 1995). However, different mechanisms have been proposed for the other $As_{(V)}$ surface complexes formed during adsorption on ferrihydrite by Waychunas et al. (1993) and Manceau (1995). Waychunas et al. (1993) claimed the presence of a monodentate surface complex, while Manceau (1995) disputed this and proposed instead a bidentate mononuclear complex. On the basis of As-Fe distances, Fendorf et al. (1997) reported the existence of three different $As_{(V)}$ surface complexes: a monodentate complex, a bidentate binuclear complex, and a bidentate mononuclear complex. According to these authors, the monodentate complex was dominant at low surface coverage, while bidentante complexes were favored at higher surface coverage. The bidentate mononuclear complex, probably associated with greater distortion of goethite surface groups, occurred subordinately and required higher surface coverage to

overcome the large activation energy barrier to its formation (Fendorf et al., 1997). Similar results were confirmed by Waychunas et al (2005) for $As_{(V)}$ adsorption on hematite.

1.2.2. Phosphate adsorption on Fe-hydroxide

Several studies progressively improved the understanding of P_i adsorption on iron hydroxide (Parfitt and Atkinson, 1976; Tejedor-Tejedor and Anderson, 1990; Persson et al., 1996; Arai and Sparks, 2001; Kwon and Kubicki, 2004; Khare et al., 2007; Elzinga and Sparks, 2007). Although researchers agreed that the adsorption of P_i on iron hydroxide occurs by the formation of inner-sphere surface complexes, there was some disagreement on the mechanism and surface species. Similar to $As_{(V)}$, the mechanism of P_i adsorption on iron hydroxide varied with pH and surface coverage (Kwon and Kubicki, 2004; Elzinga and Sparks, 2007). In general, adsorption of P_i on ferrihydrite decreases with increasing pH and is non-responsive to changes in ionic strength within the pH range of 4-7.5, but is slightly increased with increasing ionic strength at pH >7.5 (Arai and Sparks, 2001).

Using infrared spectroscopy, Parfitt and Atkinson (1976) reported the formation of inner-sphere binuclear surface complexes of the type Fe–O–P–O–Fe on dried Fe oxides and hydroxides after P_i adsorption. Using an *in situ* FTIR technique, Tejedor-Tejedor and Anderson (1990) provided evidence for the formation of three types of P_i surface complexes on goethite: protonated bridging bidentate, non-protonated bridging bidentate, and non-protonated monodentate complexes. Persson et al. (1996) reported the formation of three types of protonated ortho-P_i monodentate surface complexes on goethite which vary in molecular symmetries (C3v, C2v, and C3v for HPO_4^{2-}, $H_2PO_4^-$, and H_3PO_4, respectively). Arai and Sparks (2001) suggested the formation of non-protonated bidentate binuclear surface complexes at pH >7.5, but neither

confirmed nor ruled out the formation of protonated monodentate mononuclear complexes and/or protonated bidentate binuclear complexes at pH <7.5. Similarly, Kwon and Kubicki (2004) suggested four possible P_i surface species: a diprotonated bidentate complex at pH 4-6, either a mono-protonated monodentate or non-protonated bidentate complex at pH 7.5-7.9, and a deprotonated monodentate complex at pH 12.8. For hematite surfaces, Elzinga and Sparks (2007) obtained three different P_i complexes having different relative proportions at different pH and P_i surface coverage conditions. Two protonated P_i surface complexes, a monodentate binuclear (bridging) complex and a monodentate mononuclear complex were present at pH 3.5-7.0, with the former being favored at low pH and high surface coverage. At higher pH levels (8.5-9.0), a third non-protonated monodentate mononuclear complex was identified, along with a protonated monodentate mononuclear complex (Elzinga and Sparks, 2007). Combining data from both phosphorous K-edge XANES and UV-visible spectroscopy of aqueous Fe(III)-Pi solutions with XANES analyses of mineral and adsorbed forms of P_i, Khare et al. (2007) found bidentate binuclear surface complexes to be in greater proportion than monodentate surface complexes on ferrihydrite at pH 6 and 750 mM/kg P_i.

1.2.3. Competitive adsorption/desorption of $As_{(v)}$ and P_i on Fe-hydroxide

Many previous studies have been performed to understand the mechanism of competitive adsorption/desorption of inorganic oxyanions, including $As_{(V)}$, $As_{(III)}$, carbonate, bicarbonate, chromate, molybdate, nitrate, P_i, selenate, selenite and sulfate, and of organic acids in different combinations on various metal oxides and clay minerals (Roy et al., 1986; Manning and Goldberg, 1996; Ali and Dzombak, 1996; Geelhoed et al., 1997; Wijnja and Schulthess, 2000; Gao and Mucci, 2001; Liu et al., 2001; Zhao and Stanforth, 2001; Ronson and McQuillan, 2002;

Violante and Pigma, 2002; Wu et al., 2002; Gao and Mucci, 2003; Antelo et al., 2005; Stachowicz et al., 2007). Arsenate and P_i have higher adsorption affinity on iron hydroxide than several other oxyanions (Manning and Goldberg, 1996; Geelhoed et al., 1997). Both $As_{(V)}$ and P_i have tetrahedral structure and individually occupy an estimated area of 61 $Å^2$ on the goethite surface during adsorption (Hingston, 1981). Some recent studies attempted to understand the multi-competitive interactions of $As_{(V)}$ with other anions in the presence of cations such as Ca, Mg, and Na (Smith et al., 2002; Stachowicz et al., 2008).

During single-anion adsorption experiments, Liu et al., (2001) obtained similar amounts of Pi and $As_{(V)}$ adsorption on goethite at pH 3.0-8.5. Experiments using initial equi-molar concentrations of $As_{(V)}$ and Pi indicated greater adsorption of $As_{(V)}$ on Fe, Mn, and Ti oxides and on Fe-rich clays, butgreater adsorption of P_i on Al oxides and Al-rich clays (Violante and Pigma, 2002). Similarly, competitive anion-adsorption experiments on goethite and gibbsite indicated a greater inhibitory effect of $As_{(V)}$ on sorption of P_i at pH<6.0, with slightly more $As_{(V)}$ adsorption, but similar adsorption of both anions under basic conditions (Manning and Goldberg, 1996; Liu et al., 2001). Zhao and Stanforth (2001) obtained an equal amount of adsorption of $As_{(V)}$ and P_i on goethite during simultaneous loading, but slightly higher total surface coverage than for either ion alone. The sorption of $As_{(V)}$ and P_i decrease with increasing initial $P_i/As_{(V)}$ and $P_i/As_{(V)}$ ratios, respectively on goethite (Violante and Pigma, 2002). Similarly, a greater decrease in P_i adsorption on goethite with increasing amount of $As_{(V)}$ is observed than *vice versa* (Liu et al., 2001; Violante and Pigma, 2002). Smith et al. (2002) reported greater adsorption of $As_{(V)}$ on soils in the presence of Ca^{2+} due to the change in surface charge characteristics of adsorption sites in soils. Similarly, the presence of Ca^{2+} or Mg^{2+} ions was found to enhance the adsorption of P_i on goethite (Stachowicz et al., 2008).

The competitive desorption of $As_{(V)}$ from goethite and amorphous Fe hydroxide surfaces caused by exchange with P_i is very effective (Jackson and Miller, 2000). P_i-induced desorption of adsorbed $As_{(V)}$ on goethite is relatively rapid, releasing >35% of the total adsorbed As (O'Reilly et al., 2001). However, O'Reilly et al. (2001) reported that a significant amount of As remained bound to goethite even after 5 months of P_i-induced desorption. The addition of P_i to As-contaminated sediment and soil was also found to enhance As desorption, due to the competitive exchange of P_i for adsorbed $As_{(V)}$ on sediment/soil components (Woolson et al., 1973; Qafoku et al., 1999; Wasay et al., 2000; Alam et al., 2001; Kaplan and Knox, 2004). Phosphoric acid was found to be very effective in rapidly displacing As from contaminated soil, both by providing P_i to compete with $As_{(V)}$ for adsorption sites and by dissolving As-harboring metal oxides present in the soil (Tokunaga and Hakuta, 2002). Application of P_i fertilizers to As-contaminated soil increases the solubility, mobility, and bioavailability of As by increasing the water soluble fraction via replacement of $As_{(V)}$ by P_i (Peryea and Kammereck, 1997; Cao and Ma, 2004). Likewise, a proportionate desorption of P_i occurred at low As additions, but As adsorption continued even after P_i desorption reached a maximum at higher As concentrations (Lambkin and Alloway, 2003).

Competitive adsorption/desorption experiments have indicated that $As_{(V)}$ and P_i compete for the same adsorption sites on soil and sediment phases; however, these experiments also have indicated the presence of some anion-specific adsorption sites on Fe hydroxide (Hingston et al., 1971; Manning and Goldberg, 1996; Liu et al., 2001). The observations that the total surface coverage during simultaneous loading of $As_{(V)}$ and P_i is greater than that for single anion loadings (Zhao and Stanforth, 2001) and that adsorption of $As_{(V)}$ continues even after maximum desorption of P_i is reached (Lambkin and Alloway, 2003), indicate the existence of anion-

specific adsorption sites on Fe-hydroxide surfaces. However, the possibility of precipitation occurring along with complexation on adsorbent surfaces at higher loadings of $As_{(V)}$ and P_i makes these results difficult to interpret (Zhao and Stanforth, 2001; Ler and Stanforth, 2003). Despite the fairly well-known single ion adsorption mechanisms for $As_{(V)}$ and P_i, the anion-specific sites on iron hydroxide during competitive adsorption have not yet been fully elucidated.

1.2.4. Phosphate-induced flushing and co-precipitation of arsenate-apatite

Phosphorous-induced leaching of As from contaminated soil has been studied extensively (Peryea and Kammereck, 1997; Qafoku et al., 1999; Wasay et al., 2000; Alam et al., 2001; Tokunaga and Hakuta, 2002; Kaplan and Knox, 2004; Cao and Ma, 2004), but very little work (e.g., Grisafe and Hummel, 1970; Twidwell et al., 1994) has been done to study the co-precipitation of As along with P_i minerals. Arsenate is able to substitute for P_i to form continuous solid solutions of fluor- and chlor-apatites (Grisafe and Hummel, 1970).

Reynolds et al. (1999) incubated soil samples amended with Na_2HAsO_4 and Na_2HPO_4 under N_2 atmosphere for 41 days, followed by aeration for 7 days, to study the effect of P_i on As dynamics during soil flooding and aeration cycles. Under anaerobic conditions, they noticed a decrease in sorption of As, higher reduction rate of $As_{(V)}$ in the presence of P_i, and formation of arsenopyrite. No apatite-like phases were identified, probably due to the lack of Ca and low pH (<6) during flooding. Upon re-aeration, however, oxidative destruction of arsenopyrite occurred, with concomitant precipitation of Fe and Mn hydroxide s, which increased the adsorption of As.

Twidwell et al. (1994) and other workers at Montana Tech (Wilson, 1998; Orser, 2001) have provided detailed information about the precipitation mechanism, and thermodynamic data for several As-bearing apatite-like minerals. Arsenic can be efficiently removed from solution by

forming calcium $As_{(V)}$ at pH 8-10; however, exposure of the system to air (i.e., CO_2) results in conversion of the precipitate into calcium carbonate with release of As back into the solution. Similarly, $As_{(V)}$-hydroxyapatite (without P_i) is also not stable with exposure to atmospheric CO_2, due to its conversion to carbonate. On the other hand, calcium $As_{(V)}$-P_i-hydroxyapatites are found to be stable phases with atmospheric exposure. The Montana Tech group claimed that $As_{(V)}$-P_i-hydroxyapatite, with a P:As ratio ≥ 7, has a very low solubility (<10 ppb) and thus greater stability against atmospheric exposure and greater suitability for wastewater treatment. However, the potential for this technique to fix As in contaminated soil has not yet been evaluated.

1.3. Research problems and objectives

1.3.1. Surfactant-modified zeolite as a PRB material for fly ash disposal facilities

Considering the long history of production of enormous volumes of coal fly ash and its past disposal in unlined facilities, the potential fly ash-induced contamination of surface and groundwater is a serious environmental risk across the US. The US Environmental Protection Agency (EPA) is currently proposing rule to regulate CCPs. The proposed rule would include CCPs as waste materials that require regulation under either Subtitle C or Subtitle D of the Resource Conservation and Recovery Act (RCRA) which until now exempts CCPs as a special waste (USEPA, 2010). Therefore, development of effective and economic *in situ* techniques to control the dispersion of hazardous trace elements from older CCP disposal facilities to surrounding groundwater and surface water is very important, potentially saving millions of dollars for the electrical power industry. The following hypotheses were tested in the first part of the dissertation research:

- Coal fly ash contains a sizable leachable fraction of pollutant elements.

- SMZ has the potential to adsorb the various anionic species in fly ash leachates.
- SMZ is a suitable permeable reactive barrier material for controlling the potential migration of leachable contaminants from fly ash disposal facilities.

This part of the study was aimed at (1) determining the types and concentrations of trace elements released from one Class C and three Class F fly ashes, using short-term and long-term leaching experiments, and (2) evaluating the effectiveness of SMZ as a permeable reactive barrier material for attenuation of trace elements leached from fly ash disposal facilities. The ability of SMZ to remove trace elements from fly ash leachate was determined using batch and column experiments. The ultimate goal of this study was to develop and test a SMZ-based, cost-effective PRB to contain toxic trace elements associated with coal fly ash.

1.3.2. Competitive adsorption/desorption of $As_{(V)}$ and P_i on Fe-Hydroxide

The competitive adsorption of $As_{(V)}$ and P_i by Fe hydroxide is very important for assessing the leachability and bio-accessibility of $As_{(V)}$ in the environment.

The primary goal of the second part of this dissertation was to better understand P_i-induced desorption and mobilization of As in the soil environment by experimentally studying the competitive adsorption/desorption of $As_{(V)}$ and P_i at the ferric hydroxide-water interface. In this part of the study, the following hypotheses were tested:

- $As_{(V)}$ and P_i compete for similar adsorption sites on ferric hydroxide.
- Both $As_{(V)}$ and P_i show similar adsorption preference on ferric hydroxide.
- $As_{(V)}$ and P_i are able to desorb the pre-equilibrated co-oxyanion from the ferric hydroxide surface.

1.3.3. Flushing and co-precipitation of As in contaminated soil by P_i

Contamination of soil and groundwater has resulted at numerous industrial sites in the southeastern US from the use of arsenical herbicides during the 1950s and 1960s. Although *in situ* chemical fixation of soil $As_{(V)}$ using ferrous sulfate (FS) treatment solutions has been found to be successful under aerobic conditions (Yang et al., 2007), this remediation technique cannot be used for anaerobic systems. Under anaerobic conditions, iron hydroxide precipitated on soil particles during FS treatment would be subject to reductive dissolution, potentially releasing the adsorbed $As_{(V)}$. Therefore, a new *in situ* chemical fixation method is needed for remediation of contaminated soils and sediments in anaerobic systems.

The use of excess P_i in the presence of dissolved Ca for flushing $As_{(V)}$ from the soil and co-precipitating it along with apatite-like materials has not been previously tested. Therefore, the final portion of the dissertation study was aimed at evaluating the potential of P_i-based methods for *in situ* fixation of arsenic in contaminated soil. Flushing of arsenic from the soil with P_i-rich chemicals (e.g., H_3PO_4) and subsequent co-precipitating of As as apatite-like solid phases were evaluated through batch experiments. The general objectives of this study were achieved by testing the following hypotheses:

- Phosphoric acid will leach $As_{(V)}$ from the contaminated soil.
- Addition of excess P_i and Ca to the soil will cause co-precipitation of As-bearing apatite-like phases.
- Mineralization of As in apatite-like phases will significantly decrease the mobility of As in contaminated soil.

1.4. Structure of the dissertation

This dissertation consists of six chapters, including the Introduction (Chapter 1) and the Summary (Chapter 6). The main body of the dissertation consists of four chapters, each representing a self-contained paper. Chapter2 and Chapter 3 are related to fly ash leaching and treatment of fly ash leachate with surfactant modified zeolite (SMZ), respectively. while Chapter 4 examines $As_{(V)}$ and P_i adsorption/desorption equilibria and kinetics on ferric hydroxide. Finally, Chapter 5 presents research on P_i-treatment of As-contaminated soil.

The first paper (Chapter 2) describes the leaching of alkaline and acidic fly ashes collected from different coal-fired power plants in the southeastern United States. The fly ash leaching was performed in batch and column experiments using doubly-deionized (DDI) water and synthetic acid rain (SAR) as leaching solutions. Short-term and long-term batch leaching of the four fly ashes were performed to determine the mobilities of several priority pollutant elements. To evaluate equilibrium as well as kinetically controlled leaching of these elements, serial batch leaching and column leaching experiments were performed. Leaching tests indicated that the fly ash samples contain environmentally leachable trace elements, and economic and effective leachate treatment methods are desired to control dispersion of these elements into surrounding surface waters and groundwater resources from unlined fly ash disposal facilities.

Because fly ash contains leachable amounts of several potentially toxic trace elements, effective methods are needed to reduce the potential for release of these elements to the environment from fly ash disposal facilities. Chapter 3 evaluates the ability of SMZ to attenuate trace elements in fly ash leachates using batch and column treatment experiments. . Quantitative comparison of the elemental composition of SMZ-treated and untreated leachate indicated that SMZ was effective in decreasing the concentrations of oxyanion and cationic trace elements

associated with coal fly ash, and supports the potential use of SMZ in permeable reactive barriers to control the dispersion of heavy metals and metalloids from ash disposal sites.

The third paper (Chapter 4) describes individual ion adsorption, as well as competitive adsorption, of $As_{(V)}$ and P_i on ferric hydroxide. Adsorption isotherms, envelopes, kinetics, and As K-edge EXAFS analysis were determined experimentally and used for understanding the equilibrium adsorption of $As_{(V)}$ and P_i in single ion and competitive settings. Freundlich and competitive Langmuir models were used to predict the equilibrium adsorption of $As_{(V)}$ and P_i. The triple layer model was employed to describe the adsorption envelopes using bidentate surface complexes. Single and competitive adsorption/desorption kinetics for $As_{(V)}$ and P_i were studied in batch experiments using different loading schemes. Some selected kinetic samples were further studied using As K-edge EXAFS to investigate the changes in $As_{(V)}$ surface complexation with time during individual adsorption or competitive adsorption/desorption. The research findings indicated that $As_{(V)}$ was preferred species for adsorption on ferric hydroxide than P_i. Similarly, this study also indicated that both oxyanions have limited ability to desorb the previously sorbed co-oxyanion from the ferric hydroxide surface.

Finally, Chapter 5 examines P_i-treatment of As-contaminated soil collected from an industrial site located in the Gulf region of the southeastern United States. This soil was contaminated with As due to the one-time application of arsenolite as an herbicide in the 1950s. A phosphate-based remediation method with the potential to fix arsenic in both oxidizing and reducing subsurface systems was evaluated using batch treatment experiments. The P_i treatment was primarily aimed at initial flushing of As from the soil with ortho-phosphoric acid, followed by precipitation of As in apatite-like phases. In this study, batch treatment experiments with contaminated soil were performed as a function of pH. Sorption isotherms and envelopes of P_i on

BH soil in the absence or presence of additional Ca were determined along with the associated mobilities of As. This study demonstrated the potential application of P_i-Ca treatment for in situ chemical fixation of As in contaminated soil at environmentally relevant pH conditions.

REFERENCES

Ahmed, K. M., Bhattacharya, P., Hasan, M. A., Akhter, S. H., Alam, S.M.M., Bhuyian, M.A.H., Imam, M. B., Khan, A.A., Sracek O. (2004) Arsenic enrichment in groundwater of the alluvial aquifers in Bangladesh: an overview. Applied Geochemistry 19, 181-200.

Alam, M.G.M., Tokunaga, S., and Maekawa, T. (2001) Extraction of arsenic in a synthetic arsenic-contaminated soil using Pi. Chemosphere 43 (8), 1035-1041.

Ali, M.A. and Dzombak, D. A. (1996) Competitive sorption of simple organic acids and sulfate on goethite. Environ. Sci. Technol., 30 (4), 1061-1071.

American Coal Ash Association. Coal combustion product (CCP) production & use survey results. American Coal Ash Association, http://www.acaa-usa.org; 2011.

Antelo, J., Avena, M., Fiol, S., López, R., and Arce, F. (2005) Effects of pH and ionic strength on the adsorption of Pi and As(V) at the goethite–water interface. Journal of Colloid and Interface Science 285(2), 476-486.

Arai, Y. and Sparks, D.L. (2001) ATR–FTIR spectroscopic investigation on Pi adsorption mechanisms at the ferrihydrite–water interface. Journal of Colloid and Interface Science 241, 317–326.

ATSDR (2000) Case Studies in Environmental Medicine- Arsenic Toxicity. ATSDR Publication No.: ATSDR-HE-CS-2002-0003 U.S. Department of Health and Human Services, Agency for Toxic Substances and Disease Registry, Division of Toxicology and Environmental Medicine, p. 42.

Auer, S., Kuzel, H.J., Pöllmann, H., and F. Sorrentino (1995) Investigation on MSW fly ash treatment by reactive calcium aluminates and phases formed. Cement and Concrete Research 25 (6), 1347-1359.

Baker, M.J., Blowes, D.W., and Ptacek, C.J. (1998) Laboratory development of permeable reactive mixtures for the removal of phosphorus from onsite wastewater disposal systems. Environ. Sci. Technol. 32(15), 2308-2316.

Bates, M.N., Smith, A.H., and Hopenhayn-Rich, C. (1992) Arsenic ingestion and internal cancers: A Review. American Journal of Epidemiology 135 (5), 462-476.

Bauer,M. and Blodau, C. (2006) Mobilization of arsenic by dissolved organic matter from iron oxides, soils and sediments. Science of the Total Environment 354 (2-3), 179-190.

Belzile, N., Tessier, A. (1990) Interactions between Arsenic and Iron Oxyhydroxides in Lacustrine Sediments. Geochimica et Cosmochimica Acta 54 (1), 103-109.

Benner, S.G., Blows, D.W., and Ptacek, C.J. (1997) A full-scale porous reactive wall for prevention of acid mine drainage. Ground Water Monitoring and Remediation XVII (4), 99-107.

Benner, S.G., Blowes, D.W., Gould, W.D., Herbert, R.B., and Ptacek, C. J. (1999) Geochemistry of a Permeable Reactive Barrier for Metals and Acid Mine Drainage. Environ. Sci. Technol. 33 (16), 2793-2799.

Bhattacharyya, S., Donahoe, R.J., and Patel, D. (2009) Experimental study of chemical treatment of coal fly ash to reduce the mobility of priority trace elements. Fuel 88(7), 1173-1184.

Blowes, D.W., Ptacek, C.J., Benner, S.G., McRae, C.W.T., Bennett. T.A. and Puls, R.W. (2000) Treatment of inorganic contaminants using permeable reactive barriers. Journal of Contaminant Hydrology 45(1-2), 123-137.

Bool, L.E. III, and Helble, J.J. (1995) A laboratory study of the partitioning of trace elements during pulverized coal combustion. Energy and Fuels 9, 880-887.

Bournonville, B., Nzihou A., Sharrock, P., and Depelsenaire, G. (2004) Stabilization of heavy metal containing dusts by reaction with phosphoric acid: study of the reactivity of fly ash. Journal of Hazardous Materials. B116, 65-74.

Bowman, R.S. (1996) Surface-altered zeolites as permeable barriers for in situ treatment of contaminated groundwater. Phase I Topical Report DE-Ar21-95MC32108, US Department of Energy, Morgantown, West Virginia, p. 50.

Bowman, R. S., Li, Z., Roy, S. J., Burt, T., Johnson, T.L., and Johnson, R.L., 1999. Surface-altered zeolites as permeable barriers for in situ treatment of contaminated groundwater. Phase II Topical Report DE-AR21-95MC32108, U.S. Department of Energy, Pittsburgh, Pennsylvania, p. 58.

Bowman, R.S. (2003) Review: Applications of surfactant-modified zeolites to environmental remediation. Microporous and Mesoporous Materials 61, 43-56.

Cantrell, K.J., Kaplan, D.I., Wietsma, T.W. (1995) Zero-valent iron for the in situ remediation of selected metals in groundwater. Journal of Hazardous Materials 42, 201-212.

Cao, X. and Ma, L.Q. (2004) Effects of compost and Pi on plant arsenic accumulation from soils near pressure-treated wood. Environmental Pollution 132, 435–442.

Carbonell-Barrachina, A.A., Rocamora, A., García-Gomis, C., Martínez-Sánchez, F., and Burló, F. (2004) Arsenic and zinc biogeochemistry in pyrite mine waste from the Aznalcóllar environmental disaster. Geoderma 122, 195-203.

Clarke, L.B. (1993) The fate of trace elements during coal combustion and gasification: an overview. Fuel 72 (6), 731-736.

Crannell, B.S., Eighmy, T.T., Krzanowski, J.E., Eusden, J.D. Jr., Shaw, E.L., Francis, C.A. (2000) Heavy metal stabilization in municipal solid waste combustion bottom ash using soluble Pi. Waste Management 20, 136-148.

Cullen, W.R. and Reimer, K.J. (1989) Arsenic speciation in the environment. Chem. Rev. 89, 713-764.

Das, D., Samanta, G., Mandal, B.K., Chowdhury, T.R.,Chanda, C.R., Chowdhury, P.P., Basu, G.K., Chakraborti, D. (1996) Arsenic in groundwater in six districts of West Bengal, India. Environ. Geochem. Health 18, 5-15.

Derie, R. (1996) A new way to stabilize fly ash from municipal incinerators. Waste Management 16(8), 711-716.

Dixit, S. and Hering, J.G. (2003) Comparison of $arsenic_{(V)}$ and $arsenic_{(III)}$ sorption onto iron oxide minerals: Implications for arsenic mobility. Environ. Sci. Technol. 37, 4182-4189.

Donahoe, R.J. (2004) Secondary mineral formation in coal combustion byproduct disposal facilities: implications for trace element sequestration. In: Gieré, R. and Stille, P. (eds) Energy, waste and the environment: a geochemical perspective, Geological Society of London, Special Publications, 236, 641-658.

Donahoe, R.J., Bhattacharyya, S., and Ladwig, K.J. (2007) Chemical fixation of trace elements in coal fly ash. University of Kentucky Center for Applied Energy Research, Ash Library, http://www.flyash.info, p. 22.

Elzinga, E.J. and Sparks, D.L. (2007) Phosphate adsorption onto hematite: An in situ ATR-FTIR investigation of the effects of pH and loading level on the mode of Pi surface complexation. J. Colloid Interface Sci. 308, 53–70.

Fendorf, S., Eick, M.J., Grossl, P., Sparks, D.L. (1997) Arsenate and chromate retention mechanisms on goethite. 1. Surface structure. Environ. Sci. Technol., 1997, 31, 315-320

Fernández-Turiel, J.L., de Carvalho, W., Cabanas, M., Querol, X., and Lopez-Soler, A. (1994) Mobility of heavy metals from coal fly ash. Environmental Geology 23 , 264-270.

Fuller, C.C., Davis, J.A., Waychunas, G.A. (1993). Surface chemistry of ferrihydrite: Part 2. Kinetics of $As_{(V)}$ adsorption and coprecipitation. Geochim. Cosmochim. Acta, 57(10), 2271-2282.

Gao, Y. and Mucci, A. (2001) Acid base reactions, phosphate and arsenate complexation, and their competitive adsorption at the surface of goethite in 0.7 M NaCl solution. Geochim. Cosmochim. Acta 65, 2361-2378.

Gao, Y. and Mucci, A. (2003) Individual and competitive adsorption of Pi and As(V) on goethite in artificial seawater. Chemical Geology 199 (1-2), 91-109.

Geelhoed, J.S., Hiemstra, T., and Van Riemsdijk, W.H. (1997) Phosphate and sulfate adsorption on goethite: single anion and competitive adsorption. Geochim. Cosmochim. Acta 61, 2389-2396.

Gieré, R., Carleton, L.E., and Lumpkin, G.R. (2003) Micro- and nanochemistry of fly ash from a coal-fired power plant. American Mineralogist88 (11-12), 1853-1865.

Gillham, R.W. and O'Hannesin, S.F. (1994) Enhanced degradation of halogenated aliphatics by zero-valent iron. Groundwater 32(6), 958-967.

Given, P.H. and Miller, R.N. (1987) The association of major, minor and trace inorganic elements with lignites. III. Trace elements in four lignites and general discussion of all data from this study. Geochim. Cosmochim. Acta 51, 1843-1853.

Glasser, F.P. (2004) Coal combustion wastes: characterization, reuse and disposal. In: Gieré, R. and Stille, P. (eds) Energy, waste and the environment: a geochemical perspective, Geological Society of London, Special Publications, 236, 2211-222.

Goldberg, S. and Johnston, C.T. (2001) Mechanisms of arsenic adsorption amorphous oxides evaluated using macroscopic measurements, vibrational spectroscopy, and surface complexation modeling. J. Colloid Interface Sci. 234, 204-216.

Goldberg, S. (2002) Competitive adsorption of arsenate and arsenite on oxides and clay minerals. Soil Sci. Soc. Am. J. 66, 413-421.

Goodarzi, F., Huggins, F.E., and Sanei, H. (2008) Assessment of elements, speciation of As, Cr, Ni and emitted Hg for a Canadian power plant burning bituminous coal. Int. J. Coal Geology 74, 1–12.

Grisafe, D.A. and Hummel, F.A. (1970) Pentavalent Ion substitutions in the apatite structure Part A. Crystal chemistry. J. Solid State Chem. 2, 160-l66.

Grossl, P.R., Eick, M., Sparks, D.L., Goldberg, S., and Ainsworth, C.C. (1997) Arsenate and chromate retention mechanisms on goethite. 2. Kinetic evaluation using a pressure-jump relaxation technique. Environ. Sci. Technol. 31, 321-326.

Guerin, T.F., Horner, S., McGovern, T., and Davey, B. (2002). An application of permeable reactive barrier technology to petroleum hydrocarbon contaminated groundwater. Water Research 36(1), 15-24.

Haggerty, G.M. and Bowman, R.S. 1994. Sorption of chromate and other inorganic anions by organo-zeolite. Environ. Sci. Technology, Vol. 28, 452-458.

Hassett, D.J., Pflughost-Hassett, D.F., and Heebink, L.V. (2005) Leaching of CCBs-observations from over 25 years of research. Fuel 84, 1378-1383.

Harvey, C.F., Swartz, C.H., Badruzzaman, A. B. M., Keon-Blute, N., Yu, W., Ali, A.M., Jay, J., Beckie, R., Niedan, V., Brabander, D., Oates, P.M., Ashfaque, K.N., Islam, S., Hemond, H.F., and Ahmed, M. F. (2002) Arsenic mobility and groundwater extraction in Bangladesh. Science 298, 1602-1606.

Hernandez, L., Probst, A., Probst, J. L., and Ulrich, E. (2003) Heavy metal distribution in some French forest soils: Evidence for atmospheric contamination. Sci. Tot. Environ 312, 195–219.

Hingston, F.J. (1981) A review of anion adsorption. In: Anderson, M.A. and Rubin, A.J. (eds.) Adsorption of inorganics at solid-liquid interfaces. Ann Arbor Sci. Publ., Ann Arbor, MI, 51-90.

Hingston, F.J., Posner, A.M., and Quirk, J.P. (1971) Competitive adsorption of negatively charged ligands on oxide surfaces. Discuss. Faraday Soc. 52:334-342.

Hossain, M.F. (2006) Arsenic contamination in Bangladesh-An overview. Agriculture, Ecosystems and Environment 113, 1-16.

Hsia, T.H., Lo, S.L., Lin, C.F., and Lee, D.Y. (1994) Characterization of arsenate adsorption on hydrous iron oxide using chemical and physical methods. Colloids and Surfaces A: Physicochemical and Engineering Aspects 85, 1-7.

Huang, W.J. and Lo, J.S. (2004) Synthesis and efficiency of a new chemical fixation agent for stabilizing MSWI fly ash. Journal of Hazardous Materials. B112, 79-86.

Islam, F.S., Gault, A. G., Boothman, C., Polya, D. A., Charnock, J.M., Chatterjee, D., and Lloyd, J.R. (2004) Role of metal-reducing bacteria in arsenic release from Bengal delta sediments. Nature 430 (6995), 68-71.

Iyer, R. (2002) The surface chemistry of leaching coal fly ash. Journal of Hazardous Materials, B93, 321-329.

Jackson, R. and Grainge, J. W. (1975) Arsenic and cancer. Canadian Medical Association Journal 113 (5), 396-401. Soil Sci. Soc. Am. J. 64, 1616–1622.

Jackson, B.P. and Miller, W.P. (2000) Effectiveness of Pi and Hydroxide for Desorption of Arsenic and Selenium Species from Iron Oxides.pdf

Jain, A., Raven, K.P., and Loeppert, R.H. (1999) Arsenite and arsenate Adsorption on Ferrihydrite: Surface Charge Reduction and Net OH- Release Stoichiometry. Environ. Sci. Technol. 33 (8), 1179–118

Jankowski, J., Ward, C.R., French, D., Groves, S. (2006) Mobility of trace elements from selected Australian fly ashes and its potential impact on aquatic ecosystems. Fuel 85, 243-256.

Jegadeesan,G., Al-Abed, S.R., and Pinto, P. (2008) Influence of trace metal distribution on its leachability from coal fly ash. Fuel 87 (10-11), 1887-1893.

Jia, Y., Xu, L., Wang, X., and Demopoulos, G.P. (2007) Infrared spectroscopic and X-ray diffraction characterization of the nature of adsorbed arsenate on ferrihydrite. Geochimica et Cosmochimica Acta 71(7), 1643-1654.

Kalbitz, K. and Wennrich, R. (1998) Mobilization of heavy metals and arsenic in polluted wetland soils and its dependence on dissolved organic matter. The Science of The Total Environment
209(1), 27-39.

Kalyoncu, R.S. (2000) Coal combustion products. US Geological Service Minerals Information.

Kaplan, D.I . and Knox, A.S. (2004) Enhanced Contaminant Desorption Induced by Pi Mineral Additions to Sediment. Environ. Sci. Technol. 38, 3153-3160.

Karagas, M.R., Stukel, T.A., Tosteson, T.D. (2002) Assessment of cancer risk and environmental levels of arsenic in New Hampshire. Int. J. Hyg. Environ. Health 205, 85-94.

Khare, N., Martin, J.D., and Hesterberg, D. (2007) Pi bonding configuration on ferrihydrite based on molecular orbital calculations and XANES fingerprinting Geochim. Cosmochim. Acta 71(18), 4405-4415.

Kim, A.G. (2002) CCB leaching summary: survey of methods and results. Proceedings: Coal Combustion By-Products and Western Coal Mines: A Technical Interactive Forum, Golden, CO, April 16-18, 23p.

Külaots, I., Hurt, R.H., and Suuberg, E.M. (2004) Size distribution of unburned carbon in coal fly ash and its implications. Fuel 83 (2), 223-230.

Kutchko, B.G. and Kim, A.G. (2006) Fly ash characterization by SEM-EDS. Fuel 85, 2537-2544.

Kwon, K.D. and Kubicki, J.D. (2004) Molecular orbital theory study on surface complex structures of Pis to iron hydroxides: calculation of vibrational frequencies and adsorption energies. Langmuir, 2004, 20 (21), 9249-9254

Lambkin, D.C. and Alloway, B.J., 2003. As(V)-induced Pi release from soils and its effect on plant phosphorus. Water, Air, and Soil Pollution 144, 41–56.

Lecuyer, I., Bicocchi, S., Ausset, P., and Lefevre, R. (1996) Physico-chemical characterization and leaching of desulphurization coal fly ash. Waste Management and Research 14, 15-28.

Leppert, D. (1990) Heavy metal sorption with clinoptilolite zeolite: alternatives for treating contaminated soil and water. Mining Engineering 42(6), 604-608.

Ler, A., and Stanforth, R. (2003) Evidence for surface precipitation of phosphate on goethite. Environ. Sci. Technol. 37, 2694-2700.

Li, Z. and Bowman, R.S. (1997) Counterion effects on the sorption of cationic surfactant and chromate on natural clinoptilolite. Environ. Sci. and Technology 31, 2407-2412.

Li, Z., Roy, S. J., Zou, Y. and Bowman, R.S. (1998) Long-term chemical and biological stability of surfactant-modified zeolite. Environ. Sci. Technol. 32, 2628-2632.

Liu, F., De Cristofaro, A., and Violante, A. (2001) Effect of pH, phosphate and oxalate on the adsorption/desorption of arsenate on/from goethite. Soil Science 166(3), 197-208.

Manceau A. (1995) The mechanism of anion adsorption on iron oxides: Evidence for the bonding of As(V) tetrahedra on free $Fe(O,OH)_6$ edges. Geochim. Cosmochim. Acta 59, 3647-3653.

Mandal, B.K. and Sujuki, K.T. (2002) Arsenic round the world: a review. Talanta 58, 201-235.

Manning, B.A. and Goldberg, S. (1996) Modeling competitive adsorption of arsenate with phosphate and molybdate on oxide minerals. SSAJ 1, 121-131.

Manning, B.A., and S. Goldberg. (1997) Adsorption and stability of arsenic(III) at the clay mineral-Water interface. Environ. Sci. Technol. 31, 2005–2011.

Mardon, S.M., Hower, J.C., O'Keefe, J.M.K., Marks, M.N., and Hedges, D. H. (2008) Coal combustion by-product quality at two stoker boilers: Coal source vs. fly ash collection system design. Int. J. Coal Geology 75, 248-254.

Masscheleyn, P.H., Delaune,R.D., and Patrick, W.H. Jr. (1991) Effect of redox potential and pH on arsenic speciation and solubility in a contaminated soil. Envlron. Sci. Technol. 25, 1414-1419.

McBride, M.B. (1994) Environmental Chemistry of Soils. Oxford University Press, New York, p. 406.

McCarthy, G.J., Butler, R.D., Grier, D.G., Adamek, S.D., Parks, J.A., and Foster, H.J. (1997) Long-term stability of landfilled coal combustion by-products. Fuel. 76(8), 697-703.

McCarthy, G.J., Grier, D.G., Wisdom, M.A., Petersen, R.B., Lerach, S.L., Jarabek, R.L., Walsh, J.J., and Winburn, R.S. (1999) Coal Combustion By-Product Diagenesis II. International Ash Utilization Symposium, October 18-20. Lexington, KY: Center for Applied Energy Research, University of Kentucky, Paper # 67, 9 pp.

McGeehan, S.L., Naylor, D.V., and Shafii, B. (1992) Statistical evaluation of arsenic adsorption data using linear-plateau regression analysis. Soil Sci. Soc. Am. J. 56, 1130-1133.

Miller, R.N. and Given, P.H. (1986) The association of major, minor and trace inorganic elements with lignites. I. Experimental approach and study of a North Dakota lignite. Geochim. Cosmochim. Acta, 50, 2033-2043.

Miller, R.N. and Given, P.H. (1987) The association of major, minor and trace inorganic elements with lignites. II. Minerals, and major and minor elements profiles, in four seams. Geochimica et Cosmochimica Acta, 51, 1311-1322.

Morrell, J.J., Keefe, D., and Baileys, R.T. (2003) Copper, Zinc, and Arsenic in Soil Surrounding Douglas-Fir Poles Treated with Ammoniacal Copper Zinc As(V) (ACZA). J. Environ. Qual., 32, 2095-2099.

Morrison, S.J. and Spangler, R.R. (2006) Chemical barriers for controlling groundwater contamination. Environmental Progress 12 (3), 175-181.

Mucci A., Richard L.F., Lucotte M., and Guignard C. (2000) The Differential Geochemical Behavior of Arsenic and Phosphorus in the Water Column and Sediments of the Saguenay Fjord Estuary, Canada. Aquatic Geochemistry 6, 293-324.

National Research Council (2006) Managing Coal Combustion Residues in Mines. National Research Council of the National Academies, the National Academies Press, Washington, D.C., p. 238.

Natusch, D.F.S., Wallace, J.R., Evans, C.A. Jr. (1974) Toxic Trace Elements: Preferential Concentration in Respirable Particles. Science 183 (4121), 202-204.

Newsam, J.M. (1986) The zeolite cage structure. Science 231, 1093-1099.

Nickson, R., McArthur, J.M., Burgess, W., Ahmed, K.M., Ravenscroft, P., and Mizanur Rahmanñ, M. (1998) Arsenic poisoning of Bangladesh groundwater. Nature 395, 348.

Nickson, R., McArthur, J.M., Ravenscroft, P., Burgess, W., and Ahmed, K.M. (2000) Mechanism of arsenic release to groundwater, Bangladesh and West Bengal. Applied Geochemistry 15, 403–413.

Nordstrom, D.K. (2002) Worldwide occurrences of arsenic in ground water. Science 296 (5576), 2143-2145.

O'Reilly, S.E., Strawn, D. G., and Sparks, D.L. (2001) Residence time effects on arsenate adsorption/desorption mechanisms on goethite. Soil Sci. Soc. Am. J. 65, 67-77.

Oremland, S. and Stolz, J.F. (2003) The ecology of arsenic. Science 300, 939-944.

Orser, T., 2001. Removal of arsenic from waste water solutions as storable stable precipitates. MS Thesis, Department of Metallurgical and Materials Engineering, Montana Tech of The University of Montana.

Otero-Rey, J.R., Mato-Fernandez, M.J., Moreda-Pineiro, J., Alonso-Rodriguez, E., Muniategui-Lorenzo, S., Lopez-Mahia, P. and Prada-Rodriguez, D. (2005) Influence of several parameters on As and Se leaching from coal fly ashes. Analytica Chimica Acta 531, 299-305.

Ouki, S.K. (1997) Performance of Natural Zeolites for the Treatment of Mixed Metal-Contaminated Effluents. Waste Management and Research, 15(4), 383-394.

Ouki, S.K., Cheeseman, C., and Perry, R. (1993) Effects of conditioning and treatment of chabazite and clinoptilolite prior to lead and cadmium removal. Environ. Sci. Technol. 27(6), 1108-1116.

Parfitt, R.L. and Atkinson, R.J. (1976) Pi adsorption on goethite (α-FeOOOH). Nature 264, 740-742.

Persson, P., Nilsson, N., and Sjoberg, S. (1996) Structure and bonding of ortho-phosphate ions at the iron oxide-aqueous interface. J. Colloid Interface Sci. 177, 263-275.

Peryea, F.J. and Kammereck, R. (1997) Pi-enhanced movement of arsenic out of lead arsenate-contaminated topsoil and through uncontaminated subsoil. Water, Air, and Soil Pollution 93, 243-254.

Qafoku, N.P., Kukier, U., Sumner, M.E., Miller, W.P., and Radcliffe, D.E. (1999) Arsenate displacement from fly ash in amended soils. Water, Air, and Soil Pollution 114, 185-198.

Qi, Y. and Donahoe, R.J. (2008) The environmental fate of arsenic in surface soil contaminated by historical herbicide application. Science of The Total Environment 405, 246-254.

Raven, K.P., Jain, A., and Loeppert, R.H. (1998) Arsenite and arsenate adsorption on ferrihydrite: kinetics, equilibrium, and adsorption envelopes. Environ. Sci. Technol. 32 (3), 344-349 •

Reynolds, J.G., Naylor, D.V., and Fendorf, S.E. (1999) Arsenic sorption in phosphate-amended soils during flooding and subsequent aeration. Soil Sci. Soc. Am. J. 63, ll49-1156.

Robinson, G.R. Jr., Larkins, P., Boughton, C.J., Reed, B.W., and Sibrell, P.L. (2007) Assessment of contamination from arsenical pesticide use on orchards in the Great Valley region, Virginia and West Virginia, USA. J. Environ. Qual., 36:654-663.

Ronson, T.K. and McQuillan, A.J. (2002) Infrared spectroscopic study of calcium and Pi ion coadsorption and of brushite crystallization on TiO_2. Langmuir, 18: 5019-5022.

Roy, W.R., Hassett, J.J., and Griffin, R.A. (1986) Competitive coefficients for the adsorption of As(V), molybdate, and Pi mixtures by soils. Soil Sci. Soc. Am. J. 50, ll76-1182.

Ruhl, L., Vengosh, A., Dwyer, G.S., Hsu-Kim, H., and Deonarine, A. (2010) Environmental impacts of the coal ash spill in Kingston, Tennessee: An 18-month survey. Environ. Sci. Technol., 44, 9272-9278.

Simcox, N.J., Fenske, R.A., Wolz, S.A., Lee, I.C., Kalman, D.A. (1995) Pesticides in household dust and soil: exposure pathways for children of agricultural families. Environmental Health Perspectives 103 (12), 1126-1134.

Slomp, C.P., Van der Gasst, S.J., and Van Raaphorst, W. (1996) Phosphorus binding by poorly crystalline iron oxides in North Sea sediments. Marine Chemistry 52, 55-73.

Smedley, P.L. and Kinniburgh, D.G. (2002) A review of the source, behaviour and distribution of arsenic in natural waters. Applied Geochemistry 17, 517-568.

Smedley, P.L., Kinniburgh, D.G., Macdonald, D.M.J., Nicolli, H.B., Barros, A.J., Tullio, J.O., Pearce, J.M., Alonso, M.S. (2005)Arsenic associations in sediments from the loess aquifer of La Pampa, Argentina. Applied Geochemistry 20, 989-1016.

Smith, R.D. (1980) The trace element chemistry of coal during combustion and the emissions from coal-fired plants. Prog Energy Combust Sci 1980, 6, 53-119.

Smith, E., Naidu, R., and Alsto, A.M. (2002) Chemistry of inorganic arsenic in soils II. Effect of phosphorus, sodium, and calcium on arsenic sorption. Journal of Environmental Quality 31, 557-563.

Smyth, D.J.A., Shikaze, S.G., and Cherry, J.A. (1997) Hydraulic performance of permeable barriers for in situ treatment of contaminated groundwater. Land Contamination and Reclamation 5, 131-137. 1997.

Sposito, G. (1984) The surface chemistry of soils. Oxford University Press, New York, p. 234.

Stachowicz, M., Hiemstra, T., and van Riemsdijk, W.H. (2007) Arsenic-bicarbonate interaction on goethite particles. Environ. Sci. Technol., 41, 5620-5625.

Stachowicz, M., Hiemstra, T., and van Riemsdijk, W.H. (2008) Multi-competitive interaction of As(III) and As(V) oxyanions with Ca^{2+}, Mg^{2+}, PO_3^{-4} , and CO_2^{-3} ions on goethite. Journal of Colloid and Interface Science 320, 400-414.

Steinnes, E. and Friedland, A. J. (2006) Metal contamination of natural surface soils from long-range atmospheric transport: Existing and missing knowledge. Environmental Reviews 14, 169–186. doi

Stüben, D., Berner, Z., Chandrasekharam, D., and Karmakar, J. (2003) Arsenic enrichment in groundwater of West Bengal, India: geochemical evidence for mobilization of As under reducing conditions. Applied Geochemistry 18, 1417-1434.

Sun, X. and Donner, H.E. (1996) An investigation of arsenate and arsenite bonding structures on goethite by FTIR. Soil Science 161 (12), 865-872.

Tejedor-Tejedor, M.I. and Anderson, M.A. (1990) Protonation of phosphate on the surface of goethite as studied by CIR-FTIR and electrophoretic mobility. Langmuir 6, 602–611.

Tishmack, J.K. and Burns, P.E. (2004) The chemistry and mineralogy of coal and coal combustion products. In: Gieré, R. and Stille, P. (eds) Energy, waste and the environment: a geochemical perspective, Geological Society of London, Special Publications, 236, 223-246.

Tokunaga, S. and Hakuta, T. (2002) Acid washing and stabilization of an artificial arsenic-contaminated soil. Chemosphere 46, 31-38.

Twidwell, L.G., Plessas, K.O., Comba, P.G. and Dahnke, D.R. (1994) Removal of arsenic from wastewaters and stabilization of arsenic bearing waste solids: Summary of experimental studies. Journal of Hazardous Materials 36, 69-80.

USEPA, 2010. Hazardous and solid waste management system: identification and listing of special wastes; disposal of coal combustion residuals from electric utilities. Federal Register 75(118), 35127-35264.

Violante, A. and Pigna, M. (2002) Competitive sorption of arsenate and phosphate on different clay minerals and soils. Soil Sci. Soc. Am. J. 66, 1788–1796.

Wasay, S.A., Parker, W., Van Geel, P.J., Barrington, S., and Tokunaga, S. (2000) Arsenic pollution of a loam soil: Retention form and decontamination. Soil and Sediment Contamination 9(1), 51-64.

Waybrant, K.R., Blowes, D.W., and Ptacek, C.J. (1998) Selection of reactive mixtures for use in permeable reactive walls for treatment of mine drainage. Environ. Sci. Technol. 32 (13), 1972-1979.

Waychunas, G.A., Rea, B.A., Fuller, C.C., and Davis, J.A. (1993) Surface chemistry of ferrihvdrite: Part 1. EXAFS studies of the geometry of coprecipitated and adsorbed arsenate. Geochim. Cosmochim. Acta 57:2251-2269.

Waychunas G. A., Davis J. A., and Fuller C. C. (1995) Geometry of sorbed arsenate on ferrihydrite and crystalline FeOOH: Re-evaluation of EXAFS results and topological factors in predicting sorbate geometry, and evidence for monodentate complexes. Geochim. Cosmochim. Acta 59, 3655-3661.

Waychunas, G., Trainor T. , Eng, P., Catalano, J., Brown, G., Davis, J., Rogers, J. and Bargar, J. (2005) Surface complexation studied via combined grazing-incidence EXAFS and surface diffraction: arsenate on hematite (0001) and (10–12). Analytical and Bioanalytical Chemistry 383, 12-27.

Wijnja, H. and Schulthess, C.P. (2000) Interaction of carbonate and organic anions with sulfate and selenate adsorption on an aluminum oxide. Soil Science Society of America Journal 64, 898-908.

Wilson, S.R. (1998) Removal of arsenic from ASARCO acid plant blowdown water as stable, storable precipitates. MS Thesis, Department of Metallurgical and Materials Engineering, Montana Tech of The University of Montana.

Woolson, E.A., Axley, J.H. and Kearney, P.C. (1973) Chemistry and phytotoxicity of arsenic in soils. II. Effects of time and phosphorus. Soil Science Society of America Journal 37, 254-259

Wu, C.H. Wu, Kuo, C.Y., Lin, C.F., and Lo, S.L. (2002) Modeling competitive adsorption of molybdate, sulfate, selenate, and selenite using a Freundlich-type multi-component isotherm. Chemosphere 47, 283-292.

Yang, L. (2005) Evaluation of in situ chemical fixation for remediation of arsenic contaminated soil. PhD Dissertation, University of Alabama, p. 173.

Yang, L. and Donahoe, R.J. (2007) The form, distribution and mobility of arsenic in soils contaminated by arsenic trioxide, at sites in southeast USA. Applied Geochemistry 22, 320-341.

Yang, L., Donahoe, R.J., Redwine, J.C. (2007) In situ chemical fixation of arsenic-contaminated soils: An experimental study. Science of The Total Environment, 387, 28-41.

Yudovich, Y.E., Ketris, M.P. (2005) Arsenic in coal: a review. International Journal of Coal Geology 61, 141-196.

Zhao, H. and Stanforth, R. (2001) Competitive adsorption of Pi and As(V) on goethite. Environ. Sci. Technol. 35, 4753-4757.

CHAPTER – 2

LEACHABILITY OF ELEMENTS IN ALKALINE AND ACIDIC COAL FLY ASH SAMPLES DURING BATCH AND COLUMN LEACHING TESTS[a]

Abstract

Three acidic (HA, HB, and MA) and one alkaline (PD) fly ash samples collected from four different power plants were subjected to batch and column leaching tests to evaluate the leachability of several elements. Jar leaching tests (up to 120 h), serial batch leaching tests (35 days), and long-term (up to 70 weeks) batch leaching tests were performed using doubly deionized (DDI) water, and column leaching tests (131–150 pore volumes) were conducted using a synthetic acid rain (SAR) solution. The results of batch and column leaching tests showed that different proportions of As, Cr, Mo, Sb, Se, and V were leached by DDI water and SAR from the four fly ash samples. The increasing leachate concentrations of As, Cr, Mo, Sb, Se (except PD fly ash), and V with time indicated that the long-term release of these elements was controlled by the dissolution of glassy fly ash particles. Mobilization of As from HA fly ash, Cr from PD fly ash, and Se from both HA and PD fly ash also showed a bimodal leaching pattern during column leaching tests, potentially indicating the association of these elements with different fly ash

---

[a] This chapter represents a journal article that has been published in *Fuel*, DOI: 10.1016/j.fuel.2012.06.013.

fractions. In general, Mo, Sb, and Se showed high mobilities, while only small amounts of Cr were released from the fly ash samples. Boron, Ca, K, Mg, Mn, and Na were released very rapidly during the initial phases of both serial and column leaching tests. These elements were likely enriched in surface-bound, highly soluble loose particles. During long-term batch leaching tests, HB and MA fly ash leachate concentrations of Ba, Co, Mn, Ni, and Zn decreased with time, indicating possible adsorption or co-precipitation with secondary minerals. Because many of the older fly ash disposal facilities are unlined, these sites are potential sources of hazardous elements to the environment. Therefore, development of effective and economic methods to contain trace elements within the disposal facility site is desirable to prevent contamination of groundwater and surface water resources.

KEYWORDS: coal fly ash, leaching, trace elements, contamination

2.1. Introduction

Millions of tons of coal combustion products (CCPs) are produced every year by coal-fired power plants. CCPs include fly ash, bottom ash, boiler slag, flue gas desulfurization (FGD) materials, and various gases (Kalyoncu, 2000). Fly ash, the most voluminous fraction of CCPs, is fine particulate inorganic matter collected thorough mechanical processes, electrostatic precipitators, and fabric filters from the flue gas produced by the combustion of pulverized coal in the boiler assembly. In 2010, 67.7 million short tons of coal fly ash were produced in the US, accounting for 52.0% of the total CCPs (American Coal Ash Association, 2011). Although the beneficial use of fly ash and other CCPs has varied in recent years (37.9% or 27.7 short tons of

fly ash were recycled and used in 2010), the majority of the fly ash is buried in impoundment lagoons or dry landfills along with other unused CCPs (American Coal Ash Association, 2011).

Fly ash is a heterogeneous material primarily consisting of amorphous aluminosilicate spheres with minor amounts of iron-rich spheres, some crystalline phases, and a small amount of unburned carbon (Jegadeesan et al., 2008; Külaots et al., 2004; Kutchko and Kim, 2006; Tishmack et al., 2004). The composition of fly ash depends on the composition of source coal and co-feed materials, combustion technology, pollution control technology, and fly ash handling technology (Mardon et al., 2008; National Research Council, 2006). Coal is mainly composed of organic derivatives with a small amount of inorganic materials such as primary detrital minerals (e.g., quartz, feldspar, clays, mica, and zircon), and secondary minerals (e.g., calcite and sulfides) (Glasser, 2004; Miller and Given, 1986). Several hazardous elements, such as As, Be, Cd, Co, Cr, Hg, Mn, Ni, Pb, Sb, and Se are present in small quantities in coal (Bool and Helble, 1995). During the gas-suspension combustion of pulverized coal, most of the carbon and sulfur components of coal convert to gaseous form, while the inorganic mineral components of coal undergo partial or complete thermal transformation (Clarke, 1993). As the temperature decreases during fly ash collection, volatilized trace elements in the hot flue gas re-deposit on ash particles (Goodarzi et al., 2008). Therefore, trace elements are more enriched on the surface of the ash particles, compared to the interior (Lecuyer et al., 1996; Natusch et al., 1974; Smith, 1980). Furthermore, trace elements tend to be enriched in the finer fly ash fraction collected at lower temperature than they are in the coarser fly ash fraction collected at higher temperature (Mardon et al, 2008).

Fly ash deposited in lagoons or dry landfills undergoes mineralogical and chemical transformations, with gains, losses, or redistribution of major, minor, or trace elements, along

with alteration of its physical properties (McCarthy et al., 1997; 1999). During these chemical and mineralogical transformations, a significant proportion of the trace elements can be released into the environment. Therefore, fly ash deposited in unlined disposal facilities can be a potential source of several hazardous elements (Donahoe, 2004). Many studies have been carried out to evaluate the mechanism of trace element release from fly ash into the environment using various leaching schemes and solutions (e.g., Hassett et al., 2005; Jankowski et al., 2006; Kim, 2002; Mattigod et al., 1990; Otero-Rey et al., 2005). Fernández-Turiel et al. (1994) reported that 1.5%–36.4% of the total concentration of each element in fly ash is extractable under natural leaching conditions. Jankowski et al. (2006) reported higher mobilities for As, Mo, and Se from acidic and alkaline fly ashes at high initial pH conditions, while B showed no simple relationship between mobility and leachant pH. Long-term leaching of alkaline fly ash showed an initial increase in leachate As, B, and Se concentrations to maximum values, and then a gradual decrease due to the formation of ettringite (Jankowski et al., 2006; Mattigod et al., 1990). Jegadeesan et al. (2008) reported moderate leaching of Fe, Pb, and Cr from Class F fly ash at acidic pH conditions, and saw a significant release of As at pH < 4 (due to dissolution) and pH > 9 (due to desorption).

Because older CCP disposal facilities were typically unlined, leachable trace elements in fly ash may become part of the local hydrogeology. Therefore, these older disposal facilities pose a greater risk of being persistent sources of contaminants to the environment than lined facilities. Development of economic and effective remediation techniques to contain hazardous trace elements within unlined fly ash disposal facilities is very important to ensure the protection of groundwater and surface water resources. The objective of this study was to evaluate the leachability of As, Cr, Mo, Se, Sb, and other elements from one alkaline and three acidic fly ash

samples derived from Powder River Basin and Eastern Bituminous coals, respectively. The leachability of each element was calculated using data from serial and column leaching tests with respect to its environmentally available concentrations in the fly ash samples.

2.2. Materials and methods

2.2.1. Fly ash samples and characterization

Three acidic (Class F) fly ash samples (HA, HB, and MA) and one alkaline (Class C) fly ash sample (PD) were collected from four different coal-fired power plants located in the southeastern United States. The acidic fly ash samples were derived from the combustion of Eastern Bituminous coals and the alkaline fly ash was the combustion product of Powder River Basin coal. The fly ash samples were air-dried and homogenized prior to their use in experiments. The specific surface area of each fly ash sample was determined by the single-point BET method with a flow of 30% N_2 in He using a Leybold-Inficon mass spectrometer to detect the gasses. The bulk ash mineralogy was identified with a Brüker D8 Advance powder diffractometer. The unburned carbon content of the fly ash samples was determined by loss-on-ignition (LOI) tests (Hassett and Eylands, 1999). The environmentally available elements in the fly ash samples were extracted with a microwave-assisted partial acid digestion using USEPA Method 3051A (USEPA, 2007).

2.2.2. Background soil

A yellow, sandy background soil (5–20 cm depth) was collected from Fort Walton Beach, Florida. This soil was selected as a background soil for the column experiments because of its good hydraulic conductivity and low concentrations of environmentally available trace

elements. Furthermore, the background soil collection site is located in the Gulf region of the southeastern United States, which is the regional location of the power plants where the fly ash samples were collected. The background soil was air dried, passed through a 2 mm screen to remove larger debris, and thoroughly mixed. The mineralogy of the soil was studied by X-ray diffraction (XRD) analyses of the bulk soil as well as the clay-sized (<2 μm) fraction of the soil. The clay-sized soil fraction was separated by flotation according to Stoke's Law. The environmentally available elements in the background soil were extracted by microwave-assisted partial acid digestion (USEPA, 2007). The soil pH was measured at a 1:1 solid:liquid ratio using USEPA Method 9045D (USEPA, 2004).

2.2.3. Measurement of fly ash pH

The general surface reactivity of the fly ash particles was observed by measuring pH at different fly ash concentrations and equilibration times. The pH was measured immediately after mixing 0.5 g of fly ash into 1.0 L of DDI water (>18 MΩ doubly deionized water produced by a Barnstead NANOpure system) and again after 12 h of agitation. Then an additional 0.5 g sample of fresh fly ash was added to the previous mixture, followed by immediate measurement of pH (initial pH) and measurement of pH after 12 h of agitation (final pH). Successively, 0.5 g additional fresh fly ash was added into the mixture to make a thicker fly ash-water slurry, and pH was measured immediately and after 12 h of agitation following each fly ash increment.

2.2.4 Fly ash leaching experiments

Several different leaching schemes were used for evaluating the mobility and leachability of elements from the four fly ash samples. DDI water was selected as the leachant solution for jar

leaching, long-term batch leaching, and serial batch leaching experiments to avoid providing an external supply of sulfate and thus better evaluate the potential for precipitation of secondary minerals. The synthetic acid rain (SAR) (USEPA, 1994), a dilute solution of H_2SO_4 and HNO_3 with pH = 4.20 ± 0.05, was used for fly ash leaching in column experiments. The jar and batch leaching experiments ensured dynamic contact between the fly ash particles and the leachant (DDI water) through constant agitation, while the column leaching experiments were intended to mimic natural leaching of fly ash by infiltrating acid rain water.

Aqueous solutions were separated from the fly ash after jar and batch leaching experiments by centrifugation at 8500 rpm for 20 min. All aqueous samples were filtered through 0.2µm nylon syringe filters, acidified to 2% HNO_3 with OPTIMA® ultrapure nitric acid, and stored in a refrigerator until chemical analysis with a Perkin Elmer Optima 3000DV inductively coupled plasma optical emission spectrometer (ICP-OES). Concentrations of sulfate in some selected fly ash leachates were determined by ion chromatography (Dionex LC 20 Chromatography Enclosure).

2.2.4.1. Jar leaching tests

Jar leaching tests were carried out to determine temporal leaching trends and equilibration times for the different elements. The jar leaching experiments were performed at a 1:30 solid:liquid ratio. For these tests, 60 g of each fly ash were mixed with 1.8 L of DDI water in a 2 L bottle and agitated on an orbital platform shaker at 200 rpm. About 20 mL of the supernatant solution were removed from each jar at 1, 4, 8, 12, 24, 36, 48, 72, 96, and 120 h for chemical analysis.

2.2.4.2. Long-term batch leaching experiments

A long-term (up to 70 weeks) leaching scheme was employed to evaluate the leaching behavior of several elements during extended fly ash-DDI water interaction. For each fly ash sample, multiple leaching sets were prepared by mixing 3 g fly ash and 45 mL of DDI water in 50 mL centrifuge tubes. The fly ash-water mixtures were continuously agitated until sample collection. At each sampling time, duplicate aliquots of each fly ash leachate solution were collected for chemical analysis by sacrificing two tubes.

The leachate pH values and chemical compositions of the long-term leaching tests were used for calculating the saturation indices for several potential secondary minerals (Table S2.1) with the geochemical code PHREEQC (Parkhurst and Appelo, 1999). All solutions during geochemical simulations were allowed to equilibrate with atmospheric CO_2 and O_2. The precipitation potential of a secondary mineral from fly ash leachate solution was determined by evaluating its state of saturation (undersaturation or oversaturation). The leachate solution must be oversaturated with respect to a mineral phase for its spontaneous precipitation. The degree of undersaturation or oversaturation of a leachate with respect to a particular mineral was determined in terms of the saturation index (SI), calculated using Eq. (2.1):

$$SI = \log(IAP/K_{SP}) \ldots (2.1)$$

where IAP is the ion activity product and K_{sp} is the solubility constant for a particular mineral (Drever, 1997). If the SI value was greater than 0, then the leachate solution was considered to be oversaturated with respect to that particular mineral, and the solution was likely to spontaneously precipitate that mineral, barring any kinetic constraints.

Furthermore, the leachate pH values and concentrations of different elements mobilized during long-term batch leaching tests were analyzed using statistical tools. Two-tailed Pearson

correlation matrices and principal component analyses (PCA) were performed for each experiment. The Pearson correlation matrices show the bivariate relationship between two variables, while the PCA is a multivariate statistical analysis that can show associations between variables, such as whether different elements have similar leaching behaviors over time. The PCA transforms the original n number of variables (leachate pH and number of elements) into the same number of uncorrelated orthogonal variables, known as principle components (PCs). The first principal component represents the maximum variance associated with variables, and the successive components represent progressively smaller uncorrelated variances. Prior to the PCA, elemental concentrations were log-transferred to minimize the influence of higher values. The PCs were extracted by analyzing the correlation matrix with an eigenvalue > 1. Finally, the PCs were simplified by varimax rotation (an orthogonal rotation that increases the participation of the variables with higher contribution and reduces the participation of the variables with smaller contribution) with Kaiser Normalization. Both correlation matrices and PCA were performed using SPSS 12.0 for Windows.

2.2.4.3. Serial batch leaching experiments

Serial batch leaching experiments were conducted to estimate the cumulative mobility of elements from the fly ash samples. In serial batch leaching, the limitation of fly ash particle solubility on leachate element concentration is prevented by periodic removal of the supernatant, followed by the addition of a fresh aliquot of the same leachant. Serial batch leaching experiments were performed by agitating 3 g of fly ash with 45 mL of DDI water in 50 mL centrifuge tubes. For each fly ash, duplicate leaching sets were prepared. After each 24-h leaching cycle, the leachate was separated from the fly ash by centrifugation, and 45 mL of fresh

DDI water was added for the next leaching cycle. The serial leaching procedure was repeated for a total of 35 days.

2.2.4.4. Column leaching experiments

One acidic fly ash sample (HA) and the basic fly ash (PD) sample were selected for the column leaching experiments. For each fly ash sample, a 40.6 cm long by 8.7 cm diameter Plexiglas column was packed with background soil (17.5 cm) at the bottom and fly ash (17.5 cm) at the top. Approximately 950 g of HA fly ash and 1125 g of PD fly ash were used for column packing. Similarly, 1400 g of background soil was used in each column. The background soil was prevented from leaving the bottom of the column by a fabric filter reinforced with a 1 mm Teflon screen which rested on a perforated stainless steel plate. The packed column was placed in an upright position with the top open to the air. A second fabric filter/Teflon screen assembly was used to separate the fly ash and background soil layers to prevent mixing of these materials in the column during leaching. The SAR was selected as the column leachant to mimic natural leaching in an ash disposal facility. Two 25-L carboys were used as SAR leachant reservoirs and a Gilson Minipuls 3 peristaltic pump was used to control fluid flow through the column. Before starting the top-to-bottom fluid flow, the pore volume (PV) of each column was measured by bottom-up saturation of the packed material with SAR. The volume of SAR required to saturate the column materials was recorded as the column PV. For column-HA and column-PD, PVs were determined as 750 cm^3 and 760 cm^3 with porosities of 36% and 37%, respectively. Effluent solutions from each column were collected at higher frequency in the early stages of the experiment. During each sampling event, the fluid flow rate was measured to calculate the total

effluent volume. The average flow rate (in cm^3/min) for column-HA and column-PD were calculated as 1.31 and 1.28, respectively.

2.2.5. Leachability of elements

The leachability of an element from each fly ash sample was calculated for both serial batch and column leaching experiment data sets. The cumulatively leached amount of an element was calculated for serial leaching experiments by Eq. (2.2) and for column leaching experiments by Eq. (2.3):

$$C_C = \frac{\sum (C_i \times V_i)}{S} \ldots (2.2)$$

$$C_C = \frac{\sum \left(\frac{C_{i-1} + C_i}{2} \times \frac{(FR)_{i-1} + (FR)_i}{2} \times \Delta T_i \right)}{S} \ldots (2.3)$$

where C_c is the cumulatively leached amount of an element (mg/kg), C_i is the concentration of an element in leachate collected at sampling event i (mg/L), V_i is the volume of an individual leachate sample (L) collected during serial leaching, S is the fly ash sample weight (kg), $(FR)_i$ and $(FR)_{i-1}$ are the flow rates (L/h) corresponding to sampling events i and i–1, respectively, and ΔT_i is the time between sampling events i and i–1 (h). For both serial and column leaching experiments, the % leached value was calculated for each element by Eq. (2.4):

$$\%\,\text{leached} = C_C / C_{env} \times 100 \ldots (2.4)$$

where C_{env} is the environmentally available concentration of an element as determined by partial acid digestion (mg/kg) (USEPA, 2007). This % leached value is similar to the relative solubility value calculated by Kim et al. (2003), but uses the environmentally available amount of the element, instead of the total concentration of the element in fly ash.

2.3. Results and discussion

2.3.1 Background soil

The background soil consisted of predominantly quartz (>99%) with trace amounts of chlorite, muscovite, and kaolinite. The soil pH was determined to be 7.11. The soil concentrations (in mg/kg) of As, Cr, B, and Mo were found to be 1.3, 3.0, 26, and 2.8, respectively. Trace element concentrations measured for this soil were within the ranges reported for background soils in Florida (Chen et al., 1999). Environmentally available concentrations (in mg/kg) of some other elements in the background soil sample were 26, 152, 1083, 292, 78, and 83, for B, Ca, Fe, Si, K, and Na, respectively.

2.3.2. Characterization of fly ash samples

2.3.2.1. Physical/mineralogical characterization

X-ray diffraction (XRD) analysis showed that quartz (SiO_2), mullite ($Al_6Si_2O_{13}$), and hematite/maghemite (Fe_2O_3) are present in different proportions in all fly ash samples. These minerals have been reported as common constituents in coal fly ash by several previous researchers (Gieré et al., 2003; Hower et al., 1999). Furthermore, amorphous materials such as Fe-Al-Si glass spherules and unburned carbon are also present in significant portions in fly ash (Külaots et al., 2004; Kutchko and Kim, 2006; Tishmack et al., 2004). The carbon contents of these fly ash samples, as determined by LOI, are 6.74%, 6.37%, 14.7%, and 3.66% for HA, HB, MA, and PD, respectively. Single point BET surface areas for HA, HB, MA, and PD are 3.18, 2.11, 3.46, and 4.43 m^2/g, respectively.

2.3.2.2. Trace elements in fly ash samples

Environmentally available major, minor, and trace element concentrations (in mg/kg) in the fly ash samples are presented in Table 2.1. Aluminum, Ca, Fe, and Si are present in significant amounts in all fly ash samples. The acidic fly ash samples have the highest K concentrations while the alkaline fly ash, PD, has a greater concentration of Na. Although PD fly ash is very rich in Ca, no Ca-rich mineral phase was identified. However, the high Ca content and alkaline pH indicate the presence of amorphous lime (CaO) in PD fly ash.

Table 2.1. Environmentally available elements in fly ash samples (mg/kg)

Elements	HA	HB	MA	PD	LOD[b]
Al	21,800	14,010	9,310	19,210	0.001
As	82	167	158	17	0.006
B	166	168	117	903	0.077
Ba	312	246	316	217	0.002
Ca	4,860	7,580	5,730	32,350	0.015
Co	19	17	13	4.6	0.004
Cr	50	52	30	18	0.002
Cu	73	79	63	23	0.001
Fe	19,590	18,310	12,110	16,140	0.003
K	3,160	1,690	1,570	638	0.077
Mg	1,890	1,300	1,130	5,060	0.001
Mn	74	45	71	62	0.001
Mo	13	20	12	5.4	0.001
Na	722	460	616	1910	0.009
Ni	37	38	34	7.5	0.003
Pb	27	28	24	12	0.005
Sb	3.7	3.5	2.7	1.5	0.007
Se	7.7	23	14	12	0.002
Si	7,290	2,180	3,880	3,110	0.015
Sr	287	557	317	538	0.001
Ti	713	634	615	579	0.010
V	103	121	90	56	0.019
Zn	67	89	103	69	0.001

[b]ICP-OES level of detection values in mg/L

Several trace elements such as As, B, Co, Cr, Cu, Mo, Ni, Pb, Se, Sr, Ti, V, and Zn are found in different concentrations in all fly ash samples (Table 2.1). Boron is highly enriched in PD fly ash. However, the concentrations of As, Co, Cr, Cu, Ni, and Pb are lower in PD than in the acidic fly ash samples. In fly ash, more than 50% of the total As, Se, and Zn are concentrated primarily in non-silicate constituents, while minor and major elements (except Ca) are typically associated with silicates (Kim and Kazonich, 2004). Therefore, the total concentrations of major (except Ca), minor, and some trace elements (As, Se, and Zn) in the fly ash samples could be greater than the amount extracted by the partial digestion method used in this study.

Although determination of solid phase trace element speciation was outside of the scope of this study, most of the As in fly ash has been reported to be present as $As_{(V)}$ (Huffman et al., 1994; Huggins et al., 2007; Shoji et al., 2002). However, in some fly ash samples, particularly those which were derived from high-sulfur bituminous coal, a minor amount of $As_{(III)}$ (10–15% of the total As) has also been reported (Huggins et al., 2007). Similarly, most of the Se in fly ash has been reported to exist as $Se_{(IV)}$ (Huggins et al., 2007). Shoji et al. (2002) found that speciation of Cr was coal specific: up to 30% of the total Cr in fly ash derived from western coal was $Cr_{(VI)}$, while almost 100% of the total Cr in fly ash derived from Eastern Bituminous coal was $Cr_{(III)}$.

2.3.2.3. Surface reactivity of fly ash

The surfaces of the fly ash particles are considered to be more chemically reactive than the interior of the particles (Linton et al., 1976). The surface reactivity of fly ash is qualitatively determined by measuring the pH of a water-fly ash mixture immediately after incremental additions of fly ash (initial pH) and again after some equilibration time (final pH). Fig. 2.1

illustrates the pH measured at different fly ash contents and equilibration times. For HB and MA fly ashes, the measured pH was not mass dependent. But for PD fly ash, higher pH values were measured with increasing fly ash content in the mixture. A similar trend was observed for HA fly ash up to 8 g/L of fly ash-water mixture.

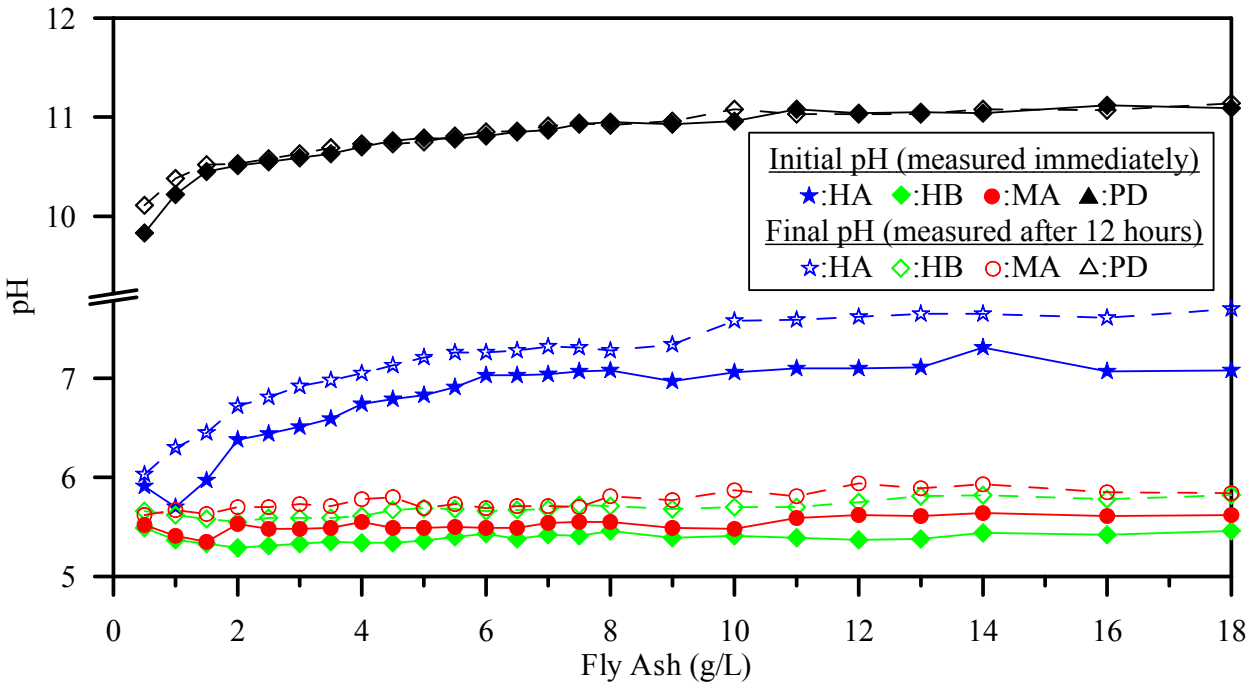

Fig. 2.1. The pH of water-ash slurries measured immediately (Initial pH) and 12 hours after (Final pH) the incremental addition of fly ash.

Measurement of the 'initial pH' and 'final pH' values for incremental additions of each fly ash indicated distinct trends for alkaline and acidic fly ash. Fig. 2.1 shows that the 'initial pH' was consistently more acidic than the 'final pH' for the acidic fly ash measurements, indicating a more acidic surface than the bulk mass of these fly ash particles. Furthermore, it was also found that the longer the reaction time (up to 10 weeks), the higher the pH (Section 2.3.4) of the acidic fly ash slurries. However, the surface and bulk particle contributions to pH are rather obfuscating

for PD fly ash. There was no difference between the 'initial pH' and 'final pH' for PD fly ash at concentrations ≥ 2 g/L, however at <2 g/L of ash, the 'initial pH' was slightly more acidic than the 'final pH' (Fig. 2.1). The decreasing pH values over time observed during long-term leaching of PD fly ash (section 2.3.4.) may indicate a more acidic bulk particle than the surface, or could reflect consumption of hydroxyl ion by precipitation of secondary minerals over time.

2.3.3. Results of jar leaching tests

Fig. 2.2 shows solution pH trends and concentrations of some trace elements released during jar leaching of the fly ash samples (see Fig. S2.1 for other element trends). Leachate pH slightly increased until 20 h and stabilized thereafter for HB, MA, and PD fly ash samples. However, the leachate pH for HA fly ash decreased slightly during the early stages of leaching, but increased to about 7 after 30 h. For all fly ash samples, As, Mo, Se and B showed initial increases in mobility with time. Leaching of Cr from HA and PD, of Se and Si from HA, HB, and MA of Ba, K, and Sr from PD, and of Al from HA also showed similar trends. Such increases in the concentrations of these elements with increasing contact time could be related to slow dissolution or diffusion from the particle interior. Some other elements, however, showed an opposite leaching trend, i.e., their leachate concentrations decreased with increasing contact time. For example, the mobilities of Cr and Al for HB and MA, of Sr for HA, of Ba for HA, HB, and MA, and of Mg, Se for PD decreased with time, potentially due to the co-precipitation of these elements in secondary minerals or adsorption on primary or secondary minerals in fly ash (Donahoe, 2004; Bhattacharyya, 2010). In general, the leaching of Ca, K (except from PD), and Na was constant over time for all fly ash samples.

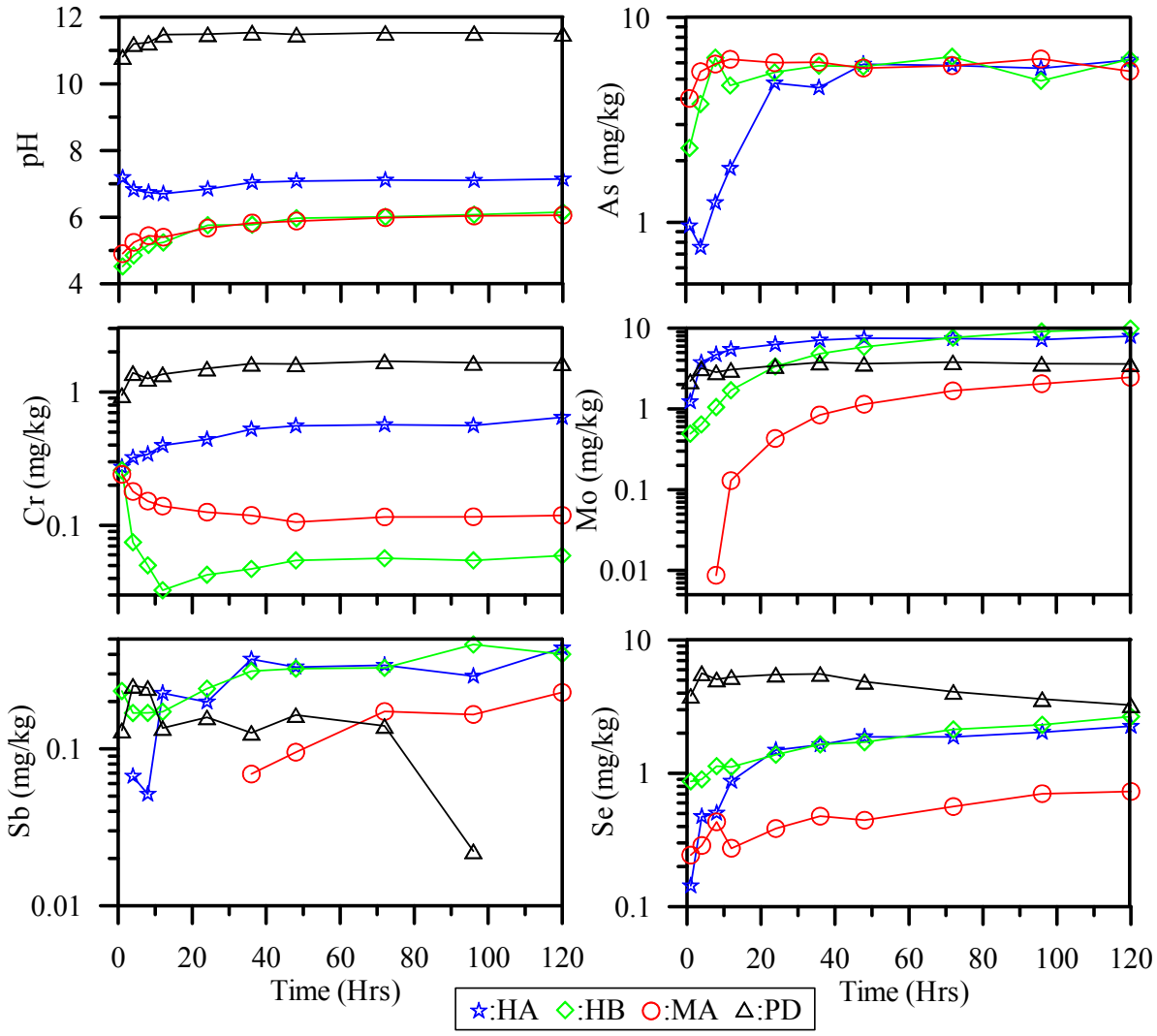

Fig. 2.2. Leachate pH trends and concentrations of some trace elements mobilized during fly ash jar leaching tests.

2.3.4. Results of long-term batch leaching experiments

2.3.4.1. Mobilization of oxyanion-forming trace elements

The leachate pH and concentrations of some oxyanion-forming trace elements mobilized during long-term batch leaching experiments are presented in Fig. 2.3. Acidic fly ash samples (HA, HB, and MA) showed increasing leachate pH until 10 weeks; pH became circum-neutral,

thereafter. However, the alkaline fly ash, PD, showed a gradual decrease in leachate pH during the entire length of these experiments.

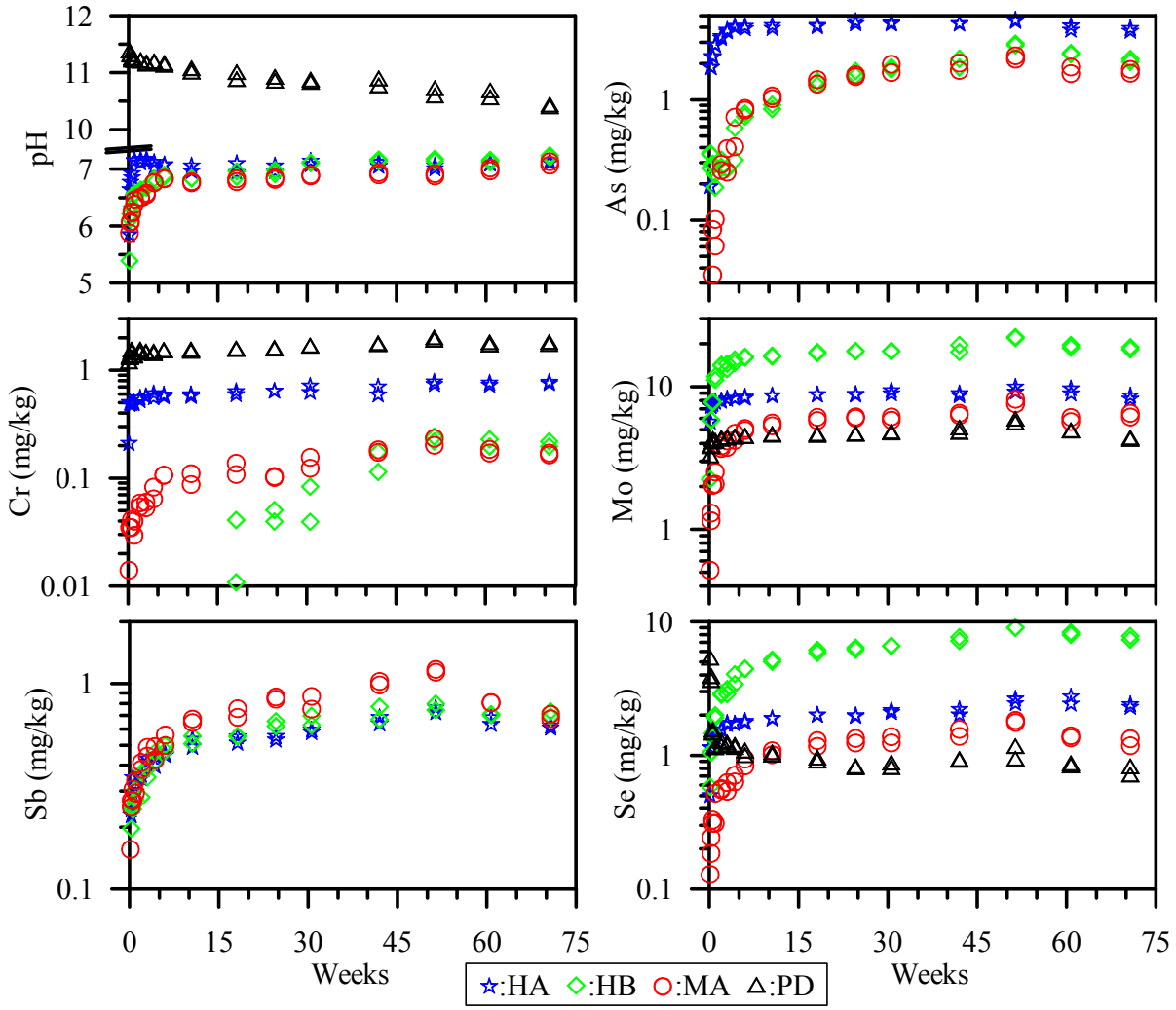

Fig. 2.3. Leachate pH trends and concentrations of some trace elements mobilized during fly ash long-term batch leaching experiments.

Mobilization of As, Cr, Mo, Sb, Se, and V from the acidic fly ash samples by DDI water increased with time (Figs. 2.3 and S2.2). Similar leaching trends were observed for Cr, Mo, and V for PD fly ash, although the mobility of Se decreased with time. PHREEQC modeling indicated that As, Cr, Mo, Sb, Se and V existed as oxyanions in all fly ash leachate solutions.

Oxyanion-forming trace elements have been reported to exist in different oxidation states in fly ash leachates. Some researchers (Jackson and Miller, 1998; Wagde and Hutton, 1987) reported that As and Se in fly ash leachate are mostly in the form of $As_{(V)}$ and $Se_{(IV)}$. Antimony in fly ash leachate was found to exist mostly as $Sb_{(III)}$ by Narukawa et al. (2005); however, Miravet et al. (2006) reported that most of the Sb in an acidic fly ash leachate was $Sb_{(V)}$, with only minor amounts of $Sb_{(III)}$. Both $V_{(V)}$ and $V_{(IV)}$ have been reported in fly ash leachates (Wang et al., 1995).

In coal fly ash, As, Cr, Mo, Sb, Se, and V can be present as surface enrichment, impurities in crystalline components, or as discrete accessory crystalline phases (Linton et al., 1976; Vassilev and Vassileva, 1997). Jankowski et al. (2006) reported a significant fraction of As was distributed in fly ash matrices. Aluminosilicate glass in fly ash is a less stable phase in the aqueous environment than mullite and quartz (Querol et al., 2002), and would slowly undergo dissolution during leaching experiments. The PHREEQC simulations also indicated that the fly ash leachates were undersaturated with respect to quartz, mullite, and amorphous silica. Therefore, the increasing leachate concentrations of As, Cr, Mo, Sb, and Se (except PD fly ash) with time likely resulted from the slow dissolution of fly ash particles. Furthermore, the undersaturated condition of the leachate solutions with respect to a V-bearing phase, CaV_2O_6, found in fly ash samples (Groen and Craig, 1994) could also slowly release V over time. However, the potential cause of the observed decreasing concentrations of Se in PD fly ash leachate with time is interesting to consider because it is counter-intuitive to expect decreasing temporal mobilization of oxyanion species such as $Se_{(IV)}$ or $Se_{(VI)}$ from an alkaline fly ash (pH > 10.5) (Iwashita et al., 2005). No oversaturated Se-bearing phases were found during PHREEQC modeling of PD fly ash leachates. Although adsorption of Se on potential secondary minerals

could be possible, Bhattacharyya (2010) showed very limited sorption of Se on fresh PD fly ash. Another potential cause of decreased Se concentrations in PD fly ash leachate with time could be co-precipitation with secondary minerals. Nonetheless, PD fly ash leachate solutions as well as all acidic fly ash leachate solutions were undersaturated with the most commonly cited secondary mineral for Se sequestration, ettringite (Hassett et al., 2005; Iwashita et al., 2005; Jankowski et al., 2006).

3.4.2. Mobilization of major, minor, and cation-forming trace elements

The concentrations of some major, minor, and cation-forming trace elements mobilized during long-term batch leaching of fly ash samples are presented in supplementary material (Fig. S2.2). Concentrations of Al in HA and HB fly ash leachates increased during the first 5 weeks of leaching, but decreased or remained constant thereafter. Concentrations of Al in MA fly ash leachates showed a decreasing trend from the beginning. The early increase in Al concentrations in HA and HB leachates could be associated with dissolution of Al-rich micro-particles; however, the decreasing leachate concentrations of Al would indicate the onset of precipitation of oversaturated Al-bearing secondary minerals such as diaspore, gibbsite, bohemite, and kaolinite. Nearly constant leachate concentrations of Al for all acidic fly ash samples after 25 weeks would indicate a steady-state dissolution of mineral/glass phases in fly ash along with the precipitation of oversaturated secondary Al-minerals. The concentrations of other major elements such as Ca, K, Mg, and Na remained approximately constant throughout the 70 week leaching experiments (Fig. S2.2). The acidic fly ash leachates were undersaturated with respect to calcite, gypsum, lime, and portlandite. Similarly, fly ash leachates were also undersaturated with respect to some potential secondary minerals containing Ca, K, Mg, and Na, such as

arcanite, aphthitalite, brucite, dawsonite, dolomite, epsomite, and thenardite throughout the experiments. However, the acidic fly ash leachates were oversaturated with respect to some other secondary minerals such as alunite, beidellites, gismondine, mesolite, montmorillonites, and scolecite. Boron, which had concentrations almost an order of magnitude lower in acidic fly ash leachates than in PD fly ash leachate, also showed constant concentrations over time. The PHREEQC simulations indicated that all fly ash leachates are undersaturated with respect to boric acid. Several previous studies (e.g., Jankowski et al., 2006) showed B to be a very labile element in fly ash because of its surface enrichment on the smallest fly ash particles. The persistent increase in Si concentrations in acidic fly ash leachates indicates a continuous dissolution of aluminosilicate glass phases in fly ash samples. Although leachate solutions were supersaturated with respect to some silicate minerals such as beidellite, gismondine, kaolinite, mesolite, and scolecite and these minerals could potentially precipitate, it appears that the concentration of Si in the acidic fly ash leachates was primarily controlled by dissolution of amorphous silica glass particles.

Cationic trace elements leached from acidic fly ash samples showed mixed temporal mobility trends. Mobilization of Ba, Co, Mn, Ni, and Zn from HB and MA fly ash samples decreased with time. The PHREEQC simulations indicated that the HB and MA fly ash leachates were oversaturated with respect to barite, birnessite, and manganite, potentially transferring Ba and Mn from solution to solid phases. Contrary to the mobilization trend for Ba from HB and MA fly ashes, its mobilization from HA fly ash increased over time, and the PHREEQC simulations showed that the HA fly ash leachates were essentially at equilibrium with barite and undersaturated with respect to other Ba-bearing phases such as witherite, alstonite, and barytocalcite. Although HA fly ash has a relatively higher environmentally available

concentration of Mn, its leachate Mn concentrations are much lower than those measured in HB and MA fly ash leachates. The concentrations of Mn in HA fly ash leachate decreased until the 7^{th} week and then gradually increased over time. The early decrease in Mn concentration in HA leachate could be caused by the precipitation of birnessite or manganite; however, the subsequent low but consistent Mn concentration increase in HA fly ash leachate could potentially indicate a slow, persistent release of aluminosilicate glass-bound Mn by dissolution. Because HB and MA leachates were undersaturated with respect to all potential secondary minerals containing Co (e.g., bieberite, sphaerocobaltite), Ni (e.g., morenosite, nickel carbonate), and Zn (e.g., hydrated zinc sulfates, hydrozincite, smithsonite), the leaching of these elements from HB and MA fly ash samples may have been controlled by sorption on primary minerals such as hematite/maghemite or on secondary minerals. Similarly, the observed slightly increasing concentrations of Sr in HA and HB fly ash leachates with time could also be linked to the slow release of Sr from the dissolution of glassy fly ash particles; however, the consistently decreasing concentrations of Sr observed in MA fly ash leachates would require transfer of Sr from solution to the solid phase. Because MA fly ash leachates were undersaturated with respect to celestite and strontianite, it is likely that the primary or secondary minerals in MA fly ash fly ash would have sorbed aqueous Sr from leachate solutions over time. Bhattacharyya (2010) reported that both HB and MA fly ash samples have some sorption capacities for Ni and Sr.

The alkaline fly ash PD showed a gradual decrease in leachate concentrations of Al, Ba, and Ca with time (Fig. S2.2). These elements had relatively high concentrations in early leachates and would have been mobilized from the surface-bound highly soluble fly ash particles such as lime, anhydrite, and glass of varying composition (Groen and Craig, 1994). The PHREEQC simulations indicated that the PD fly ash leachates were undersaturated with respect

to lime, anhydrite, and gypsum, but were oversaturated with respect to Al-, Ba-, and Ca-bearing secondary minerals such as gismondine, witherite, alstonite, barytocalcite, mesolite, calcite, scolecite, boehmite, diaspore, gibbsite, dawsonite, and kaolinite. Therefore, it is likely that precipitation of secondary minerals was responsible for the observed decreasing concentrations of Al, Ba, and Ca in the PD fly ash leachates over time. Furthermore, these potential secondary minerals could have also sequestered trace elements such as Se through co-precipitation and resulted in its decreased leachate concentrations over time.

The PD fly ash leachate concentrations of some other elements such as K, Mg, and Na increased with time. Potential secondary minerals such as arcanite, brucite, and thenardite were undersaturated in PD fly ash leachates. Concentrations of Si and Sr in PD leachates increased initially, but then decreased gradually after 10 weeks. The observed early increase in leachate concentrations of Sr could be related to release from soluble fractions of fly ash, such as fine particles, and the later decrease in its concentration could be related to either adsorption/co-precipitation on/with other phases or to precipitation of an oversaturated secondary mineral such as strontianite. The likely sources of Si in PD fly ash leachate are amorphous silica or other silicate phases. The PD fly ash leachates over time were undersaturated with respect to amorphous silica but oversaturated with respect to some secondary silicate minerals such as gismondine, kaolinite, and dawsonite. Precipitation of these secondary silicate minerals would have resulted in the observed slow decrease in Si concentrations over time in PD fly ash leachates.

Despite PHREEQC modeling predictions of the potential precipitation of several secondary minerals, and the strong indication of such precipitation shown by decreasing concentrations of some elements in the fly ash leachates over time, no new minerals were

identified by XRD analysis of reacted fly ash samples at the end of 70 weeks of leaching. However, it is not unusual for XRD to not detect likely secondary minerals if they either precipitated in small amounts (<2% of the bulk sample) or as amorphous phases (Donahoe, 2004).

3.4.3. Correlation and principal component analyses

In all acidic fly ash leachates, As, Cr, Mo, Sb, Se, and V show significant positive correlations with pH and with each other (Table S2.2 through S2.4), and have dominant positive PC1 (except for Cr and Sb concentrations in HB fly ash leachates where variance is explained largely by PC2) (Fig. 2.4a-c and Table S2.6-S2.8). These elements show significant positive correlation with Si in acidic fly ash leachates. In general, these anion-forming elements and Si are closely distributed on PC1 vs. PC2 plots (Fig. 2.4), and their mobilization from acidic fly ash samples could have been primarily controlled by continuous dissolution of fly ash glass particles. Elements such as Al, Ba, Co, Mn, Ni, Sr, and Zn leached from HB and MA fly ashes show significant negative correlation with pH and significant positive correlations with each other. However, the pH of HA fly ash leachates does not significantly correlate with Al and Ba, and has a significant negative correlation with Mn. Elements such as Ba, Co, Mn, Ni, Sr, and Zn are aligned together on the PC1 vs. PC2 plot for MA fly ash leachates (Fig. 2.4c) with dominant negative loading of PC1, but these elements show a relatively greater spread on the PC1 vs. PC2 plot of HB fly ash leachates (Fig. 2.4b). For HB fly ash leachates, Ba concentration variance is explained by PC1, Mn is associated with negative PC2, Co and Ni have dominant positive PC3, Sr has a large negative PC3, and Zn has a dominant PC4 (Table S2.7). Considering the correlations and PC distributions, the temporal mobilizations of Ba, Co, Mn, Ni, Sr, and Zn from

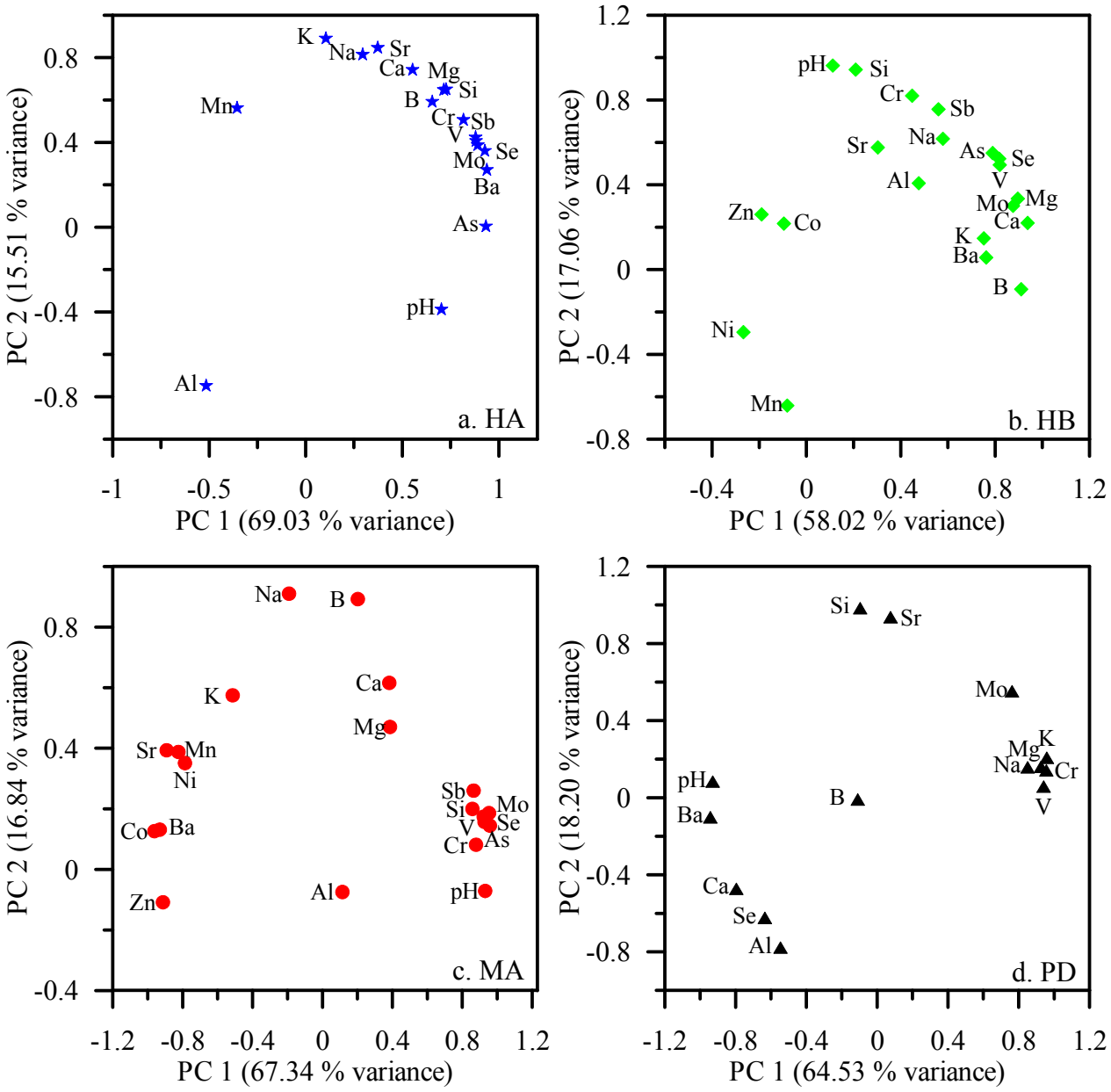

Fig. 2.4. Principal component PC1 vs. PC2 plots for fly ash leachate solutions.

MA fly ash are inferred to have been primarily controlled by early rapid dissolution of finer/soluble fly ash fractions and subsequent congruent precipitation/adsorption of/on secondary phases. However, incongruent precipitation/adsorption phenomena are inferred to have controlled the temporal mobilizations of Ba, Co, Mn, Ni and Zn from HB fly ash. Because the

release of Sr from HB fly ash was constant through time, its mobilization is likely to have been equilibrium-controlled. Aluminum leached from HA fly ash shows significant negative correlation with all other elements (except As and Mo) (Table S2.2). For HA and MA fly ash samples, Al is completely isolated on PC1 vs. PC2 plots (Figs. 2.4a and 2.4c). Aluminum concentration variance is largely explained by a negative PC2 value in HA fly ash leachates, but primarily by PC4 and PC3 in HB and MA fly ash leachates. The mobilization of Ba from HA fly ash is more associated with anion-forming trace elements (As, Cr, Mo, Sb, Se, and V) with dominant participation in PC1, while mobilization of Mn shows a close association with Ca, K, Na, and Sr with dominant participation in PC2. Furthermore, B, Mg, and Si mobilized from HA fly ash are explained by both PC1 and PC2 and have significant correlations with anion-forming elements, as well as with Ca, K, Na, and Sr. The mobilizations of Ca, K, Na, and Sr from HA fly ash are likely controlled by the initial dissolution of soluble particles, and their concentrations remained almost constant over time. However, the mobilizations of B and Mg from HA fly ash are controlled by the persistent slow dissolution of glassy fly ash particles after an initial rapid release into the leachate solution. For HB fly ash leachates, B, Ca, K, and Mg concentrations are largely explained by PC1, while Na has significant PC1 and PC2 loadings (Table S2.7). For MA fly ash leachates, B and Na have large PC2 loadings, Ca and Mg concentrations are associated with PC3, and K has significant loading in PC1, PC2 (dominant), and PC3 (Table S2.8). The mobilizations of B, K, and Na from Ma fly ash and of B, Ca, K, and Mg from HB fly ash were mostly constant through time after their initial rapid release into the leachate solutions. Calcium and Mg in MA fly ash and Na in HB fly ash showed increasing mobilities, likely as the result of slow dissolution of fly ash particles with time.

Chromium, K, Mg, Mo, Na, and V released from PD fly ash show significant positive correlations with each other, and are grouped together on a PC1 vs. PC2 plot with a large PC1 loading (Fig. 2.4d). These elements all show significant negative correlations with pH. The leaching of these elements was primarily controlled by the slow dissolution of fly ash particles with time. The PD fly ash leachate Ba, Ca, and Se concentrations are primarily explained by PC1 (negative values), while B is uniquely loaded with PC3 and Al has a slightly greater association with PC2 (Fig. 2.4d and Table S2.9). Leachate concentrations of Al, Ba, and Ca are positively correlated with pH. Unlike the other oxyanion-forming trace elements, Se shows a close association with Ca and Al during PD fly ash leaching. The mobilizations of Al, Ba, Ca, and Se were controlled by rapid dissolution of small particles at the initial stages of leaching, but their long-term mobilization was limited by their precipitation/co-precipitation in secondary minerals. Silicon and Sr mobilized from PD fly ash show strong positive correlation with each other (Table S2.5) and are clustered together on the PC1 vs. PC2 plot with their variance explained by PC2 (Fig. 2.4d and Table S2.9). Mobilization of Si and Sr was initially dominated by dissolution of PD fly ash particles, but switched to being precipitation-dominated with time.

3.5. Results of serial batch leaching experiments

Fig. 2.5 shows variations in the concentrations of some trace elements and pH during serial batch leaching of the fly ash samples (for all other elements, see Fig. S2.3). The initial high pH of PD fly ash leachate decreased by more than a unit within 10 days, with a slower decrease

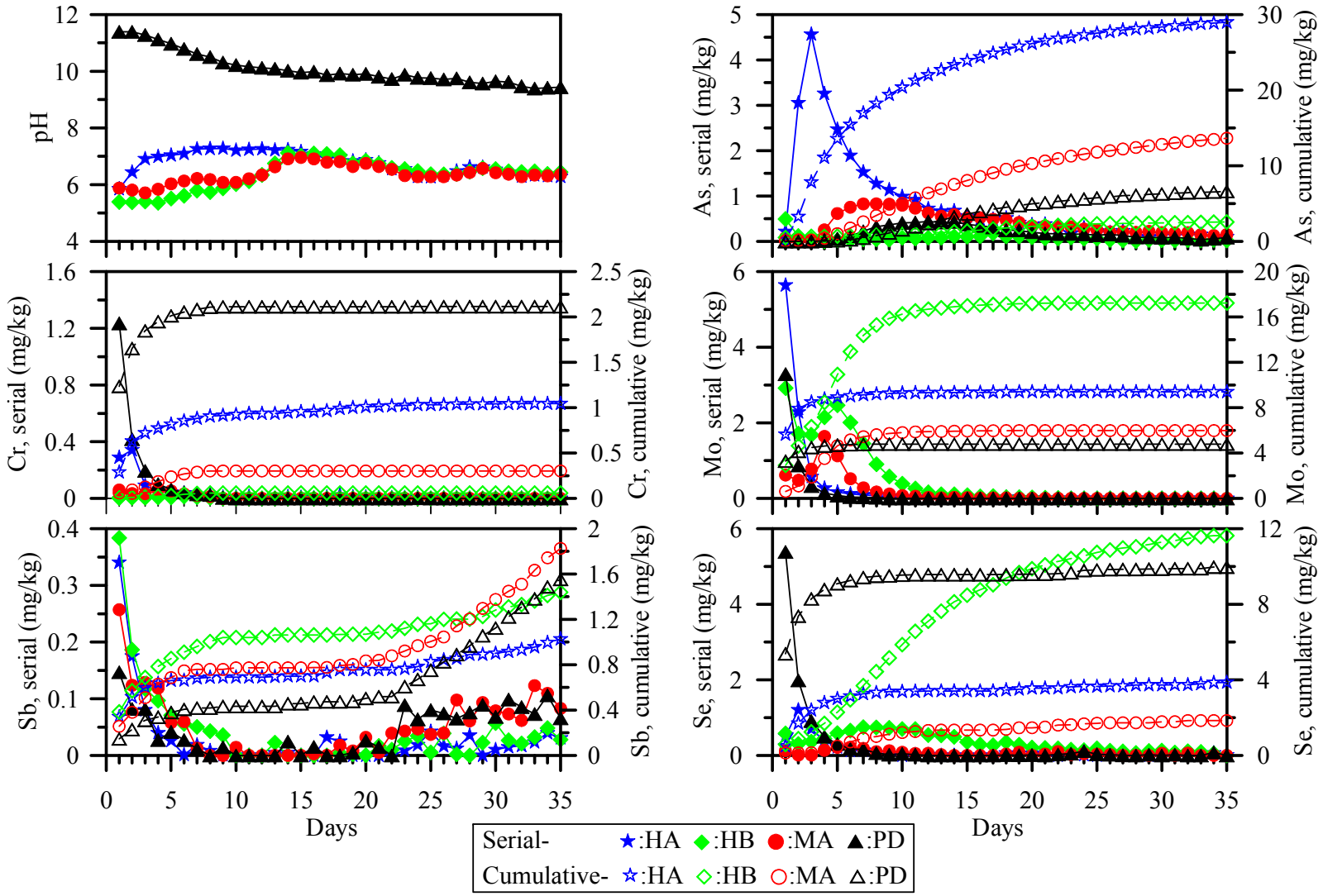

Fig. 2.5. Leachate pH trends and the serial and cumulative concentrations of some trace elements mobilized during fly ash serial batch leaching experiments.

thereafter to a pH of about 9.4 by the end of the 35 day leaching period. HA fly ash leachate increased rapidly in pH over the first 3 leaching cycles, hovered about 7 for the next 3 weeks, and then decreased to about 6.3 during the last 10 days of leaching. HB and MA fly ash leachates gradually increased in pH to approximately 7 during the first 2 weeks of leaching, and then gradually decreased to about 6.4 during the last 10 days.

For all fly ash samples, the initially high concentrations of Ca in the leachates decreased exponentially in subsequent leaching cycles (Fig. S2.3). Most of the Ca leached from the acidic fly ash samples was removed during the first four leaching cycles. Cumulatively, PD fly ash released almost five times more Ca than the acidic fly ash samples. Most of the other elements with dominant cationic aqueous species and B showed similar leaching patterns, with high initial leachate concentrations, followed by rapid decrease in concentrations after a few early leaching cycles. However, mobilization of Al from HA fly ash and of Mg from PD fly ash increased with time during the early leaching cycles and then remained nearly constant for the remainder of the experiments.

Mobilizations of Ba from HB and MA, of Se from HB, and of Mo from HB and MA fly ash samples increased with time during the early leaching cycles, and then decreased over the rest of the leaching period. Antimony showed large initial mobilization which then tailed off within 10 leaching cycles, but after 20 days, its mobilization again increased for all fly ash samples (Fig. 2.5). During serial leaching of HA fly ash, concentrations of As peaked in the 3rd leaching cycle and gradually decreased thereafter. In contrast, several additional leaching cycles were required for the other fly ash samples to reach peak leachate As concentrations. For MA, PD, and HB fly ashes, the peak arsenic leaching event occurred at the 7th, 12th, and 17th leaching cycles, respectively. Although HB and MA fly ashes have higher environmentally available As

contents, HA fly ash released the most cumulative As during the serial batch leaching experiments, followed by MA, PD, and HB.

The early high mobilization of most of the fly ash elements could have resulted from the dissolution of soluble surface-bound particles, while the low but persistent leaching (e.g., leaching of As from HA), the onset of relatively higher mobilization after a few initial leaching cycles (e.g., leaching of V from HB and MA), or the reemergence of increasing mobilization after tailing off of initial high mobilization (e.g., leaching of Sb from all fly ash samples) could be related to the slow dissolution of glassy fly ash particles or diffusion of these elements from the interior of particles into the leaching solution.

2.3.6. Results of column leaching experiments

Fig. 2.6 shows effluent solution pH and some trace element concentrations for HA and PD column experiments (see Fig. S2.4 for other element plots). For both HA and PD fly ash columns, pH increased rapidly at the beginning of the experiments. Equilibrium pH was attained after the circulation of about 7 PVs and 16 PVs of SAR for column-HA and column-PD, respectively. Thereafter, effluent pH was nearly constant at ~7 for HA fly ash. But for column-PD, effluent pH showed a decreasing trend after the circulation 42 PVs of SAR and increased to 10.2 by the end of the column leaching experiment.

Elemental leaching behavior during the column experiments can be broadly grouped into two categories: unimodal and bimodal leaching (Fig. 2.6). Most of the elements existing as cationic aqueous species and a few elements present as anionic aqueous species (i.e., Mo for both fly ashes and Cr and Sb for HA fly ash) showed a unimodal leaching pattern; however, the peak leaching of these elements may have occurred at different time points. Boron, Ca, K, Mg, Mn,

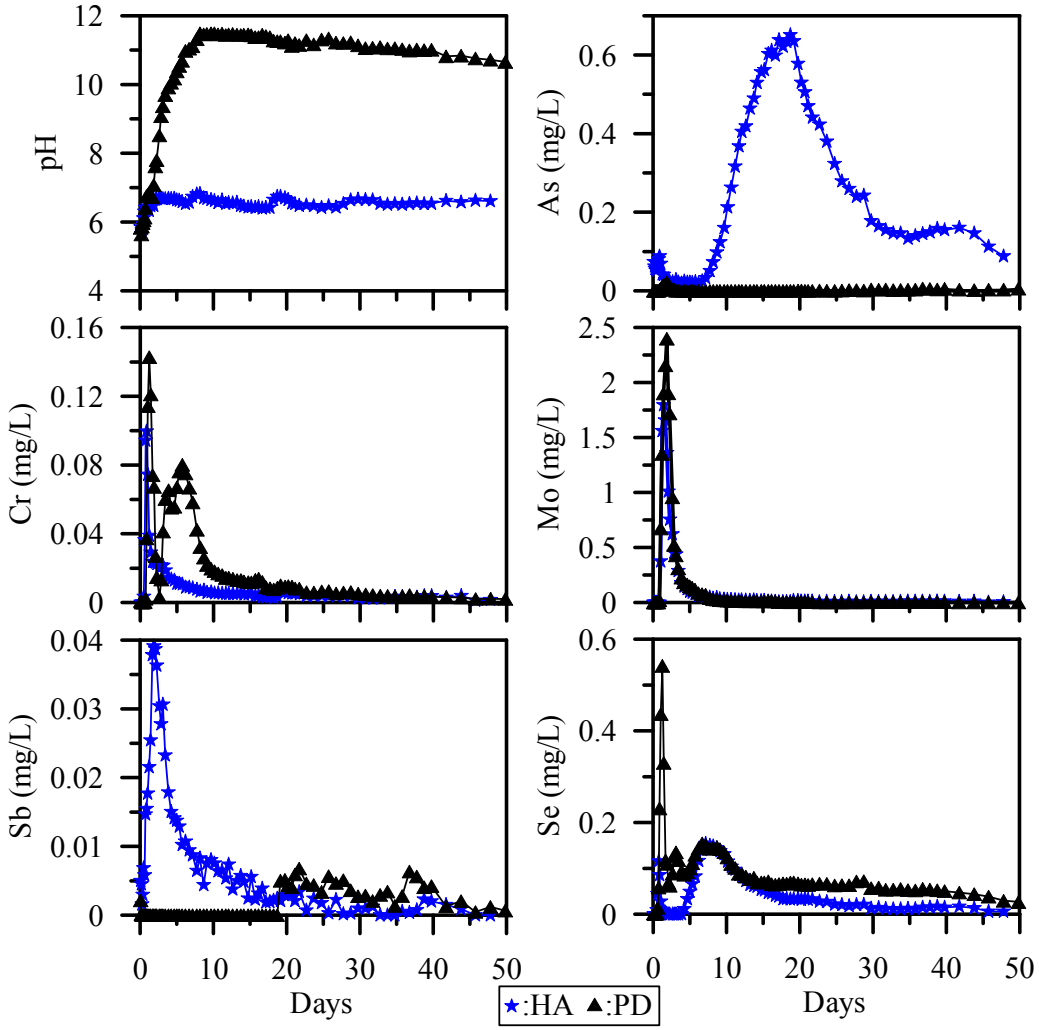

Fig. 2.6. Effluent pH trends and concentrations of some trace elements mobilized during HA and PD fly ash column leaching experiments.

Mo, and Na showed very early (PV ~1.2 to 2.4) peak leaching from HA and PD fly ashes, then rapidly (1–2 PV after the peak leaching event) decreased in concentration and tailed off. In general, the peak leaching of most of these elements was slightly slower for PD fly ash compared to HA fly ash. This rapid and short leaching behavior represents the soluble surface-enriched fraction of these elements. Warren and Dudas (1984) reported the presence of submicron-sized lime (CaO) fragments on the surface of fly ash particles, potentially derived from the

decarbonation of limestone and/or dolomite impurities in the feed coal. Although Warren and Dudas also found the external surfaces of glassy fly ash particles to be enriched in Al, Fe, and Mg (Warren and Dudas, 1984), Al was not leached significantly from HA fly ash. However, Al was released from PD fly ash with a large peak at about 10 PV and subsequently showed continued, but decreasing leaching over time during the column leaching experiment (Fig. S2.4). However, Fe was not detected in HA and PD fly ash column effluents.

Arsenic concentrations in column-HA effluents; Ba, Cr, K, Sb, and Sr concentrations in column-PD effluents; and Se, Si, and V concentrations in both column experiments showed a bimodal leaching pattern (Fig. 2.6 and Fig. S2.4). However, the relative sizes and timing of the leaching peaks for the different elements were not necessarily similar. In general, the first leaching peaks for these elements mostly coincided with the peaks of the elements having a unimodal leaching pattern, and are probably also associated with the removal of loosely-bound elements from the fly ash particle surfaces. The second leaching peak for these elements was relatively broader and lower in concentration than the first peak. Some elements (e.g., As and Zn for HA fly ash; Ba, Se, and Sr for PD fly ash; and Si and V for both fly ash samples) showed lower but steady leaching after the second peak, possibly due to the dissolution of glass or other soluble minerals in the fly ash or due to diffusion of these elements from the interiors of fly ash particles. Some elements with unimodal leaching patterns, such as Al and Ca in PD fly ash, also showed this protracted concentration tailing (Fig. S2.4).

2.3.7. Leachability of elements in fly ash

The leachabilities of the different elements calculated using Eqn. (2.4) as the percentage of the total environmentally available fly ash concentration mobilized during serial batch and

column leaching experiments are presented in Table 2.2. In general, leachability varied with the element, fly ash sample, and leaching method. Iyer (2002) reported that the surface area of the ash particles, as well as the combustion system, desulfurization process, and fly ash collection techniques used, could affect the water leachability of trace elements from coal fly ash. Particularly, it has been observed that greater proportions of the oxyanion-forming trace elements tend to leach from alkaline fly ash samples because of the higher solubility of these elements at elevated pH (Jankowski et al., 2006). In this study, the leaching method utilized has also been shown to play a significant role in determining the leachability of elements from coal fly ash. Despite being a relatively aggressive leaching solution, SAR resulted in significantly lower calculated leachabilities for most elements during column leaching than for DDI water (less aggressive) during serial batch leaching tests. The constant agitation and longer leachant-ash particle contact times during serial batch leaching resulted in the significantly higher mobilities of elements.

The distribution of trace elements between different fly ash fractions could also play an important role in the leaching of trace elements. An attempt was made to compare the leachabilities of some trace elements such as As, Cr, Mo, Sb and Se with the results of sequential chemical extractions performed on these fly ash samples in a previous study (Bhattacharyya, 2010). Element distributions in these fly ash samples were previously studied by Bhattacharyya (2010) using a 7-step sequential chemical extraction procedure. The sequential chemical extraction procedure uses increasingly more aggressive extractant solutions to separate elements associated with different fly ash fractions: (1) water soluble, (2) exchangeable, 3) carbonate bound, (4) easily reducible (bound to Mn oxides), (5) moderately reducible (bound to amorphous Fe/Al oxides), (6) poorly reducible (bound to crystalline Fe/Al oxides), (7) oxidizable (bound to

organics/sulfides). Elements associated with the first three fractions are considered to be mobile, while the easily reducible through the poorly reducible fractions are increasingly stable in oxidizing environments, but become unstable under reducing conditions. The oxidizable and sulfide fraction is considered to be stable in reducing environments.

Table 2.2. Leachability of elements determined from results of serial and column leaching tests

Elements	Cumulatively Leached (mg/kg)							% Leached						
	Serial					Column		Serial					Column	
	HA	HB	MA	PD		HA	PD	HA	HB	MA	PD		HA	PD
Al	186	25	14	2,360		2.5	1,280	0.9	0.2	0.1	12.3		0.01	6.6
As	29	2.6	14	6.6		23	1.3	35.5	1.5	8.6	39.0		28.3	7.6
B	28	44	38	642		19	602	16.8	25.9	32.8	71.1		9.5	66.8
Ba	3.3	136	11	127		0.4	38	1.1	55.3	3.4	58.5		0.1	17.4
Ca	1,710	2,640	2,830	10,100		948	6,980	35.2	34.8	49.4	31.2		19.5	21.6
Co	0.2	1.0	0.9	0.0		0.0	0.0	0.8	5.7	6.7	0.0		0.0	0.0
Cr	1.0	0.1	0.3	2.1		0.6	1.3	2.1	0.1	1.0	11.9		1.2	7.1
K	263	348	223	60		104	42	8.3	20.6	14.2	9.4		3.3	6.6
Mg	133	169	234	574		71	6.2	7.0	13.0	20.7	11.3		3.8	0.1
Mn	1.8	5.0	6.5	0.0		0.1	0.1	2.4	11.2	9.1	0.0		0.1	0.1
Mo	9.4	17	6.0	4.8		6.0	4.7	74.3	86.5	49.8	88.9		46.5	86.6
Na	232	212	324	557		132	463	32.1	46.1	52.6	29.2		18.3	24.2
Ni	0.5	3.0	3.5	0.2		0.0	0.1	1.4	8.0	10.2	2.5		0.1	1.0
Sb	1.0	1.4	1.8	1.5		0.4	0.2	28.1	41.0	67.2	100.0		11.8	15.2
Se	3.9	11.6	1.8	10.0		3.2	7.5	50.2	50.6	13.2	83.1		41.6	62.7
Si	307	207	256	1,420		149	267	4.2	9.5	6.6	45.6		2.0	8.6
Sr	24	123	85	344		1.4	306	8.4	22.1	26.7	63.9		0.5	57.0
V	2.3	9.1	18	0.0		6.5	13	2.2	7.5	20.4	0.0		6.3	23.4
Zn	0.9	13	7.1	1.0		10	1.7	1.3	14.3	6.9	1.5		15.5	2.4

2.3.7.1 Arsenic

Nearly 36% and 39% of the environmentally available As was leached from HA and PD fly ash samples, respectively, during 35 cycles of serial batch leaching (Table 2.2). Similarly, 28% of the environmentally available As was leached from HA fly ash during column leaching. However, only a small fraction of the available As was leached from HB (1.5%) and MA (8.6%)

fly ash samples during serial batch leaching tests and from PD fly ash (7.6%) during the column leaching experiment. The higher leachability of As for HA and PD fly ash samples could be related to the presence of relatively larger fractions (15% and 22% for HA and PD fly ashes, respectively) of water soluble and/or exchangeable As in these fly ash samples (Bhattacharyya, 2010). On the other hand, HB and MA fly ashes have relatively low amounts (5–7%) of water soluble or exchangeable As. However, as noted above, the low mobilization of As from PD fly ash during the column leaching experiment could also have been related to the lack of agitation and short residence time of the leachant in column-PD. For all fly ash samples, only a very small fraction (2–4%) of the environmentally available As was acid soluble, while more than a quarter of the As in all of the acidic fly ash samples and about 8% of the As in PD fly ash were extracted as easily reducible. In contrast, more than 50% of the As in all of the fly ash samples was associated with moderately reducible amorphous iron/aluminum oxides, and the remaining As was either associated with crystalline Fe oxides or bound to organics/sulfides (Bhattacharyya, 2010). Because the moderately/poorly reducible and oxidizable fractions of As are effectively immobile for the leaching tests utilized in this study, a portion of the As associated with the acid soluble or easily reducible fractions was also leached from HA fly ash during serial batch and column leaching experiments and from PD fly ash during serial batch leaching.

2.3.7.2 Chromium

Unlike other oxyanion-forming trace elements, the mobilization of environmentally available Cr from the acidic fly ash samples was very low (≤2%) during both serial batch and column leaching experiments (Table 2.2). About 12% and 7% of the environmentally available Cr were leached from PD fly ash during serial batch and column leaching experiments,

respectively. Most (35–54%) of the Cr in the acidic fly ash samples is associated with the relatively immobile crystalline iron/aluminum oxide fraction (Bhattacharyya, 2010). Other researchers (Jegadeesan et al., 2008; Kim and Kazonich, 2004) have previously reported silicate-associated Cr in fly ash. Only 2–7% of the environmentally available Cr was reported by Bhattacharyya (2010) to be associated with the water soluble or exchangeable fractions of these acidic fly ash samples. Jegadeesan et al. (2008) also showed a very small fraction of Cr as being water soluble or exchangeable in Class F fly ash. More than 21% of the environmentally available Cr was reported to be water soluble or exchangeable in PD fly ash (Bhattacharyya, 2010); hence a relatively larger leachability of Cr from PD fly ash was calculated for the serial batch and column leaching experiments. Furthermore, the relatively higher leachability of Cr from PD fly ash compared to the acidic fly ash samples could be related to the high leachate pH and resulting dominance of the mobile $Cr_{(VI)}$ species (Shoji et al., 2002). However, the acidic fly ash leachate solutions with the less-mobile $Cr_{(III)}$ species (Shoji et al., 2002) and low pH resulted in only minor (0.1–2.1%) leaching of Cr during serial batch and column leaching experiments.

2.3.7.3 Molybdenum

All of the fly ash samples showed large Mo mobilities during both serial batch and column leaching experiments. About 74% (HA), 86% (HB), 50% (MA), and 89% (PD) of the environmentally available Mo were leached during serial batch leaching, while about 47% (HA) and 87% (PD) of the environmentally available Mo were leached during column leaching experiments (Table 2.2). The high leachability of Mo from all of the fly ash samples studied was related to the presence of large amounts of water soluble and/or exchangeable Mo in all fly ash samples (Bhattacharyya, 2010). Large proportions of the Mo in HA, HB, and PD fly ash samples

are associated with the water soluble (nearly 80%) or exchangeable (10–20%) fractions, while 25% and 49% of the Mo in MA fly ash was associated with the water soluble and exchangeable fractions, respectively (Bhattacharyya, 2010). The presence of such large mobile (i.e., water soluble and exchangeable) fractions of Mo indicates a significant enrichment of Mo on fly ash particle surfaces. The relatively lower leachability of Mo from MA fly ash could be related to the significant amount (21%) of immobile (bound to crystalline Fe/Al oxides) Mo in this sample (Bhattacharyya, 2010).

2.3.7.4 Antimony

Significant proportions of the environmentally available Sb were leached from all fly ash samples during serial batch and column leaching tests. During the serial batch leaching experiments, 28%, 41%, 67%, and 100% of the environmentally available Sb were leached from HA, HB, MA, and PD fly ash samples, respectively (Table 2.2). However, only about 12% and 15% of the environmentally available Sb were leached from HA and PD fly ash samples, respectively, during column leaching experiments. In contrast, only 10–13% of the available Sb in the acidic fly ash samples and 47% of the Sb in PD fly ash was water soluble (Bhattacharyya, 2010). Because only an insignificant amount of Sb was extracted as exchangeable and acid soluble in all fly ash samples, the easily reducible fraction of Sb was also leached during serial batch leaching experiments. While most of the water soluble Sb was removed from HA fly ash, only a minor amount of the water soluble Sb in PD fly ash was removed during column leaching experiments.

2.3.7.5 Selenium

Similar to the mobilization of Mo and Sb, significant fractions of the environmentally available Se was mobilized from HA, HB, and PD fly ash samples. More than 50% of the environmentally available Se was leached from HB and HA fly ash samples, while 83% of the environmentally available Se in PD fly ash was leached during the serial batch leaching tests (Table 2.2). However, only 13% of the environmentally available Se was mobilized from MA fly ash by serial batch leaching. Similarly, column leaching tests removed nearly 42% and 63% of the environmentally available Se from HA and PD fly ash samples, respectively. Because only 13%, 34%, 7%, and 28%, respectively, of the available Se in HA, HB, MA, and PD fly ash samples were reportedly present in the water soluble fraction (Bhattacharyya, 2010), significant fractions of Se associated with the reducible fly ash fractions were also mobilized during the serial batch and column leaching experiments. Except for serial batch leaching of PD fly ash, the leachate concentrations of Se varied with progression of the serial batch and column leaching experiments. The use of successive leaching cycles and continual circulation of fresh SAR during the serial and column leaching experiments, respectively, could have mobilized the otherwise relatively immobile Se fractions from these fly ash samples, and resulted in an overall greater mobility. The greater leachability of Se from the PD fly ash sample is consistent with the leaching behavior of Se from alkaline fly ash samples reported elsewhere (e.g., Jankowski et al., 2006).

2.3.7.6 Other elements

Some major elements such as Ca, K, Na, and Mg were leached in different proportions during serial batch and column leaching experiments. Mattigod et al. (1990) also reported significant fractions of Ca, Mg, K, and Na in water extracts of fly ash samples. Serial batch

leaching of the fly ash samples removed 30% or more of the environmentally available Ca and Na. Similarly, about 20% of the Ca and Na were leached from HA and PD fly ash samples during column leaching experiments. From 7–20 % of the available K and Mg were mobilized from all fly ash samples during serial batch leaching experiments, but less than 7% of these elements were leached from HA and PD fly ash samples during the column experiments. Although only 4–10% of the environmentally available Si was leached from the acidic fly ashes, more than 45% was mobilized from the alkaline fly ash during the column leaching experiments. Similarly, very small amounts of Al were mobilized from the acidic fly ash samples, but 12% and 7% were removed from the alkaline fly ash during serial batch and column leaching experiments, respectively. The relatively higher leachabilities of Al and Si from PD fly ash are consistent with the pH dependence of Al-oxides/hydroxides and amorphous silica solubilities. Because the solubilities of Al-oxides/hydroxides and amorphous silica are low to very low at circum-neutral pH conditions (Langmuir, 1997), the mobilities of Al and Si were small for the acidic fly ash samples. However, because the solubilities of Al-oxides/hydroxides and amorphous silica increase with increasing pH (Langmuir, 1997), the alkaline fly ash leached greater amounts of Al and Si. Nevertheless, smaller Al and Si mobilities were obtained for PD fly ash during column leaching experiments, compared to the values obtained for serial batch leaching, potentially due to the absence of dynamic solution-particle interactions. Despite the large Fe contents of these fly ash samples (Table 1), no detectable Fe was mobilized during either the serial batch or column leaching experiments. The low leachability of Fe from these fly ash samples is consistent with the low solubilities of Fe oxide minerals such as hematite and maghemite present in these fly ash samples (Kim and Kazonich, 2003; Sadiq and Lindsay, 1988).

Boron showed significant mobilization from all fly ash samples studied (Table 2). Approximately 17–33% of the environmentally available B from acidic fly ash samples and 71% of the B from PD fly ash sample were mobilized during serial batch leaching tests. Similarly, 10% and 67% of the B was leached from HA and PD fly ash samples during column leaching tests. Jankowski et al. (2006) also reported B as the most labile elements in alkaline fly ash. Strontium showed high mobilization (57–64%) from PD fly ash during both serial batch and column leaching experiments, and was moderately leached (8–27%) from acidic fly ash samples during serial batch leaching tests. Only 0–10% of the environmentally available Co, Mn, Ni, V (except MA), and Zn (except HB) were removed from fly ash samples during serial batch leaching tests. Similarly, very small amounts (<1%) of the Mn (both HA and PD), Mg (PD), Sr and Ba (HA) were leached from the fly ash samples during the column leaching experiments. Some other elements, such as Cu, Pb, and Ti, were not mobilized during either leaching test.

2.4. Conclusions

Microwave-assisted partial acid digestion of coal fly ash samples showed the presence of several environmentally available trace elements (e.g., As, Co, Cr, Ni, Sb, Se, Ti, V, and Zn). The acidic fly ash samples (HA, HB, and MA) were significantly richer in these trace elements than the alkaline fly ash, PD. PD fly ash contained significantly more B than the acidic fly ash samples. Batch and column leaching tests showed that varying fractions of the As, Cr, Mo, Sb, Se, and V in the coal fly ash samples were leachable. For all fly ash samples, leaching tests indicated that Mo, Sb, and Se were the most labile and Cr was the least mobile of the oxyanion-forming trace elements.

The leachate concentrations of As, Cr, Mo, Sb, Se (except PD fly ash), and V increased with time during long-term batch leaching tests, indicating that these oxyanion-forming trace elements resulted from the dissolution of glassy fly ash particles. However, the leachate concentrations of Ba, Co, Mn, Ni, and Zn for HB and MA fly ash samples decreased with time, indicating adsorption or co-precipitation of these elements during long-term leaching tests. Similarly, mobilization of Al, Ba, Ca, and Si (after 10 weeks) from PD fly ash also decreased over time, suggesting the precipitation of these elements in secondary minerals such as calcite, barytocalcite, gibbsite, gismondine, and kaolinite.

Boron, Ca, K, Mg, Mn, and Na were released very rapidly during the initial phases of serial batch and column leaching experiments. Although As and Se (except PD) were released during the early phases of serial batch and column leaching tests, their concentrations later decreased over time. Some elements such as As (HA), Cr (PD) and Se showed a bimodal leaching pattern during column leaching tests. Molybdenum is very labile with 47–89% mobility for all fly ash samples. Approximately 30–35 % of the environmentally available As was mobilized from HA fly ash during column and serial leaching tests. Similarly, 28–67% of the Sb was leached from the acidic fly ash samples and 100% of the Sb was leached from PD fly ash during serial batch leaching tests, and about 12–15% of the Sb was leached from HA and PD fly ash samples during column leaching tests. Greater proportions (42–63%) of the environmentally available Se were leached from HA and PD fly ash samples during column leaching than during serial leaching tests. Similarly, 16% (HA), 26% (HB), 33% (MA) and 71% (PD) of the environmentally available B was leached during serial leaching tests, while 10% (HA) and 67% (PD) of B was mobilized during column leaching tests.

The leaching tests performed in this study indicate that the major long-term environmental challenge for the management of coal fly ash is to control the potential leakage of leachate from fly ash disposal facilities into the environment. Once the leachate plume from a fly ash disposal facility reaches groundwater or surface water, it could potentially contaminate drinking water supplies. In particular, the older unlined fly ash disposal facilities pose a greater contamination risk than the lined disposal facilities. Therefore, development of economic and efficient methods for containing the hazardous trace elements within the fly ash disposal facility sites is needed.

Acknowledgments: The authors would like to thank E.Y. Graham, S. Bhattacharyya, Z. Yue, and B.E. Hollon for their help with laboratory work. Suggestions from two anonymous reviewers were very helpful in revising and improving the original manuscript.

REFERENCES

American Coal Ash Association. Coal combustion product (CCP) production & use survey results. American Coal Ash Association, http://www.acaa-usa.org; 2011.

Bhattacharyya S. Investigation of natural weathering processes and artificial treatment techniques in the attenuation of toxic metals from coal fly ash. Doctoral Dissertation, The University of Alabama, 2010.

Bool LE III and Helble JJ. A laboratory study of the partitioning of trace elements during pulverized coal combustion. Energy & Fuels 1995;9:880-7.

Chen M, Ma LQ, Harris WG. Baseline concentrations of 15 trace elements in Florida surface soils. J Environ Qual 1999;28:1173-81.

Clarke LB. The fate of trace elements during coal combustion and gasification: an overview. Fuel 1993;72:731-6.

Donahoe RJ. Secondary mineral formation in coal combustion byproduct disposal facilities: implications for trace element sequestration. In: Gieré R, Stille, P editors. Energy, waste

and the environment: a geochemical perspective: Geological Society of London, Special Publications 236; 2004, p. 641-58.

Drever JI. The geochemistry of natural waters: surface and groundwater environments. 3rd ed. New Jersey:Prentice Hall; 1997.

Fernández-Turiel JL, de Carvalho W, Cabanas M, Querol X, Lopez-Soler A. Mobility of heavy metals from coal fly ash. Environ Geol 1994;23:264-70.

Gieré R, Carleton LE, Lumpkin GR. Micro- and nanochemistry of fly ash from a coal-fired power plant. Am Min 2003;88:1853-65.

Glasser FP. Coal combustion wastes: characterization, reuse and disposal. In: Gieré R, Stille, P editors. Energy, waste and the environment: a geochemical perspective: Geological Society of London, Special Publications 236; 2004, p. 211-22.

Goodarzi F, Huggins FE, Sanei H. Assessment of elements, speciation of As, Cr, Ni and emitted Hg for a Canadian power plant burning bituminous coal. Inter J Coal Geol 2008;74:1-12.

Groen JC, Craig JR. The inorganic geochemistry of coal, petroleum, and their gasification/combustion products. Fuel Processing Technology 1994;40:15-48.

Hassett DH, Eylands KE. Mercury capture on coal combustion fly ash. Fuel 1999;78:243-8.

Hassett DJ, Pflughost-Hassett DF, Heebink LV. Leaching of CCBs- observations from over 25 years of research. Fuel 2005;84:1378-1383.

Hower JC, Rathbone RF, Robertson JD, Peterson G, Trimble AS. Petrology, mineralogy, and chemistry of magnetically-separated sized fly ash. Fuel 1999;78:197-203.

Huffman GP, Huggins FE, Shah N, and Zhao J. Speciation of arsenic and chromium in coal and combustion ash by XAFS spectroscopy. Fuel Process Technol 1994;39:47-62.

Huggins FE, Senior CL, Chu P, Ladwig K, Huffman GP. Selenium and arsenic speciation in fly ash from full-scale coal-burning utility plants. Environ Sci Technol 2007;41:3284-89.

Iwashita A, Sakaguchi Y, Nakajima T, Takanashi H, Ohki A, Kambara S. Leaching characteristics of boron and selenium for various coal fly ashes. Fuel 2005;84:479-485.

Iyer R. The surface chemistry of leaching coal fly ash. J Hazard Mater 2002;B93:321-9.

Jackson BP, Miller WP. Arsenic and selenium speciation in coal fly ash extracts by ion chromatography-inductively coupled plasma mass spectrometry. J Anal Atom Spectrom 1998;13:1107-12.

Jankowski J, Ward CR, French D, Groves S. Mobility of trace elements from selected Australian fly ashes and its potential impact on aquatic ecosystems. Fuel 2006;85:243-256.

Jegadeesan G, Al-Abed SR, Pinto P. Influence of trace metal distribution on its leachability from coal fly ash. Fuel 2008;87:1887-93.

Kalyoncu RS. Coal combustion products. US Geological Survey Minerals Yearbook-2001; 2000.

Kim AG, Kazonich G, Dahlberg M. (2003) Relative solubility of cations in Class F fly ash. Environ Sci Technol 2003;37:4507-11.

Kim AG, Kazonich G. The Silicate-non-silicate distribution of metals in fly ash and its effect on solubility. Fuel 2004;83:2285-92.

Kim AG. CCB leaching summary: survey of methods and results. Proceedings: Coal Combustion By-Products and Western Coal Mines: A Technical Interactive Forum, Golden, CO, April 16-18; 2002.

Külaots I, Hurt RH, Suuberg EM. Size distribution of unburned carbon in coal fly ash and its implications. Fuel 2004;83:223-230.

Kutchko BG, Kim AG. Fly ash characterization by SEM-EDS. Fuel 2006;85:2537-44.

Langmuir D. Aqueous environmental geochemistry. 1st ed. New Jersey: Prentice Hall; 1997.

Lecuyer I, Bicocchi S, Ausset P, Lefevre R. Physico-chemical characterization and leaching of desulphurization coal fly ash. Waste Management & Research 1996;14:15-28.

Linton RW, Loh A, Natusch DF, Evans CAJr., Williams P. Surface predominance of trace elements in airborne particles. Science 1976;191:852-4.

Mardon SM, Hower JC, O'Keefe JMK, Marks MN, Hedges DH. Coal combustion by-product quality at two stoker boilers: Coal source vs. fly ash collection system design. Inter J Coal Geol 2008;75:248-54.

Mattigod SV, Rai D, Eary LE, Ainsworth CC. Geochemical factors controlling the mobilization of inorganic constituents from fossil fuel combustion residues: I. Review of the major elements. J Environ Qual 1990;19:188-201.

McCarthy GJ, Butler RD, Grier DG, Adamek SD, Parks JA, Foster HJ. Long-term stability of landfilled coal combustion by-products. Fuel 1997;76:697-703.

McCarthy GJ, Grier DG, Wisdom MA, Petersen RB, Lerach SL, Jarabek RL, Walsh JJ, Winburn RS (1999) Coal combustion by-product diagenesis II. International Ash Utilization Symposium, October 18-20. Lexington, KY, Center for Applied Energy Research, University of Kentucky, Paper # 67; 1999.

Miller RN, Given PH. The association of major, minor and trace inorganic elements with lignites. I. Experimental approach and study of a North Dakota lignite. Geochim Cosmochim Acta 1986;50:2033-43.

Miravet R, López-Sánchez JF, Rubio R. Leachability and analytical speciation of antimony in coal fly ash. Analytica Chimica Acta 2006;576:200-6.

Narukawa T, Takatsu A, Chiba K, Riley KW, French DH. Investigation on chemical species of arsenic, selenium and antimony in fly ash from coal fuel thermal power stations. J Environ Monit 2005;7:1342-8.

National Research Council (2006) Managing coal combustion residues in mines. National Research Council of the National Academies, the National Academies Press, Washington DC; 2006.

Natusch DFS, Wallace JR, Evans CAJr. Toxic trace elements: preferential concentration in respirable particles. Science 1974;183:202-4.

Otero-Rey JR, Mato-Fernandez MJ, Moreda-Pineiro J, Alonso-Rodriguez E, Muniategui-Lorenzo S, Lopez-Mahia P, Prada-Rodriguez D. Influence of several parameters on As and Se leaching from coal fly ash samples. Analytica Chimica Acta 2005;531:299-305.

Parkhurst DL, Appelo CAJ. 1999. User's guide to PHREEQC (Version 2)-A computer program for speciation, batch-reaction, one-dimensional transport, and inverse geochemical calculations. US Geol Survey, Water Resour Invest:Rep 99-4259;1999.

Querol X, Moreno N, Umaña JC, Alastuey A, Hernández E, López-Soler A, Plana F. Synthesis of zeolites from coal fly ash: an overview. Fuel 2002;50:413-423.

Sadiq M, Lindsay WL.The Solubility Product of Soil Maghemite. Soil Science 1988;146:1-5.

Shoji T, Huggins FE, Huffman GP, Linak WP, Miller CA. XAFS spectroscopy analysis of selected elements in fine particulate matter derived from coal combustion. Energy & Fuels 2002;16:325-9.

Smith RD. The trace element chemistry of coal during combustion and the emissions from coal-fired plants. Prog Energy Combust Sci 1980;6:53-119.

Tishmack JK, Burns PE. The chemistry and mineralogy of coal and coal combustion products. In: Gieré R, Stille, P, editors. Energy, waste and the environment: a geochemical perspective: Geological Society of London, Special Publications 236; 2004, p. 223-46.

USEPA. Method 1312b: Synthetic precipitation leaching procedure. Revision 0, November 1994, US Environmental Protection Agency, USA; 1994.

USEPA. Method 3051A: Microwave-assisted acid digestion of sediments, sludges, soils and oils. Revision 1, February 2007, US Environmental Protection Agency, USA; 2007.

USEPA. Method 9045D: Soil and waste pH. Revision 4, November 2004, US Environmental Protection Agency, USA; 2004.

Vassilev SV, Vassileva CG. Geochemistry of coals, coal ashes and combustion wastes from coal-fired power stations. Fuel Processing Technology 1997;51:19-45.

Wadge A, Hutton M. The leachability and chemical speciation of selected trace elements in fly ash from coal combustion and refuse incineration. Environ Pollution 1987;48:85-99.

Wang J, Tomlinson MJ, Caruso JA. Extraction of trace elements in coal fly ash and subsequent speciation by high-performance liquid chromatography with inductively coupled plasma mass spectrometry. J Anal Atom Spectrom 1995;10:601-7.

Warren CJ, Dudas MJ. Weathering processes in relation to leachate properties of alkaline fly ash. J Environ Qual 1984;13:530-8.

SUPPLEMENTARY MATERIAL FOR CHAPTER – 2

LEACHABILITY OF ELEMENTS IN ALKALINE AND ACIDIC COAL FLY ASH SAMPLES DURING BATCH AND COLUMN LEACHING TESTS

The following supporting materials are provided for this chapter:

Fig. S2.1. Leachate concentrations of elements mobilized during fly ash jar leaching tests.

Fig. S2.2. Leachate concentrations of elements mobilized during long-term batch leaching of fly ash samples.

Fig. S2.3. Serial and cumulative concentrations of elements mobilized during serial batch leaching experiments.

Fig. S2.4. Effluent concentrations of elements mobilized during HA and PD fly ash column leaching experiments.

Table S2.1. Mineral solubility product data from llnl.dat used by PHREEQC to calculate mineral saturation indices.

Table S2.2. Correlation matrix for leachate pH and concentrations of elements mobilized during long-term leaching of HA fly ash (n =31).

Table S2.3. Correlation matrix for leachate pH and concentrations of elements mobilized during long-term leaching of HB fly ash (n =31).

Table S2.4. Correlation matrix for leachate pH and concentrations of elements mobilized during long-term leaching of MA fly ash (n =31).

Table S2.5. Correlation matrix for leachate pH and concentrations of elements mobilized during long-term leaching of PD fly ash (n =31).

Table S2.6. Loadings of leachate pH and element concentrations on two significant (eigenvalues >1) principal components for long-term leaching of HA fly ash.

Table S2.7. Loadings of leachate pH and element concentrations on two significant (eigenvalues >1) principal components for long-term leaching of HB fly ash.

Table S2.8. Loadings of leachate pH and element concentrations on two significant (eigenvalues >1) principal components for long-term leaching of MA fly ash.

Table S2.9. Loadings of leachate pH and element concentrations on two significant (eigenvalues >1) principal components for long-term leaching of PD fly ash.

Fig. S2.1. Leachate concentrations of elements mobilized during fly ash jar leaching tests.

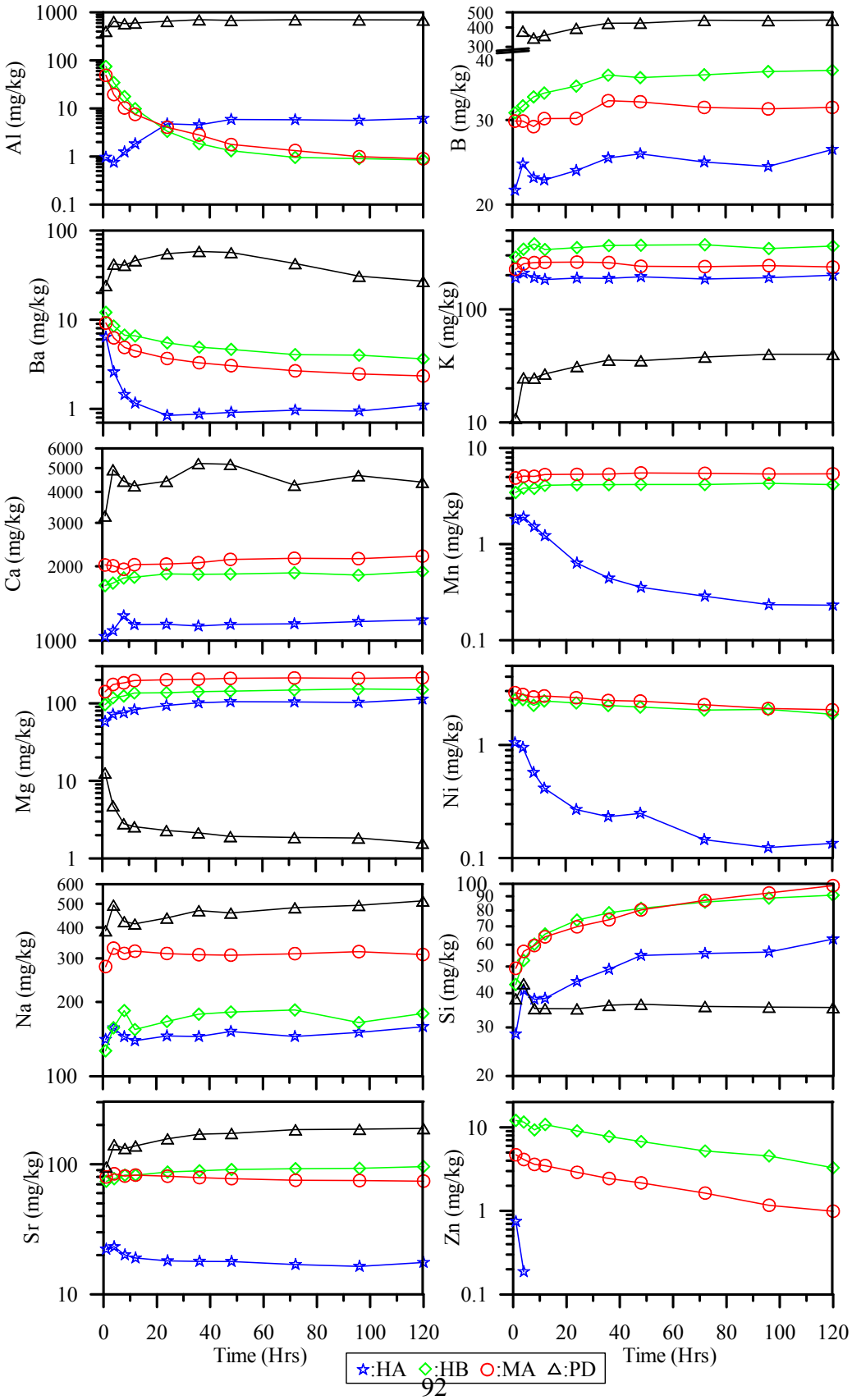

Fig. S2.2. Leachate concentrations of elements mobilized during long-term batch leaching of fly ash samples.

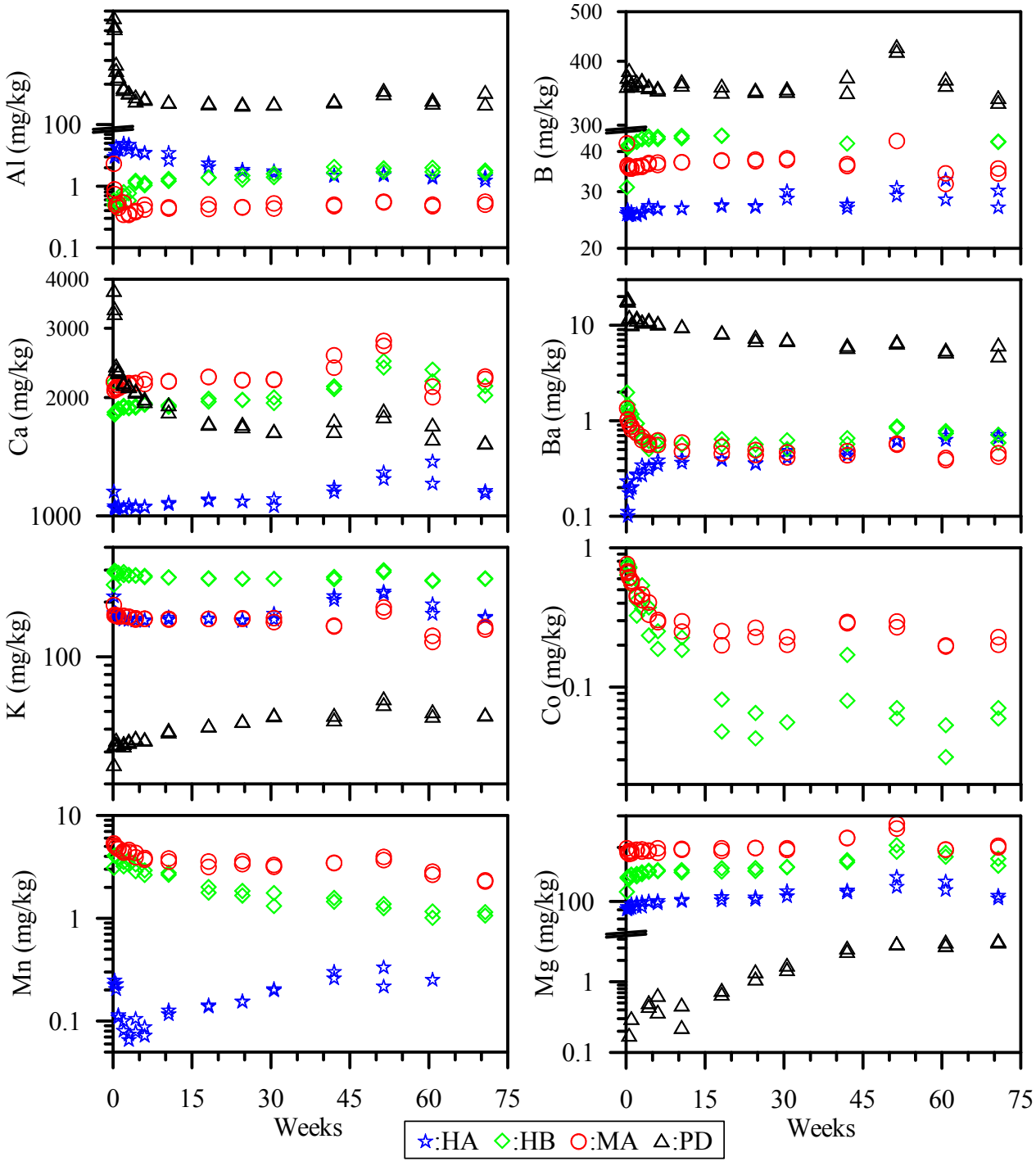

Fig. S2.2. Concentrations of elements mobilized during long-term leaching experiments of fly ash samples (contd…)

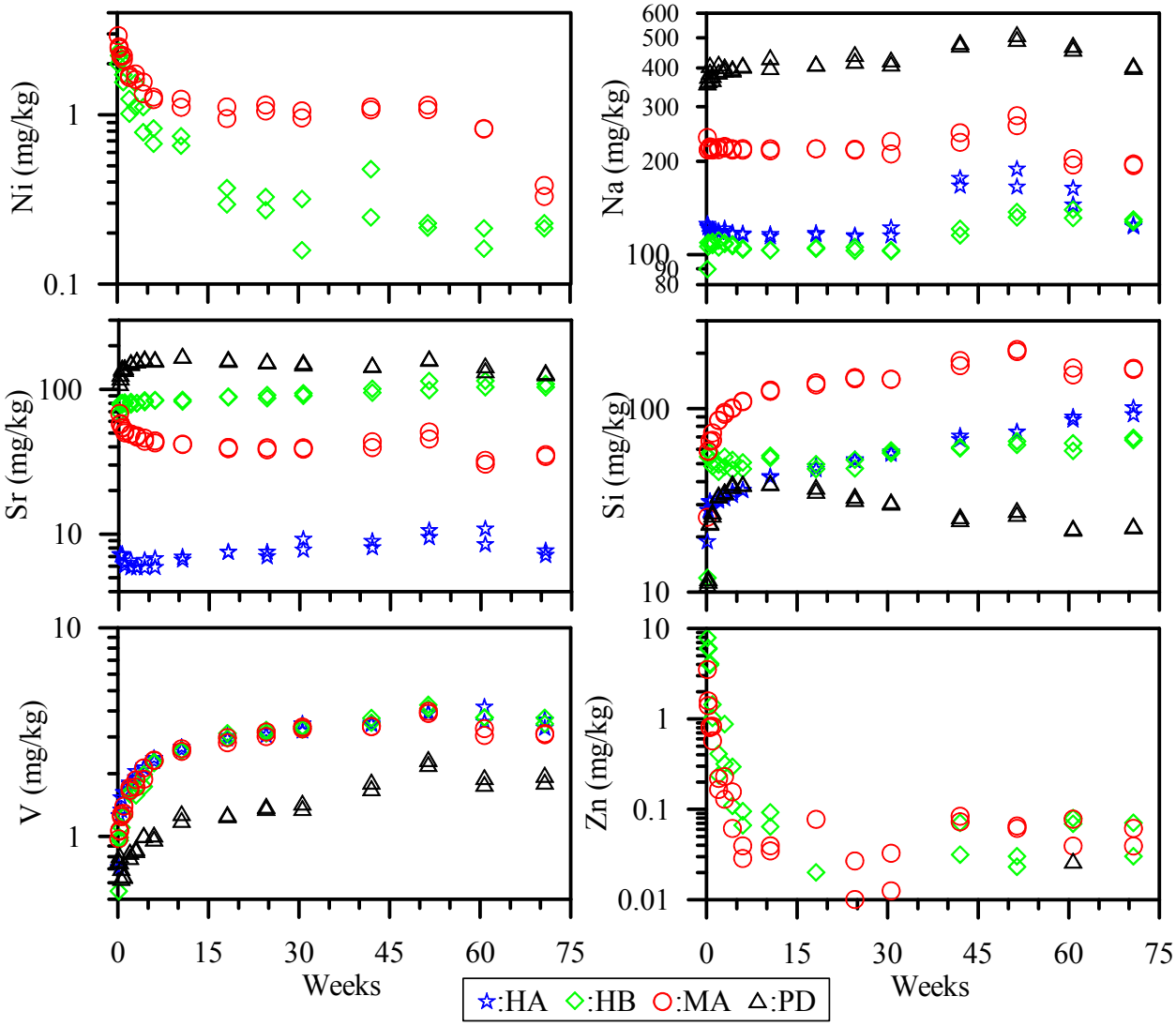

Fig. S2.3. Serial and cumulative concentrations of elements mobilized during serial batch leaching experiments.

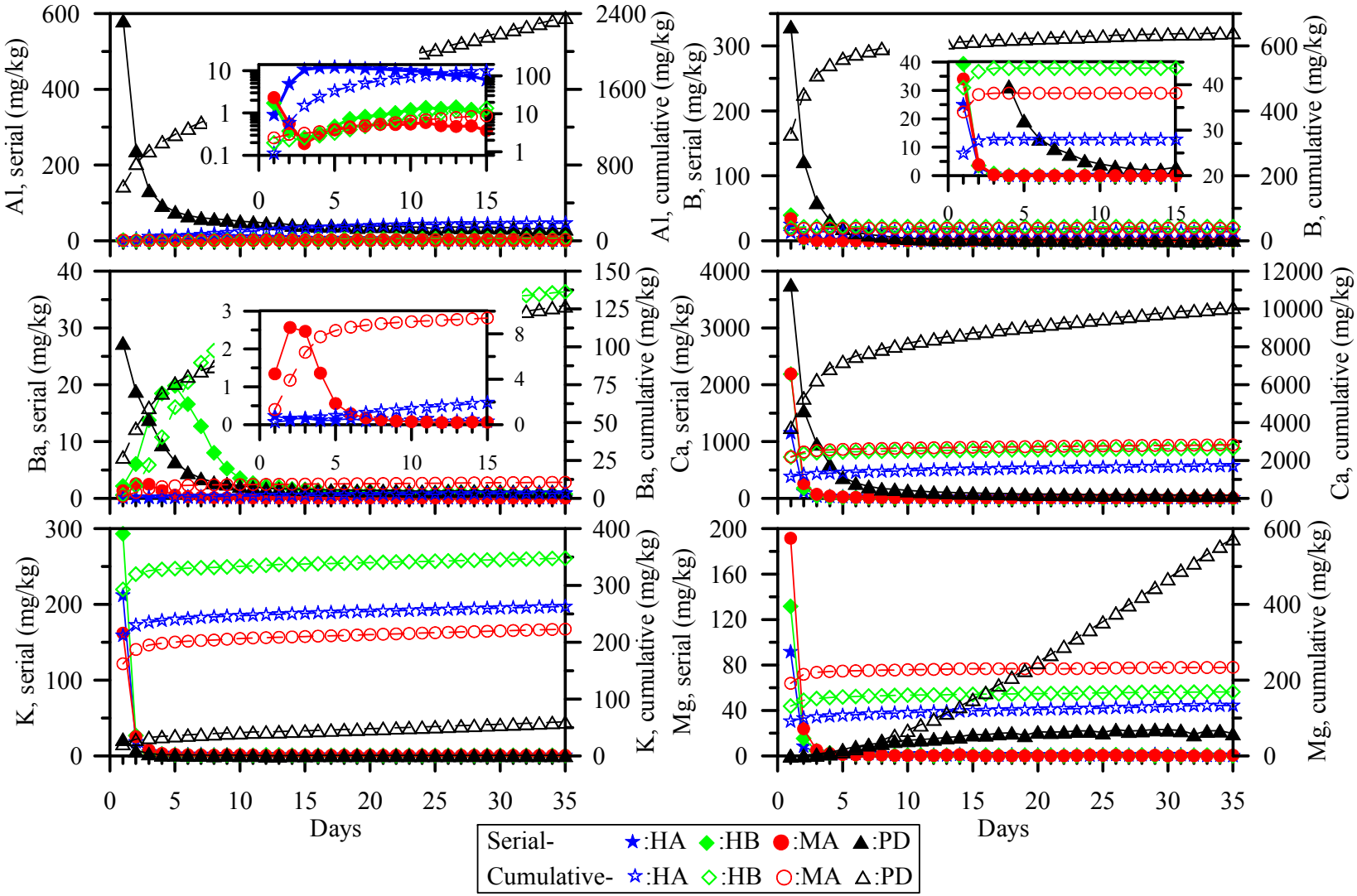

Fig. S2.3. Serial and cumulative concentrations of elements mobilized during serial batch leaching experiments (cont.).

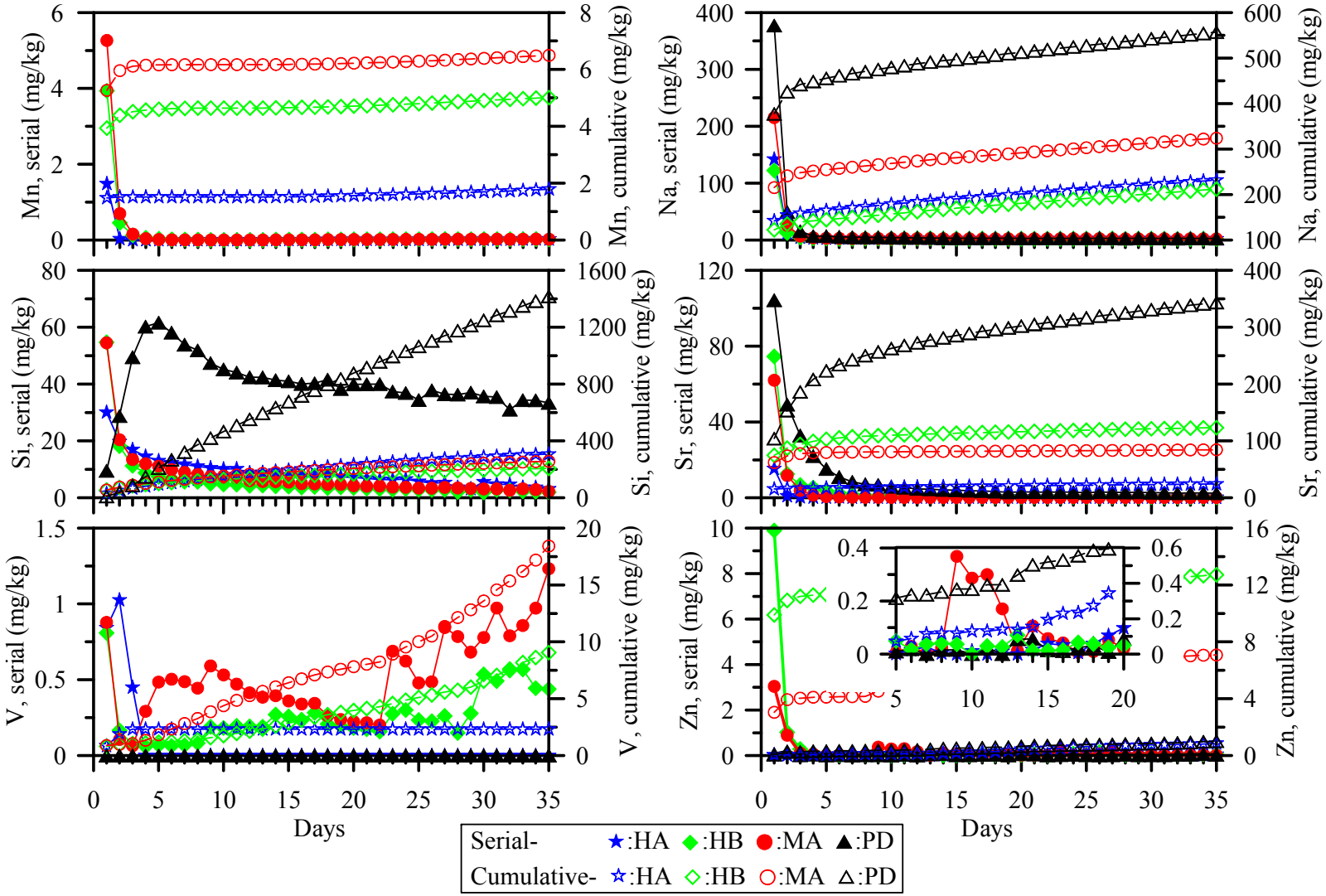

Fig. S2.4. Effluent concentrations of elements mobilized during HA and PD fly ash column leaching experiments.

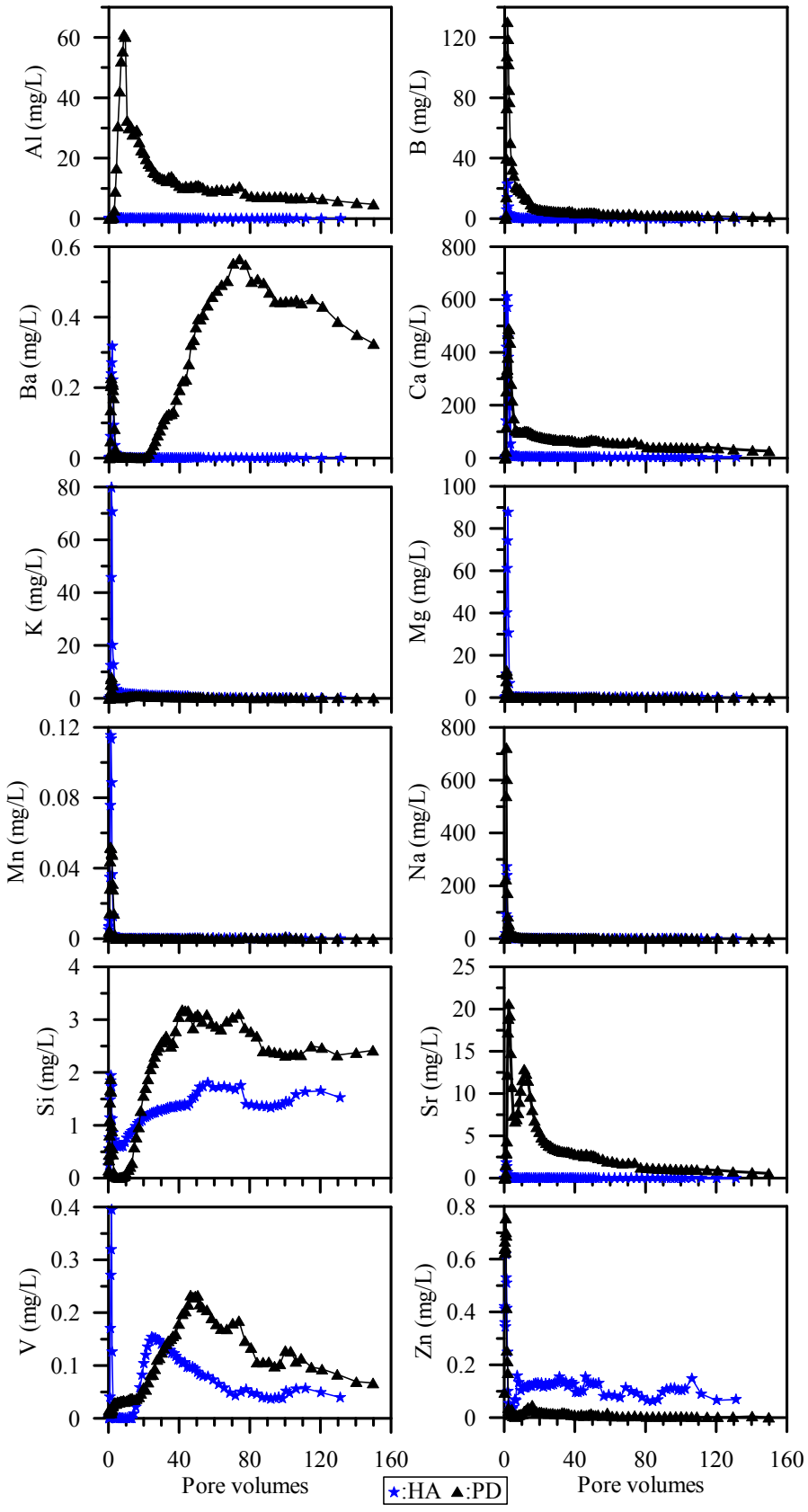

Table S2.1. Mineral solubility product data from llnl.dat used for PHREEQC modeling.

Minerals	Log (Ksp)
Alstonite ($BaCa(CO_3)_2$)	2.58
Alunite ($KA_{l3}(OH)_6(SO_4)_2$)	0.09
Amorphous silica (SiO_2)	-2.79
Aphthitalite ($NaK_3(SO_4)_2$)	-3.89
Arcanite (K_2SO_4)	-1.9
Barite ($BaSO_4$)	-10.07
Barytocalcite ($BaCa(CO_3)_2$)	2.74
Beidellites ($(CaMg)_{.165}(KNa)_{.33}Al_{2.33}Si_{3.67}O_{10}(OH)_2$)	5.51 to 5.86
Bieberite ($CoSO_4 \cdot 7H_2O$)	-2.57
Birnessite ($Mn_8O_{14} \cdot 5H_2O$)	-85.55
Bohemite (AlO_2H)	7.82
Boric Acid ($B(OH)_3$)	-0.1583
Brucite ($Mg(OH)_2$)	16.55
Ca, K, Mg, Na-Montmorillonites	2.19 to 2.57
Calcite ($CaCO_3$)	1.89
CaV_2O_6	-51.36
Celestite ($SrSO_4$)	-5.71
Dawsonite ($NaAlCO_3(OH)_2$)	4.52
Diaspore ($AlHO_2$)	7.41
Dolomite ($CaMg(CO_3)_2$)	2.62
Epsomite ($MgSO_4 \cdot 7H_2O$)	-1.96
$Ca_6Al_2(SO_4)_3(OH)_{12} \cdot 26H_2O$	62.54
Gibbsite ($Al(OH)_3$)	7.99
Gismondine ($Ca_2Al_4Si_4O_{16} \cdot 9H_2O$)	41.72
Gypsum ($CaSO_4{:}2H_2O$)	-4.53
Hydrated zinc sulfates ($CaSO_4 \cdot nH_2O$, n = 1, 4, or 7)	-1.7 to -0.45
Hydrozincite ($Zn_5(OH)_6(CO_3)_2$)	30.31
Kaolinite ($Al_2Si_2O_5(OH)_4$)	7.08
Lime (CaO)	33.03
Manganite (MnO(OH))	-0.16
Mesolite ($Na_{.676}Ca_{.657}Al_{1.99}Si_{3.01}O_{10} \cdot 2.647H_2O$)	13.91
Morenosite ($NiSO_4 \cdot 7H_2O$),	-2.09
Nickel carbonate ($NiCO_3$)	3.51
Portlandite ($Ca(OH)_2$)	22.85
Quartz (SiO2)	-4.11
Scolecite ($CaAl_2Si_3O_{10} \cdot 3H_2O$)	16.23
Smithsonite ($ZnCO_3$)	0.52
Sphaerocobaltite ($CoCO_3$)	-0.18
Strontianite	-0.32
Thenardite (Na_2SO_4)	-0.35
Witherite ($BaCO_3$)	-3.05
Mullite ($Al_6Si_2O_{13} + 18H^+ = 6Al^{3+} + 5H_2O + 2H_4SiO_4$)	50.50[a]

[a] Data prepared and compiled from Robie and Hemingway [1] by Ph. Blanc and others, available at http://thermoddem.brgm.fr/fichiers/Phreeqc_lv1_thermoddem_lvl1_no-org_15dec11.txt

Table S2.2. Correlation matrix for leachate pH and concentrations of elements mobilized during long-term leaching of HA fly ash (n =31).

HAFA	pH	Al	As	B	Ba	Ca	Cr	Mg	Mn	Mo	Se	Sb	Sr	Si	K	Na	V
pH	1																
Al	0.03	1															
As	0.77#	-0.51#	1														
B	0.23	-0.71#	0.53#	1													
Ba	0.35	-0.74#	0.63#	0.82#	1												
Ca	-0.03	-0.68#	0.28	0.70#	0.78#	1											
Cr	0.66#	-0.79#	0.82#	0.78#	0.83#	0.55#	1										
Mg	0.31	-0.72#	0.62#	.81#	0.82#	0.86#	0.77#	1									
Mn	-0.45*	-0.29	-0.04	0.04	-0.12	0.11	-0.03	0.22	1								
Mo	0.69#	-0.68#	0.91#	0.76#	0.71#	0.47#	0.90#	0.78#	0.13	1							
Se	0.63#	-0.76#	0.85#	0.78#	0.89#	0.66#	0.95#	0.86#	0.05	0.92#	1						
Sb	0.59#	-0.79#	0.87#	0.75#	0.86#	0.66#	0.93#	0.87#	0.14	0.92#	0.97#	1					
Sr	-.70#	-0.75#	-0.33	0.36*	0.30	.63#	-0.13	0.38*	0.40*	-0.13	-0.01	0.02	1				
Si	0.35	-0.84#	0.56#	0.79#	0.94#	0.77#	0.85#	0.78#	0.00	0.67#	0.86#	0.84#	0.24	1			
K	-0.35	-0.48#	-0.08	0.33	0.311	0.72#	0.10	0.53#	0.70#	0.09	0.16	0.26	0.69#	0.33	1		
Na	0.05	-0.52#	0.25	0.56#	0.54#	0.82#	0.46#	0.74#	0.45#	0.46#	0.50#	0.57#	0.45*	0.58#	0.85#	1	
V	0.48#	-0.86#	0.81#	0.83#	0.90#	0.71#	0.91#	0.88#	0.09	0.90#	0.96#	0.97#	0.16	0.89#	0.28	0.56#	1

Correlation is significant at the 0.01 level (2-tailed), * Correlation is significant at the 0.05 level (2-tailed)

Table S2.3. Correlation matrix for leachate pH and concentrations of elements mobilized during long-term leaching of HB fly ash (n =31).

HBFA	pH	Al	As	B	Ba	Ca	Co	Cr	Mg	Mn	Mo	Ni	Se	Sb	Sr	Zn	Si	K	Na	V
pH	1																			
Al	0.83#	1																		
As	0.75#	0.91#	1																	
B	0.77#	0.64#	0.70#	1																
Ba	-0.85#	-0.60#	-0.39*	-0.55#	1															
Ca	0.41*	0.73#	0.82#	0.55#	-0.05	1														
Co	-0.86#	-0.90#	-0.81#	-0.63#	0.76#	-0.54#	1													
Cr	0.63#	0.79#	0.90#	0.62#	-0.19	0.84#	-0.60#	1												
Mg	0.79#	0.84#	0.88#	0.86#	-0.45*	0.81#	-0.69#	0.87#	1											
Mn	-0.77#	-0.95#	-0.94#	-0.57#	0.52#	-0.73#	0.92#	-0.81#	-0.77#	1										
Mo	0.95#	0.86#	0.79#	0.81#	-0.82#	0.55#	-0.93#	0.65#	0.82#	-0.83#	1									
Ni	-0.88#	-0.91#	-0.82#	-0.65#	0.77#	-0.56#	1.00#	-0.63#	-0.72#	0.93#	-0.94#	1								
Se	0.88#	0.96#	0.95#	0.75#	-0.63#	0.73#	-0.92#	0.82#	0.88#	-0.96#	0.93#	-0.94#	1							
Sb	0.93#	0.93#	0.91#	0.76#	-0.72#	0.61#	-0.90#	0.76#	0.85#	-0.90#	0.93#	-0.92#	0.97#	1						
Sr	0.78#	0.85#	0.91#	0.73#	-0.40*	0.73#	-0.73#	0.94#	0.87#	-0.86#	0.77#	-0.75#	0.89#	0.85#	1					
Zn	-0.89#	-0.64#	-0.48#	-0.65#	0.92#	-0.22	0.80#	-0.34	-0.58#	0.59#	-0.91#	0.83#	-0.70#	-0.75#	-0.52#	1				
Si	0.73#	0.51#	0.57#	0.66#	-0.45*	0.25	-0.37*	0.62#	0.70#	-0.42*	0.57#	-0.41*	0.59#	0.67#	0.68#	-0.46#	1			
K	-0.16	-0.44*	-0.31	0.20	0.24	-0.23	0.50#	-0.18	0.00	0.54#	-0.21	0.47#	-0.35	-0.30	-0.21	0.17	0.27	1		
Na	0.59#	0.62#	0.72#	0.70#	-0.17	0.72#	-0.41*	0.90#	0.86#	-0.57#	0.57#	-0.45*	0.66#	0.62#	0.85#	-0.34	0.71#	0.13	1	
V	0.88#	0.95#	0.95#	0.74#	-0.63#	0.69#	-0.92#	0.80#	0.86#	-0.95#	0.92#	-.93#	0.99#	0.98#	0.88#	-0.69#	0.60#	-0.33	0.63#	1

Correlation is significant at the 0.01 level (2-tailed), * Correlation is significant at the 0.05 level (2-tailed)

Table S2.4. Correlation matrix for leachate pH and concentrations of elements mobilized during long-term leaching of MA fly ash (n =31).

MAFA	pH	Al	As	B	Ba	Ca	Co	Cr	Mg	Mn	Mo	Ni	Se	Sb	Sr	Zn	Si	K	Na	V
pH	1																			
Al	-0.55#	1																		
As	0.85#	-0.24	1																	
B	-0.14	0.51#	0.16	1																
Ba	-0.96#	0.66#	-0.79#	0.22	1															
Ca	0.49#	-0.05	0.73#	0.49#	-.38*	1														
Co	-0.96#	0.52#	-0.86#	0.09	0.95#	-.43*	1													
Cr	0.87#	-0.29	0.96#	0.04	-0.78#	0.73#	-0.84#	1												
Mg	0.47#	0.01	0.68#	0.33	-0.39*	0.86#	-0.40*	0.68#	1											
Mn	-0.93#	0.36*	-0.87#	0.19	0.87#	-0.39*	0.93#	-0.88#	-0.41*	1										
Mo	0.95#	-0.47#	0.93#	0.06	-0.92#	0.64#	-0.96#	0.90#	0.60#	-0.89#	1									
Ni	-0.97#	0.50#	-0.85#	0.17	0.94#	-0.43*	0.97#	-0.86#	-0.43*	0.97#	-0.95#	1								
Se	0.90#	-0.34	0.98#	0.1	-0.86#	0.70#	-0.91#	0.95#	0.65#	-0.88#	0.96#	-0.89#	1							
Sb	0.83#	-0.33	0.97#	0.17	-0.80#	0.77#	-0.83#	0.93#	0.73#	-0.78#	0.93#	-0.80#	0.98#	1						
Sr	-0.95#	0.61#	-0.79#	0.32	0.96#	-0.29	0.95#	-0.79#	-0.28	0.93#	-0.89#	0.96#	-0.84#	-0.76#	1					
Zn	-0.83#	0.90#	-0.57#	0.33	0.89#	-0.29	0.82#	-0.60#	-0.23	0.66#	-0.79#	0.80#	-0.67#	-0.63#	0.84#	1				
Si	0.88#	-0.39*	0.96#	0.1	-0.83#	0.78#	-0.85#	0.96#	0.72#	-0.84#	0.94#	-0.86#	0.97#	0.97#	-0.80#	-0.68#	1			
K	-0.75#	0.46#	-.65#	0.58#	0.73#	-0.25	0.69#	-0.75#	-0.29	0.80#	-0.64#	0.75#	-0.67#	-0.62#	0.81#	0.60#	-0.68#	1		
Na	-0.22	0.24	0.05	0.70#	0.24	0.58#	0.23	0.00	0.50#	0.37*	-0.03	0.31	0.04	0.17	0.42*	0.21	0.09	0.46#	1	
V	0.90#	-0.33	0.99#	0.13	-0.86#	0.69#	-0.91#	0.95#	0.67#	-0.88#	0.96#	-0.89#	0.99#	0.97#	-.84#	-.66#	0.97#	-0.65#	0.04	1

Correlation is significant at the 0.01 level (2-tailed), * Correlation is significant at the 0.05 level (2-tailed)

Table S2.5. Correlation matrix for leachate pH and concentrations of elements mobilized during long-term leaching of PD fly ash (n =31).

PDFA	pH	Al	B	Ba	Ca	Cr	Mg	Mo	Se	Sr	Si	K	Na	V
pH	1													
Al	0.52#	1												
B	0.40*	0.33	1											
Ba	0.84#	0.85#	0.38*	1										
Ca	0.74#	0.95#	0.42*	0.95#	1									
Cr	-0.89#	-0.59#	-0.12	-0.83#	-0.75#	1								
Mg	-0.93#	-0.37*	-0.25	-0.76#	-0.59#	0.88#	1							
Mo	-0.64#	-0.74#	-0.03	-0.81#	-0.80#	0.83#	0.64#	1						
Se	0.54#	0.98#	0.29	0.85#	0.94#	-0.60#	-0.39*	-0.73#	1					
Sr	-0.07	-0.73#	-0.02	-0.40*	-0.58#	0.28	-0.06	0.63#	-0.66#	1				
Si	0.04	-0.75#	-0.22	-0.35	-0.57#	0.08	-0.23	0.39*	-0.67#	0.90#	1			
K	-0.92#	-0.56#	-0.24	-0.85#	-0.76#	0.93#	0.89#	0.83#	-0.57#	0.22	0.02	1		
Na	-0.68#	-0.50#	0.1	-0.71#	-0.61#	0.88#	0.76#	0.88#	-0.48#	0.38*	0.09	0.80#	1	
V	-0.93#	-0.45*	-0.26	-0.78#	-0.67#	0.91#	0.95#	0.75#	-0.44*	0.15	-0.05	0.94#	0.82#	1

Correlation is significant at the 0.01 level (2-tailed), * Correlation is significant at the 0.05 level (2-tailed)

Table S2.6. Loadings of leachate pH and element concentrations on two significant (eigenvalues >1) principal components for long-term leaching of HA fly ash.

Variables	PC 1 (69.03% variance)	PC 2 (15.51 % variance)
pH	**0.70**	-0.39
Al	-0.52	**-0.75**
As	**0.93**	0.00
B	**0.66**	0.59
Ba	**0.94**	0.27
Ca	0.55	**0.74**
Cr	**0.82**	0.51
K	0.10	**0.89**
Mg	**0.72**	0.65
Mn	-0.36	**0.56**
Mo	**0.89**	0.39
Na	0.30	**0.81**
Sb	**0.88**	0.41
Se	**0.93**	0.36
Si	**0.73**	0.65
Sr	0.37	**0.85**
V	**0.88**	0.42

Table S2.7. Loadings of leachate pH and element concentrations on two significant (eigenvalues >1) principal components for long-term leaching of HB fly ash.

Variables	PC1 (58.02% variance)	PC2 (17.067% variance)	PC3 (13.36% variance)	PC4 (5.63% variance)
pH	0.11	**0.96**	0.02	0.15
Al	0.48	0.41	0.32	**0.64**
As	**0.79**	0.55	-0.23	0.05
B	**0.91**	-0.09	-0.38	-0.05
Ba	**0.76**	0.06	-0.48	-0.15
Ca	**0.94**	0.22	-0.11	0.17
Co	-0.10	0.22	**0.96**	0.02
Cr	0.45	**0.82**	-0.27	0.21
K	**0.75**	0.15	0.20	-0.58
Mg	**0.90**	0.33	-0.04	0.18
Mn	-0.08	**-0.64**	0.62	-0.38
Mo	**0.88**	0.30	-0.18	-0.32
Na	0.58	**0.62**	-0.43	0.28
Ni	-0.27	-0.30	**0.89**	0.05
Sb	0.56	**0.76**	-0.01	-0.04
Se	**0.82**	0.52	-0.19	0.07
Si	0.21	**0.94**	0.04	0.11
Sr	0.30	0.58	**-0.59**	0.27
V	**0.82**	0.49	0.00	-0.12
Zn	-0.19	0.26	-0.09	**0.86**

Table S2.8. Loadings of leachate pH and element concentrations on two significant (eigenvalues >1) principal components for long-term leaching of MA fly ash.

Variables	PC1 (67.34% variance)	PC2 (16.83% variance)	PC3 (6.76% variance)
pH	**0.93**	-0.07	0.26
Al	0.11	-0.07	**0.75**
As	**0.93**	0.14	0.21
B	0.20	**0.89**	-0.05
Ba	**-0.93**	0.13	-0.13
Ca	0.38	0.62	**0.64**
Co	**-0.96**	0.13	-0.14
Cr	**0.88**	0.08	0.43
K	-0.51	**0.57**	-0.50
Mg	0.39	0.47	**0.67**
Mn	**-0.82**	0.39	-0.35
Mo	**0.95**	0.93	0.18
Na	-0.19	**0.91**	0.18
Ni	**-0.79**	0.35	-0.32
Sb	**0.87**	0.26	0.38
Se	**0.93**	0.16	0.30
Si	**0.86**	0.20	0.46
Sr	**-0.89**	0.39	-0.16
V	**0.92**	0.17	0.33
Zn	**-0.91**	-0.11	0.15

Table S2.9. Loadings of leachate pH and element concentrations on two significant (eigenvalues >1) principal components for long-term leaching of PD fly ash.

Variables	PC1 (64.53% variance)	PC2 (18.20% variance)	PC3 (10.96% variance)
pH	**-0.93**	0.08	0.27
Al	-0.55	**-0.78**	0.25
B	-0.11	-0.01	**0.94**
Ba	**-0.94**	-0.10	0.21
Ca	**-0.80**	-0.47	0.34
Cr	**0.96**	0.14	0.11
K	**0.96**	0.21	-0.06
Mg	**0.93**	0.16	-0.13
Mo	**0.76**	0.55	0.26
Na	**0.85**	0.16	0.42
Se	**-0.63**	-0.62	0.34
Si	-0.10	**0.98**	-0.07
Sr	0.08	**0.94**	0.23
V	**0.94**	0.06	-0.08

REFERENCE

Robie RA, Hemingway B. Thermodynamic properties of minerals and related substances at 298.15 K and 1 Bar (105 Pascals) pressure and at higher temperatures. US Geol Survey Bull 2131,1995.

CHAPTER – 3

ATTENUATION OF TRACE ELEMENTS IN COAL FLY ASH LEACHATES BY SURFACTANT-MODIFIED ZEOLITE[a]

Abstract

Potential leaching of trace elements from older, unlined fly ash disposal facilities is a serious threat to groundwater and surface water contamination. Therefore, effective methods for containing the pollutant elements within the unlined coal combustion products (CCPs) disposal facilities are required to minimize any potential impact of leachate emanating from such facilities into the nearby environment. Because surfactant-modified zeolite (SMZ) has the potential to sequester both cationic and anionic trace elements from aqueous solutions, bench-scale batch and column experiments were performed to test its ability to remediate trace elements in leachates generated from both alkaline and acidic fly ash samples. Fly ash leachate treatment results showed the potential application of SMZ as an effective permeable reactive barrier (PRB) material to control the dispersion of heavy metals and metalloids from ash disposal sites.

[a] This chapter represents a journal article that has been published in *Journal of Hazardous Materials 229–230, 201-208, 2012*. Similarly, a part of this chapter was also published as a proceeding paper: "Neupane, G. and Donahoe, R. J. (2009) Potential use of surfactant-modified zeolite to treat leachate from fly ash disposal sites. University of Kentucky Center for Applied Energy Research, Ash Library:133-neupane2009, 19 pp.

Quantitative comparison of the elemental composition of SMZ-treated and untreated leachates indicated that SMZ was effective in decreasing the concentrations of trace elements in fly ash leachates. Similarly, SMZ treatment column experiments showed the delayed peak leaching events and overall reductions in leachate concentrations of trace elements. The effectiveness of SMZ column treatments, however, decreased with time potentially due to the saturation of sorption sites.

KEYWORDS: Coal fly ash, Leachate, Surfactant-modified zeolite, Trace elements, Permeable reactive barrier.

3.1. Introduction

Coal-fired power plants produce large volumes of coal combustion products (CCPs), including fly ash, bottom ash, boiler slag, flue gas desulfurization materials, and different gasses (Kalyoncu, 2000). In 2010, 67.7 million short tons of fly ash were produced by coal-fired power plants in the US, accounting for 52.0% of the total CCPs (American Coal Ash Association). Although the beneficial use of fly ash and other CCPs has varied in recent years (37.9% or 27.7 short tons of fly ash were recycled and used in 2010), the majority of the fly ash is buried in impoundment lagoons or dry landfills along with other unused CCPs (American Coal Ash Association). Fly ash contains numerous trace elements which can potentially pose health hazards to humans; therefore, development of feasible and effective techniques to control the dispersion of hazardous trace elements from older, unlined CCP disposal facilities to local hydrology is very important for the protection of potable water resources.

Several previous studies have attempted the treatment of municipal solid waste (MSW) fly ash (Auer et al., 1995; Bournonville et al., 2004; Crannell et al., 2000; Derie, 1996); however, there have been relatively few studies which focused on controlling the mobility of trace elements from coal fly ash (Bhattacharyya et al., 2009; Donahoe et al., 2007). Auer et al. (1995) noted that the addition of reactive calcium aluminates to sulfate rich MSW fly ash resulted in the formation of ettringite-like minerals, partially sequestering some trace elements. A ferrous sulfate treatment method developed for fixing arsenic in a contaminated soil (Yang et al., 2007) was also tested for immobilizing trace elements in coal fly ash (Bhattacharyya et al., 2009; Donahoe et al., 2007). It was found that ferrous sulfate treatment at a 1:30 solid: liquid ratio was effective in decreasing the synthetic acid rain leachability of several trace elements associated with coal fly ash (Bhattacharyya et al., 2009).

Zeolites are hydrated aluminosilicate minerals characterized by cage-like structures with high internal and external surface areas (Bowman, 2003; Newsam, 1986). The availability, low cost (about $60 – $100 per metric ton), and high cation exchange capacity make natural zeolites very useful material for treatment of contaminated water (Bowman, 1996). Although natural zeolites are effective in removing cationic species from aqueous solutions (Leppert, 1990), they are not useful for removing oxyanions due to their negative surface charge (Haggerty and Bowman, 1994). However, the external surface of natural zeolite can be altered to make it suitable to adsorb oxyanions (Haggerty and Bowman, 1994). When natural zeolite is treated with cationic surfactant solution with concentration> critical micelle concentration (CMC), its surface becomes a positively charged surface suitable for adsorbing anionic counterions (Haggerty and Bowman, 1994).

Despite the potential to sequester trace elements from aqueous solution and its relatively low cost ($350 – $500 per ton (Bowman, 1996; Ranck et al., 2005), SMZ has not previously been tested for remediation of trace elements in fly ash leachate. In the current study, we performed bench-scale batch and column experiments to evaluate the effectiveness of SMZ to remediate trace elements in fly ash leachates.

3.2. Materials and methods

3.2.1. Background soil

A yellow sandy background soil (5 – 20 cm) was collected from Fort Walton Beach, FL. The background soil was air dried, passed through a 2 mm screen to remove larger debris, and thoroughly mixed. Mineralogy of the soil was studied with X-ray diffraction analyses of the bulk soil and clay-sized (<2 μm) soil fractions using a Brüker D8 Advance powder diffractometer. The clay-sized soil fraction was separated by flotation according to Stoke's Law. The soil pH was measured at a 1:1 soil:water ratio (USEPA, 2004). The environmentally available elements in the background soil were extracted by microwave-assisted partial acid digestion (USEPA, 2007) and analyzed with a Perkin Elmer Optima 3000DV inductively coupled plasma-optical emission spectrometer (ICP-OES).

3.2.2. Fly ash samples and characterization

Three acidic (Class F) and an alkaline (Class C) fly ash samples were collected from four different coal-fired power plants located in the southeastern United States. The acidic fly ashes (HA, HB, and MA) and alkaline fly ash (PD) were the combustion products of Eastern Bituminous coals and Powder River Basin coal, respectively. The fly ash samples were air-dried

and homogenized prior to their use in experiments. The specific surface area of each fly ash sample was determined by the single-point BET method using a device with flow of 30% N_2 in He using a Leybold-Inficon mass spectrometer to detect the gasses. Similarly, bulk mineralogy was identified with X-ray diffraction. The unburned carbon contents in fly ash samples were determined by loss-on-ignition tests (Hassett and Eylands, 1999). Similarly, the environmentally available elements in the fly ash samples were extracted by microwave-assisted partial acid digestion (USEPA, 2007).

3.2.3. Surfactant-modified zeolite

Natural zeolite was obtained from the St. Cloud Mining Company located in Winston, NM. St. Cloud zeolite is rich in clinoptilolite (74%) with smaller amounts of smectite (5%), quartz/cristobilite (10%), feldspar (10%), and illite (Sullivan et al., 1997). Its external CEC was reported to be in the range of 70 – 90 mequiv./kg (Sullivan et al., 1997, 2003). Quaternary amine hexadecyltrimethylammonium bromide (HDTMA-Br) with a CMC of 0.9 mM (Li and Bowman, 1997) was used for the zeolite surface modification. The HDTMA-Br has been used by several previous researchers (Bowman, 2003; Chutia et al., 2009; Li et al., 1998) for surface modification of zeolites. Furthermore, Campos and Bucher (2007) reported that HDTMA-modified zeolite was very effective in removing arsenic from aqueous solution. At higher concentrations, HDTMA-Br selectively exchanges with inorganic cations on the external zeolite surface and forms a stable surfactant bilayer with anion exchange properties. It has been reported that this exchange occurs to the level of the zeolite's external CEC (Bowman, 2003; Haggerty and Bowman, 1994; Li et al., 2003). A method modified from Li et al. (2003) was used for the surface modification of the natural zeolite. For the surface modification, zeolite was agitated for

three days at 1:3.75 zeolite: 0.04 M HDTMA-Br solution ratio in polypropylene bottles. The initial concentration (0.04 M) of surfactant in the surfactant solution was far greater than the CMC (0.9 mM) value (Li and Bowman, 1997); therefore the surfactant should have formed the HDTMA bilayer on the zeolite surface. After being allowed to settle for 24 hours, the supernatant solution was discarded, and the SMZ was agitated with reagent water (>18MΩ) at 1:4 solid: liquid ratio for 24 hours to remove the excess HDTMA-Br. The rinsed SMZ was finally collected by vacuum filtration, air dried at room temperature, and homogenized.

3.2.4. Fly ash leachate

Fly ash leachate solutions were prepared by equilibrating the fly ash samples with DDI (>18MΩ doubly de-ionized water produced by a Barnstead NANOpure system) water at a 1:15 solid: liquid ratio. For each fly ash, 450 mL of DDI water were added to 30 g of fly ash sample in a 500 mL polypropylene bottle, and the mixture was agitated for 48 hours. Then the leachate was filtered through a 0.2 μm filter for use in the SMZ batch treatments. About 20 mL of each filtered leachate solution was reserved for chemical analysis.

3.2.5. SMZ treatment batch experiments

Fly ash leachate was treated with different amounts of SMZ in batch experiments. The batch treatments were conducted by equilibrating 40 mL of fly ash leachate in 50 mL centrifuge tubes with 0.027 g, 0.133 g, 0.267 g, 0.400 g, and 0.533 g of SMZ, which represent, respectively, 1%, 5%, 10%, 15%, and 20% by weight of the 2.667 g of fly ash that was used to generate 40 mL of leachate at a 1:15 solid:liquid ratio. A 24-h equilibration time was selected for use in the batch experiments, which has been used in previous studies (Ghiaci et al., 2004; Warchoł et al.,

2006). Other studies of oxyanion adsorption have shown equilibration in substantially less time. For example, adsorption of $Cr_{(VI)}$ on surfactant-modified zeolite has been achieved in <10 min to 4 h (Cordoves et al., 2008; Majdan et al., 2006; Zeng et al., 2010). Batch SMZ treatments were conducted in duplicate. All tubes were agitated at 200 rpm for 24 hours. At the end of the experiments, the supernatant solutions were centrifuged at 8500 rpm for 20 min, filtered through 0.2 μm syringe filters, acidified to 2% with OPTIMA HNO_3, and stored in a refrigerator until chemical analysis.

3.2.6. SMZ treatment column experiments

A representative acidic fly ash (HA) and the alkaline fly ash (PD) were selected for the SMZ treatment column experiments. For each fly ash, two columns were dry-packed into 40.6 cm long Plexiglas tubes with a large internal diameter (8.7 cm) to minimize the wall effects during unsaturated flow experiments. In one column, SMZ (5 cm), background soil (17.5 cm), and fly ash (17.5 cm) were packed, from bottom to top, while background soil (17.5 cm) and fly ash (17.5 cm) were packed into the other column (see Supplementary Fig. S3.1). To obtain the desired height for the fly ash layers, a total of 950 g of HA fly ash was used in each column (HA and HA-SMZ), while 1,125 g of PD fly ash was used in each of the other two columns (PD and PD-SMZ). Similarly, 1,400 g of background soil was used in each column. For each SMZ column, 400 g of SMZ was used. Loss of SMZ or background soil was prevented by placing a fabric filter reinforced with a 1-mm Teflon screen above a perforated stainless steel support plate at the base of each column. Similar fabric filter assemblies were used at the interface between different materials to prevent mixing of layers. After being packed, the columns were placed in an upright position with the tops open to air.

Synthetic acid rain (SAR), a dilute solution of H_2SO_4 and HNO_3 with pH 4.20 ± 0.05 (USEPA, 1994), was used as the leaching solution. A peristaltic pump (Gilson Minipuls 3) was used to control the fluid flow through the columns. Before beginning the column experiments, the porosity of each column was measured by saturating the column materials with bottom-up pumping of SAR. For HA, HA-SMZ, PD, and PD-SMZ columns, the porosities were measured to be 36%, 38%, 37%, and 39%, respectively. After the porosity measurement, the SAR circulation in each column was reversed to top-to-bottom. It was expected that this circulation pattern would mimic the natural leaching of fly ash in ash disposal facilities. Initially, effluent samples were collected from the base of the columns at a higher frequency but a progressively longer sampling interval was used as the experiments progressed. During each sampling event, fluid flow rate and pH were measured for each column. Average flow rates for HA, HA-SMZ, PD, and PD-SMZ columns were calculated as 1.31, 1.35, 1.28, and 1.33 cm^3/min, respectively. The average residence times of the leachate in contact with the SMZ layers in columns HA-SMZ and PD-SMZ were calculated to be 118 and 129 min, respectively. All effluent samples were filtered through 0.2 μm syringe filters, acidified to 2% with HNO_3, and stored in a refrigerator until chemical analysis.

3.2.7. Serial leaching of reacted SMZ material

At the end of the SMZ treatment column experiments, the SMZ layers from both columns were retrieved by cutting the column into 10 cm transverse-sections. The reacted SMZ material from each column was air-dried, homogenized, and subjected to SAR serial leaching at a 1:15 solid:liquid ratio. Duplicate serial leaching sets were conducted for the reacted SMZ material, but only one serial leaching was performed for the unreacted SMZ. Each leaching set consisted

of 3 g of SMZ in a 50 mL centrifuge tube with 45 mL of SAR. The SAR and SMZ mixture was agitated for 24-h in each leaching cycle. After 24-h agitation, the supernatant solution was separated by centrifugation and filtration for chemical analysis. Then a fresh 45 mL of SAR was added into the tube and kept agitated for each subsequent leaching cycle. The leaching cycle was repeated until concentrations of several analytes fell below the ICP-OES detection limit.

3.2.8. Effectiveness of SMZ treatment

The effectiveness of SMZ in removing an element of interest from the fly ash leachate during batch experiments was determined by calculating the % change (Eq. 1) in in the leachate concentration of that element after the treatment using Eq. (3.1)

$$\%\,\text{change} = \frac{C_{i\_after} - C_{i\_before}}{C_{i\_before}} \times 100 \ldots (3.1)$$

where C_{i_before} and C_{i_after} are concentrations (in mg/L) of an element (i) in the leachate before and after SMZ treatment, respectively.

The effectiveness of the SMZ barrier in attenuating an element from fly ash leachate generated during column experiments was determined by a similar approach. For the column experiments, the effectiveness of SMZ treatment was determined by calculating the cumulative % change in an element's effluent concentration for the SMZ column versus the non-SMZ column. For each element, two cumulative calculations were made: one considering the entire effluent data set and the other including only the effluent data until the crossover point was reached. The crossover point for each element was determined by visually identifying the intersection of the SMZ and non-SMZ column effluent curves after the element peak leaching event(s) for each fly ash. This approach considers that the different elements may have different mechanisms of leaching from the fly ash, transportation through the fly ash and background soil,

and adsorption or exchange at the SMZ–water interface. The different crossover times for different elements, therefore, reflect the consequences of complex and varied processes occurring along the column during leaching, transportation, and treatment. For elements which lacked an apparent intersection of SMZ and non-SMZ effluent curves, it was assumed that the crossover point occurred at the end of the experiments. And for these elements, both cumulative % changes were assumed to be the same. For each element, the cumulatively leached amount was calculated by Eq. (3.2):

$$C_c = \sum\left(\frac{C_{i-1} + C_i}{2} \times \frac{(FR)_{i-1} + (FR)_i}{2} \times \Delta T_i\right) \ldots (3.2)$$

where C_c is the cumulatively leached amount of the element (mg), C_i is the concentration of the element in effluent collected at a sampling event i (mg/L), $(FR)_i$ and $(FR)_{i-1}$ are the flow rates (L/hr) at sampling events i and i–1, respectively, and ΔT_i is the time interval between sampling events i and i–1 (h). Once Cc of an element for non-SMZ and SMZ column effluents (using the complete data set or data until the crossover point) were calculated, the cumulative % change was obtained by Eq. (3.3):

$$\text{Cumulative\% change} = \frac{C_{c-SMZ} - C_{c-nonSMZ}}{C_{c-nonSMZ}} \times 100 \ldots (3.3)$$

where C_{c-SMZ} and $C_{c-nonSMZ}$ are the cumulatively leached amounts of an element from SMZ and non-SMZ columns, respectively. For both treatments, the more negative the % change value for an element, the more effective the SMZ treatment was in removing that element from the leachate.

3.3. Results and discussion

3.3.1. Background soil

The background soil consisted of predominantly quartz (>99%) with traces of chlorite, muscovite, and kaolinite. The soil pH was determined to be 7.11. The soil concentrations (in mg/kg) of As, Cr, B, and Mo were found to be 1.3, 3.0, 26, and 2.8, respectively. Trace element concentrations measured for this soil were within the ranges reported for background soils in Florida (Chen et al., 1999). Similarly, environmentally available concentrations (in mg/kg) of some other elements in the background soil were 26, 152, 1083, 292, 78, and 83, for B, Ca, Fe, Si, K, and Na, respectively.

3.3.2. Fly ash samples

X-ray diffraction analysis of the fly ash samples showed the presence of quartz, mullite, and hematite/maghemite in different proportions. These minerals were reported as common constituents in coal fly ash (Gieré et al., 2003; Hower et al., 1999). Furthermore, significant proportions of the fly ash samples are represented by amorphous materials such as Fe-Al-Si glass spherules and unburned carbon (Külaots et al., 2004; Kutchko and Kim, 2006; Tishmack and Burns, 2004). The carbon contents of these fly ash samples were determined to be 6.74%, 6.37%, 14.7%, and 3.66% for HA, HB, MA, and PD, respectively. Single point BET surface areas for HA, HB, MA, and PD were determined to be 3.18, 2.11, 3.46, and 4.43 m^2/g, respectively.

Aluminum, Ca, and Fe are dominant elements in all of the fly ash samples (Table S3.1). Although PD fly ash is very rich in Ca, no Ca-rich mineral phase was identified. Trace elements such as As, B, Ba, Cr, Cu, Mo, Ni, Pb, Se, Sr, Ti, V, and Zn are also present in varied concentrations in all fly ash samples. Boron is highly enriched in PD, compared to the other fly ash samples. However, As, Co, Cr, Cu, Ni, Pb, and V concentrations are lower in PD than in the

other fly ash samples. In fly ash, more than 50% of the total As, Se, and Zn are concentrated primarily in non-silicate constituents, while minor and major elements (except Ca) are typically associated with silicates (Kim and Kazonich, 2004). Therefore, the total concentrations of minor, major (except Ca), and some trace elements (As, Se, and Zn) could be greater than the amount extracted by partial acid digestion.

3.3.3. Fly ash leachates

All fly ash leachates had different proportions of leachable major, minor and trace elements. Calcium was the dominant element in leachates, followed by K, Na, Mg, Sr, Si, and B (Fig. 3.1). The concentrations of Ca in HA, HB, MA, and PD leachates were 80, 132, 153, and 234 mg/L, respectively. Compared to the acidic fly ash leachates, PD leachate had a two orders of magnitude higher concentration of Al, but two orders of magnitude lower concentration of Mg. In addition, PD leachate was enriched in B and Ba. All fly ash leachates were very rich in sulfate (≥280 mg/L). Trace elements such as As, Co, Cr, Mo, Ni, Sb, Se, V, and Zn were present at various concentrations in fly ash leachates (Fig. 3.1). Geochemical modeling using PHREEQC (Parkhurst and Appelo, 1999) indicates that As, Cr, Mo, Sb, Se and V exist in the leachate solutions as oxyanions. This speciation is also supported by previous studies. Oxyanion-forming trace elements such as As, Sb, Se, and V are reported to exist in different oxidation states in fly ash leachates. Wadge and Hutton (1987) reported that As and Se in fly ash water extracts are mostly in the form of $As_{(V)}$ and $Se_{(IV)}$. Antimony in fly ash leachate was found mostly as $Sb_{(III)}$ by Narukawa et al. (2005); however, Miravet et al. (2006) reported that most of the Sb in acidic fly ash leachate was $Sb_{(V)}$, with only minor amounts of $Sb_{(III)}$. Both $V_{(V)}$ and $V_{(IV)}$ were reported in fly ash leachates (Wang et al., 1995).

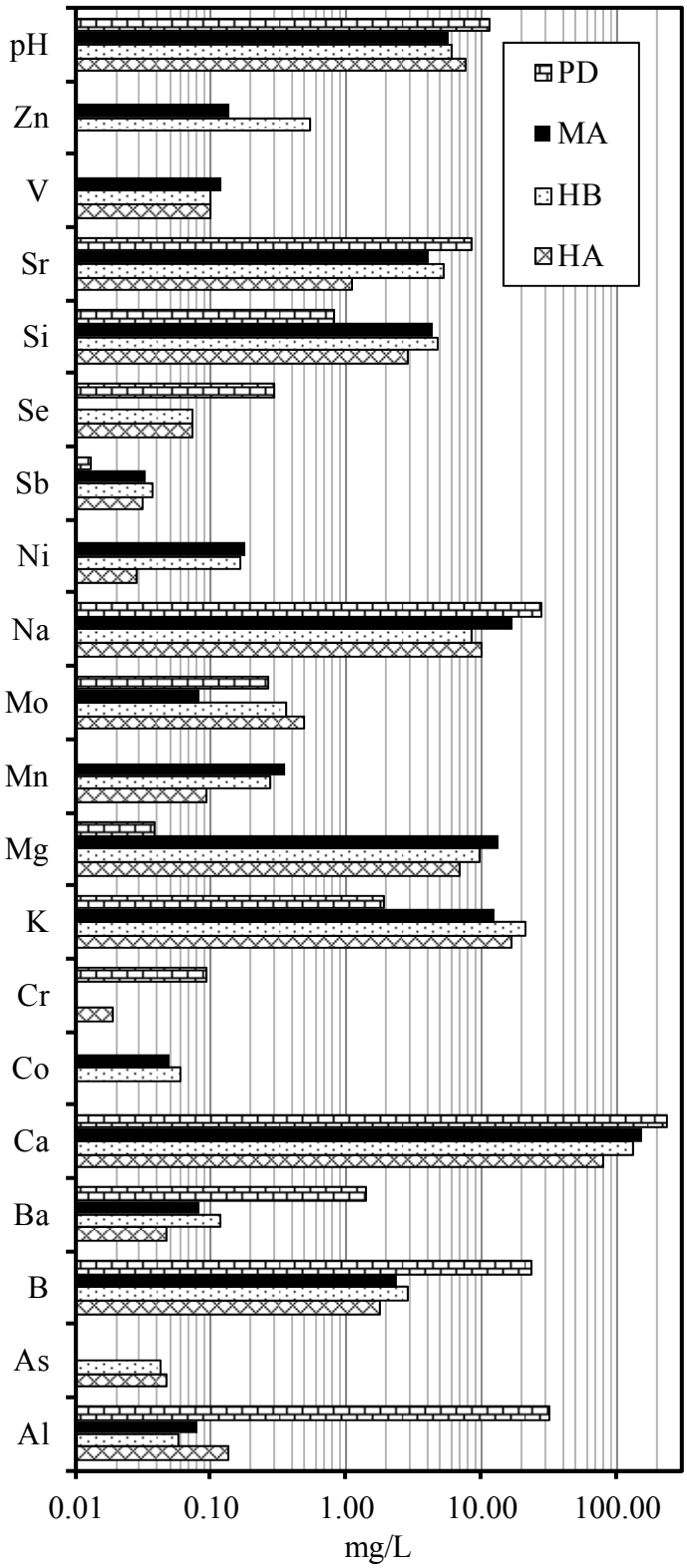

Fig. 3.1. Elemental composition of fly ash leachates

3.3.4. SMZ treatment batch experiments

The concentrations of several trace elements such as As, Cr, Mo, and V in fly ash leachates were decreased after SMZ batch treatments (Figs. 3.2 and Fig. S3.2). The positively charged external surface of SMZ is very conducive for the adsorption of anionic species (Haggerty and Bowman, 1994). Treatment also decreased the leachate concentrations of Al, Ba, Ca, K (except PD), Ni, Sr, and Zn. During surfactant modification, the internal surface charge of the zeolite remains unchanged, as the cationic $HDTMA^+$ is too large to enter the internal structural channelways (Haggerty and Bowman, 1994). Therefore, SMZ retains the ability to adsorb cationic aqueous species, but in diminished amounts (Bhattacharyya, 2010; Li et al., 2006). The SMZ treatment increased the concentration of K, but decreased the amount of Na, in PD leachate (Fig. S3.2). The increased concentrations of Mg, Na (except MA and PD), K (PD only), and Si in leachates after SMZ treatment indicate the occurrence of cation exchange reactions and/or dissolution of zeolite. The concentration of B in leachates was not changed by SMZ treatment. Bhattacharyya (2010) also found that SMZ was not effective in adsorbing B from synthetic leachate, largely due to boron's neutral aqueous species.

In general, increasing amounts of SMZ used during batch treatments resulted in greater reductions in the concentrations of several leachate constituents. Increased removal of elements with increasing SMZ content during treatment was observed for Cd (HB only), Cr, Mo (except MA), and Sr (except HA). However, for other elements (e.g., As, Se, and V), there was no significant improvement in removal of these elements with addition of SMZ in excess of 10%.

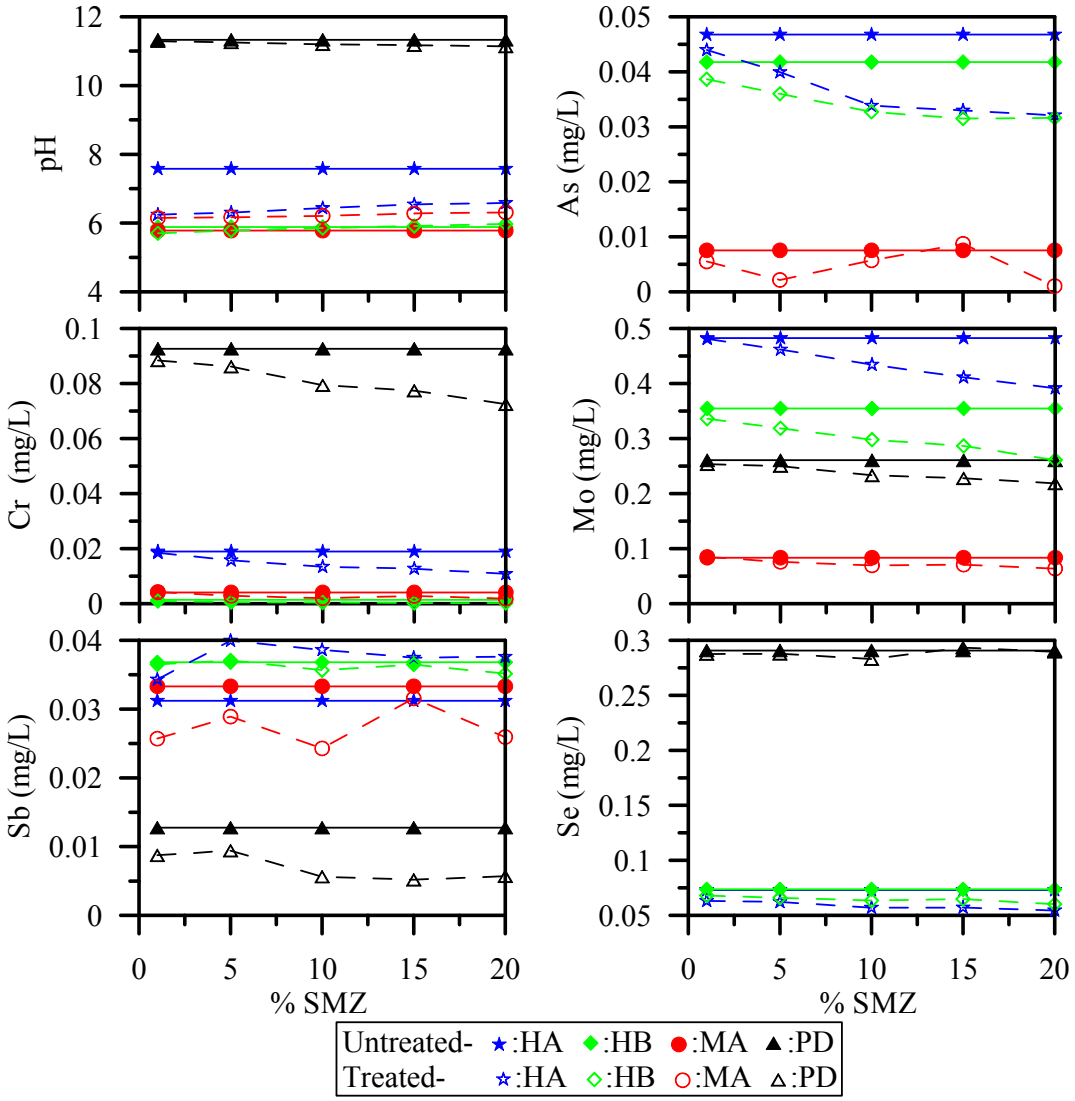

Fig. 3.2. Trace elements in fly ash leachates before and after SMZ treatments

3.3.5. SMZ treatment column experiments

The pH and concentrations of some trace elements in column experiment effluent solutions are shown in Fig. 3.3 (see Fig. S3.3 for other elements). Rapid increase in pH (from <6 to ~6.5) was observed in HA and HA-SMZ effluents. Consistently, effluent pH was higher for column HA-SMZ than for column HA (Fig. 3.3). Effluents from both columns PD and PD-SMZ (Fig. 3.3) showed similar evolution of pH throughout the experiments. Both columns showed an increase in pH from 5.5 to more than 11 over 10 days, followed by a slow decrease for the

remainder of the experiments. In the literature, various pH conditions have been reported as optimum for the adsorption of oxyanions on SMZ. Leyva-Ramos et al. (2008) found an optimum pH of 6 for $Cr_{(VI)}$ adsorption. A lower pH for $Cr_{(VI)}$ adsorption and a circum-neutral pH for $As_{(V)}$ adsorption were suggested as optimum values by Yusof et al. (2008). Other studies, however, have reported a wide range of pH (6–10) over which removal of $As_{(V)}$ and $Cr_{(VI)}$ from solution was effective (Chutia et al., 2009; Leyva-Ramos et al., 2008; Zeng et al., 2010). Such a wide range of working pH would make SMZ a good material to contain trace elements in the environment.

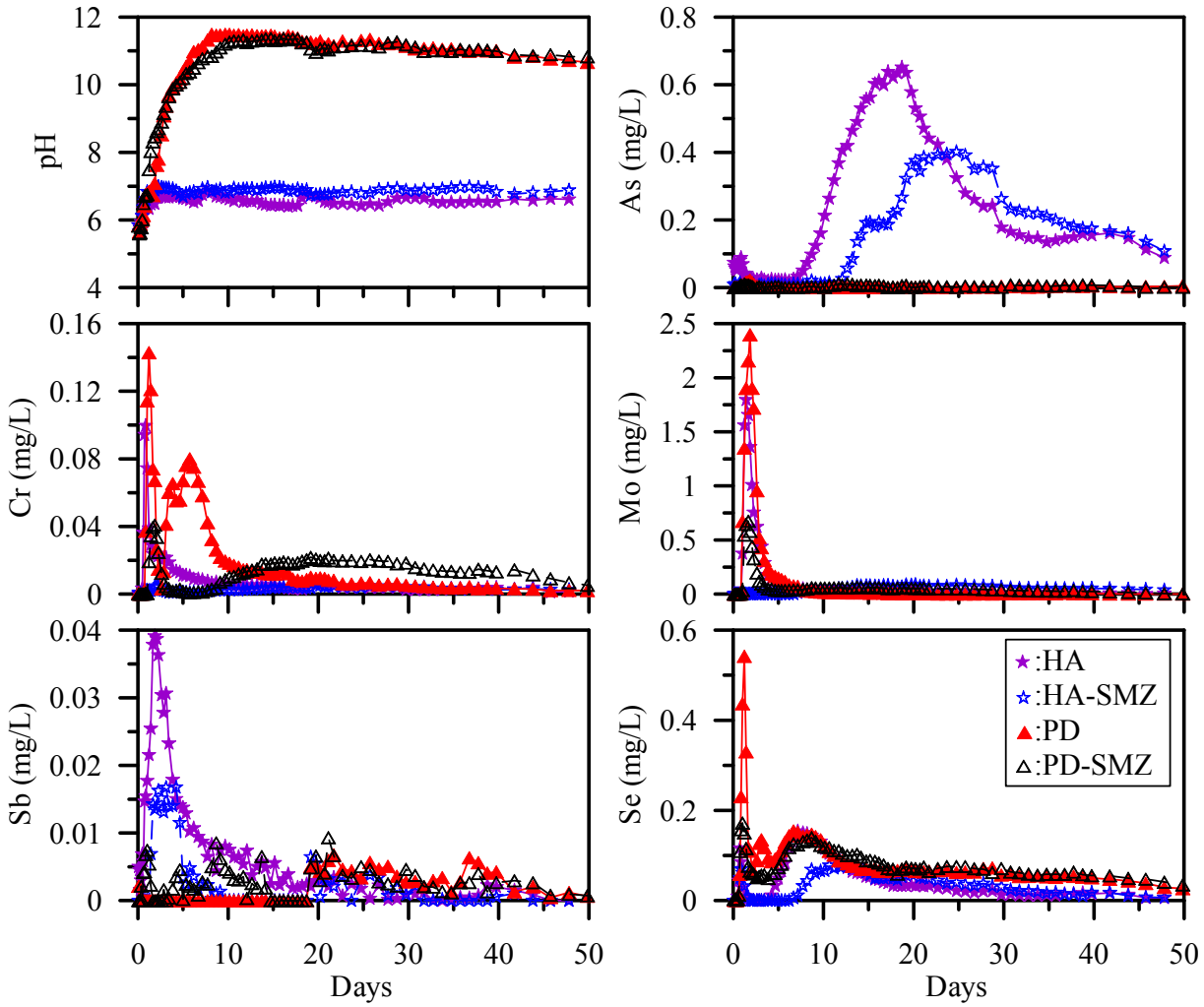

Fig. 3.3. Aqueous compositions of SMZ and non-SMZ column effluents

Fig. 3.3 shows that SMZ treatment decreased and delayed the peak leaching of As, Cr, Mo, Sb, Se, and V from column HA-SMZ compared to column HA. Of these elements, reductions in the concentrations of Cr, Mo, and Se were very significant. The SMZ treatment of PD fly ash helped decrease the peak leaching concentrations of As, Cr, Mo, and Se (Fig. 3.3). Three different mechanisms: precipitation, surface anion exchange reactions, and Lewis acid-base interactions have been proposed for SMZ sequestration of oxyanions from aqueous solutions (Chutia et al., 2009; Haggerty and Bowman, 1994; Li et al., 1997; Sullivan et al., 1997, 1998, 2003; Wingenfelder et al., 2006). Of these mechanisms, surface anion exchange reactions could be at work during SMZ treatments, and the decreased removal of these oxyanion elements from the leachate (e.g., Cr from PD-SMZ column) with time could have resulted from the saturation of such exchange sites.

Peak effluent concentrations of Ba, K, and Na were also decreased for column HA-SMZ (Fig. S3.3). However, some elements, such as Al, Mn, Si, Sr, and Zn, were leached more from column HA-SMZ than from column HA (Fig. S3.3). Boron, Ca, and Mg were leached in similar amounts from both columns. The peak effluent concentrations of some other elements, such as Al, B, Na, Sr, V, and Zn, were lower for column PD-SMZ than for column PD (Fig. S3.3). However, peak effluent concentrations of Ca, K, Mg, Mn, and Si were higher for column PD-SMZ than for column PD.

Fly ash has been reported to have some adsorption capacity for trace elements (Bhattacharyya, 2010), and it has also been tested as a remediation material for stabilization and solidification of heavy metals in contaminated soils (Dermatas and Meng, 2003). Bhattacharyya (2010) performed several sorption experiments using both weathered and fresh fly ash samples to determine their ability to sequester trace elements. Although fresh HB, MA, and PD fly ashes

were reported to have some sorption capacities for As, V, Mo, Ni, and Sr, their weathered counterparts had very limited sorption capacity for these elements (Bhattacharyya, 2010). Therefore, the sorption ability of fly ash cannot be relied upon to contain its labile fraction of trace elements over long time periods. Moreover, it is likely that the decreased sorption capacity of weathered fly ash would consequently result in an enhanced mobilization of trace elements, particularly from old fly ash disposal facilities. Some previous studies have also suggested that weathering processes could result in the formation of secondary minerals that would help sequester trace elements by precipitation, adsorption, and co-precipitation (Donahoe, 2004). But no new minerals were detected in the reacted fly ash at the end of the column experiments.

3.3.6. Effectiveness of SMZ treatments of fly ash leachates

Fig. 3.4 shows the % change in concentration of selected elements in fly ash leachates after the SMZ batch treatments (see Table S3.2 for all other elements). Both cationic and anionic aqueous species present in fly ash leachates were removed to different extents by SMZ. Larger amounts of SMZ resulted in higher removal of several trace elements from fly ash leachates during batch treatment experiments. For example, 10% SMZ treatment reduced the concentration of As by 28%, 22%, and 24% in HA, HB, and MA fly ash leachates, respectively. For HA, HB, MA, and PD fly ash leachates, 10% SMZ treatment decreased the concentration of Cr by 29%, 69%, 51%, and 14%, respectively. Similarly, leachate concentrations of Mo, Ni, Se, Sr, and V were decreased up to 16%, 15%, 22%, 15%, and 13%, respectively, by 10% SMZ treatments. Bhattacharyya (2010) also showed significant removal V, Mo, and Cr over As and Se by SMZ from a synthetic fly ash leachate solution.

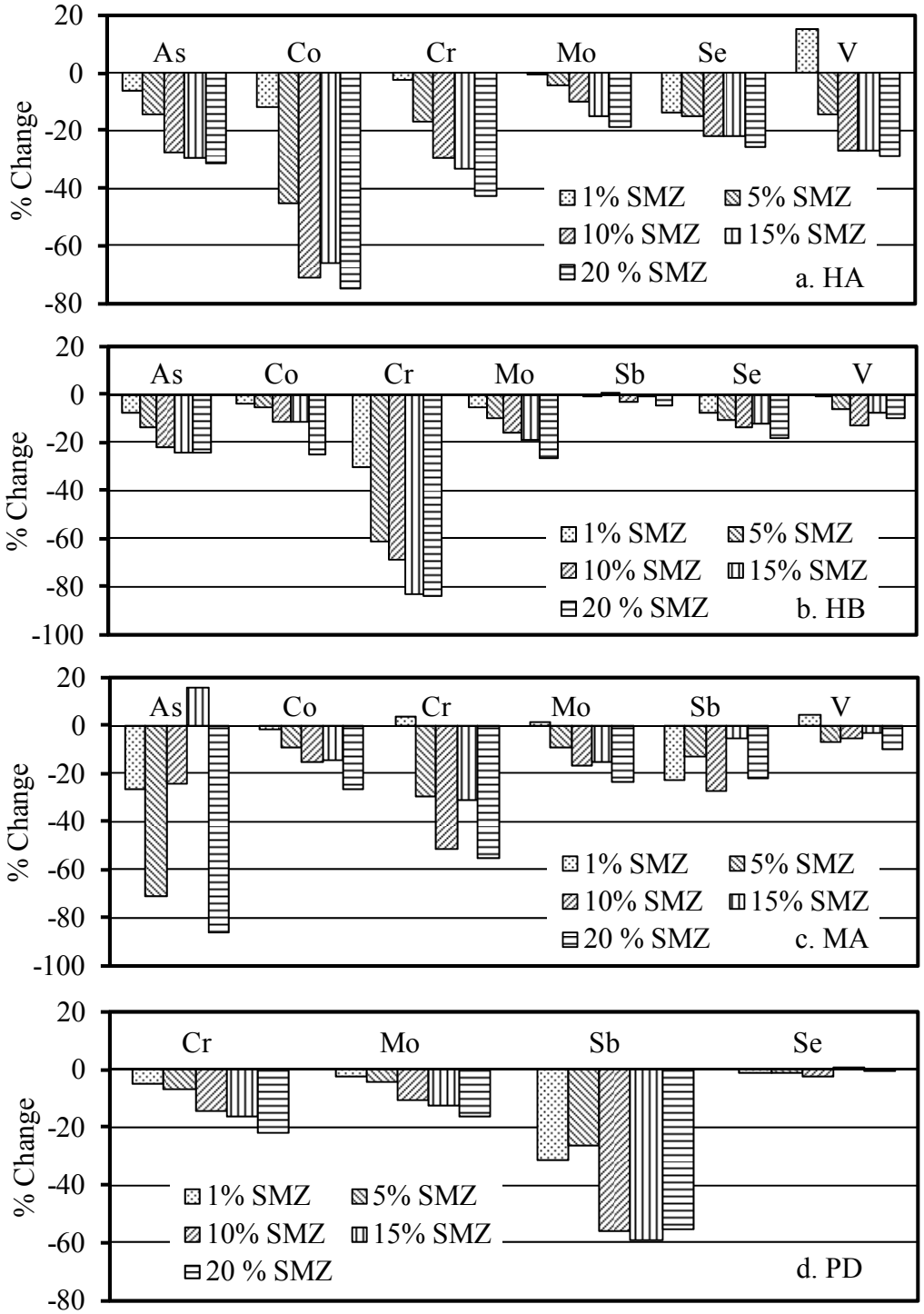

Fig. 3.4. Percentage change in element concentrations in leachates after SMZ treatments

Fig. 3.5 shows the cumulative % change in mobility of some elements during column experiments (see Table S3 for other elements). For column HA-SMZ, the mobility of As, Cr, Mo, Sb, Se, and V were decreased by 20%, 42%, 16%, 55%, 10%, and 62%, respectively, compared to column HA. Until the crossover point, the mobilities of As, Cr, Mo, Se, and V were decreased by an even greater extent: 53%, 81%, 98%, 50%, and 71%, respectively. Previously, Bowman et al. (1999) demonstrated the ability of SMZ-based PRBs to remove oxyanions from contaminated groundwater. In contrast, the treatment results of PD fly ash in column experiments were not very conclusive. Cumulatively, more As, Cr, Mo, and Sb leached over the course of the experiments from column PD-SMZ than from column PD. However, until the crossover point, 25%, 78%, and 64% less As, Cr, and Mo, respectively, were leached from column PD-SMZ. The mobilities of Se and V were decreased in column PD-SMZ effluent, but 11% higher Sb was leached from this column (Fig. 3.5). The SMZ treatment was ineffective in attenuating B from HA leachate; however, it immobilized 18% of B in PD leachate until the crossover point. At higher pH, negatively charged 'borate' is the dominant aqueous species of B, while at lower pH, neutral boric acid is the dominant aqueous species (Woods, 1994). The SMZ likely adsorbed the borate anion from the high pH PD leachate but not the neutral boric acid species from the low-pH HA leachate. Bhattacharyya (2010) also reported poor sorption of B on SMZ at pH 4 through 7.

Furthermore, the presence of competing co-ions can hinder the adsorption of desirable species from the leachates. The fly ash leachates were enriched in sulfate which could compete with other oxyanion-forming trace elements during batch and column treatment experiments. However, as noted above, the gradual increase in concentration of some trace elements in column SMZ effluents after the crossover was more likely related to saturation of SMZ external

adsorption sites rather than sulfate-induced competitive displacement, because sulfate concentrations in column effluents peaked and tailed off early in the experiments. In addition, the adsorption kinetics of sulfate has been reported to be very slow compared to other species (Vujaković et al., 2000).

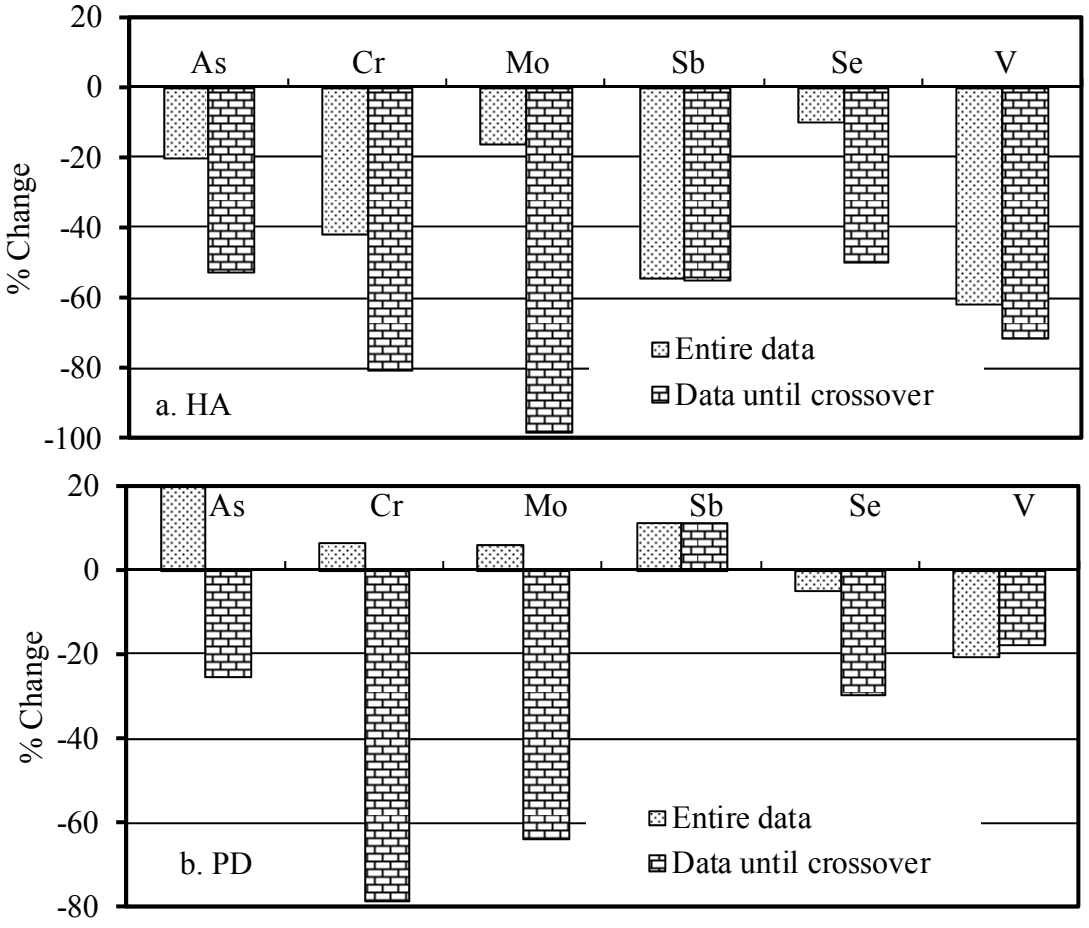

Fig. 3.5. Cumulative % change in element concentrations in effluents from SMZ columns

3.3.7. Stability of reacted SMZ

Fig. 6 shows pH and some trace elements mobilized during SAR serial leaching of reacted and fresh SMZs (see Fig. S3.4 for other elements). Leachate produced by reacted SMZ from column PD-SMZ had higher pH than the other two leachates; however, all of these

materials showed an overall decrease in leachate pH with progressive leaching cycles. Mobilizations of several elements from reacted SMZs were negligible, particularly after early leaching cycles. Steady leaching of Si was observed for reacted and fresh SMZ materials; particularly, after the first 1–2 leaching cycles (Fig. S3.4). Furthermore, the stability of HDTMA bound to zeolite has been reported to be very high, remaining intact even after multiple washings with high ionic-strength solutions at both high- and low-pH conditions (Li et al. 1997). Li et al. (1997) also reported a strong resistance of SMZ to biodegradation.

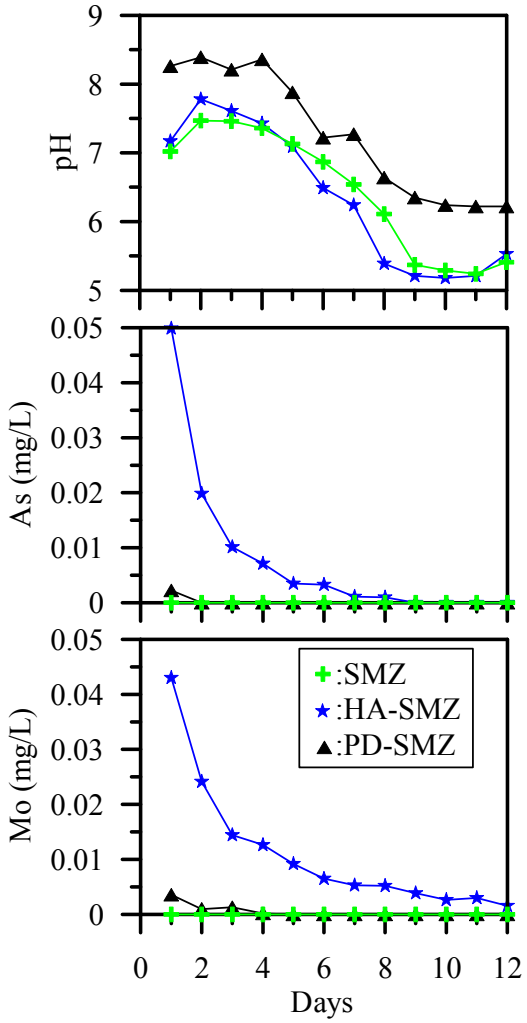

Fig. 3.6. pH and As mobilized during serial SAR leaching of SMZs

3.4. Summary and conclusions

Fly ash contains significant amounts of environmentally available and leachable trace elements which are potentially hazardous to the environment and to human health. Therefore, older unlined fly ash disposal facilities may pose a risk of contamination to the environment. Surfactant-modified zeolite (SMZ) has the potential to sequester both cationic and anionic trace elements from aqueous solutions, but has not previously been tested for remediation of trace elements in fly ash leachate. Bench-scale batch and column fly ash leachate treatment experiments performed to test the ability of SMZ to remediate trace elements in fly ash leachates showed its potential application as a PRB material for controlling the dispersion of trace elements from fly ash disposal facilities. Rapid adsorption kinetics also supports the application of SMZ as a PRB material.

The SMZ treatment batch experiments decreased trace element concentrations in leachate generated from acidic and alkaline fly ash samples. Up to 30% of the As, Mo, and V; up to 80% of the Cr; and up to 20% of the Se and Sr were removed from the fly ash leachates after batch treatment experiments with 10% SMZ. Similarly, SMZ treatment delayed the peak leaching events of several trace elements, and it also decreased the total leachate trace element concentrations in column effluent solutions. Elements with dominant oxyanion species (e.g., As, Cr, Se, Mo, etc.) were attenuated in greater proportions. Before the crossover point, more than 50% of the As, Se, and Sb; 80% of the Cr; 95% of the Mo; and 70% of the V were decreased in the effluent from column HA-SMZ compared to column HA effluents. Similarly, effluent from column PD-SMZ had less than 79% of the Cr, 64% of the Mo, 29% of the Se, and 59% of the Sr compared to effluent from column PD. However, the effectiveness of SMZ treatment for

immobilizing trace elements in fly ash leachate diminished after the crossover point, indicating a relatively short effective lifetime of a SMZ PRB in the ash disposal environment.

Acknowledgements

This research was supported in part by funding from the Electric Power Research Institute and Southern Company Services, Inc. The author would like to thank E.Y. Graham, S. Bhattacharyya, Z. Yue, and B. E. Hollon for their help with analytical and laboratory work. Suggestions from Dr. J. Abedi-Koupai and two other anonymous reviewers were helpful in revising the original manuscript.

REFERENCES

American Coal Ash Association (2011) Coal combustion product (CCP) production & use survey results. American Coal Ash Association, http://www.acaa-usa.org, p. 1.

Auer, S., Kuzel, H.J., Pöllmann, H., and Sorrentino, F. (1995) Investigation on MSW fly ash treatment by reactive calcium aluminates and phases formed. Cement and Concrete Research 25, 1347-1359.

Bhattacharyya, S., Donahoe, R.J., and Patel, D. (2009) Experimental study of chemical treatment of coal fly ash to reduce the mobility of priority trace elements. Fuel 88, 1173-1184.

Bhattacharyya, S. (2010) Investigation of natural weathering processes and artificial treatment techniques in the attenuation of toxic metals from coal fly ash. Doctoral Dissertation, The University of Alabama, p. 255.

Bournonville, B., Nzihou A., Sharrock, P., and Depelsenaire, G. (2004) Stabilization of heavy metal containing dusts by reaction with phosphoric acid: study of the reactivity of fly ash. J. Haz. Mater. 116, 65-74.

Bowman, R.S. (1996) Surfactant-altered zeolites as permeable barriers for in situ treatment of contaminated groundwater, In: Proc. Industry Partnerships to Deploy Environmental Technology Meeting, Morgantown, WV, p. 41.

Bowman, R. S., Li, Z., Roy, S. J., Burt, T., Johnson, T.L., and Johnson, R.L. (1999) Surface-altered zeolites as permeable barriers for in situ treatment of contaminated groundwater.

Phase II Topical Report DE-AR21-95MC32108, U.S. Dept. of Energy, Pittsburgh, Pennsylvania, p. 58.

Bowman, R.S. (2003) Review: Applications of surfactant-modified zeolites to environmental remediation. Microporous and Mesoporous Materials 61, 43-56.

Campos, V. and Buchler, P.M. (2007) Anionic sorption onto modified natural zeolites using chemical activation. Environ. Geol. 52, 1187-1192.

Chen, M., Ma, L.Q., and Harris, W.G. (1999) Baseline concentrations of 15 trace elements in Florida surface soils, J. Environ. Qual. 28, 1173-1181.

Chutia, P., Kato, S., Kojima, T., and Satokawa, S. (2009) Adsorption of As(V) on surfactant-modified natural zeolites. J. Hazard. Mater. 162, 204-211.

Cordoves, A.I.P., Valdés, M.G., Fernández, J.C.T., Luis, G.P., García-Calzón, J.A., García, M.E.D. (2008) Characterization of the binding site affinity distribution of a surfactant-modified clinoptilolite. Microporous and Mesoporous Materials 109, 38-48.

Crannell, B.S., Eighmy, T.T., Krzanowski, J.E., Eusden, J.D. Jr., Shaw, E.L., Francis, C.A. (2000) Heavy metal stabilization in municipal solid waste combustion bottom ash using soluble phosphate. Waste Management 20, 136-148.

Derie, R. (1996) A new way to stabilize fly ash from municipal incinerators. Waste Management 16, 711-716.

Dermatas, D. and Meng, X. (2003) Utilization of fly ash for stabilization/solidification of heavy metal contaminated soils. Eng. Geol. 70, 377-394.

Donahoe, R.J., 2004. Secondary mineral formation in coal combustion byproduct disposal facilities: implications for trace element sequestration. In: Gieré, R. & Stille, P. (eds) Energy, waste and the environment: a geochemical perspective, Geological Society of London, Special Publications, 236, 641-658.

Donahoe, R.J., Bhattacharyya, S. and Ladwig, K.J. (2007) Chemical fixation of trace elements in coal fly ash. University of Kentucky Center for Applied Energy Research, Ash Library, http://www.flyash.info, p. 17.

Ghiaci, M., Kia, R., Abbaspur, A., and Seyedeyn-Azad, F. (2004) Adsorption of chromate by surfactant-modified zeolites and MCM-41 molecular sieve. Separation and Purification Technology 40, 285-295.

Gieré, R., Carleton, L.E. and Lumpkin, G.R. (2003) Micro- and nanochemistry of fly ash from a coal-fired power plant, Am. Min. 88, 1853-1865.

Haggerty, G.M. and Bowman, R.S. (1994) Sorption of chromate and other inorganic anions by organo-zeolite. Environ. Sci. & Technology 28, 452-458.

Hassett, D.H. and Eylands, K.E. (1999) Mercury capture on coal combustion fly ash. Fuel 78, 243-248.

Hower, J.C., Rathbone, R.F., Robertson, J.D., Peterson, G., and Trimble, A.S. (1999) Petrology, mineralogy, and chemistry of magnetically-separated sized fly ash, Fuel 78, 197-203.

Kalyoncu, R.S. (2000) Coal combustion products. US Geological Service Minerals Yearbook-2001.

Kim, A.G. and Kazonich, G. (2004) The Silicate-non-silicate distribution of metals in fly ash and its effect on solubility, Fuel 83, 2285-92.

Külaots, I., Hurt, R.H. and Suuberg, E.M. (2004) Size distribution of unburned carbon in coal fly ash and its implications. Fuel 83, 223-230.

Kutchko, B.G. and Kim, A.G. (2006) Fly ash characterization by SEM-EDS, Fuel 85, 2537-2544.

Leppert, D. (1990) Heavy metal sorption with clinoptilolite zeolite: alternatives for treating contaminated soil and water. Mining Engineering 42, 604-608.

Leyva-Ramos, R., Jacobo-Azuara, A., Diaz-Flores,P.E., Guerrero-Coronado, R.M., Mendoza-Barron, J., and Berber-Mendoza, M.S. (2008) Adsorption of chromium(VI) from an aqueous solution on a surfactant-modified zeolite, Colloids and Surfaces A: Physicochem. Eng. Aspects 330, 35–41.

Li, Z. and Bowman, R.S. (1997) Counterion effects on the sorption of cationic surfactant and chromate on natural clinoptilolite. Environ. Sci. Technol. 31, 2407-2412.

Li, Z., Roy, S. J., Zou, Y. and Bowman, R.S. (1998) Long-term chemical and biological stability of surfactant-modified zeolite. Environ. Sci. Technol. 32, 2628-2632.

Li, Z., Alessi, D., and Allen, L. (2002) Influence of cationic surfactant on the sorption of metal cations on zeolite. J. Environ. Qual. 31, 1106-1114.

Majdan, M., Pikus, S., Rzączyńska, Z., Iwan, M., Maryuk, O., Kwiatkowski, R., Skrzypek, H. (2006). Characteristics of chabazite modified by hexadecyltrimethylammonium bromide and of its affinity toward chromates. Journal of Molecular Structure 791, 53-60.

Miravet, R., López-Sánchez, J.F., and Rubio, R. (2006) Leachability and analytical speciation of antimony in coal fly ash, Anal. Chim. Acta 576, 200-206.

Narukawa, T., Takatsu, A., Chiba, K., Riley, K.W., and French, D.H. (2005) Investigation on chemical species of arsenic, selenium and antimony in fly ash from coal fuel thermal power stations, J. Environ. Monit. 7, 1342-1348.

Newsam, J.M. (1986) The zeolite cage structure. Science 231, 1093-1099.

Parkhurst, D.L. and Appelo, C.A.J. (1999) User's guide to PHREEQC (Version 2)-A computer program for speciation, batch-reaction, one-dimensional transport, and inverse geochemical calculations. U.S. Geol. Surv., Water Resour. Invest. Rep. 99-4259, 326 p.

Ranck, J.M. , Bowman, R.S., Weeber, J.L., Katz, L.E., and Sullivan, E.J. (2005) BTEX removal from produced water using surfactant-modified zeolite, J. Environ. Eng. 131, 434-442.

Sullivan, E.J., Hunter, D.B., and Bowman, R.S. (1997) Topological and thermal properties of surfactant-modified clinoptilolite studied by tapping-mode™ atomic force microscopy and high-resolution thermogravimetric analysis. Clays and Clay Minerals 45, 42-53.

Sullivan, E.J., Hunter, D.B., and Bowman, R.S. (1998) Fourier Transform Raman spectroscopy of sorbed HDTMA and the mechanism of chromate sorption to surfactant-modified clinoptilolite. Environ. Sci. Technol. 32, 1948-1955.

Sulivan E.J., Bowman, R.S., and Legiec, I.A. (2003) Sorption of arsenic from soil-washing leachate by surfactant-modified zeolite. J. Environ. Qual. 32, 2387-2391.

Tishmack, T.K. and Burns, P.E. (2004) The chemistry and mineralogy of coal and coal combustion products, in: R. Gieré, P. Stille (Eds.), Energy, waste and the environment: a geochemical perspective: Geological Society of London, Special Publications 236, London, pp. 223-246.

USEPA (1994) Method 1312: Synthetic precipitation leaching procedure. Revision 0, November 1994, US Environmental Protection Agency, USA, p. 30.

USEPA (2004) Method 9045D: Soil and waste pH. Revision 4, November 2004, US Environmental Protection Agency, USA, p. 5.

USEPA (2007) Method 3051A: Microwave-assisted acid digestion of sediments, sludges, soils and oils. Revision 1, February 2007, US Environmental Protection Agency, USA, p. 30.

Vujaković, A.D., Tomašević-Čanović, M.R., Daković, A.S., and Dondur, V.T. (2000). The adsorption of sulphate, hydrogenchromate and dihydrogenphLosphate anions on surfactant-modified clinoptilolite. Applied Clay Science 17, 265-277.

Wadge, A., and Hutton, M. (1987) The leachability and chemical speciation of selected trace elements in fly ash from coal combustion and refuse incineration, Environ. Pollution 48, 85-99.

Wang, J., Tomlinson, M.J., and Caruso, J.A. (1995) Extraction of trace elements in coal fly ash and subsequent speciation by high-performance liquid chromatography with inductively coupled plasma mass spectrometry, J. Anal. Atom. Spectrom. 10, 601-607.

Warchoł, J., Misaelides, P., Petrus, R., and Zamboulis, D. (2006) Preparation and application of organo-modified zeolitic material in the removal of chromates and iodides. J. Hazard. Mater. 137, 1410-1416.

Wingenfelder, U., Furrer, G., and Schulin, R. (2006) Sorption of antimonate by HDTMA-modified zeolite. Micropor. Mesopor. Mat. 95, 265-271.

Woods, W.G. (1994) An introduction to boron: history, sources, uses, and chemistry. Environ. Health Persp. 102, 5-11.

Yang, L., Donahoe, R.J., Redwine, J.C. (2007) In situ chemical fixation of arsenic-contaminated soils: An experimental study. Sci. Total Environ. 387, 28-41.

Yusof, A.M. and Malek, N.A.N.N. (2008) Removal of Cr(VI) and As(V) from aqueous solutions by HDTMA-modified zeolite Y. J. Hazard. Mater. 162, 1019-1024.

Zeng, Y., Woo, H., Lee, G., and Park, J. (2010) Removal of chromate from water using surfactant modified Pohang clinoptilolite and Haruna chabazite. Desalination 257, 102-109.

SUPPLEMENTARY MATERIAL FOR CHAPTER – 3

ATTENUATION OF TRACE ELEMENTS IN COAL FLY ASH LEACHATES BY SURFACTANT-MODIFIED ZEOLITE

The following supporting materials are provided for Chapter – 3:

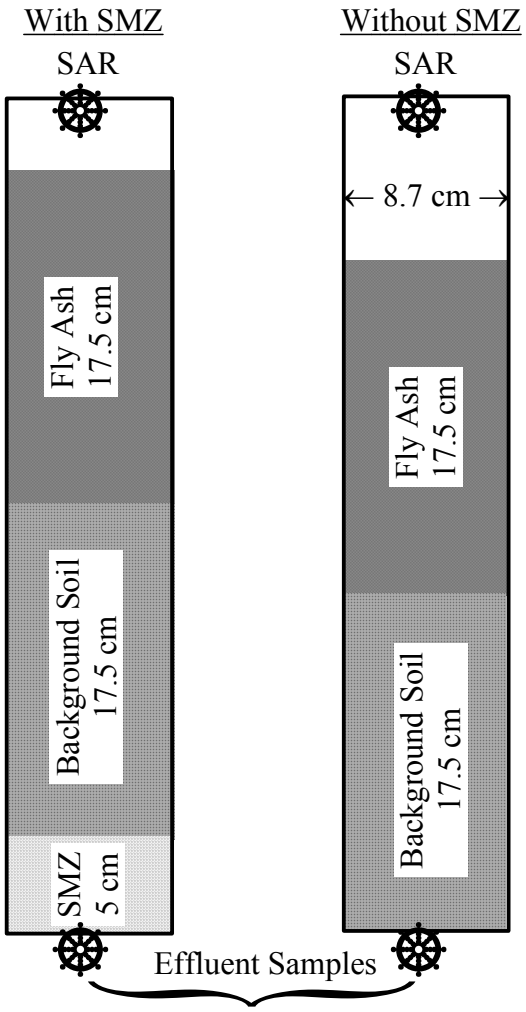

Fig. S3.1. Schematic diagram showing SMZ and non-SMZ column experiments

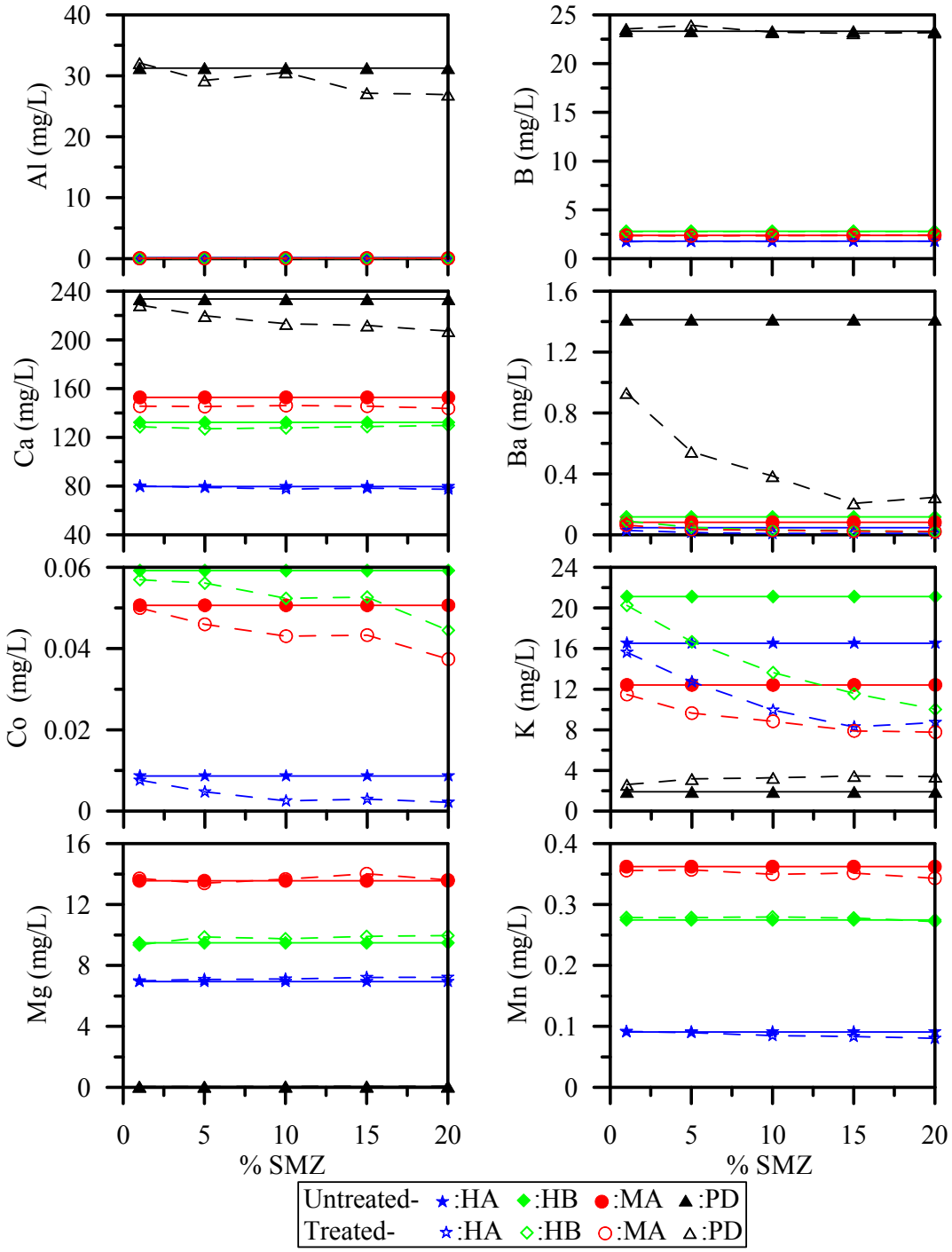

Fig. S3.2. Fly ash leachate compositions before and after SMZ treatment batch experiments

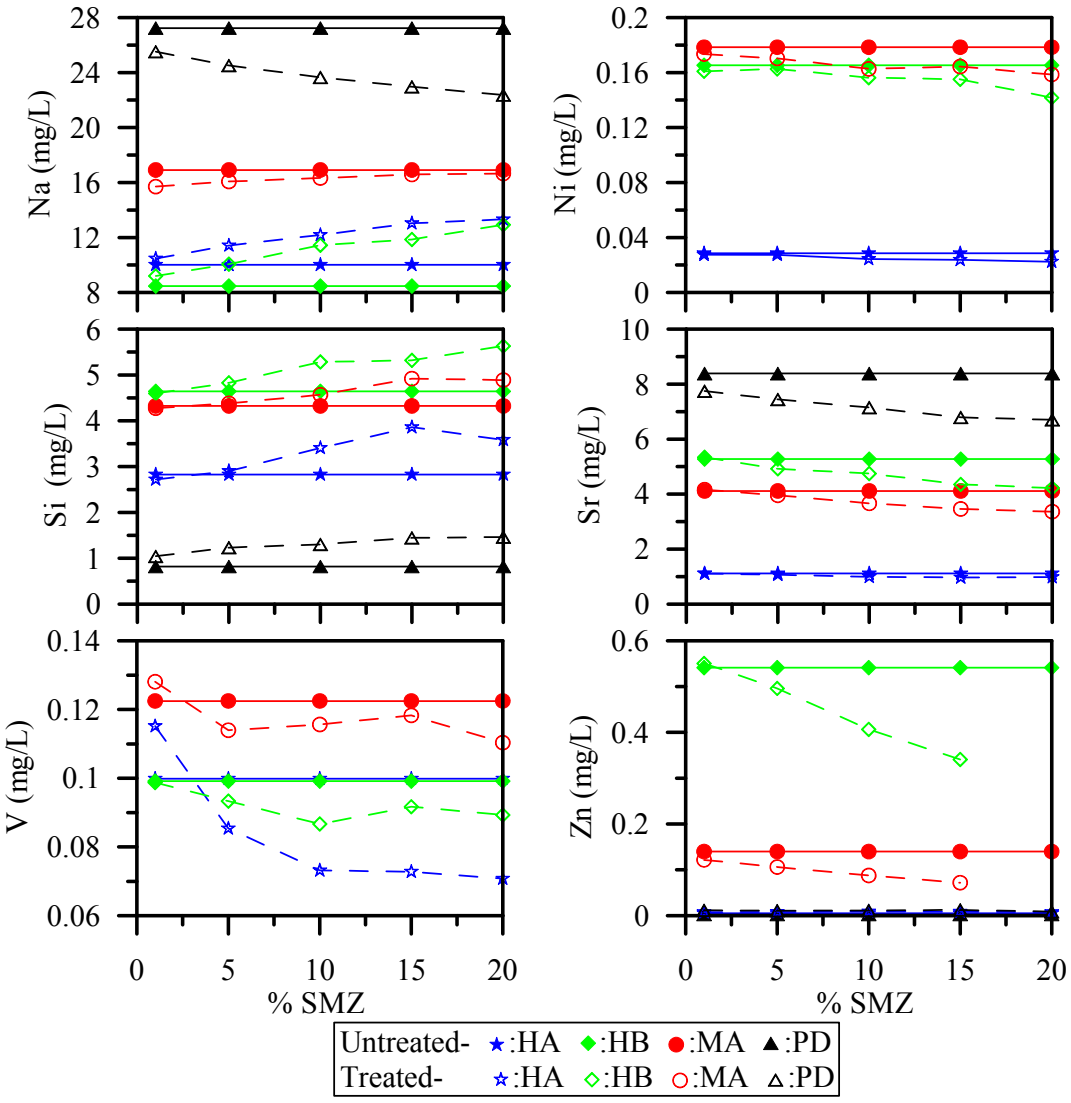

Fig. S3.2. Fly ash leachate compositions before and after SMZ treatment batch experiments

(contd…)

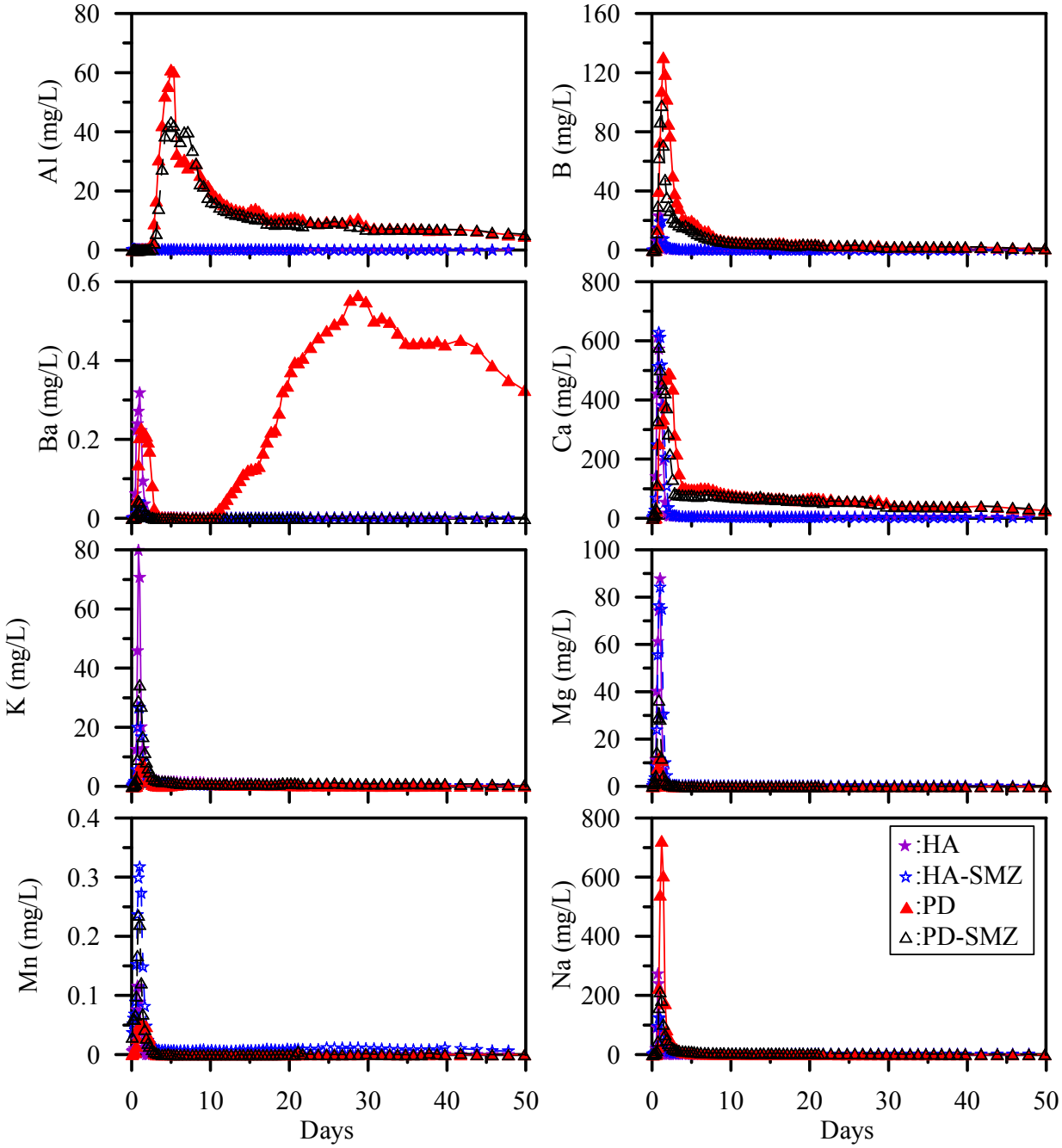

Fig. S3.3. Effluent pH and elemental compositions of SMZ and non-SMZ column experiments

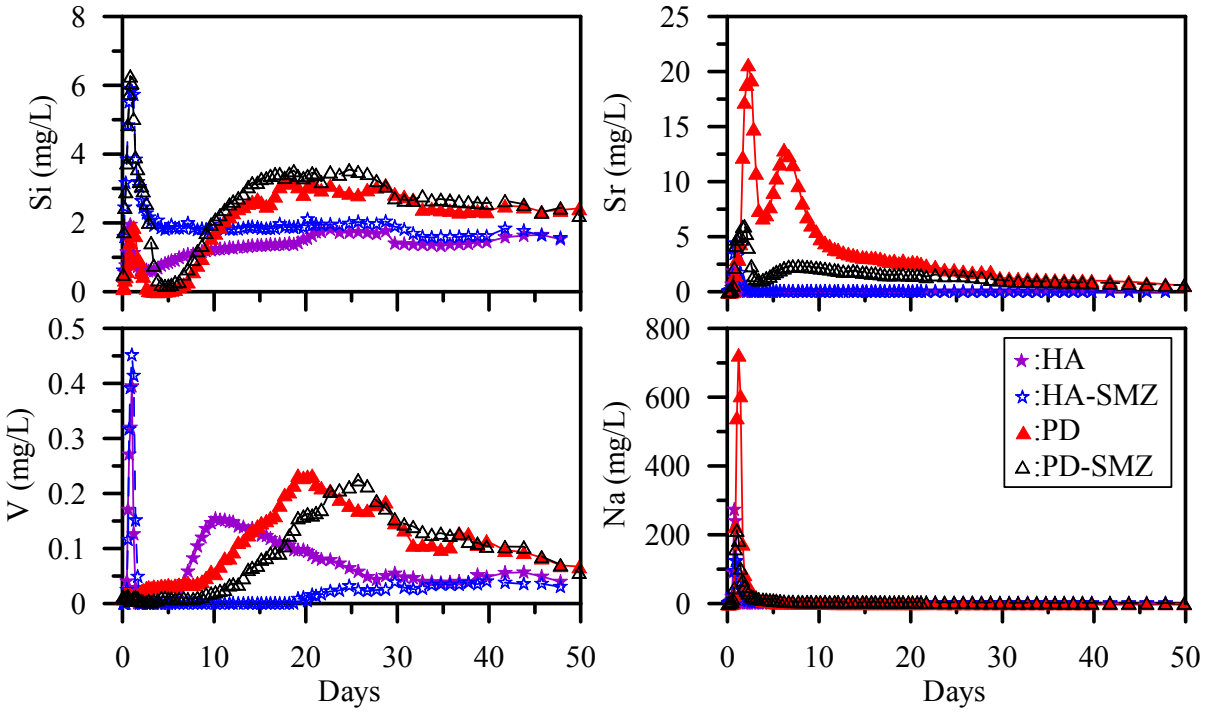

Fig. S3.3. Effluent pH and elemental compositions of SMZ and non-SMZ column experiments

(contd)

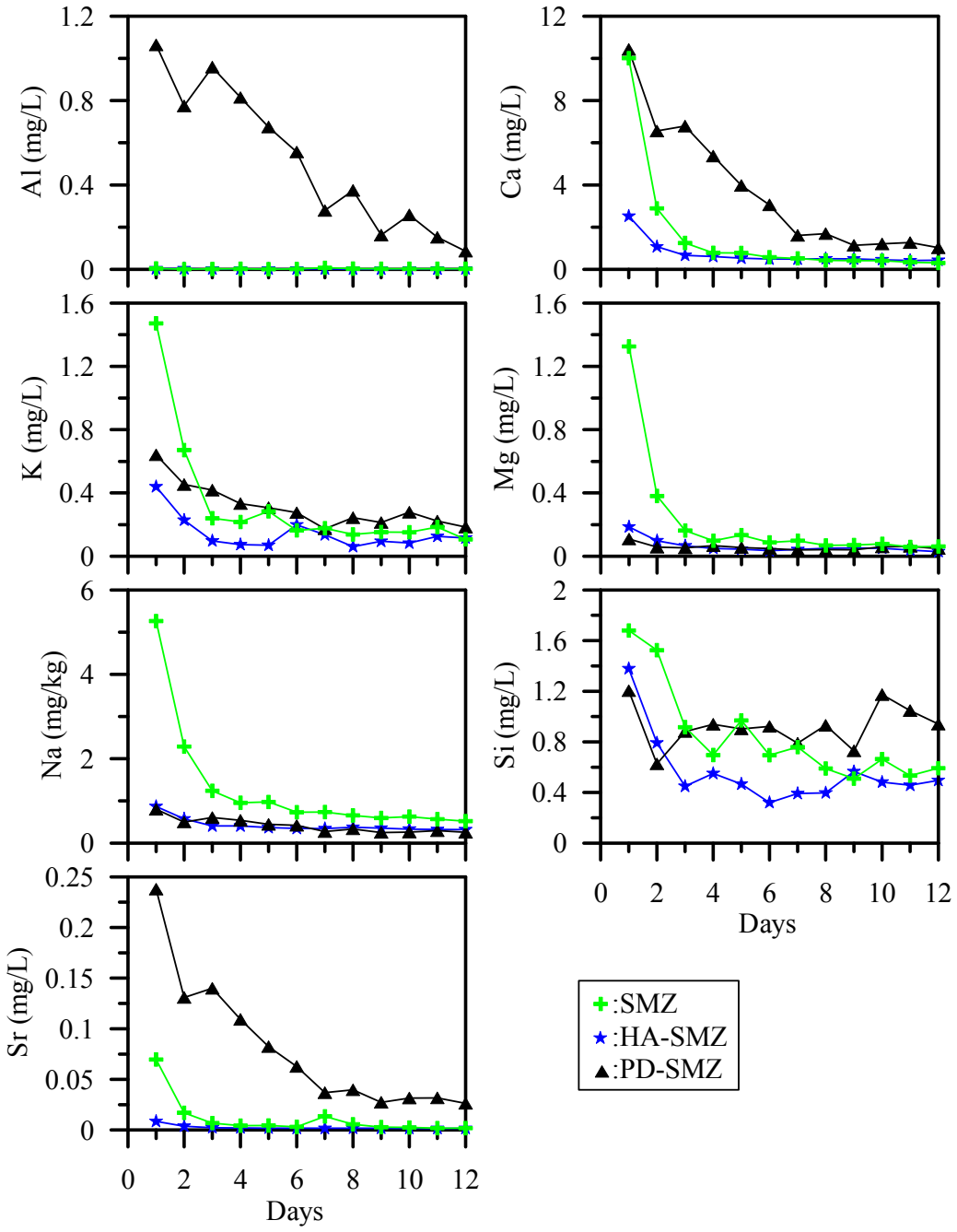

Fig. S3.4. Additional elements mobilized during serial SAR batch leaching of SMZs

Table S3.1. Environmentally available elemental composition of fly ashes (mg/kg)

Elements	HA	HB	MA	PD	LOD[a]
Al	21,800	14,010	9,310	19,210	0.001
As	82	167	158	17	0.006
B	166	168	117	903	0.077
Ba	312	246	316	217	0.002
Ca	4,860	7,580	5,730	32,350	0.015
Co	19	17	13	4.6	0.004
Cr	50	52	30	18	0.002
Cu	73	79	63	23	0.001
Fe	19,590	18,310	12,110	16,140	0.003
K	3,160	1,690	1,570	638	0.077
Mg	1,890	1,300	1,130	5,060	0.001
Mn	74	45	71	62	0.001
Mo	13	20	12	5.4	0.001
Na	722	460	616	1910	0.009
Ni	37	38	34	7.5	0.003
Pb	27	28	24	12	0.005
Sb	3.7	3.5	2.7	1.5	0.007
Se	7.7	23	14	12	0.002
Si	7,290	2,180	3,880	3,110	0.015
Sr	287	557	317	538	0.001
Ti	713	634	615	579	0.010
V	103	121	90	56	0.019
Zn	67	89	103	69	0.001

[a]ICP-OES level of detection values in mg/L

Table S3.2. Percentage change in element concentrations in fly ash leachates after SMZ treatment

	% change																		
% SMZ	Al	As	B	Ba	Ca	Co	Cr	K	Mg	Mn	Mo	Na	Ni	Sb	Se	Si	Sr	V	Zn
HA																			
1	-84	-6	-3	-38	0	-12	-3	-5	1	1	0	5	-4	10	-13	-4	0	15	
5	-88	-15	-2	-67	-1	-45	-17	-23	2	-1	-4	14	-4	28	-15	3	-4	-14	
10	-87	-28	-2	-81	-2	-71	-29	-40	2	-7	-10	22	-15	24	-22	20	-11	-27	
15	-84	-29	0	-77	-2	-66	-33	-50	4	-8	-15	30	-17	20	-22	36	-13	-27	
20	-88	-31	0	-82	-3	-75	-43	-47	4	-12	-19	33	-21	21	-25	27	-12	-29	
HB																			
1	-49	-7	-1	-23	-3	-4	-30	-4	-1	1	-5	9	-3	-1	-8	-1	1	0	2
5	-72	-14	-1	-59	-4	-5	-61	-21	4	1	-10	19	-2	1	-10	4	-7	-6	-8
10	-70	-22	-1	-73	-3	-12	-69	-35	3	2	-16	35	-5	-3	-14	14	-10	-13	-25
15	-64	-25	-1	-76	-3	-11	-83	-45	5	1	-19	40	-6	-1	-12	15	-17	-8	-37
20	-70	-24	0	-84	-2	-25	-84	-53	5	-1	-26	53	-14	-5	-18	21	-20	-10	-49
MA																			
1	-72	-27	-1	-23	-5	-1	4	-8	1	-2	1	-7	-3	-23		-1	1	5	-13
5	-82	-71	-3	-58	-5	-9	-30	-22	-1	-1	-9	-5	-5	-13		1	-4	-7	-24
10	-83	-24	-1	-64	-4	-15	-51	-29	1	-3	-17	-3	-9	-27		6	-11	-6	-37
15	-78	16	0	-70	-5	-15	-31	-36	3	-3	-15	-2	-8	-5		14	-16	-3	-49
20	-78	-86	0	-74	-6	-26	-55	-37	0	-5	-24	-2	-11	-22		13	-18	-10	-52
PD																			
1	3		1	-34	-2		-5	37	12		-3	-6	-100	-31	-1	27	-8		
5	-6		3	-61	-6		-7	66	13		-4	-10	-100	-26	-1	50	-11		
10	-2		0	-73	-9		-14	72	51		-10	-13	-100	-56	-3	59	-15		
15	-13		-1	-85	-9		-16	82	59		-12	-16	-100	-59	1	76	-19		
20	-14		-1	-83	-11		-22	79	82		-16	-18	-100	-55	0	78	-20		

Table S3.3. Percentage change in mobility of elements after SMZ column treatment

Elements	Cumulatively leached from HA columns					
	For entire data			For data until crossover		
	SMZ (mg)	Non-SMZ (mg)	% Change	SMZ (mg)	Non-SMZ (mg)	% Change
Al	3.8	2.5	55	0.53	0.77	-31
As	19	23	-20	6.7	14	-53
B	21	19	10	20	19	9
Ba	0.08	0.36	-78	0.05	0.32	-86
Ca	1058	948	12	835	601	39
Cr	0.32	0.55	-42	0.06	0.33	-81
K	61	99	-38	28	56	-50
Mg	100	71	40	85	64	34
Mn	1.3	0.1	1169	0.44	0.10	361
Mo	5.1	6.0	-16	0.11	5.2	-98
Na	277	132	110	144	127	13
Sb	0.19	0.41	-55	0.17	0.38	-55
Se	2.9	3.2	-10	0.82	1.6	-50
Si	190	142	34	178	116	53
Sr	5.6	1.3	316	4.9	1.3	281
V	2.5	6.5	-62	1.5	5.2	-71
Zn	5.3	10	-49	1.6	0.86	88
Elements	Cumulatively leached from PD columns					
	For entire data			For data until crossover		
	SMZ (mg)	Non-SMZ (mg)	% Change	SMZ (mg)	Non-SMZ (mg)	% Change
Al	1092	1276	-14	396	459	-14
As	0.39	0.23	69	0.016	0.021	-25
B	531	603	-12	229	280	-18
Ba	0.05	37.8	-100	0.05	0.33	-84
Ca	6345	6978	-9	2167	2244	-3
Cr	1.4	1.3	7	0.18	0.82	-79
K	137	42	228	54	10	430
Mg	29	6.2	368	27	5.9	363
Mn	0.31	0.08	310	0.27	0.07	288
Mo	5.0	4.7	6	1.2	3.2	-64
Na	624	463	35	301	408	-26
Sb	0.25	0.23	11	0.25	0.23	11
Se	7.1	7.5	-5	1.4	2.0	-29
Si	270	267	1	18	2.1	782
Sr	139	307	-55	105	256	-59
V	10	13	-20	9.1	11	-18
Zn	1.2	1.7	-29	0.38	0.69	-45

CHAPTER – 4

COMPETITIVE ADSORPTION/DESORPTION OF ARSENATE AND PHOSPHATE AT THE FERRIC HYDROXIDE–WATER INTERFACE

Abstract

Excess input of P from agricultural land can result in eutrophication of surface watersand can also mobilize As from soil and sediment by competitive desorption. Metal oxyhydroxides (e.g., goethite and ferrihydrite) present in soils and sediments as discrete mineral phases or grain coatings play a significant role in controlling the environmental mobility of arsenate ($As_{(V)}$) and phosphate (P_i) because of their high adsorption capacities for these oxyanions. In this study, single- and competitive-ion adsorption of $As_{(V)}$ and P_i on ferric hydroxide in 0.1 M NaCl were investigated using adsorption isotherms, adsorption envelopes, adsorption/desorption kinetics, and As K-edge EXAFS spectroscopy. Adsorption isotherms at pH 4, 8, and 11 were constructed for both oxyanions with initial concentrations of 0.07 mM to 6.67 mM, in single- as well as in competitive-ion adsorption experiments. Single-ion adsorption envelopes for $As_{(V)}$ (C_i = 0.12 mM and 0.65 mM) and P_i (C_i = 0.16 mM and 0.86 mM), as well as competitive adsorption envelopes for $As_{(V)}$ and P_i (C_i = 0.35 mM and 0.75 mM), were prepared in the pH range from 4 to 11. The kinetics of individual ion and competitive adsorption/desorption of $As_{(V)}$ and P_i on ferric-hydroxide were studied at pH 4 and 8, using 1.5 mM of $As_{(V)}$ and/or P_i. Selected samples from the kinetics experiments were also subjected to As K-edge EXAFS study for understanding the changes with time in $As_{(V)}$ complexation on ferric-hydroxide in the presence/absence of P_i.

The experimental results indicate that adsorption of these oxyanions on ferric-hydroxide decrease with increasing pH. Both oxyanions showed similar adsorption behavior during single-ion adsorption experiments; however, $As_{(V)}$ was preferentially adsorbed during competitive adsorption experiments. Similarly, more $As_{(V)}$ was adsorbed when it was loaded into a P_i-equilibrated system than *vice versa*. Furthermore, more pre-equilibrated P_i was desorbed by by the added $As_{(V)}$ than *vice versa*. Triple-layer model simulations using bidentate surface complexes slightly under-predicted the adsorption of $As_{(V)}$ and P_i at low (value?) and high (value?) pH, but over-predicted adsorption at intermediate pH (6.5-8. During kinetic experiments, the rate of $As_{(V)}$ and P_i interactions on ferric hydroxide decreased after initial rapid adsorption/desorption. The early rapid adsorption/desorption was attributed to surface interactions, while the subsequent slower reactions were controlled by rate-limiting diffusion processes. The adsorption/desorption kinetics of $As_{(V)}$ and P_i showed good compliance with pseudo-second order, Elovich, and power-function equations. Both oxyanions competed for adsorption on ferric-hydroxide and each of them showed limited capacity to desorb the other. The As K-edge EXAFS analysis indicated the presence mononuclear (^{2}E) and binuclear (^{2}C) bidentate $As_{(V)}$ surface complexes. Combined Fe coordination numbers (CN) increased with increasing time, and decreased with the addition of P_i to the system. After the addition of P_i to the $As_{(V)}$-equilibrated system, the combined Fe CN decreased by about 38% and 18% at pH 4 and 8, respectively. Relatively, the proportion of higher Fe CN associated with ^{2}E surface complexes compared to ^{2}C surface complexes was decreased by the addition of P_i. Study indicated that the excessive input of P_i to As-contaminated geomedia due to the overuse of fertilizers could mobilize As through competitive desorption.

Key Words: Arsenate, Phosphate, Ferric hydroxide, Adsorption, Desorption, As K-edge EXAFS

4.1. Introduction

Phosphorus is an essential element that is often regarded as a growth-limiting nutrient in pristine aquatic ecosystems (Smil, 2000). However, excess P in the environment due to the over-application of chemical as well as animal-based fertilizers on agricultural land has created severe problems by promoting eutrophication of surface waters (Correll, 1998; Withers et al., 1999). Eutrophication and algal blooms can impair the water quality in recreational, industrial, and drinking water bodies and threaten human and ecological health (Anderson et al., 2002). On the other hand, As is a known toxic element (Nriagu, 2002). An acute dose of 50 to 300 mg of As is lethal for humans due to gastrointestinal, respiratory, cardiovascular, neurological or other body system failures (ATSDR, 2000). Similarly, chronic exposure to As has been proven to cause several different cancers (Jackson and Grainge, 1975; Bates et al., 1992). Widespread As contamination of groundwaterby natural processes has affected millions of people in several countries in the world (Bundschuh et al., 2012; Nordstrom, 2002; Smedley and Kinniburgh, 2002). Localized anthropogenic As contamination can occur through the use of As-based pesticides (Robinson et al., 2007), herbicides (Yang and Donahoe, 2007), or wood preservatives (Morrell et al., 2003), and by mining and smelting activities (Carbonell-Barrachina et al., 2004), potentially creating severe environmental problems for the surrounding groundwater and surface water resources.

In the environment, inorganic As can exist in several different valance states (-3, 0, +3, +5), depending on the prevailing pH and redox conditions (Cullen and Reimer, 1989). In natural waters, As mostly occurs as inorganic +3 (arsenite, $As_{(III)}$) and +5 (arsenate, $As_{(V)}$), although some organic species have been reported in waters severely impacted by industrial pollution (Smedley and Kinniburgh, 2002). In the environment, phosphorous only occurs in the

pentavalent form as ortho-phosphates (P_i), pyro-phosphates, longer-chain polyphosphates, and several organic phosphate species (Correll, 1998). In terms of geochemical processes, P_i and $As_{(V)}$ demonstrate similar chemical behavior in low-temperature oxic environments. Ortho-arsenic (H_3AsO_4) and ortho-phosphoric (H_3PO_4) acids have similar aqueous species and dissociation constants. Both $As_{(V)}$ and P_i have tetrahedral structures with thermochemical radii of 2.48 Å and 2.38 Å, respectively (da Silva and Williams, 2001). Considering the mono-protonated aqueous species at neutral pH, Kish and Viola (1999) estimatexd the partial negative charge on O to be a -0.895 in $As_{(V)}$ and -0.952 in P_i, with a partial charge of +1.125 and + 1.263 on the central As and P atom, respectively.

Both P_i and $As_{(V)}$ exhibit high degrees of adsorption on Fe, Mn, and Al hydroxides (Mucci et al., 2000). In natural soils and sediments, these anions are mostly associated with iron hydroxides (Belzile and Tessier, 1990; Slomp et al., 1996). Adsorption of $As_{(V)}$ and P_i involves ligand exchange with H_2O and OH^- at the iron hydroxide-water interface. On the basis of As-Fe distances, Fendorf et al. (1997) reported the existence of three surface complexes: a monodentate complex, a bidentate binuclear complex, and a bidentate mononuclear complex. Waychunas et al. (2005) also reported the presence of these complexes on a face of a single hematite crystal. Using an in situ FTIR technique, Tejedor-Tejedor and Anderson (1990) provided evidence for the formation of three types of P_i surface complexes on goethite: protonated bridging bidentate, non-protonated bridging bidentate, and non-protonated monodentate complexes. Combining data from both phosphorous K-edge XANES analysis of mineral and adsorbed forms of P_i and UV-visible spectroscopy of aqueous Fe(III)-P_i solutions, Khare et al. (2007) found a greater proportion of bidentate binuclear surface complexes than monodentate surface complexes on ferrihydrite at pH 6.

Arsenate and P_i have higher adsorption affinities on iron hydroxide than those of several other oxyanions (Manning and Goldberg, 1996; Geelhoed et al., 1997). Previous competitive adsorption/desorption experiments have shown that both $As_{(V)}$ and P_i largely compete for the same adsorption sites on soil and its constituents (Hingston et al., 1971; Manning and Goldberg, 1996; Liu et al., 2001). Zhao and Stanforth (2001) reported greater total surface coverage of $As_{(V)}$ and P_i in competitive-ion adsorption experiments than in single-ion adsorption experiments on goethite. The addition of P_i to As-contaminated sediment and soil enhanced the mobility of As by competitively exchanging P_i for $As_{(V)}$ (Alam et al., 2001). Lambkin and Alloway (2003) also reported proportionate desorption of P_i from soil at low $As_{(V)}$ additions. Furthermore, Lambkin and Alloway (2003) observed continual adsorption of $As_{(V)}$, even after the maximum desorption of P_i was achieved. Such experimental results could be interpreted as evidence for the existence of anion-specific adsorption sites on Fe-hydroxide. However, changes in $As_{(V)}$ complexation on ferric hydroxide in the presence of P_i have been poorly understood.

The main objective of this study was the quantitative comparison of $As_{(V)}$ and P_i adsorption on ferric hydroxide with single-ion and competitive-ion loadings. Single- and competitive-ion adsorption envelopes were used to understand the adsorption affinity of $As_{(V)}$ and P_i at the ferric-hydroxide -water interface. Similarly, equilibrium single- as well as competitive-ion adsorption isotherms for both $As_{(V)}$ and P_i at pH 4, 8, and 11 were constructed to understand the adsorption behavior of these ions. Time-dependent adsorption/desorption experiments for $As_{(V)}$ and P_i using individual, simultaneous, and sequential loadings were performed to quantify the rates of adsorption/desorption reactions. Selected samples from the kinetic study were analyzed by As K-edge EXAFS to elucidate changes in $As_{(V)}$ complexation on ferric hydroxide over time with the introduction of P_i at pH 4 and 8.

4.2. Materials and methods

4.2.1. Ferric hydroxide

The ferric hydroxide used in this study was synthesized at room temperature (~21˚ C) by oxidation of a ferrous sulfate solution. Ferrous sulfate was selected to prepare ferric hydroxide because it has been used previously in our laboratory as a treatment solution for *in situ* chemical fixation of As and other elements in contaminated soil and coal fly ash samples (Bhattacharyya et al., 2009; Yang et al., 2007). About 200 g of analytical grade ferrous sulfate ($FeSO_4 \bullet 7H_2O$) was placed in a 2 L reaction vessel containing 1 L of >18 MΩ doubly de-ionized (DDI) water produced by a Barnstead NANOpure™ system. A magnetic stirrer was used to agitate the solution continuously. During ferrous sulfate treatment of arsenic-contaminated soil performed by Yang et al. (2007), the soil particle surface helped catalyze the oxidation of Fe^{2+} and precipitate ferric hydroxide. The soil also buffered the acidity produced during Fe^{2+} oxidation. However, in the absence of soil particle catalysis and buffering, homogeneous precipitation of adequate quantities of ferric hydroxide from the ferrous sulfate solution was not feasible. Therefore, 30% hydrogen peroxide was added to the solution in multiple steps (about 10 mL in one addition) to enhance the oxidation process. Simultaneously, drops of a 5 M NaOH solution were gradually added to raise the pH to 8 and promote the formation of ferric hydroxide. The ferric-hydroxide precipitate was rinsed in two cycles to remove the sulfate. The first rinsing cycle consisted of several serial additions of DDI water to the reaction vessel, followed by agitation, settling, and decantation. The sulfate concentration of the decanted water was measured by ion chromatography (Dionex LC 20 Chromatography Enclosure). Once the sulfate concentration of the decanted rinse water fell below 0.2 mg/L, the pH of the suspension was increased to 11 by the dropwise addition of 5 M NaOH, which resulted in desorption of sulfate

from the ferric hydroxide. The ferric hydroxide was again serially rinsed multiple times with DDI water until the sulfate concentration in the decanted water fell below the IC detection limit (0.02 mg/L). Finally, the synthesized ferric hydroxide was separated by vacuum filtration, freeze-dried and analyzed by X-ray diffraction (XRD) using a Brüker D-8 Advance powder X-ray diffractometer. The XRDpattern of the synthesized ferric hydroxide resembled that of two-line ferrihydrite (Zhang et al., 2009). Therefore, it was used as ferrihydrite during surface complexation modeling. The surface area of the ferric-hydroxide was determined with a TriStar 3000 BET Surface Analyzer (Micrometrics Inc.). The BET surface area of 273 m^2/g measured for this ferric hydroxide was within the typical range (200-350 m^2/g) of reported ferrihydrite BET surface areas (Dzombak and Morell, 1990). However, a surface area of 600 m^2/g (Fukushi and Sverjensky, 2007) was used for the surface complexation model (SCM), because of the uncertainty in BET surface area measurement of ferric hydroxide. The point of zero net proton charge (PZNPC) of the ferric hydroxide was estimated to be 8.1 by acid-base titration.

4.2.2. Adsorption isotherms

4.2.2.1. Experimental

Single- and competitive-ion adsorption isotherms for $As_{(V)}$ and P_i were determined at pH 4, 8, and 11 by equilibrating different concentrations of these sorbate ions with 1 g/L ferric hydroxide at room temperature in a 0.1 M NaCl background electrolyte solution. Arsenate and P_i stock solutions were prepared from analytical grade $Na_2HAsO_4 \bullet 7H_2O$ salt and 85% H_3PO_4, respectively, and their concentrations determined by inductively coupled plasma-optical emission spectroscopy (ICP-OES) using a Perkin Elmer Optima 3000DV. Separate 13.33 mM stock solutions of $As_{(V)}$ and P_i were prepared and lower concentration solutions were obtained by

dilution. For each experiment, 45 mg of ferric hydroxide were weighed in a 50 mL centrifuge tube and pre-conditioned in background electrolyte at a specific pH for 24 h. Then a calculated amount of $As_{(V)}$ and/or P_i solution(s) was/were added to achieve the desired initial concentrations (C_i) of these sorbates. The C_i values of $As_{(V)}$ and P_i ranged from 0.07 mM to 6.67 mM during the adsorption isotherm experiments. The ferric hydroxide-electrolyte mixture with added $As_{(V)}$ and/or P_i was agitated for 24 h. Any change in pH during the experiment was adjusted to ±0.05 of the specified pH value with 0.1 M HCl and NaOH solutions. After equilibration, samples were centrifuged at 8,500 rpm for 20 minutes, filtered through 0.2 μm nylon syringe filters, acidified to 2% HNO_3 with OPTIMA® ultrapure nitric acid, and stored in a refrigerator until chemical analysis. Aqueous As and P concentrations were analyzed by ICP-OES and directly used as the equilibrium $As_{(V)}$ and P_i concentrations. The adsorbed amount of $As_{(V)}$ or P_i was calculated as the difference between C_i and equilibrium concentration (C_e) of these sorbates in the supernatant solution.

4.2.2.2. Isotherm Modeling

The single- and competitive-ion adsorption of $As_{(V)}$ and P_i was modeled using the Freundlich isotherm and competitive Langmuir isotherm models, respectively (Table 4.1). For each isotherm, the goodness of model fit was determined by calculating the coefficient of determination (R^2) with Eq. 4.1:

$$R^2 = \frac{\sum_{i=1}^{n}\left(q_m - \overline{q_e}\right)^2}{\sum_{i=1}^{n}\left(q_m - \overline{q_e}\right)^2 + \sum_{i=1}^{n}\left(q_m - q_e\right)^2} \quad ...(4.1)$$

where q_e is the adsorbed amount (mmol/g), q_m is the model-derived sorbed amount (mmol/g), and $\overline{q_e}$ is the average equilibrium sorbed amount (mmol/g) of oxyanion. The closer the value of

R^2 is to 1.0, the better the model is in predicting sorption. The R^2 value for each isotherm was obtained by using the n values of experimental and corresponding model datasets.

Table 4.1. Isotherm equations, their linear forms, and model fitting parameters.

Isotherms		Linear Form	Fitting Parameters
Freundlich[a]	$q_e = KC_e^n$	$\log q_e = \log K + n \log C_e$	K and n
Competitive Langmuir[b]	$q_{e(As_{(V)})} = \frac{b_{As_{(V)}} C_{e(As_{(V)})} N_{\max(As_{(V)})}}{1 + b_{As_{(V)}} C_{e(As_{(V)})} + b_{P_i} C_{e(P_i)}}$ $q_{e(P_i)} = \frac{b_P C_{e(P_i)} N_{\max(P_i)}}{1 + b_{As_{(V)}} C_{e(As_{(V)})} + b_{P_i} C_{e(P_i)}}$ Model fitted by trial-and-error with the help of Solver add-in in Microsoft Excel; maximized the sum of R^2 for both $As_{(V)}$ and P_i		$N_{\max(As(V))}$, $N_{\max(P)}$, $b_{(As(V))}$ and $b_{(P)}$

[a]Freundlich (1906), [b]Butler and Ockrent (1930)

4.2.3. Adsorption envelopes

4.2.3.1. Experimental

Single- as well as competitive-ion adsorption envelope batch experiments were performed to evaluate the complexation of P_i and $As_{(V)}$ on ferric-hydroxide as a function of pH (4-11). Two sets of single-ion adsorption envelopes were determined for $As_{(V)}$ with C_i of 0.12 mM and 0.65 mM, and for P_i with C_i of 0.16 mM and 0.86 mM. Similarly, equimolar C_i of 0.35 mM or 0.75 mM for both $As_{(V)}$ and P_i were used for construction of competitive adsorption envelopes. For each batch experiment, 45 mg ferric-hydroxide was weighed in a 50 mL centrifuge tube and a known volume of 0.1 M NaCl solution at the pH of interest was added. The pH of ferric-hydroxide suspension was adjusted and equilibrated for 24 h. Then $As_{(V)}$ (or P_i) was spiked to the desired C_i at that pH. For competitive adsorption, both $As_{(V)}$ and P_i were spiked together. The final volume of suspension in each tube was maintained at 45±0.2 mL by adding a pH-adjusted blank 0.1 M NaCl solution. Any change in solution pH was corrected. After 24

hours of agitation, the final pH was measured and the supernatant solution was collected by centrifugation and filtration.

4.2.3.2. Triple layer modeling

The triple layer model (TLM) (Yates et al., 1974; Davis and Leckie, 1978; Hayes and Leckie, 1986) was used to describe the single- as well as competitive-ion adsorption of $As_{(V)}$ and P_i on ferric-hydroxide as a function of pH. This model represents the ferric-hydroxide surface with three planes having different characteristics, the 0-plane, β-plane, and d-plane. For these planes, three charge-potential relationships (Eqs. 2-4) are defined using the surface charges (in Coulomb/m^2) of the 0-plane (σ_0) and d-plane (σ_d), the surface potentials (in V) of the 0-plane (ψ_o) , β-plane (ψ_β), and d-plane (ψ_d), and the capacitance (in F/m^2) between the 0-plane – β-plane (C_1) and the β-plane – d-plane (C_2) using the following equations:

$$\psi_0 - \psi_\beta = \sigma_0/C_1 \ldots (4.2)$$

$$\psi_\beta - \psi_d = -\sigma_d/C_2 \ldots (4.3)$$

$$\sigma_d = -(8RTc\varepsilon_0 D)^{0.5} \sinh(F\psi_d/2RT) \ldots (4.4)$$

where c is the concentration of a 1:1 background electrolyte, ε_0 is the permittivity of vacuum, D is the dielectric constant of water, F is the Faraday constant, R is the gas constant, and T is the temperature in K (Goldberg, 1995). During modeling, C_1 and C_2 were fixed at 1.2 F/m^2 and 0.2 F/m^2, respectively. Similarly, an adsorption site density of 3.8 sites/nm^2 (Fukushi and Sverjensky, 2007) was used during surface complexation modeling.

4.2.3.3. Aqueous species, surface reactions, and equilibria

The aqueous species and reactions used in the triple layer model simulations are given in Table 4.2. The aqueous reactions and equilibria were obtained from different sources and directly used without optimization, as follows. The $As_{(V)}$ and P_i protonation equilibria were obtained from Wagman et al. (1982) and Smith and Martell (1976), respectively. The equilibria for ion-pair formation between aqueous P_i species and Na^+ were obtained from Snoeyink and Jenkins (1980). The P_i-Na^+ ion pairs were considered to be important (Gao and Mucci, 2001); however, equivalent relationships for $As_{(V)}$ are not well-defined (Fukushi and Sverjensky, 2007). Gao and Mucci (2001) speculated that the complexation of $As_{(V)}$ species with Na^+ are not as significant as the complexation of P_i species with Na^+. In this study, however, similar ion-pairs and equilibrium values were assumed for aqueous complexation of equivalent P_i and $As_{(V)}$ species with Na^+. The complexation constants for protonated P_i and $As_{(V)}$ species with Na^+ shown in Table 4.2 were derived by combining the equilibria obtained from Wagman et al. (1982), Smith and Martell (1976), and Snoeyink and Jenkins (1980).

The ferric-hydroxide surface was assumed to have chemically active amphoteric sites which could be defined as a diprotic acid (Dzombak and Morell, 1990). Protons and hydroxyl ions were considered to interact with the 0-plane by forming inner-sphere surface complexes, while ions from the background electrolyte were assumed to interact with the β-plane and form outer-sphere surface complexes. The surface acidity constants, $\log K_{+}^{int}$ and $\log K_{-}^{int}$, and electrolyte-surface complexation constants, $\log K_{Na^+}^{int}$ and $\log K_{Cl^-}^{int}$, (Table 4.3) were obtained from Zhang and Sparks (1990). Although these intrinsic constants were originally derived for goethite, Goldberg and Johnston (2001) successfully used them for ferric hydroxide. According to Goldberg and Sposito (1984), changes in values of protonation-dissociation constants were relatively less sensitive than the changes in oxyanion surface complexation affinities. The

surface complexation reactions describing the chemical interactions between surface functional groups and several aqueous species are given in Table 4.3. The species of interest (e.g., $As_{(V)}$, P_i) could interact with either the 0-plane or β-plane. Traditionally, the ions that form inner-sphere complexes are considered to interact with the 0-plane and make a charge contribution to that plane. However, the TLM yielded better results for $As_{(V)}$ adsorption on hematite and other Fe-oxides when the oxyanion-surface interaction and resultant charge were assigned to the β-plane (Arai et al., 2004; Fukushi and Sverjensky, 2007). Therefore, the charge from the non-protonated surface complexation reaction was placed on the β-plane during the TLM model simulation performed for this study. For both oxyanions, bidentate surface complexation reactions were used. The presence of a bidentate binuclear $As_{(V)}$ surface complex was indicated by the As K-edge extended X-ray absorption fine structure (EXAFS) analysis performed for this study, while

Table 4.2. Aqueous speciation reactions and equilibrium constants

Aqueous reactions	log K
$H_2O \Leftrightarrow H^+ + OH^-$	-14.00[a]
$H_3PO_4^0 \Leftrightarrow H_2PO_4^- + H^+$	-2.15[a]
$H_2PO_4^- \Leftrightarrow HPO_4^{-2} + H^+$	-7.19[a]
$HPO_4^{-2} \Leftrightarrow PO_4^{-3} + H^+$	-12.38[a]
$H_3AsO_3^0 \Leftrightarrow H_2AsO_4^- + H^+$	-2.2[b]
$H_2AsO_4^- \Leftrightarrow HAsO_4^{-2} + H^+$	-7.15[b]
$HAsO_4^{-2} \Leftrightarrow AsO_4^{-3} + H^+$	-11.53[b]
$NaCl^0 \Leftrightarrow Na^+ + Cl^-$	0.80[c]
$NaPO_4^{-2} \Leftrightarrow PO_4^{-3} + Na^+$	0.60[d]
$NaHPO_4^- \Leftrightarrow Na^+ + H^+ + PO_4^{-3}$	-11.78 [a, d]
$NaAsO_4^{-2} \Leftrightarrow AsO_4^{-3} + Na^+$	0.60[d,e]
$NaHAsO_4^- \Leftrightarrow AsO_4^{-3} + H^+ + Na^+$	-10.93 [b, d]

[a]Smith and Martell (1976), [b]Wagman et al. (1982), [c]Sverjensky et al. (1997), [d]Snoeyink and Jenkins (1980)

Table 4.3. Surface complexation reactions, species, stoichiometric and surface potential coefficients, and TLM intrinsic surface complexation constants (water assumed to be ubiquitous).

Reactions	Surface Species	$FeOH$ (m)	H^+ (n)	ψ_0 (p)	ψ_β (q)	log K^{int}
Surface hydrolysis reactions						
TLM1	$FeOH_2^+$	1	1	1	0	4.3[b]
TLM2	FeO^-	1	-1	-1	0	-9.8[b]
TLM3[a]	$FeONa$	1	-1	-1	1	-9.3[b]
TLM4[a]	$FeOH_2^+Cl^-$	1	1	1	-1	5.4[b]

Inner-sphere bidentate binuclear $As_{(V)}$ -P_i surface complexes								
Reactions	Surface Species	$FeOH$ (m)	H^+ (n)	ZO_4^{-3} (o)	ψ_0 (p)	ψ_β (q)	log K^{int} (P_i)	log K^{int} ($As_{(V)}$)
TLM5	$(FeO)_2ZO(OH)$	2	3	1	0	0	13.36[c], 12.63[d]	12.78[c], 12.96[d]
TLM6	$(FeO)_2ZO_2^-$	2	2	1	0	-1	12.42[c], 10.45[d]	10.72[c], 10.59[d]

[a]No stoichiometric coefficients given for Na and Cl; [b]Zhang and Sparks (1990); [c]single oxyanion adsorption (this study); [d]competitive oxyanion adsorption (this study).

similar surface complexation of P_i has been reported elsewhere (Tejedor-Tejedor and Anderson, 1990; Rose et al., 1997). Arai et al. (2004) considered bidentate binuclear complexation as a major mechanism for $As_{(V)}$ adsorption on hematite. While some previous studies (Tejedor-Tejedor and Anderson, 1990; Fendorf et al., 1997) also indicated the presence of monodentate complexes during adsorption of $As_{(V)}$ and P_i at lower surface coverage and high pH, such complexes were not used for TLM simulations in this study. Even though As-EXAFS indicated the presence of an edge-sharing bidentate mononuclear complex, it was not included during TLM simulations because of its similar reaction stoichiometry with the bidentate binuclear complex. It was assumed that any contribution of this complexation mechanism to adsorption was accommodated by bidentate binuclear reactions within the scope of the TLM. The protonated and non-protonated bidentate complexation reactions, the species and their coefficients, and the surface potentials and their coefficients are presented in Table 4.3. The optimized reaction affinity constants (Table 4.3) were calculated with a generalized mass law equation (Eq. 4.5):

$$K^{int} = \frac{[\text{Surface species}][H^+]^n}{[\equiv FeOH]^m[H_3ZO_4]^o} \exp\left(p\frac{F\Psi}{RT}\right) \quad \ldots (4.5)$$

where F is the Faraday constant ; Ψ is the surface potential (V) with coefficient p; R is the gas constant; T is temperature in K; and m, n, and o are stoichiometric coefficients for $FeOH$, H^+, and H_3ZO_4, respectively (Table 4.3).

4.2.3.4. Model simulation

FITEQL 4.0 (Herbelin and Westall, 1999) was used for both parameter optimization and model simulation. FITEQL is a non-linear parameter optimization and fitting program which has been used extensively in determining surface complexation constants and modeling (Manning and Goldberg, 1996). The FITEQL input file consisted of experimental adsorption data, including measured pH as $\log[H^+]$, surface hydrolysis reactions and their affinities, aqueous reactions including ion-pair formation and their reaction constants, surface electrical properties, specific surface area, and reactive surface sites. Furthermore, a relative error of 5% for total and adsorbed $As_{(V)}$ and P_i, and $\log[H^+]$ were included in the input file. For all other parameters, the default value of 1% relative error was used. The affinity values for surface complexation reactions were initially obtained from the literature and optimized during modeling. The quality of model fit was determined by calculating a goodness-of-fit parameter called WSOS/DF using Eq. 4.6 (Herbelin and Westall, 1999):

$$\text{WSOS/DF} = \frac{\sum (Y/S_Y)^2}{(n_p \times n_{II} - n_u)} \quad ...(4.6)$$

where Y is the value of the difference function (difference in value between model and experimental data point); S_Y is the FITEQL estimated experimental error, which is used as a weighting parameter in the WSOS calculation; n_p is the number of data points; n_{II} is the number of chemical components with known total and free concentrations; and n_u is the number of adjustable parameters (Herbelin and Westall, 1999). In general, the lower the calculated value of WSOS/DF, the better the model fit.

All oxyanion surface reaction affinity constants can be treated as adjustable parameters during simulations. However, FITEQL generally fails to converge when there are more than two

adjustable parameters (Hayes et al., 1991). Therefore, some reaction affinities were fixed if more than two surface complexation reactions were used for a simulation. For the competitive adsorption simulation, reaction affinities obtained from single-ion adsorption simulations were used as initial values. Then further optimization of these parameters was made by successively letting two parameters at a time to float during the simulation. Finally, the relative qualities of fit for competitive adsorption models were determined by visual inspection and calculation of WSOS/DF values.

4.2.4. Adsorption/desorption kinetics

4.2.4.1. Kinetic experiments

Single-ion adsorption kinetics, competitive ion adsorption kinetics, and co-oxyanion induced desorption kinetics of $As_{(V)}$ and P_i were studied at pH 4 and 8 at room temperature and pressure. Each experimental set consisted of a pH-adjusted 2g/L ferric-hydroxide suspension in 0.1 M NaCl electrolyte placed in a 1.5 L reaction vessel. The suspension was spiked to 1.5 mM of $As_{(V)}$ or P_i, or both, depending on the loading schemes. Three loading schemes were used at each pH:

a) Arsenate was loaded first, followed by sequential P_i loading.
b) Phosphate was loaded first, followed by sequential $As_{(V)}$ loading.
c) Both oxyanions were loaded together.

In schemes (a) and (b), P_i and $As_{(V)}$ were sequentially added after 48 h equilibration at the initial loadings of $As_{(V)}$ and P_i, respectively. Individual adsorption kinetics for $As_{(V)}$ and P_i on ferric hydroxide were obtained for the first 48 h equilibrations. With sequential additions of the

co-oxyanion, competitive adsorption kinetic data for P_i and $As_{(V)}$ were obtained for loading schemes (a) and (b), respectively. Furthermore, sequential loading of the co-oxyanion also provided the competitive desorption kinetic data for the pre-equilibrated oxyanion ($As_{(V)}$ for scheme a and P_i for scheme b). In addition, competitive adsorption kinetic data were obtained by simultaneously loading both oxyanions using scheme (c). Throughout these experiments, the suspension was agitated by magnetic stirrer; pH changes were monitored continuously and adjusted to the target value with 0.1 M NaOH/HCl. From each reaction vessel, 20 ml of suspension were extracted at each sampling event, centrifuged at 8,500 rpm for 10 min (2 min for the initial kinetic samples), filtered, acidified, and stored in a refrigerator until chemical analysis.

The adsorption of each oxyanion was calculated by subtracting the measured concentration at each sampling point from the initial concentration. The co-oxyanion induced desorption of $As_{(V)}$ or P_i was calculated by subtracting the aqueous concentration of the pre-equilibrated oxyanion (at 48 h) from its concentration at each sampling point after the sequential loading of co-oxyanion. The competitively adsorbed amount of the sequentially added co-oxyanion was calculated by a method similar to that used for single-anion adsorption.

4.2.4.2. Kinetic modeling

Pseudo-second order (Ho and Mckay, 1999), Elovich (Low, 1960), and power function (Aharoni and Sparks, 1991) equations were used for modeling single- as well as competitive-ion adsorption/desorption kinetics of $As_{(V)}$ and P_i. The primary kinetic model equations and their linear forms are given in Table 4.4. Attempts to use other kinetic equations, such as first-order

and second-order kinetic models, failed because of their inability to adequately describe the experimental data. The coefficient of determination (R^2) for each model was obtained by using the experimental and model-derived datasets.

Table 4.4. Kinetic equations, their linear forms, and model fitting parameters.

Kinetic Equations		Linear Form	Kinetic Parameters
Pseudo-second order [a]	$\frac{dq_t}{dt} = k(q_e - q_t)^2$	$\frac{t}{q_t} = \frac{1}{kq_e^2} + \frac{1}{q_e}t$	k , $h = kq_e^2$
Elovich [b]	$\frac{dq_t}{dt} = \alpha \exp(-\beta q_t)$	$q_t = \frac{1}{\beta}\ln(\alpha\beta) + \frac{1}{\beta}\ln(t)$	α, β
Power Function [c]	$q_t = at^n$	$\log q_t = \log a + n \log t$	a , n

[a] Ho and McKay (1999), [b] Low (1960), [c] Aharoni and Sparks (1991)

4.2.5. As K-edge EXAFS spectroscopy

4.2.5.1. EXAFS Samples and data collection

Selected samples from the adsorption kinetics experiments were analyzed by As K-edge (EXAFS) spectroscopy. After centrifugation, the ferric-hydroxide residue of selected samples was packed into Teflon sample holders, sealed with Kapton® tape, and stored in a refrigerator. The XAS samples were not aged more than a week before analysis. The As K-edge EXAFS spectra were collected on bending magnet beamline 9 BM B at the Advanced Photon Source, Argonne National Laboratory in Argonne, IL. The storage ring was operated at 7.0 GeV, with a maximum ring current of 100 mA. Two silicon crystals with Si(111)and Si (220) panes were used as monochromators. The monochromator energy was calibrated to 11,867 eV with 0.1 mol sodium arsenate hepta-hydrate solution prior to the As EXAFS data collection. The sample

holder was oriented at 45º to the unfocussed incident beam. Arsenic EXAFS spectra were collected from pre-edge to extended regions in 0.3 to 10 eV steps. At each step, the measurement time was 2 seconds, with a settling time of 0.5 sec. All XAS spectra were collected in fluorescence mode at room temperature by a 13-element Ge solid-state detector. For each sample, at least three spectra were collected.

4.2.5.2. EXAFS Data Reduction

Arsenic K-edge EXAFS data reduction was performed with Athena 0.8.056 software (Ravel and Newville, 2005). The spectrum for each sample was visually inspected, and any error present in the data was removed. Then at least two spectra for each sample with similar baseline and background were merged before background removal. The built-in AUTOBK algorithm (Newville et al., 1993) in Athena was used for background removal, and the spectra were normalized with respect to E_0 values determined from the second derivative of the raw spectra. Then the EXAFS data were converted from E-space to k-space and exported to Artemis 0.8.012 (Ravel and Newville, 2005) for model fitting using the IFEFFIT code (Newville, 2001). The preliminary structural parameters for the model compound were obtained with ATOMS (Ravel, 2001), using scorodite ($FeAsO_4 \bullet 2H_2O$) crystalline data (Kitahama et al., 1975). The theoretical amplitude and phase shifts for the selected paths (a single-scattering path for As–O, up to two separate single-scattering paths for As–Fe, and a multi-scattering path within the arsenate tetrahedron for $As–O_{(MS)}$) were calculated using the FEEF6 code (Zabinsky et al., 1995) and the ATOMS-generated input file. The radial structural functions were obtained by Fourier-transforming the k-space data over the Δk of 3-11 $Å^{-1}$. A Kaiser-Bessel function was used with a

dk of 1 for the Fourier transform window. Then the fitting of the EXAFS data was performed in R-space with a fitting range of 1-3.5 Å. During fitting, the values of coordination number (CN) and inter-atomic bond distance (R) were floated. The E_0 value was obtained by fitting the first shell (As-O) and fixed to that value for all other shells. The amplitude reduction factor (S_0^2) was fixed at 0.85. The Debye-Waller factor (σ^2) for the As-O single-scattering was allowed to float, while a fixed value of 0.005 was used for As-Fe shells and a value of 0.007 was used for As-$O_{(MS)}$. For each fit, the number of independent fitting variables was not allowed to exceed the number of degrees of freedom in the data. The accuracies of the model-derived parameters were 0.02±Å for R_{As-O}, 0.03±Å for R_{As-Fe}, ±14% for CN_{As-O}, and ±41% for CN_{As-Fe}.

4.3. Results and discussion

4.3.1 Adsorption isotherms

4.3.1.1. Single-ion adsorption

Adsorption isotherms for both oxyanions at pH 4, 8, and 11 are shown in Fig. 4.1. Adsorption isotherms show that at lower C_i, most of the $As_{(V)}$ and P_i were adsorbed, but gradually smaller fractions of these oxyanions were adsorbed with increasing C_i. Adsorption of both $As_{(V)}$ and P_i was strongly controlled by pH;both sorbates showed greater adsorption at pH 4 than at pH 8 and 11. Approximately two times and three times more adsorption of $As_{(V)}$ and P_i occurred at pH 4 compared to pH 8 and pH 11, respectively (Fig. 4.1). Similar pH-dependent adsorption isotherms for $As_{(V)}$ and P_i at the metal oxide-water interface have been previously determined by several researchers (e.g., Violante and Pigna, 2002).

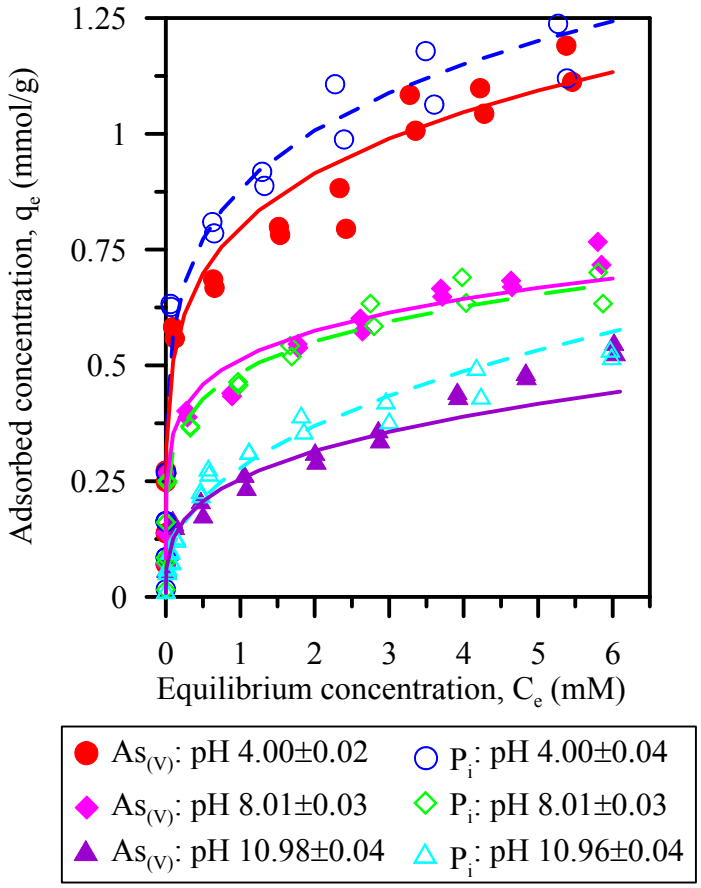

Fig. 4.1. Single-anion adsorption isotherms for $As_{(V)}$ and P_i at pH 4, 8, and 11. Lines (solid lines for $As_{(V)}$ and dashed lines for P_i) represent Freundlich isotherm model fits.

Both $As_{(V)}$ and P_i showed similar adsorption on ferric hydroxide at each pH (Fig. 4.1). Although Zeng et al. (2008) reported higher adsorption of P_i than $As_{(V)}$ on Fe/Mn hydroxide, a significant difference in their adsorption behavior was not observed in this study. The adsorption maxima for $As_{(V)}$ and P_i at pH 4 were greater than 1.15 and 1.2 mmol/g, respectively. Raven et al. (1998) reported a similar adsorption maximum (1 mmol/g) for $As_{(V)}$ on ferrihydrite at pH 4.6. Similarly, the adsorption maxima for both oxyanions at pH 8 and 11 were greater than 0.7 and 0.5 mmol/g, respectively.

The Freundlich model was able to describe the experimental isotherm data for $As_{(V)}$ and P_i at pH 4, 8, and 11 (Fig. 4.1). Model parameters and R^2 values are presented in Table 4.5. The isotherm parameters (K and n) of the Freundlich model fits were similar for $As_{(V)}$ and P_i at each pH. The Freundlich isotherm constant (K) was larger at pH 4 than at pH 8 and 11; however, the value of n was similar at pH 4 and 8, but significantly larger at pH 11, for both sorbates.

Table 4.5. Freundlic model parameters for single-ion adsorption isotherms.

pH	$As_{(V)}$	P_i
pH 4	K = 0.80, n = 0.19, R^2 = 0.960	K = 0.88, n = 0.19, R^2 = 0.964
pH 8	K = 0.51, n = 0.16, R^2 = 0.974	K = 0.49, n = 0.18, R^2 = 0.973
pH 11	K = 0.26, n = 0.31, R^2 = 0.914	K = 0.28, n = 0.40, R^2 = 0.975

4.3.1.2. Competitive adsorption

Isotherms for competitive adsorption of $As_{(V)}$ and P_i on ferric hydroxide at pH 4, 8, and 11 are shown in Fig. 4.2. During competitive adsorption, both $As_{(V)}$ and P_i retained the Type-I isotherm pattern shown during single-ion adsorption, with a greater fraction being adsorbed at lower C_i than at higher C_i. The adsorption maxima for $As_{(V)}$ and P_i at pH 4 were 0.75 and 0.50 mmol/g, respectively. Similarly, the adsorption maxima for $As_{(V)}$ at pH 8 and 11 were 0.55 and 0.44 mmol/g, respectively, while the maxima for P_i were 0.40 and 0.33 mmol/g, respectively.

Although $As_{(V)}$ and P_i exhibited similar surface complexation in single-ion adsorption experiments, relatively greater adsorption of $As_{(V)}$ occurred at all pH values in competitive adsorption experiments. Violante and Pigna (2002) also reported a preferential adsorption of $As_{(V)}$ over P_i on Fe, Mn, Ti oxides, and Fe-rich clays. The competitive Langmuir isotherm model, which has the ability to simultaneously handle the adsorption of two sorbates, was useful in describing the competitive adsorption of these oxyanions on ferric hydroxide (Fig. 4.2 and

Table 4.6). Although this model slightly over-predicted $As_{(V)}$ adsorption for intermediate concentrations at pH 4, it was able to predict $As_{(V)}$ adsorption at both lower and higher concentrations.

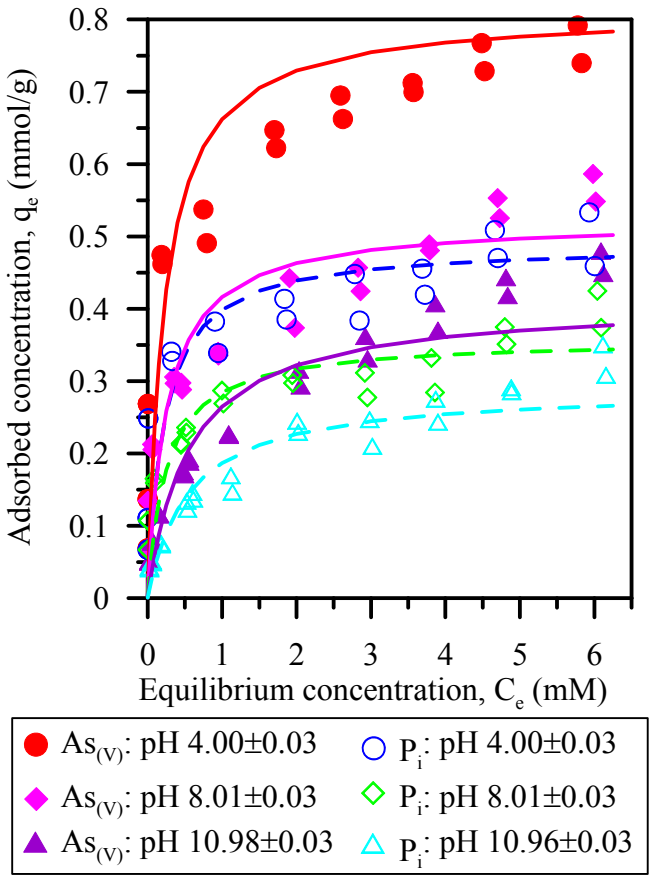

Fig. 4.2. Competitive adsorption isotherms for $As_{(V)}$ and P_i at pH 4, 8, and 11 with competitive Langmuir model fits (solid lines are for $As_{(V)}$ models, dashed lines are for P_i models).

Table 4.6. Model parameters of competitive Langmuir isotherms for $As_{(V)}$ and P_i

pH	Competitive Langmuir Model Parameters
4	$N_{max(As_{(V)})} = N_{max(P_i)} = 1.30,\ b_{As_{(V)}} = 2.77,\ b_{P_i} = 1.67,\ R^2_{max(As_{(V)})} = 0.895,\ R^2_{max(P_i)} = 0.830$
8	$N_{max(As_{(V)})} = N_{max(P_i)} = 0.88,\ b_{As_{(V)}} = 2.33,\ b_{P_i} = 1.60,\ R^2_{max(As_{(V)})} = 0.882,\ R^2_{max(P_i)} = 0.865$
11	$N_{max(As_{(V)})} = N_{max(P_i)} = 0.70,\ b_{As_{(V)}} = 1.07,\ b_{P_i} = 0.75,\ R^2_{max(As_{(V)})} = 0.900,\ R^2_{max(P_i)} = 0.900$

4.3.2. Adsorption envelopes

4.3.2.1. Single-ion adsorption

Arsenate (C_i: 0.12 mM and 0.65 mM) and P_i (C_i: 0.15 mM and 0.86 mM) adsorption envelopes, along with the TLM results, are presented in Fig. 4.3. Adsorption isotherms (Figs. 4.1 and 4.2) and envelopes (Fig. 4.3) indicated that complexation of $As_{(V)}$ and P_i on ferric-hydroxide was strongly controlled by pH. Such pH-dependent adsorption of $As_{(V)}$ and P_i could be explained by considering changes in the aqueous dissociation/speciation of H_3AsO_4 and H_3PO_4, and variation in the surface electrical properties of ferric hydroxide as a function of pH. The polyprotic acids of $As_{(V)}$ and P_i have similar aqueous protonation/deprotonation reactions and constants (Table 4.2). The overall adsorption of a polyprotic acid that provides protonated and non-protonated aqueous species through a series of successive dissociation reactions yields a broad adsorption envelope across a wide range of pH (Sigg and Stumm, 1981; Manning and Goldberg, 1996). Considering the point of zero net proton charge (PZPNC) of ferric-hydroxide (which was determined to be 8.1) and the dissociation constants of H_3AsO_4 and H_3PO_4 (given in Table 4.2), the adsorption of both $As_{(V)}$ and P_i was expected to decrease with increasing pH as the ferric-hydroxide surface as well as aqueous species become increasingly negatively charged. Either electrostatic or ligand exchange interactions between the ferric-hydroxide surface and the aqueous species couldexplain the pH-dependent adsorption of $As_{(V)}$ and P_i on ferric hydroxide. The presence of lower but significant and persistent adsorption above the PZPNC and the formation of predominantly inner-sphere complexes of $As_{(V)}$ and P_i on ferric-hydroxide (Tejedor-Tejedor and Anderson, 1990; Fendorf et al., 1997), indicate that surface interactions

were largely controlled by ligand exchange reactions at all pH values. And these interactions get a greater electrostatic impetus below the PZPNC, resulting in enhanced adsorption.

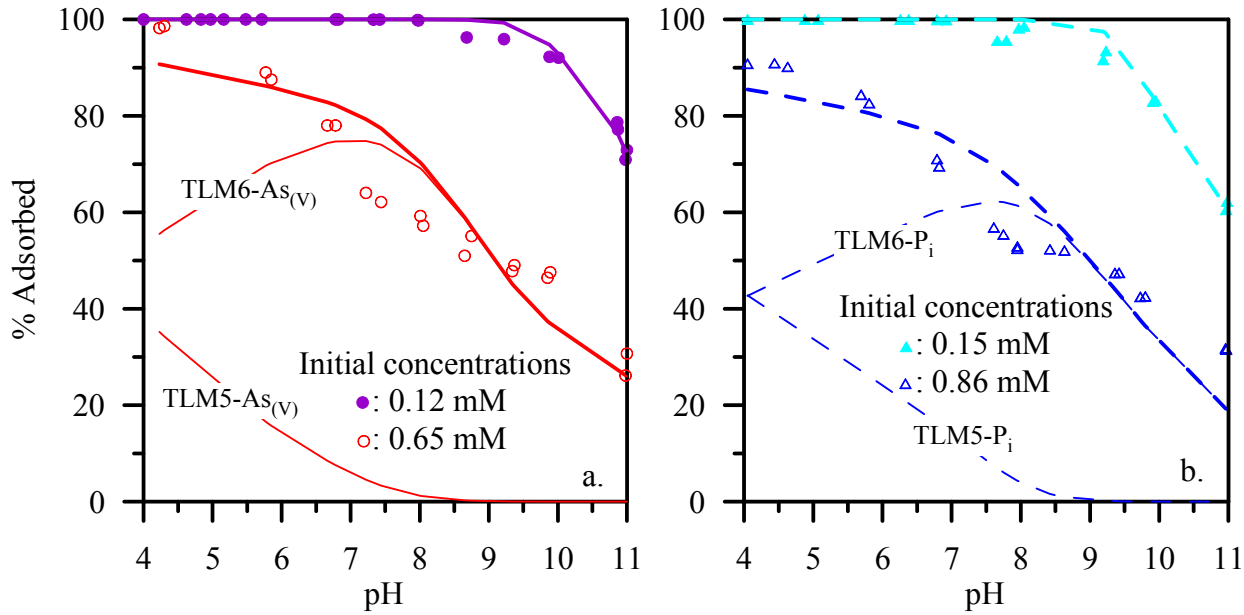

Fig. 4.3. Percent adsorption of $As_{(V)}$ (a) and P_i (b) as a function of pH and C_i in a 0.1 M NaCl electrolyte solution containing 1 g/L ferric-hydroxide. Bold solid lines (a) and bold dashed lines (b) represent the triple layer model (TLM) fit for $As_{(V)}$ and P_i, respectively. During TLM simulations, TLM6 and both TLM5 + TLM6 are used for lower and higher C_i, respectively. Thinner solid lines (a) and thinner dashed lines (b) represent the protonated (TLM5) and non-protonated (TLM6) surface complexes, as indicated on the plots.

The effect of pH on adsorption was greater at higher C_i than at lower C_i. At low C_i, adsorption of $As_{(V)}$ and P_i was complete until pH 8, and then rapidly decreased with increasing pH. At higher C_i (0.65 mM of $As_{(V)}$ and 0.86 mM of P_i), the maximum adsorption of these oxyanions occurred at about pH 4, with removal of about 98% of the $As_{(V)}$ and 91% of the P_i from solution, which resulted in surface coverages of 0.64 mmol/g and 0.78 mmol/g for $As_{(V)}$ and P_i, respectively. At pH 11, nearly 28% of the $As_{(V)}$ and 32% of the P_i was removed from the

solution. The rate of decrease in adsorption with increasing pH, however, was not constant. The adsorption envelopes for higher C_i values consisted of 4 distinct regions. With increasing pH, there was a slow decrease in adsorption at low pH (<6), followed by a relatively rapid decrease in adsorption from pH 6 to 8. Adsorption decreased again slowly from pH 8 to 10, and finally decreased more rapidly at high pH (> 10). Such a complex adsorption envelope was likely caused by the successive deprotonation of H_3AsO_4 and H_3PO_4 (Table 4.2), along with a possible change in adsorption preference of aqueous species on the increasingly negative surface of the sorbent with increasing pH.

Fig. 4.3 also shows the TLM results for both $As_{(V)}$ (Fig. 4.3a) and P_i (Fig. 4.3b) adsorption envelopes for low and high C_i values. For low C_i (0.12 mM $As_{(V)}$ and 0.15 mM P_i), only the nonprotonated bidentate surface complex (TLM6) was used for modeling. However, both protonated (TLM5) and nonprotonated (TLM6) surface complexes were used for simulating adsorption envelopes at high C_i. The surface affinity constants for these surface complexation reactions for P_i and for $As_{(V)}$ are given in Table 4.3. The surface reaction affinities obtained at low C_i were smaller than their values at higher C_i. In some other instances, however, opposite trends (i.e., smaller affinity constants with increasing surface coverage) have also been reported. For example, Balistrieri and Chao (1990) reported decreased adsorption affinities with increasing $Se_{(IV)}$ surface coverage on Fe- and Mn-oxides, and they attributed such phenomenon to surface site heterogeneity.

At the lower C_i values, the TLM predicted nearly 100% adsorption of $As_{(V)}$ and P_i at pH < 9. The model slightly over-predicted the adsorption of $As_{(V)}$ and P_i on ferric hydroxide at low C_i from pH 8 to 10. The simulations for the high C_i values underpredicted the adsorption at low

and high pH, but over-predicted adsorption at intermediate pH. For both oxyanions, the protonated surface species (TLM5) were consistently present at low pH; however, the amount adsorbed decreased with increasing pH.

4.3.2.2. Competitive adsorption

The competitive adsorptions of $As_{(V)}$ and P_i on ferric-hydroxide as a function of C_i and pH along with TLM results are presented in Fig. 4.4. As in the single-ion adsorption experiments, the maximum adsorption of $As_{(V)}$ and P_i occurred at pH 4 and then decreased with increasing pH. Unlike the similar single-ion adsorption experiments, the competitive adsorption envelopes showed a greater adsorption of $As_{(V)}$ than P_i on ferric-hydroxide.

The TLM5 and TLM6 complexation reactions were used for competitive adsorption model simulations. Reaction affinities obtained for single-oxyanion adsorption were used as initial input values for the competitive adsorption simulations. Though the complexation affinities from single-ion adsorption modeling were able to mimic the general pattern of competitive adsorption envelopes, they did not generate a satisfactory fit without further optimization. Gao and Mucci (2001) also noticed a similar phenomenon while modeling competitive adsorption envelopes of $As_{(V)}$ and P_i on goethite in artificial sea water using the Basic Stern model. Previously, Zeng et al. (2008) divided the sorption sites on sorbent into sorbate-specific and competitive sites to address a similar problem. Contrary to our results, Zeng et al. (2008) reported a greater adsorption of P_i than $As_{(V)}$ on Fe/Mn oxides in competitive experiments, and they considered P_i only sites in addition to the competitive sites on sorbent. Furthermore, Zeng et al. (2008) assumed that the same P_i complexation constants for specific

and competitive sites. The direct extension of this approach to the present scenario would be to include the $As_{(V)}$ specific and competitive sites with the same affinity values. The assumption of such $As_{(V)}$ specific sites in addition to the competitive adsorption sites during modeling might have yielded a slightly improved fit; however, the additional incorporation of $As_{(V)}$ specific sites alone should not have inherently resulted in a better fit without further optimization of affinities because their values were directly related to the complexation energy which vary with changes in surface coverage (Low, 1960). Therefore, surface complexation constants obtained after simulating the individual adsorption were used as initial input values for competitive adsorption modeling and optimized further with a series of successive simulations.

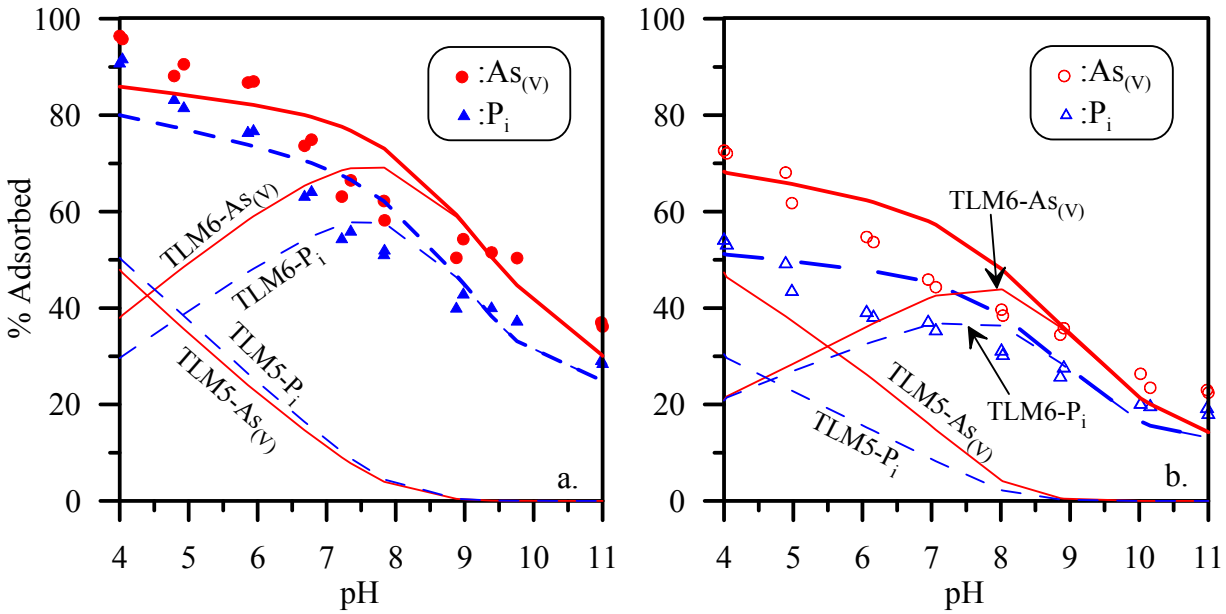

Fig. 4.4. Percent adsorption of $As_{(V)}$ and P_i as a function of pH in a 0.1 M NaCl electrolyte solution containing 1 g/L ferric-hydroxide when 0.35 mM (a) and 0.75 mM (b) of each $As_{(V)}$ and P_i loaded together. Bold solid and dashed lines represent the triple layer model fits for P_i and $As_{(V)}$, respectively. During TLM simulation, protonated (TLM5) and non-protonated (TLM6) surface complexes of both $As_{(V)}$ and P_i are considered. Percent abundances of these surface species are illustrated with thinner lines in the diagram.

The affinity values given in Table 4.3 for TLM5 and TLM 6 for $As_{(V)}$ and P_i were obtained after simulating the higher C_i adsorption data. Consistent with the observation after single-ion adsorption modeling, the smaller affinity constants were obtained for lower C_i competitive-ion adsorption than higher C_i competitive-ion adsorption. The model simulation indicated that the TLM5 (protonated) and TLM6 (nonprotonated) were the dominating surface complexes at low pH and high pH, respectively (Fig. 4.4).

4.3.3. Adsorption/desorption kinetics of $As_{(V)}$ and P_i

4.3.3.1. Single- and competitive-ion adsorption kinetics

Figs. 4.5 and 4.6 show the results of time-dependent individual- as well as competitive-ion adsorption/desorption of $As_{(V)}$ and P_i on/from ferric-hydroxide . In both figures, adsorption of $As_{(V)}$ and P_i are shown as percentage adsorbed with respect to C_i (1.5 mM) of each sorbate. In Fig. 4.5, data points until 48 h represent individual $As_{(V)}$ or P_i adsorption while data points after 48 h represent competitive adsorption/desorption of $As_{(V)}$ and P_i. Fig. 4.6 shows the competitive adsorption of $As_{(V)}$ and P_i when both oxyanions were loaded together.

Both oxyanions showed a very rapid initial adsorption (Fig. 4.5). At pH 4, about 73% of $As_{(V)}$ (surface coverage, Γ = 0.55 mmol/g) and 82% of P_i (0.61 mmol/g) were adsorbed in 5 min. Such a rapid adsorption of $As_{(V)}$ and P_i on iron oxides has been previously reported by several researchers (e.g., Grossl et al., 1997; Luengo et al., 2006). However, a sluggish adsorption was ensued after the initial rapid adsorption and reached to 97% of adsorption in 48 h. Similar kinetics but less adsorption was occurred at pH 8. In the first 5 min, about 41% of $As_{(V)}$ and 44% of P_i were removed from the solution, and their adsorption reached to about 57% and 58% in 48

h, respectively. The rapid initial uptake of oxyanions by ferric-hydroxide was attributed to adsorption on surface/near-surface sites while the later slow sorption was controlled by diffusion into the interior (e.g., Fuller et al., 1993) or surface precipitation (Zhao and Stanforth, 2001), or heterogeneous surface reactions involving surface sites with different bonding energy (Zhang and Stanforth, 2005).

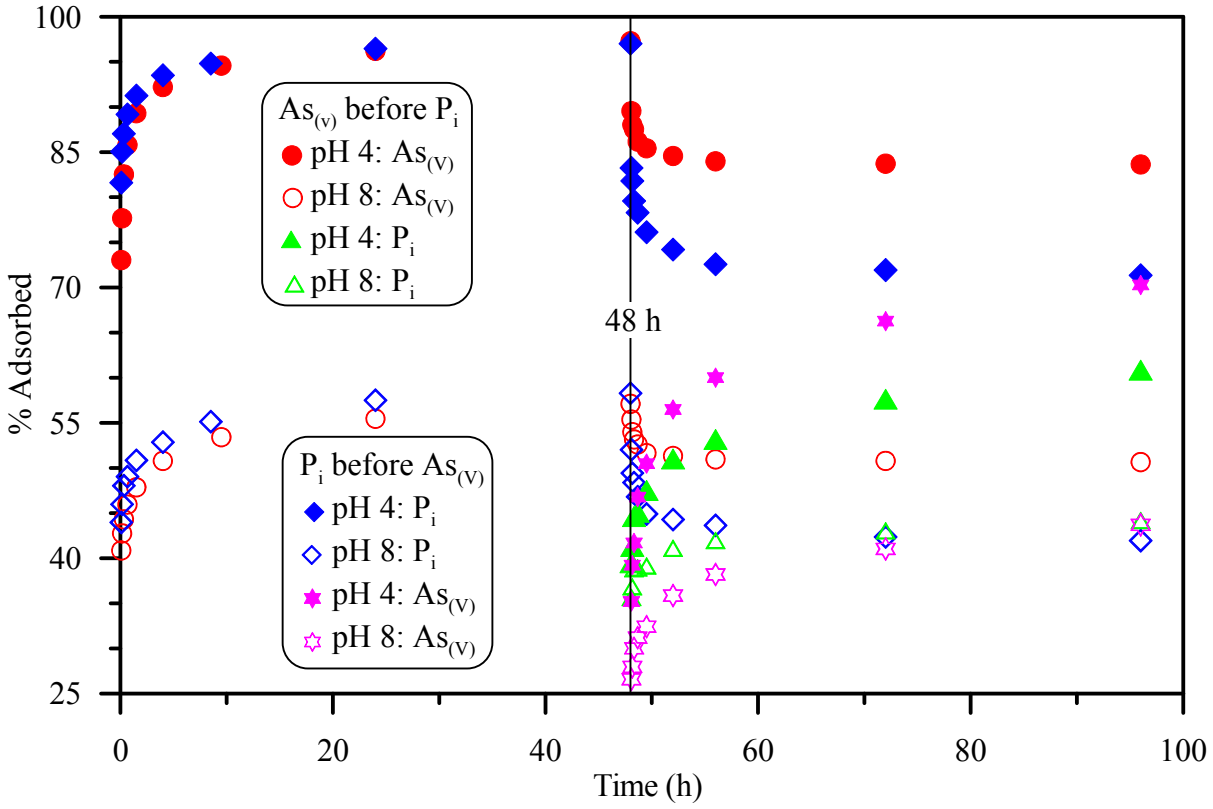

Fig. 4.5. Individual and competitive desorption kinetic of $As_{(V)}$ and P_i. At the beginning, $As_{(V)}$ or P_i stock solution is spiked to 1.5 mM at pH 4 or 8 in pH equilibrated 0.1 M NaCl solution with 2 g/L ferric-hydroxide and reacted for 48 h for individual adsorption kinetic. After 48 h, the suspension is spiked to 1.5 mM of co-oxyanion for competitive adsorption kinetic of sequentially added oxyanion and competitive desorption kinetic of initially loaded oxyanion.

Competitive adsorption kinetics of P_i and $As_{(V)}$ were studied with sequential and simultaneous loadings. Experiments for competitive adsorption kinetics with sequential loadings started at 48 h after addition of $As_{(V)}$ or P_i into the co-oxyanion pre-equilibrated (Fig. 4.5). At pH 4 and 8, nearly 40% and 36% of P_i, and 35% and 27% of $As_{(V)}$ were competitively adsorbed in 5 min after sequential loadings, respectively. With simultaneous loading (Fig. 4.6), 55% of $As_{(V)}$ and 44% of P_i were adsorbed in 5 min at pH 4. Similarly, 31% of $As_{(V)}$ and 27% of P_i were adsorbed in 5 min at pH 8. After 4 h, however, adsorption of both $As_{(V)}$ and P_i slowed as with the single-ion adsorption experiments.

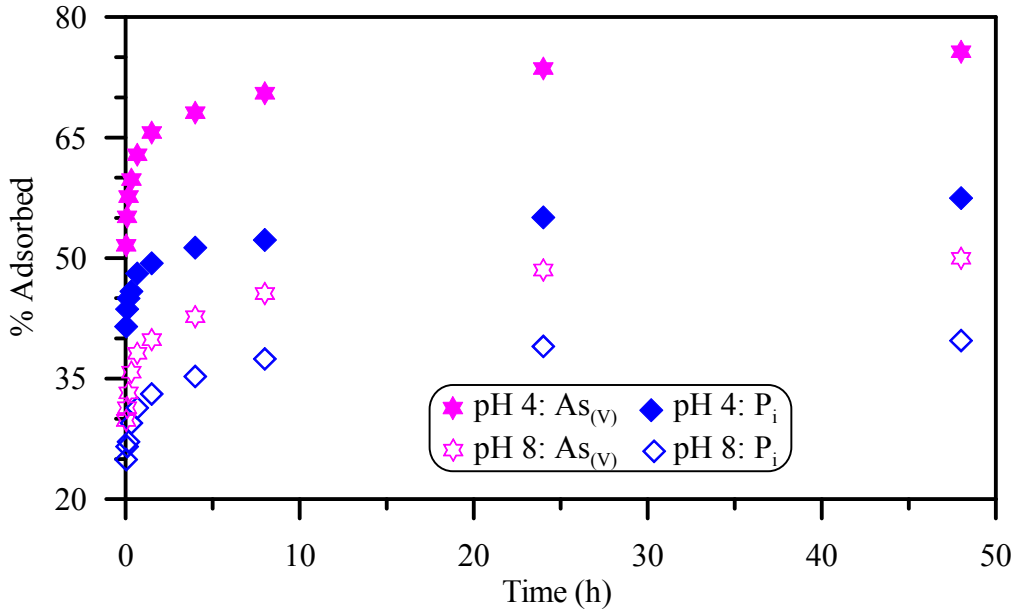

Fig. 4.6. Competitive adsorption kinetic for $As_{(V)}$ and P_i in 0.1 M NaCl solution at 2 g/L ferric-hydroxide after simultaneously spiking of both oxyanions to 1.5 M.

4.3.3.2. Competitive desorption kinetics

Competitive desorption of a pre-equilibrated oxyanion (e.g., $As_{(V)}$) was occurred after the sequential addition of co-oxyanion (e.g., P_i) (Fig. 4.5). The desorbed amount of a pre-equilibrated oxyanion was calculated by subtracting its adsorbed amount at any time after sequential addition of co-oxyanion from its adsorbed amount at equilibrium (at 48 h). Thus calculated desorbed amount of $As_{(V)}$ and P_i were plotted in Fig. 4.7 along with competitively adsorbed amount of sequentially loaded co-oxyanion. Both $As_{(V)}$ and P_i were found partially effective in desorbing co-oxyanion from the ferric-hydroxide . Jackson and Miller (2000) reported a very effective competitive desorption of $As_{(V)}$ from goethite and amorphous Fe oxide surfaces by P_i.

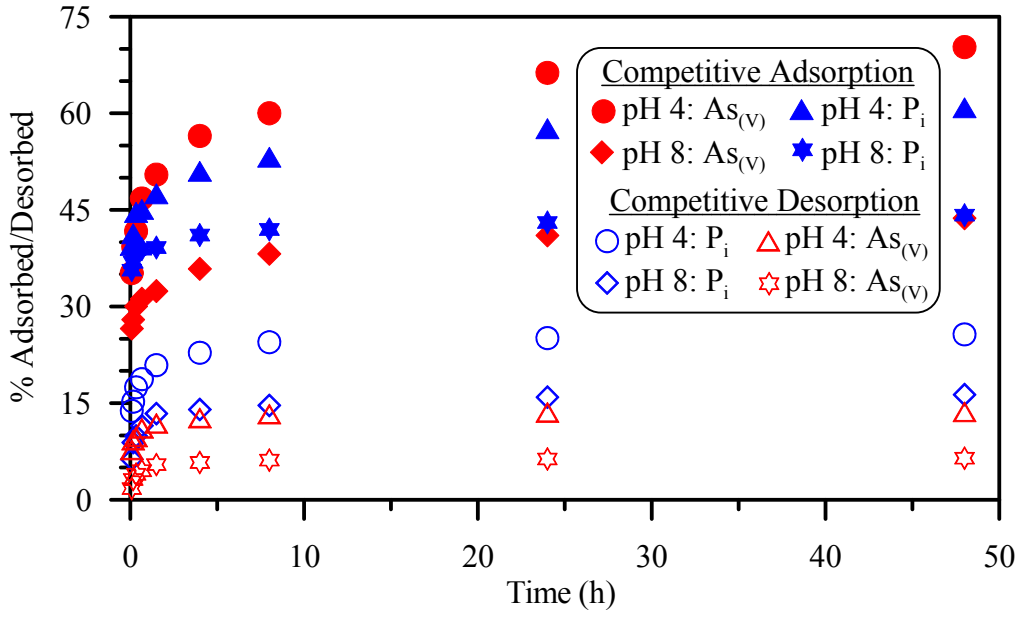

Fig. 4.7. Comparison of competitive desorption of oxyanion ($As_{(V)}$ or P_i) with competitive adsorption of sequentially loaded co-oxyanion (P_i or $As_{(V)}$)

The co-oxyanion induced desorption of $As_{(V)}$ and P_i was rapid at the beginning, which slowed with time (Fig. 4.7). The desorbed amounts of $As_{(V)}$ after 5 min of addition of P_i at pH 4 and 8 were 0.06 mmol/g and 0.01 mmol/g accounting about 8% and 2% of adsorbed amount of $As_{(V)}$, respectively. The desorbed amounts of P_i after 5 min of addition of $As_{(V)}$ at pH 4 and 8 were 0.10 mmol/g and 0.05 mmol/g accounting about 14% and 11% of adsorbed amount of P_i at 48 h, respectively. Competitive desorptions of P_i and $As_{(V)}$ were occurred persistently with increasing contact time but at diminishing rate. The co-oxyanion induced desorptions of $As_{(V)}$ and P_i increased to 0.10 mmol/g and 0.17 mmol/g at pH 4 and 0.04 mmol/g and 0.10 mmol/g at pH 8, respectively in 4 h. Very small desorptions of both oxyanions occurred after 4 h at both pH levels. Such an early rapid then a slow desorption of P_i by $As_{(V)}$ was reported by Puccia et al. (2009). The early rapid desorption of $As_{(V)}$ or P_i was also attributed to surface exchange of oxyanions while the later slower desorption was related to diffusion controlled exchanges.

4.3.3.3. Kinetic modeling

The Pseudo-second order, Elovich, and power-function kinetic models were used to describe the individual/competitive adsorption and desorption kinetic data. The kinetic parameters for these models are presented in Table 4.7 along with coefficient of determination (R^2). All three models were able to predict the general adsorption/desorption kinetics of $As_{(V)}$ and P_i. The good agreement of experimental data with the model equations indicated that diffusion process might be the rate limiting step in adsorption/desorption of $As_{(V)}$ and P_i (Aharoni and Sparks, 1991). Linear plots of pseudo-second order kinetic equations for single-ion adsorption, competitive-ion adsorption after sequential and simultaneous loadings, and

competitive-ion desorption are shown in Fig. 4.8. Adsorption and desorption of both oxyanions during different loading schemes resulted in excellence (R^2>0.99) coefficient of determination (Table 4.7). Recently, some other researchers also showed a good compliance of pseudo-second order equation to their kinetic data of P_i adsorption on multi-component $Al_{(III)}$-$Fe_{(III)}$ hydroxide (Harvey and Rhue, 2008) and α-Al_2O_3 (Del Nero et al., 2010). The good compliance of adsorption kinetic data with pseudo-second order equation can be attributed to a sorption phenomenon in which the rate-limiting step was associated with chemisorption that involves valence forces through sharing or exchange of electrons between sorbent and sorbate (Ho and McKay, 1999). This is consistent with the fact that both $As_{(V)}$ and P_i adsorbed on ferric-hydroxide forming inner-sphere surface complexes (Tejedor-Tejedor and Anderson, 1990; Waychunas et al., 1993). Similarly, Elovich equation also showed a strong ability to describe the $As_{(V)}$ and P_i adsorption/desorption kinetics (Fig. 4.9) with better than 0.88 R^2 values (Table 4.7). The Elovich equation, which is based on assumption that the adsorption energy increases with surface coverage (Low, 1960), has been previously used to describe the kinetics of adsorption/desorption adsorption/desorption of $As_{(V)}$ (Raven et al., 1998) and P_i (Chien and Clayton, 1980) on soil and its constituents. Chein and Clayton (1980) suggested that an increase in α with or without changes in β would indicate a relatively rapid reaction. However, mechanistic inference drawn from nature of α and β was deemed questionable at different situations (Sparks, 1989). The power-function equation also described the experimental data (Fig. 4.10) with R^2 > 0.76 (Table 4.7). The relatively lower R^2 values were particularly associated with desorption. Such a relatively lower R^2 value might indicate that this equation was

not equally suitable for describing desorption kinetics of these oxyanions. The power function reaction rate constants were larger for adsorption than for desorption.

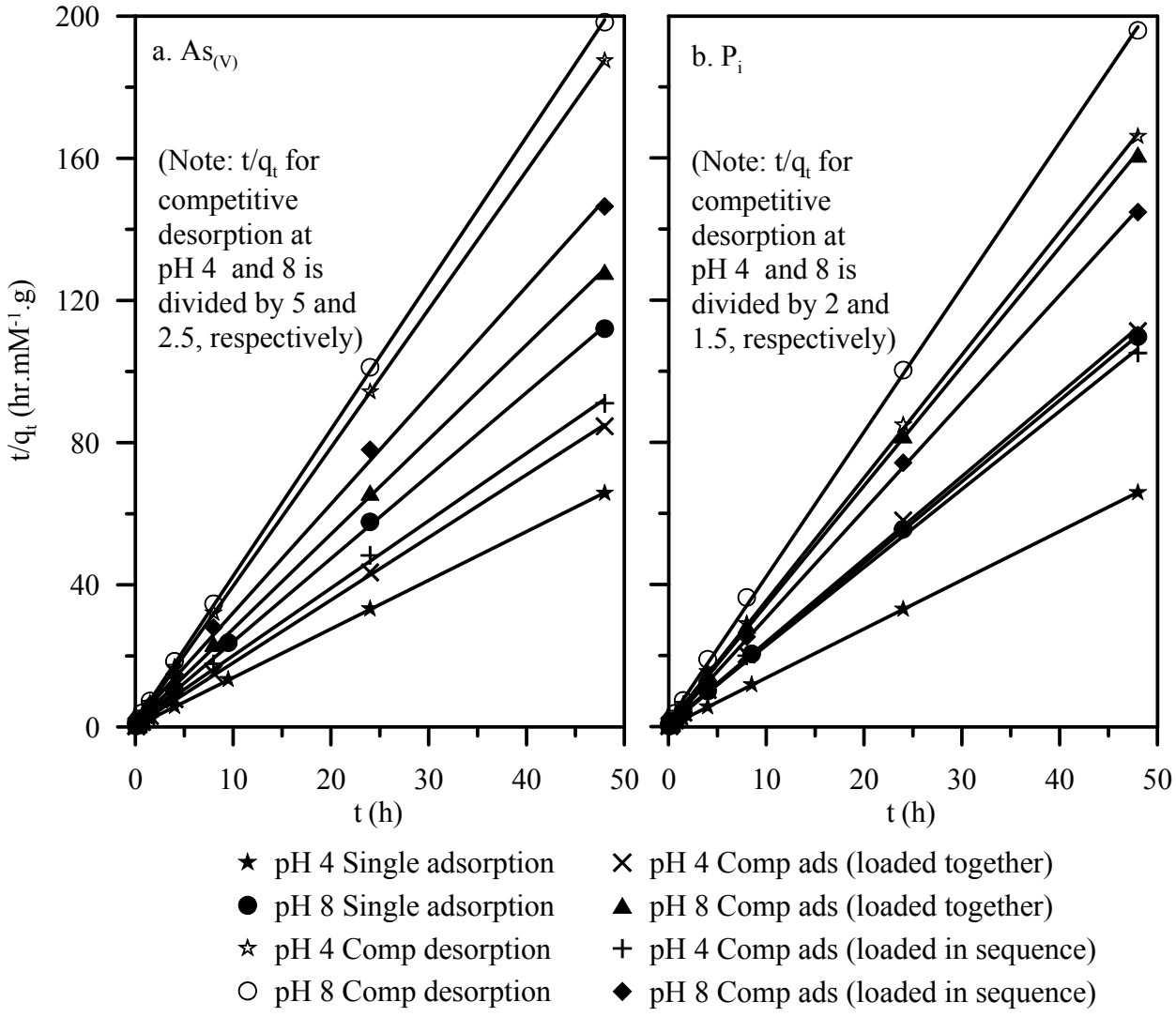

Fig. 4.8. Pseudo-second order adsorption/desorption kinetic plots for $As_{(V)}$ (a) P_i (b) different loading schemes (see Figs. 3 and 4 for detail description of loading schemes)

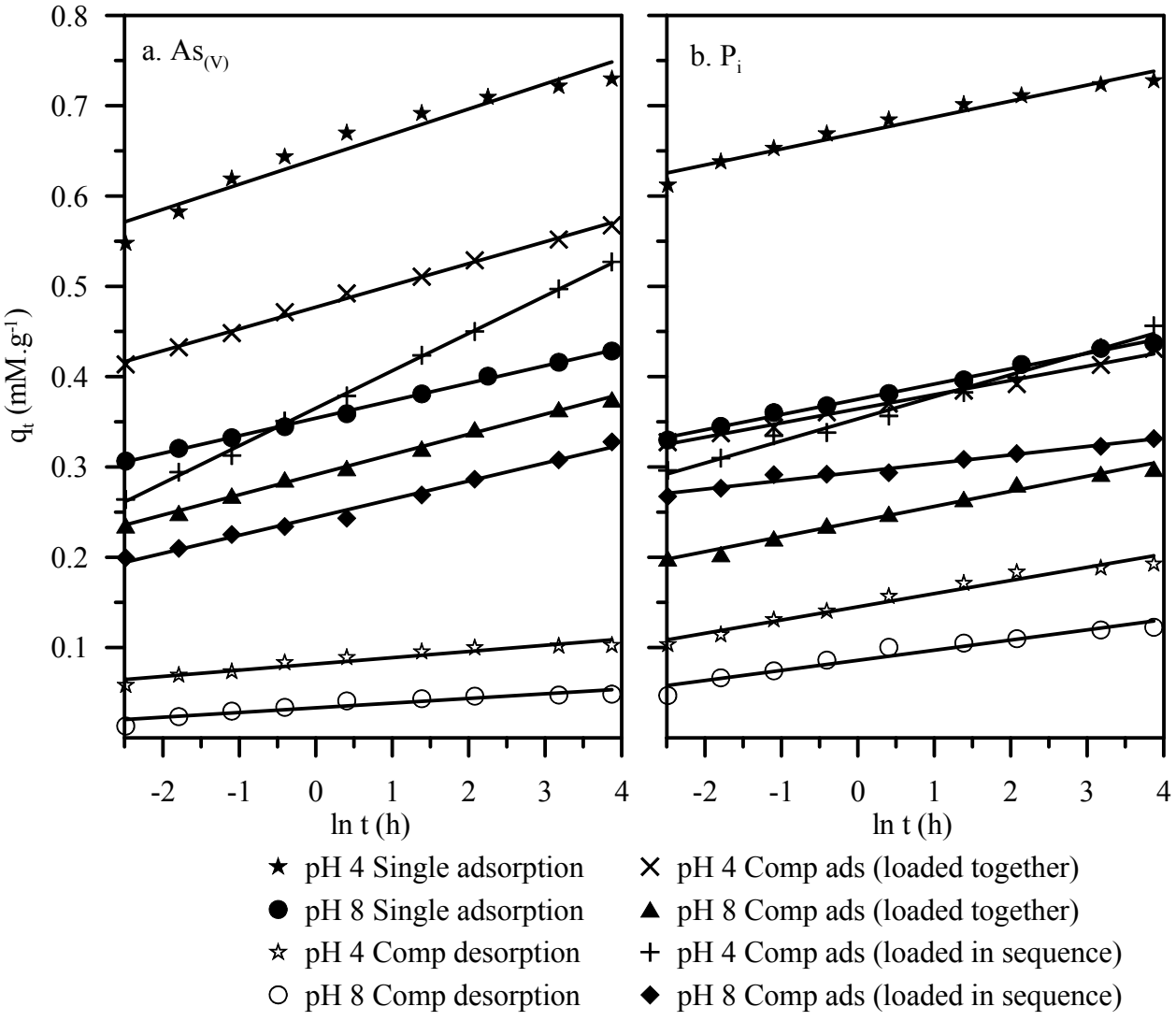

Fig. 4.9. Elovich adsorption/desorption kinetic plots for $As_{(V)}$ (a) P_i (b) different loading schemes (see Figs. 3 and 4 for detail description of loading schemes)

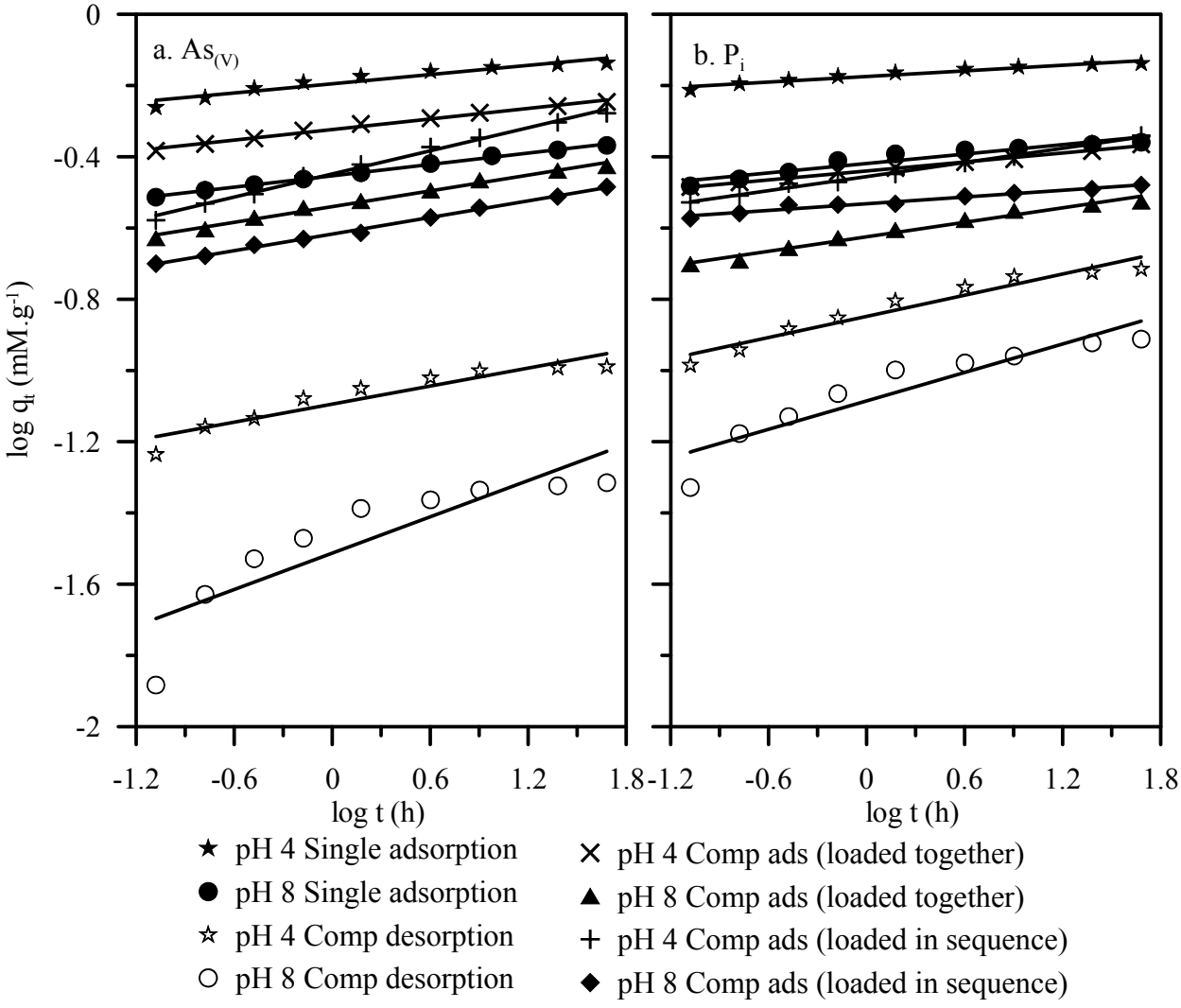

Fig. 4.10. Power-function adsorption/desorption kinetic plots for $As_{(V)}$ (a) P_i (b) different loading schemes (see Figs. 3 and 4 for detail description of loading schemes)

Table 4.7. Absorption/desorption kinetic parameters for pseudo-second order, Elovich, and power function equations

Experiments		Pseudo-second order				Elovich			Power function		
		k	h	q_e	R^2	α	β	R^2		n	R^2
P_i loaded after $As_{(V)}$	pH 4 $As_{(V)}$ adsorption	10.80	5.75	0.73	0.99996	2.81×10^8	35.95	0.94416	0.638	0.043	0.92557
	pH 8 $As_{(V)}$ adsorption	8.59	1.57	0.43	0.99971	1.61×10^6	51.52	0.99850	0.352	0.053	0.99764
	pH 4 $As_{(V)}$ desorption	56.72	0.60	0.10	0.99998	9.86×10^2	144.93	0.92463	0.080	0.084	0.88716
	pH 8 $As_{(V)}$ desorption	65.85	0.16	0.05	0.99992	3.21	193.05	0.88397	0.031	0.170	0.76374
	pH 4 P_i adsorption	5.01	1.04	0.46	0.99905	4.62×10^4	40.92	0.98835	0.350	0.066	0.99384
	pH 8 P_i adsorption	17.09	1.87	0.33	0.99982	3.40×10^{11}	104.06	0.97386	0.294	0.031	0.96896
$As_{(V)}$ loaded after P_i	pH 4 P_i adsorption	16.15	8.56	0.73	0.99998	4.80×10^{14}	33.80	0.96360	0.667	0.026	0.95423
	pH 8 P_i adsorption	11.31	2.17	0.44	0.99988	7.01×10^7	59.07	0.99740	0.373	0.044	0.99182
	pH 4 P_i desorption	18.37	0.68	0.19	0.99986	2.99×10^2	68.40	0.96777	0.142	0.099	0.94149
	pH 8 P_i desorption	20.54	0.31	0.12	0.99967	2.36×10^1	89.05	0.94148	0.082	0.133	0.86739
	pH 4 $As_{(V)}$ adsorption	3.34	0.93	0.53	0.99883	2.76×10^2	24.12	0.99874	0.356	0.108	0.99209
	pH 8 $As_{(V)}$ adsorption	6.24	0.67	0.33	0.99885	4.10×10^3	50.05	0.98926	0.241	.078	0.99586
Loaded together	pH 4 $As_{(V)}$ adsorption	8.33	2.68	0.57	0.99974	5.89×10^6	40.52	0.99626	0.473	0.052	0.98753
	pH 8 $As_{(V)}$ adsorption	8.82	1.24	0.37	0.99961	1.47×10^4	45.89	0.99624	0.288	0.074	0.99305
	pH 4 P_i adsorption	9.26	1.71	0.43	0.99946	1.83×10^8	63.61	0.99338	0.363	0.043	0.99490
	pH 8 P_i adsorption	14.92	1.33	0.30	0.99983	3.64×10^4	60.86	0.99023	0.237	0.068	0.98433

Units: Pseudo-second order: k ($g.mmol^{-1}$ hr), h ($mmol.g^{-1}$ hr), q_e ($mmol.g^{-1}$)
Elovich: α ($mmol.g^{-1}.hr^{-1}$), β ($g.mmol^{-1}$)
Power function: ($mmol.\ g^{-1}$), n ($mmol.\ g^{-1}.hr^{-1}$)

The influence of pH on adsorption/desorption kinetics could be evaluated by the close inspection of linear Elovich and power function plots. These plots (Figs.4.9 and 4.10) were mostly parallel to sub-parallel to each other except the plots for competitive adsorption with sequential loading. Therefore, reaction rates were independent of pH when oxyanions were loaded separately or simultaneously. Zhang and Stanforth (2005) also reported a parallel Elovich plots at pH 4, 7, and 10, and suggested a pH independent kinetics for $As_{(V)}$ adsorption on goethite.

4.3.3.4. Comparison of individual and competitive adsorption kinetics

At both pHs, the adsorption of each oxyanion was greater when loaded separately than together (Figs. 4.5 and 4.6). Relatively, the decrease in adsorption of P_i was greater than the decrease in adsorption of $As_{(V)}$ in competitive setting. At pH 4, near complete (97%) adsorptions of both oxyanions were resulted in during single adsorption experiments while only 76% of $As_{(V)}$ and 57% of P_i were adsorbed when loaded together. Similarly, about a three-fifths of $As_{(V)}$ and P_i were adsorbed during single adsorption experiments at pH 8 but their adsorptions decreased to 50% and 40%, respectively at the same pH during competitive experiments. Competitive loading schemes also caused a minor change in adsorption of $As_{(V)}$ in such a way that a slightly greater adsorption of $As_{(V)}$ occurred with simultaneous loading (76% at pH 4 and 50% at pH 8) than with sequential loading (70% at pH 4 and 44% at pH 8). However, almost similar adsorption of P_i (57-61% at pH 4 and 40-42% at pH 8) occurred with both loading schemes.

The presence of co-oxyanion not only decreased the partial surface coverage of an oxyanion, but it also changed the adsorption kinetics. The pseudo-second order reaction rates (k and h), Elovich constant (α), and power function rate constant (a) for competitive adsorptions of

$As_{(V)}$ and P_i were lower than these rates/constants for individual adsorption (Table 4.7). Su and Puls (2001) also noted a significant decrease in sorption kinetics of $As_{(V)}$ on zero-valent iron in the presence of P_i. However, Chen et al. (1973) reported a decrease in initial adsorption amount of P_i but not the first order sorption rate in the presence of fluoride.

4.3.3.5. Comparison between competitive adsorption of $As_{(V)}$ with competitive desorption of P_i and vice versa

The competitive adsorptions of $As_{(V)}$ and P_i after sequential loading were accompanied by competitive desorption of pre-equilibrated oxyanion (Figs. 4.5 and 4.7). Significant amount of pre-equilibrated oxyanions remained bound to ferric-hydroxide. O'Reilly et al. (2001) also reported a significant amount of As remained bound to goethite even after 5 months of P_i-induced desorption. With respect to the total adsorbed amounts of oxyanions at equilibrium (at 48 h of contact time) at each pH, only 11-14% of $As_{(V)}$ and 26-28%) P_i were desorbed. The pH independent proportionate desorptions of $As_{(V)}$ and P_i were reported by several researchers (e.g. Strauss et al., 1997). With respect to the initial concentrations, however, a greater desorption of each oxyanion occurred at pH 4 than at pH 8 (Fig. 4.7).

Using ATR-FTIR spectroscopy for studying the competitive adsorption/desorption of $As_{(V)}$ and P_i, Carabante et al. (2010) reported that the co-oxyanion induced desorption of $As_{(V)}$ and P_i occurred by replacing the deuterated surface species of pre-equilibrated oxyanion by de-deuterated surface species of sequentially loaded co-oxyanion. Previously, Puccia et al. (2009) reported a mole-for-mole exchange of sequentially loaded $As_{(V)}$ with pre-equilibrated P_i. But in our experiments, the competitive adsorption of sequentially loaded co-oxyanion was greater than the competitive desorption of pre-equilibrated oxyanion (Fig. 4.7). Furthermore, the competitive

desorption of pre-equilibrated co-oxyanion was negligible after an early rapid desorption. Such a greater competitive adsorption than the competitive desorption of co-oxyanion might suggest the presence of both anion specific and competing adsorption sites on ferric-hydroxide.

Comparatively, a greater desorption of P_i was induced by $As_{(V)}$ than *vice versa* (Fig.4.7). The greater $As_{(V)}$ induced desorption of P_i from ferric-hydroxide was consistent with the greater adsorption preference of $As_{(V)}$ after simultaneous loading or greater amount of non-exchangeable $As_{(V)}$ remained after the sequential loading of P_i. Previously, Liu et al. (2001) also reported a greater $As_{(V)}$ induced desorption of P_i than *vice versa* from goethite. Similarly, Carabante et al. (2010) also reported a requirement of five times greater concentration of P_i than $As_{(V)}$ to desorb an equivalent amount of previously adsorbed co-oxyanion on ferrihydrite.

4.3.3.6. As K-edge EXAFS analysis of kinetic samples

Some selected adsorption/desorption kinetic samples were investigated with As K-edge EXAFS analysis to determine the nature of $As_{(V)}$ complexation at the ferric-hydroxide -water interface in the presence or absence of P_i with time. Fig. 4.11 shows the k3-weighted As k-edge EXAFS spectra and their Fourier transformed spectra for kinetic samples collected at 5 min, 4 h (only for pH 4), and 24 h after addition of $As_{(V)}$ at pH 4 and 8. Similarly, Fig. 4.11 also includes EXAFS spectra of desorption kinetic samples collected at 5 min, 4 h (only for pH 4), and 24 h after addition of P_i into the reaction vessel containing $As_{(V)}$ equilibrated ferric-hydroxide . Structural parameters obtained after least-square fitting of these EXAFS spectra for samples at pH 4 and 8 are presented in Tables 4.8.

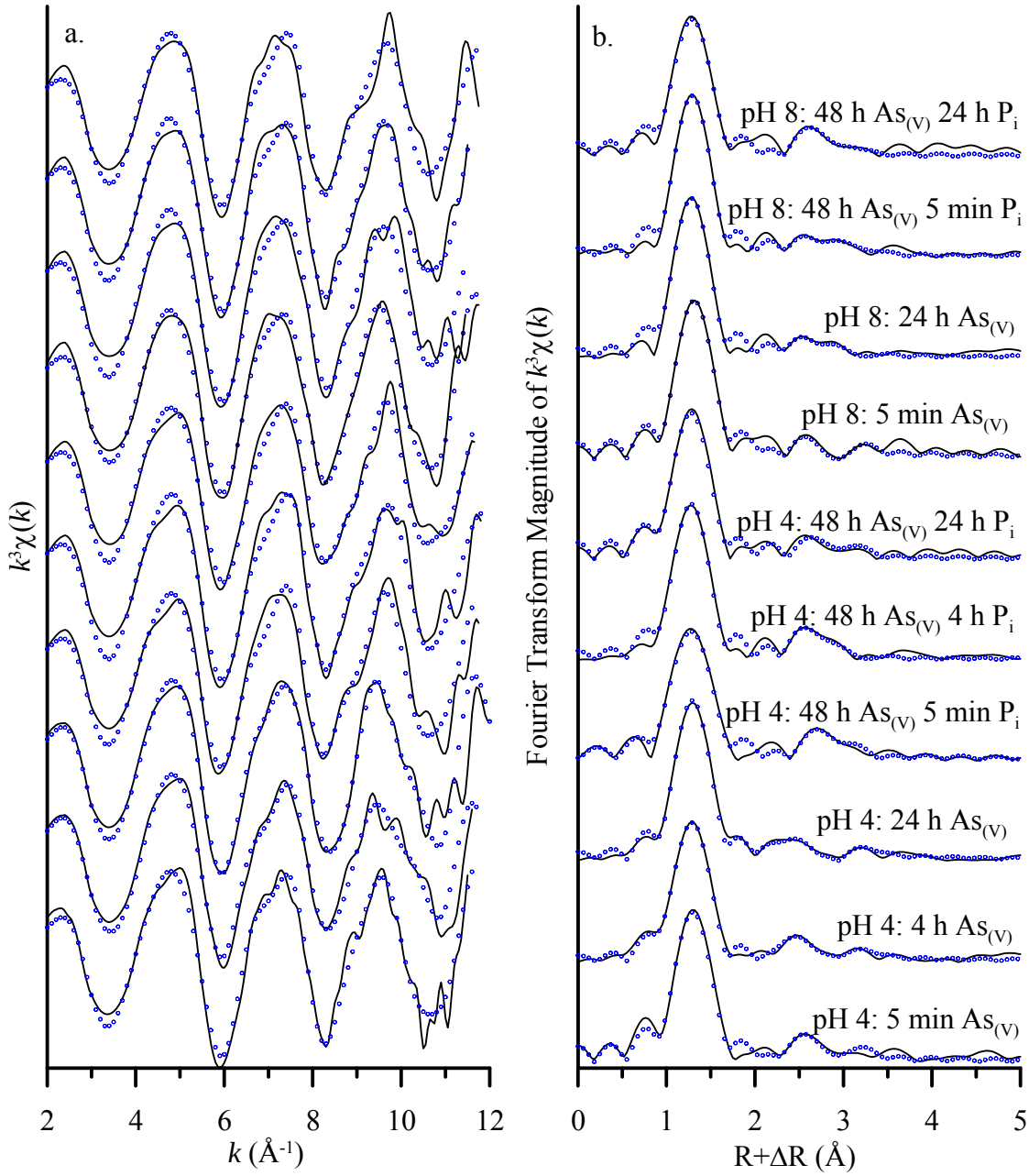

Fig. 4.11. a) Normalized and background subtracted k^3-weighted As K-edge EXAFS spectra. b) Fourier-transformed k^3-weighted As K-edge EXAFS spectra (phase shift uncorrected). Solid lines represent experimental data of $As_{(V)}$ adsorbed ferric-hydroxide samples at pH 4 and 8 while open circles represent the theoretical non-linear least-square fit to the experimental data

Each $As_{(V)}$ EXAFS spectrum shown in Fig. 4.11a is characterized by a strong sinusoidal oscillations originated from the back-scattering of surrounding oxygen atoms. Primarily, the near symmetrical k-space spectral feature between 4 to 6 $Å^{-1}$ was qualitatively used as an indication of adsorption dominated mechanism for $As_{(V)}$ interaction on ferric-hydroxide (Chen et al., 2009). Concentration of Fe in supernatants from blank ferric-hydroxide and $As_{(V)}/P_i$ reacted ferric-hydroxide at pH 4 and 8 were near or below the ICP-OES detection limit. The PHREEQC (Parkhurst and Appelo, 1999) simulations for equilibrium aqueous concentrations of Fe and C_i of $As_{(V)}$ indicated that all experimental systems were undersaturated with crystalline scorodite (K_{sp} = -25.83) and amorphous ferric arsenate (-23.0) (Langmuir et al., 2006). The As-O oscillations resulted in a strong peak in the Fourier transformed spectra (Fig. 4.11b). This peak represented the first coordination shell of four O atoms at a distance of 1.70-1.71 Å from the central As atom. Previous researchers (Waychunas et al., 1993; Foster et al.,, 1998) also reported a similar As-O distances for the adsorbed $As_{(V)}$ at the metal oxides water interface.

Two As-Fe shells were identified for the $As_{(V)}$ complexation on ferric-hydroxide. The As-Fe1 shell was located at a distance of 2.82 to 2.90 Å, and it has been attributed to the bidentate mononuclear edge sharing complex (^{2}E) (Fendorf et al., 1997; Waychunas et al., 2005).

Similarly, the As-Fe2 shell was defined with a distance of 3.29 to 3.38 Å, which has been attributed to the bidentate binuclear corner sharing complex (^{2}C) (Arai et al., 2004; Waychunas et al., 2005). A multiple scattering of $As\text{-}O_{(MS)}$ was also considered during model fitting. This $As\text{-}O_{(MS)}$ contributed a broad peak at a distance of 3.18-3.32 Å to the overall Fourier transformed magnitude. The inclusion of $As\text{-}O_{(MS)}$ slightly increased the quality of the fit; however, the consideration of this multiple scattering was not enough to discard the As-Fe1 shell as suggested by Sherman and Randall (2003).

Table 4.8. Structural parameters from the least-squares analysis of As K-edge EXAFS spectra of $As_{(V)}$ adsorbed ferric-hydroxide samples at pH 4 and 8 at different times and loading schemes

Sample	Shells	σ^2 (Å^2)[a]	ΔE_0 (eV)	R (Å)[b]	CN[c]	R-factor
pH 4: $As_{(V)}$ 5 min	As-O	0.0010	8.72	1.71	3.81	0.018
	As-Fe1	0.005[d]		2.85	0.85	
	As-Fe2	0.005[d]		3.32	1.16	
	$As\text{-}O_{(MS)}$	0.007[d]		3.25	8.95	
pH 4: $As_{(V)}$ 4 h	As-O	0.0031	9.87	1.71	4.17	0.010
	As-Fe1	0.005[d]		2.86	1.19	
	As-Fe2	0.005[d]		3.38	1.22	
	$As\text{-}O_{(MS)}$	0.007[d]		3.32	7.52	
pH 4: $As_{(V)}$ 24 h	As-O	0.0009	9.32	1.71	3.86	0.007
	As-Fe1	0.005[d]		2.83	1.22	
	As-Fe2	0.005[d]		3.38	1.21	
	$As\text{-}O_{(MS)}$	0.007[d]		3.30	8.91	
pH 4: $As_{(V)}$ 48 h P_i 5 min	As-O	0.0011	8.31	1.70	3.63	0.024
	As-Fe1	0.005[d]		2.90	0.76	
	As-Fe2	0.005[d]		3.33	1.37	
	$As\text{-}O_{(MS)}$	0.007[d]		3.21	9.65	
pH 4: $As_{(V)}$ 48 h P_i 4 h	As-O	0.0016	7.60	1.70	4.07	0.015
	As-Fe1	0.005[d]		2.88	0.56	
	As-Fe2	0.005[d]		3.29	1.07	
	$As\text{-}O_{(MS)}$	0.007[d]		3.18	9.13	
pH 4: $As_{(V)}$ 48 h P_i 24 h	As-O	0.0018	8.46	1.70	3.83	0.014
	As-Fe1	0.005[d]		2.82	0.45	
	As-Fe2	0.005[d]		3.34	1.06	
	$As\text{-}O_{(MS)}$	0.007[d]		3.21	9.76	
pH 8: $As_{(V)}$ 5 min	As-O	0.0001	8.50	1.71	3.53	0.015
	As-Fe1	0.005[d]		2.84	0.68	
	As-Fe2	0.005[d]		3.35	1.05	
	$As\text{-}O_{(MS)}$	0.007[d]		3.29	6.82	
pH 8: $As_{(V)}$ 24 h	As-O	0.0016	6.85	1.70	4.19	0.018
	As-Fe1	0.005[d]		2.84	0.71	
	As-Fe2	0.005[d]		3.29	1.29	
	$As\text{-}O_{(MS)}$	0.007[d]		3.23	8.49	
pH 8: $As_{(V)}$ 48 h P_i 5 min	As-O	0.0010	8.81	1.71	3.78	0.013
	As-Fe1	0.005[d]		2.83	0.59	
	As-Fe2	0.005[d]		3.32	1.31	
	$As\text{-}O_{(MS)}$	0.007[d]		3.25	9.69	
pH 8: $As_{(V)}$ 48 h P_i 24 h	As-O	0.0016	8.49	1.70	3.74	0.029
	As-Fe1	0.005[d]		2.89	0.55	
	As-Fe2	0.005[d]		3.31	1.14	
	$As\text{-}O_{(MS)}$	0.007[d]		3.22	6.30	

[a] Debye-Waller factor, [b] Interatomic distance, [c] Coordination number, [d] Fixed

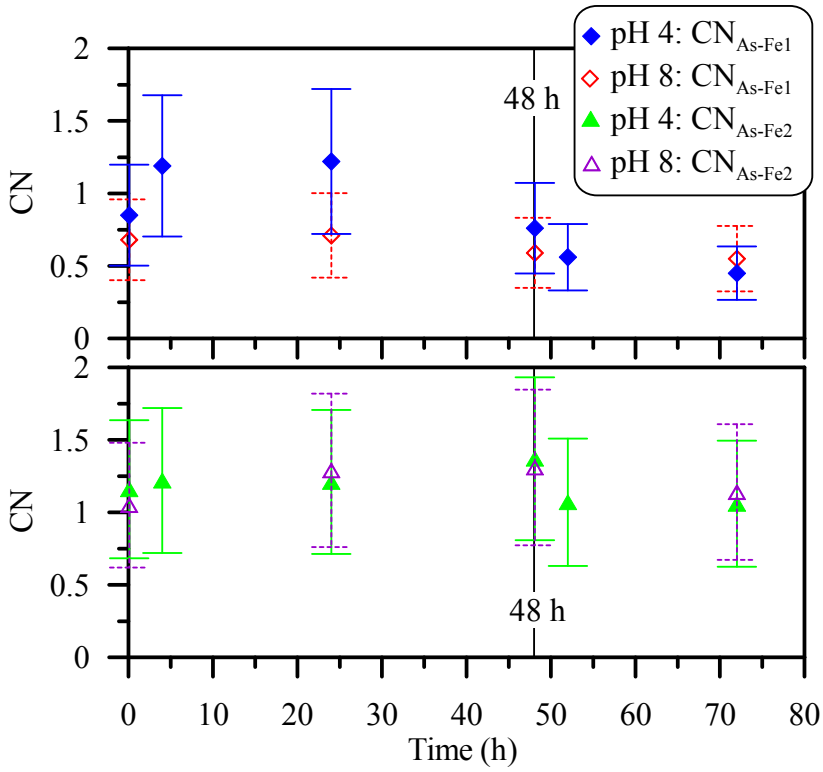

Fig. 4.12. Changes in As-Fe coordination numbers with time and addition of P_i at 48 h

Although the CN values obtained with EXAFS were relatively less accurate (±41%), the intensities of ^{2}E and ^{2}C varied in samples with time (Table 4.8 and Fig. 4.12). The CNs for ^{2}E and ^{2}C were increased with increasing contact time but decreased after addition of P_i into the system. Relatively, higher proportion of CN associated with ^{2}E was decreased with the addition of P_i than CN associated with ^{2}C. Fendorf et al. (1997) suggested greater complexation energy for ^{2}E than ^{2}C; therefore, the former might be more susceptible to desorption from ferric-hydroxide surface by P_i. The small amount of P_i induced desorption of $As_{(V)}$ at pH 8 was also reflected in relatively small decrease in combined CN of As-Fe shells (Fig. 4.12), after the addition of P_i into the $As_{(V)}$ equilibrated system at pH 8.

4.3.5. Comparison of single and competitive adsorptions

At each pH, greater adsorption of $As_{(V)}$ and P_i was occurred in single adsorption experiments than in competitive experiments. Comparatively, P_i showed a greater decrease in adsorption in competitive setting than $As_{(V)}$. When loaded together, adsorption of $As_{(V)}$ was decreased by a third while adsorption of P_i was diminished by more than a half with respect to their adsorption in single adsorption experiments (Figs. 4.1 and 4.2). The diminished adsorption of $As_{(V)}$ and P_i in competitive experiments could be attributed to adsorption inhibition by co-oxyanion or competition for adsorption sites.

For a similar C_i, the combined adsorption (adsorbed $As_{(V)}$ + adsorbed P_i) in competitive experiment was greater than the adsorption of a sorbate in single adsorption experiment. Previously, (Zhao and Stanforth, 2001) also reported a greater total surface coverage of $As_{(V)}$ and P_i in competitive experiments than in single anion experiments. However, the above inference was obtained by considering the surface coverage with respect partial C_i (or partial C_e) for competitive experiments. To see whether there was a greater total surface coverage during competitive experiments, $As_{(V)}$ and P_i isotherms at pH 4, 8, and 11 were reconstructed (Fig. 4.13) by plotting the total adsorption against total $C_{e\text{-combined}}$ (C_e of $As_{(V)}$ + C_e of P_i).The adsorption isotherms shown in Fig. 8 illustrate that there was no such enhanced adsorption during competitive experiments compared to the adsorptions of these oxyanions in single adsorption experiments. The overall competitive adsorption behaved as if it were a single adsorption system.

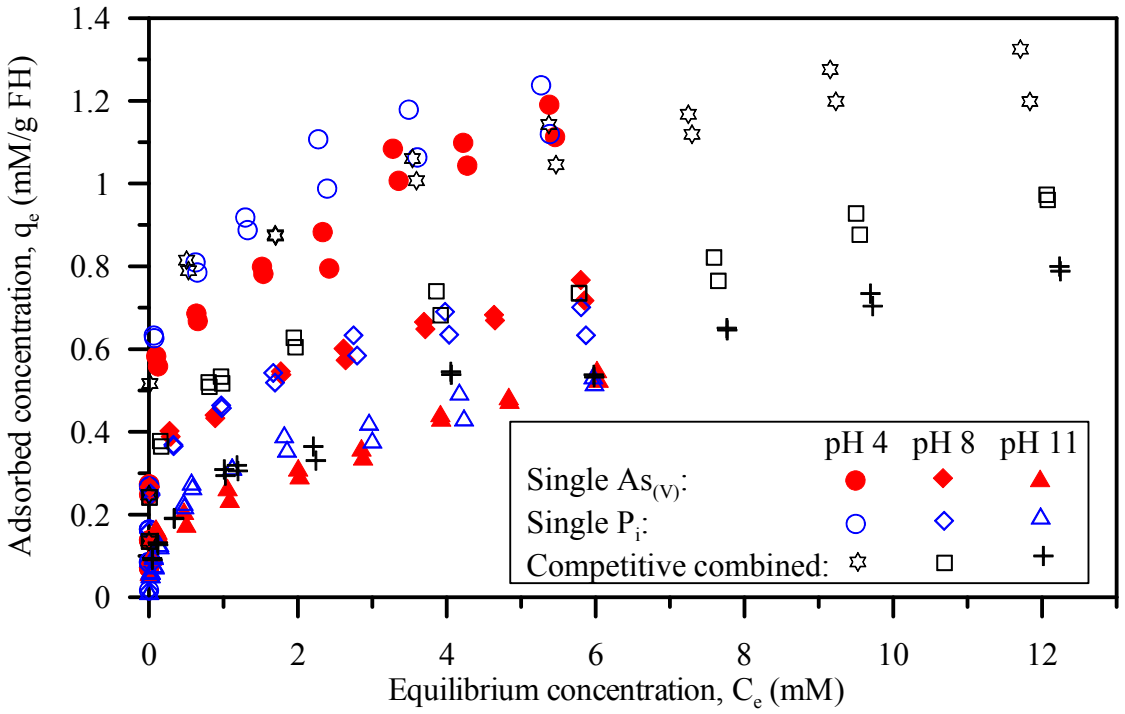

Fig. 4.13. Arsenate and P_i adsorption isotherms at pH 4, 8, and 11. The adsorbed concentration for combined data set represents sum of adsorbed $As_{(V)}$ and P_i while the sum of equilibrium concentrations of $As_{(V)}$ and P_i in equilibrium solution during competitive adsorption.

4.3.6. Preference of $As_{(V)}$ during competitive adsorption

Though both oxyanions have similar adsorption in single adsorption experiments, $As_{(V)}$ was preferentially adsorbed in competitive experiments. Previous researchers (e.g., Manning and Goldberg, 1996; Liu et al., 2001) also reported a higher adsorption affinity of $As_{(V)}$ on iron hydroxides in competitive experiments. Experiments using equimolar C_i of $As_{(V)}$ and P_i indicated a higher adsorption of $As_{(V)}$ on Fe, Mn, and Ti oxides and on Fe-rich clays (Violante and Pigna 2002) in 0.05 M KCl solutions. The adsorption preference of $As_{(V)}$ and P_i during individual as well as competitive adsorption settings were evaluated by calculating the molar adsorption ratio (MAR) of adsorbed $As_{(V)}$ to adsorbed P_i during competitive adsorption experiments. A value of MAR close to 1 indicates an equal adsorption preference for both oxyanions while a value of

MAR less than 1 or more than 1 suggests a greater or less adsorption preference of P_i than $As_{(V)}$ on ferric-hydroxide . The MARs for single adsorption were calculated using single adsorption kinetic data while the MARs for competitive adsorptions were calculated using competitive kinetic data as well as competitive adsorption isotherm data at pH 4, 8, and 11.

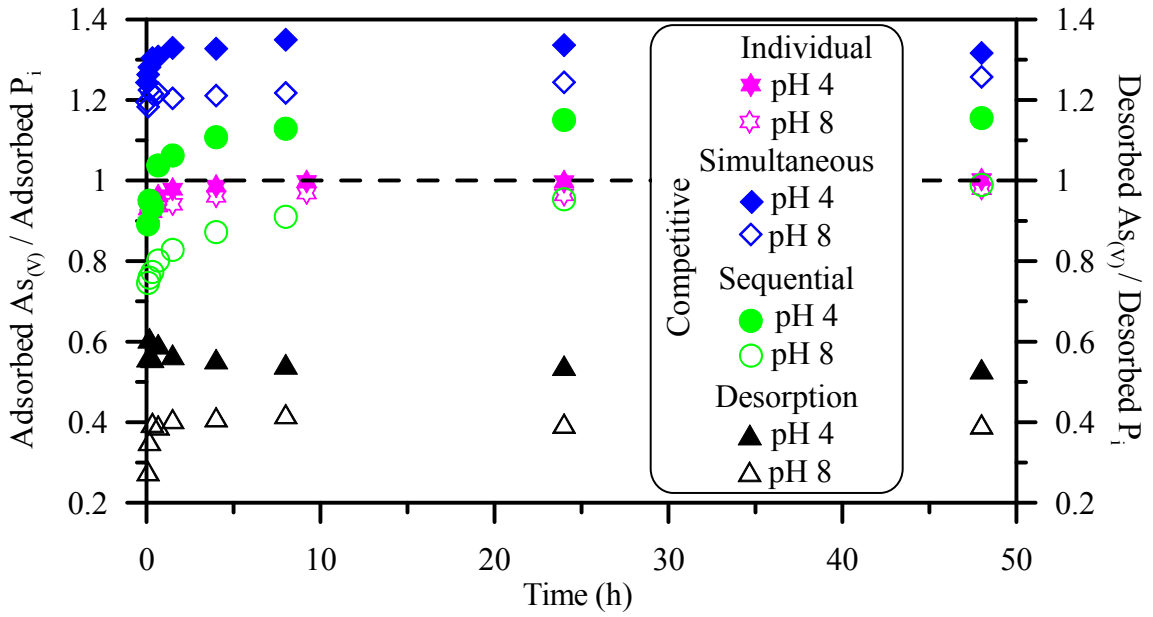

Fig. 4.14. Molar ratio (adsorbed $As_{(V)}$/adsorbed P_i and desorbed $As_{(V)}$/desorbed P_i) plots for different loading schemes.

MARs for single adsorption experiments were very close to 1 (>0.94) after 20 and 40 min at pH 4 and pH 8, respectively (Fig. 4.14). The MARs values of 0.90-0.94 might indicate a slightly faster or greater adsorption of P_i at the beginning of experiments. On the other hand, greater amount of $As_{(V)}$ than P_i was adsorbed in competitive setting at pH 4 and 8 with MAR values ranging from 1.18 to 1.35 (Fig. 4.14). For competitive adsorption with sequential loading, the MARs at pH 4 were >1 after 20 min; however, MARs were less than or close to 1 at pH 8.

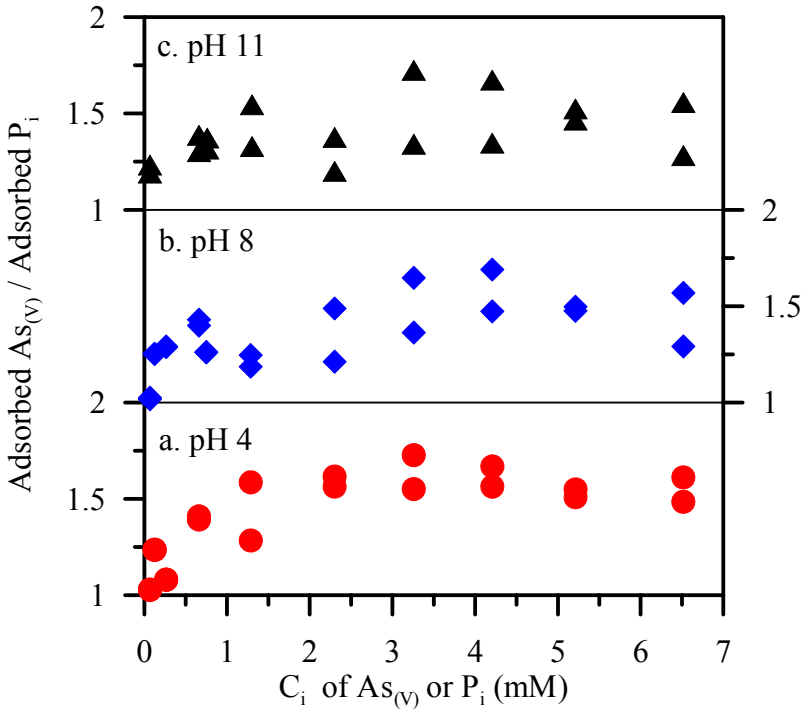

Fig. 4.15. Molar adsorption ratio of adsorbed $As_{(V)}$ and adsorbed P_i during competitive adsorption experiments at pH 4, 8, and 11. The ratio of initial concentration of $As_{(V)}$ and P_i was 1.04 ± 0.06.

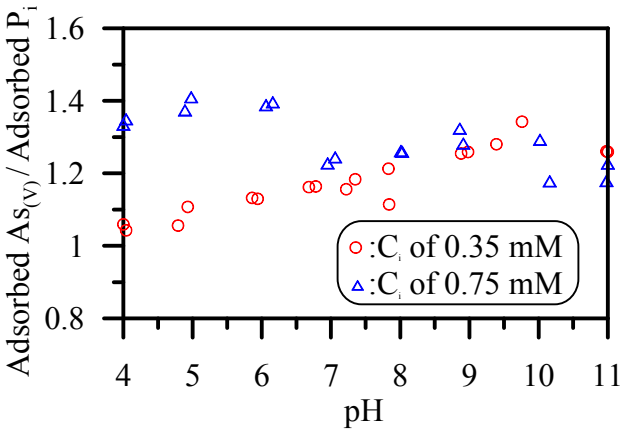

Fig. 4.16. Molar adsorption ratio of adsorbed $As_{(V)}$ and adsorbed P_i during competitive adsorption experiments as a function of pH.

Similarly, MARs of oxyanions during competitive adsorption isotherm at pH values of 4, 8, and 11 (Fig. 4.15) and adsorption envelopes (Fig. 4.16) experiments were also consistently

greater than 1. The MARs for the desorbed $As_{(V)}$ to desorbed P_i at pH 4 and 8 (Fig. 4.14) were significantly lower than 1 indicating a greater competitive desorption of P_i by $As_{(V)}$ than *vice versa*. For sequential addition of $As_{(V)}$, MAR gradually increased from <0.5 to ~1 at pH 4 and pH 8 (Fig. 4.17). While MAR decreased from 2.27 to 1.37 at pH 4 and 1.55 to 1.15 at pH 8 after the sequential addition of P_i into the systems with pre-equilibrated $As_{(V)}$. Such evolution of MAR with time for both loading schemes illustrated the preferential adsorption of $As_{(V)}$ in competitive setting. Apparently, greater MARs at pH 4 than at pH 8 for $As_{(V)}$ before P_i systems (Fig. 4.14) indicated an enhanced adsorption preference of $As_{(V)}$ at lower pH level. The potential cause for greater adsorption preference of $As_{(V)}$ in competitive setting could be attributed to different factors including greater affinity of P_i-Na^+ ion pair formation than $As_{(V)}$-Na^+ ion pairs (Gao and Mucci, 2001) or stronger bond formation during $As_{(V)}$ adsorption than Pi adsorption.

4.4. Conclusions

Arsenate and P_i show a strong adsorption affinity at the ferric-hydroxide -water interface. Their adsorption on ferric-hydroxide was largely controlled by pH and C_i. Adsorption of these oxyanions decreased with increasing pH and greater fractions of sorbates were adsorbed at lower C_i than at higher C_i. Freundlich isotherm model was able to predict the single adsorption isotherm data while competitive Langmuir model predicted the competitive adsorption of both oxyanions. Triple layer model with bidentate surface complexation reactions was used to describe the single as well as competitive adsorption envelopes. The TLM simulations slightly underpredicted the adsorption at lower and upper pH regions while overpredicted the adsorption at intermediate pH levels (6.5-8).

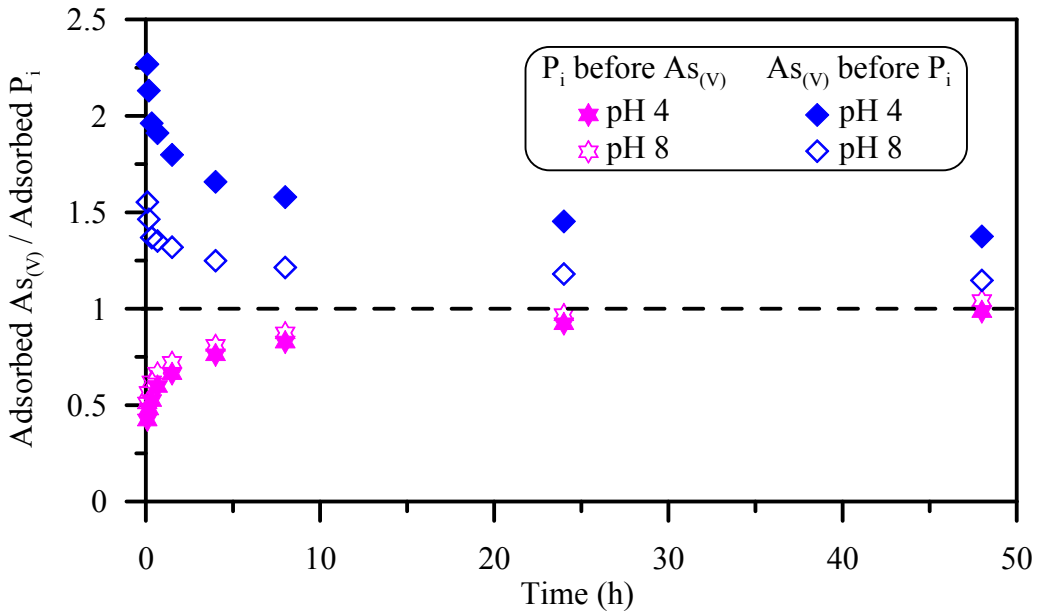

Fig. 4.17. Molar ratio (adsorbed $As_{(V)}$/adsorbed P_i) plots for data after sequential loading of co-oxyanion. For P_i before $As_{(V)}$ scheme, the adsorbed P_i is the remaining amount of adsorbed P_i after sequential addition of $As_{(V)}$ and for $As_{(V}$ before P_i system the adsorbed $As_{(V}$ is the remaining amount of adsorbed $As_{(V}$ after sequential addition of P_i. After sequential loading, the pre-equilibrated oxyanion was competitively desorbed while the sequentially loaded co-oxyanion was competitively adsorbed.

Individual as well as competitive adsorption/desorption kinetic experiments of $As_{(V)}$ and P_i indicated an early rapid interaction at the ferric-hydroxide -water interface followed by a slow interaction. For both adsorption and desorption, the early rapid kinetics were attributed to surface adsorption/desorption while the later slow kinetics were controlled by the rate limiting diffusion of oxyanions to/from the interior. Both oxyanions showed a limited ability to desorb the previously adsorbed co-oxyanion from the ferric-hydroxide. The competitive desorption of pre-equilibrated co-oxyanion (eg. $As_{(V)}$) was less than the competitive adsorption of sequentially loaded oxyanion (e., P_i). Comparatively, $As_{(V)}$ induced a greater desorption of P_i than vice versa.

The experimental adsorption/desorption kinetic data showed good compliance with pseudo-second order, Elovich, and power-function equations. The As K-edge EXAFS analysis indicated the presence of two types of inner-sphere adsorption complexes: bidentate mononuclear and bidentate binuclear complexes.

Although both $As_{(V)}$ and P_i showed a similar complexation in single adsorption experiments; however, $As_{(V)}$ was preferentially adsorbed in competitive experiments. The adsorption preference of $As_{(V)}$ was potentially related to its tendency to form stronger bond at the ferric-hydroxide-water interface than P_i.

Acknowledgements: We would like to thank Dr. S. Bhattacharyya, E. Grahm, and Z. Yue for their help during laboratory experiments and chemical analysis. P. Dhakal (University of Kentucky) is appreciated for his help in BET surface area measurement of ferric-hydroxide. This research was partly funded by Hooks Fund (UA) and student research grants from Geological Society of America (GSA) and Gulf Coast Association of Geological Societies (GCAGS). Use of the Advanced Photon Source, an Office of Science User Facility operated for the U.S. Department of Energy (DOE) Office of Science by Argonne National Laboratory, was supported by the U.S. DOE under Contract No. DE-AC02-06CH11357. We greatly appreciate beam line scientist T. Bolin for her assistance during XAS data collection.

REFERENCES

Aharoni, C. and Sparks, D.L. (1991) Kinetics of soil chemical reactions- a theoretical treatment. In D.L. Sparks and D.L. Suarez (eds) Rate of soil chemical processes, SSSA Spec. Publ. 27, 1-18.

Alam, M.G.M., Tokunaga, S., and Maekawa, T. (2001) Extraction of arsenic in a synthetic arsenic-contaminated soil using phosphate. Chemosphere 43, 1035-1041.

Anderson, D.M., Glibert, P.M., and Burkholder, J.M. (2002) Harmful algal blooms and eutrophication: Nutrient sources, composition, and consequences. Estuaries and Coasts 25, 704-726.

Arai, Y., Sparks, D.L., and Davis, J.A. (2004) Effects of dissolved carbonate on arsenate adsorption and surface speciation at the hematite-water interface. Environ. Sci. Technol. 38, 817-824.

ATSDR (2000) Case Studies in Environmental Medicine- Arsenic Toxicity. ATSDR Publication No.: ATSDR-HE-CS-2002-0003 U.S. Department of Health and Human Services, Agency for Toxic Substances and Disease Registry, Division of Toxicology and Environmental Medicine, p. 42.

Balistrieri, L.S. and Chao, T.T. (1990) Adsorption of selenium by amorphous iron oxyhydroxide and manganese dioxide. Geochim. Cosmochim. Acta 54, 739-751.

Bates, M.N., Smith, A.H., and Hopenhayn-Rich, C. (1992) Arsenic ingestion and internal cancers: A Review. Am. J. Epidem. 135, 462-476.

Belzile, N., Tessier, A. (1990) Interactions between arsenic and iron oxyhydroxides in lacustrine sediments. Geochim. Cosmochim. Acta 54, 103-109.

Bhattacharyya, S., Donahoe, R.J., and Patel, D. (2009) Experimental study of chemical treatment of coal fly ash to reduce the mobility of priority trace elements. Fuel 88, 1173-1184.

Bundschuh,J., Litter, M.I., Parvez, F., Román-Ross, G., Nicolli, H.B., Jean, J., Liu, C., López, D., Armienta, M.A., Guilherme, L.R.G., Cuevas, A.G., Cornejo, L., Cumbal, L., and Toujaguez, R. (2012) One century of arsenic exposure in Latin America: A review of history and occurrence from 14 countries. Science of the Total Environment 429, 2-35.

Butler, J.A.V. and Ockrent, C. (1930) Studies in electrocapillarity. Part III the surface tensions of solutions containing two surface-active solutes. Journal of Physical Chemistry 34, 2841-2859.

Carabante, I., Grahn, M., Holmgren, A., and Hedlund, J. (2010) In situ ATR-FTIR studies on the competitive adsorption of arsenate and phosphate on ferrihydrite. J. Colloid Interf. Sci. 351, 523-531.

Carbonell-Barrachina, A.A., Rocamora, A., García-Gomis, C., Martínez-Sánchez, F., and Burló, F. (2004) Arsenic and zinc biogeochemistry in pyrite mine waste from the Aznalcóllar environmental disaster. Geoderma 122, 195-203.

Chen, N., Jiang, D.T., Cutler, J., Kotzer, T., Jia, Y.F., Demopoulos, G.P., and Rowson, J.W. (2009) Structural characterization of poorly-crystalline scorodite, iron(III)–arsenate co-

precipitates and uranium mill neutralized raffinate solids using X-ray absorption fine structure spectroscopy. Geochim. Cosmochim. Acta 73, 3260-3276.

Chen, Y.R., Butler, J.N., and Stumm, W. (1973) Kinetic study of phosphate reaction with aluminum oxide and kaolinite. Environ. Sci. Technol. 7, 327-332.

Chien, S.H. and Clayton, W.R. (1980) Application of Elovich equation to the kinetics of phosphate release and sorption in soils. Soil Sci. Soc. Am. J. 44, 265-268.

Correll, D.L. (1998) Role of phosphorus in the eutrophication of receiving waters: A review. J. Environ. Qual. 27, 261-266.

Cullen, W.R. and Reimer, K.J. (1989) Arsenic speciation in the environment. Chem. Rev. 89, 713-764.

da Silva, J.J.R.F., Williams, R.J.P. (2001) The Biological Chemistry of the Elements: The Inorganic Chemistry of Life, 2nd ed., Oxford University Press, New York USA, 600 p.

Davis, J.A. and Leckie, J.A. (1978) Surface ionization and complexation at the oxide/water interface II. Surface properties of amorphous iron oxyhydroxide and adsorption of metal ions. J. Colloid Interf. Sci. 67, 90-107.

Del Nero, M., Galindo, C., Barillon, R., Halter, E., and Madé, B. (2010) Surface reactivity of α-Al_2O_3 and mechanisms of phosphate sorption: In situ ATR-FTIR spectroscopy and f potential studies. Soil Sci. Soc. Am. J., 342, 437- 444.

Dzombak, D.A. and Morel, F.M.M. (1990) Surface complexation modeling. Hydrous ferric oxide. John Wiley & Sons, New York.

Fendorf, S., Eick, M.J., Grossl, P., and Sparks, D.L. (1997) Arsenate and Chromate Retention Mechanisms on Goethite. 1. Surface Structure. Environ. Sci. Technol. 31, 315-320.

Foster, A.L., Brown, G.E. Jr., Tingle, T.N., and Parks, G.A. (1998). Quantitative arsenic speciation in mine tailings using X-ray absorption spectroscopy. Am. Min. 83, 553-568.

Freundlich, H. (1906) Uber die adsorption in losungen. Z. Phys. Chem. 57, 385-470.

Fukushi, K. and Sverjensky, D.A. (2007) A predictive model (ETLM) for arsenate adsorption and surface speciation on oxides consistent with spectroscopic and theoretical molecular evidence. Geochim. Cosmochim. Acta 71, 3717-3745.

Fuller, C.C., Davis, J.A., Waychunas, G.A. (1993) Surface chemistry of ferrihydrite: Part 2. Kinetics of arsenate adsorption and coprecipitation. Geochim. Cosmochim. Acta, 57, 2271-2282.

Gao, Y. and Mucci, A. (2001) Acid base reactions, phosphate and arsenate complexation, and their competitive adsorption at the surface of goethite in 0.7 M NaCl solution. Geochim. Cosmochim. Acta 65, 2361-2378.

Geelhoed, J.S., Hiemstra, T., and Van Riemsdijk, W.H. (1997) Phosphate and sulfate adsorption on goethite: single anion and competitive adsorption. Geochim. Cosmochim. Acta 61, 2389-2396.

Goldberg, S. (1995) Adsorption models incorporated into chemical equilibrium models. Chemical equilibrium and reaction models. SSSA Special Publication 42, 75-95.

Goldberg, S. and Johnston, C.T. (2001) Mechanisms of arsenic adsorption amorphous oxides evaluated using macroscopic measurements, vibrational spectroscopy, and surface complexation modeling. J. Colloid Interf. Sci. 234, 204-216.

Goldberg, S., and Sposito, G. (1984) A chemical model of phosphate adsorption by soils: I. Reference oxide minerals. Soil Sci. Soc. Am. J. 48, 772-778.

Grossl, P.R., Eick, M., Sparks, D.L., Goldberg, S., and Ainsworth, C.C. (1997) Arsenate and chromate retention mechanisms on goethite. 2. Kinetic evaluation using a pressure-jump relaxation technique. Environ. Sci. Technol. 31, 321-326.

Harvey, O.R. and Rhue, R.D. (2008) Kinetics and energetics of phosphate sorption in a multi-component Al(III)–Fe(III) hydr(oxide) sorbent system. Soil Sci. Soc. Am. J., 322, 384-393.

Hayes, K.F. and Leckie, J.O. (1986) Mechanism of lead ion adsorption at the goethite-water interface. Am. Chem. Soc. Symp. Ser. 323, 114-141.

Hayes, K.F., Redden, G., ELA, W., and Leckie, J.O. (1991) Surface complexation models: an evaluation of model parameter estimation using FITEQL and oxide mineral titration data. J. Colloid Interf. Sci. 142, 448-469.

Herbelin, A.L., Westall, J.C. (1999) FITEQL 4.0: a Computer program for determination of chemical equilibrium constants from experimental data; Report 99-01. Department of Chemistry, Oregon State University, Corvallis.

Hingston, F.J., Posner, A.M., and Quirk, J.P. (1971) Competitive adsorption of negatively charged ligands on oxide surfaces. Discuss. Faraday Soc. 52, 334-342.

Ho, Y.S. and McKay, G. (1999) Pseudo-second order model for sorption processes. Process Biochemistry 34, 451-465.

Jackson, B.P. and Miller, W.P. (2000) Effectiveness of phosphate and hydroxide for desorption of arsenic and selenium species from iron oxides. Soil Sci. Soc. Am. J. 64, 1616-1622.

Jackson, R. and Grainge, J.W. (1975) Arsenic and cancer. Canadian Medical Association Journal 113, 396-401.

Khare, N., Martin, J.D., and Hesterberg, D. (2007) Phosphate bonding configuration on ferrihydrite based on molecular orbital calculations and XANES fingerprinting. Geochim. Cosmochim. Acta 71, 4405-4415.

Kish, M.M., and Viola, R. E. (1999) Oxyanion specificity of aspartate-β-semialdehyde dehydrogenase. Inorganic Chemistry 38, 818-820.

Kitahama, K., Kiriyama, R., and Baba, Y. (1975) Refinement of the crystal structure of scorodite. Acta Crystallographica B31, 322-324.

Kuo, S. and Lotse, E.G. (1973) Kinetics of Phosphate Adsorption and Desorption By Hematite and Gibbsite. Soil Science 116, 400-406.

Lambkin, D.C. and Alloway, B.J. (2003) Arsenate-induced phosphate release from soils and its effect on plant phosphorus. Water, Air, and Soil Pollution 144, 41-56.

Langmuir, D., Mahoney, J., and Rowson, J. (2006) Solubility products of amorphous ferric arsenate and crystalline scorodite ($FeAsO_4 \cdot 2H_2O$) and their application to arsenic behavior in buried mine tailings. Geochim. Cosmochim. Acta 70, 2942-2956.

Liu, F., De Cristofaro, A., and Violante, A. (2001) Effect of pH, phosphate and oxalate on the adsorption/desorption of arsenate on/from goethite. Soil Science 166, 197-208.

Low, M.J.D., (1960) Kinetics of chemisorption of gases on solids. Chemical Review 60, 267-312

Luengo, C., Brigante, M., Antelo, J., and Avena, M. (2006) Kinetics of phosphate adsorption on goethite: Comparing batch adsorption and ATR-IR measurements. J. Colloid Interf. Sci. 300, 511-518.

Manning, B.A. and Goldberg, S. (1996) Modeling competitive adsorption of arsenate with phosphate and molybdate on oxide minerals. Soil Sci. Soc. Am. J. 60, 121-131.

Morrell, J.J., Keefe, D., and Baileys, R.T. (2003) Copper, Zinc, and Arsenic in Soil Surrounding Douglas-Fir Poles Treated with Ammoniacal Copper Zinc Arsenate (ACZA). J. Environ. Qual. 32, 2095-2099.

Mucci, A., Richard, L.F., Lucotte, M., and Guignard, C. (2000) The differential geochemical behavior of arsenic and phosphorus in the water column and sediments of the Saguenay Fjord Estuary, Canada. Aquatic Geochemistry 6, 293-324.

Newville M., Livins P., Yacoby Y., Rehr J., and Stern E. (1993) Near-edge x-ray- absorption fine-structure of Pb - a comparison of theory and experiment. Phys. Rev. B, 47, 14126–14131.

Newville, M. (2001) IFEFFIT: interactive XAFS analysis and FEFF fitting. J. Synchrotron Rad. 8, 322-324.

Nordstrom, D.K. (2002) Worldwide occurrences of arsenic in ground water. Science 296, 2143-2145.

Nriagu, J.O. (2002) Arsenic poisoning through the ages. In: Environmental Chemistry of Arsenic (W.T. Frankenberger, Editor), New York, Marcel Dekker, 1-26.

O'Reilly, S.E., Strawn, D. G., and Sparks, D.L. (2001) Residence time effects on arsenate adsorption/desorption mechanisms on goethite. Soil Sci. Soc. Am. J. 65, 67-77.

Parkhurst, D.L. and Appelo, C.A.J. (1999) User's guide to PHREEQC (Version 2)-A computer program for speciation, batch-reaction, one-dimensional transport, and inverse geochemical calculations. U.S. Geol. Surv., Water Resour. Invest. Rep. 99-4259, 326 p.

Puccia, V., Luengo, C., and Avena, M. (2009) Phosphate desorption kinetics from goethite as induced by arsenate. Colloids and Surfaces A: Physicochem. Eng. Aspects 348, 221-227.

Ravel, B. (2001). ATOMS: crystallography for the X-ray absorption spectroscopist. J. Synchrotron Rad. 8, 314-316.

Ravel, B. and Newville, M. (2005). Athena, Artemis, Hephaestus data analysis for X-ray absorption spectroscopy using IFEFFIT. J. Synchrotron Rad. 12, 537-541.

Raven, K.P., Jain, A., and Loeppert, R.H. (1998) Arsenite and arsenate adsorption on ferrihydrite: kinetics, equilibrium, and adsorption envelopes. Environ. Sci. Technol. 32, 344-349.

Robinson, G.R. Jr., Larkins, P., Boughton, C.J., Reed, B.W., and Sibrell, P.L. (2007) Assessment of contamination from arsenical pesticide use on orchards in the Great Valley region, Virginia and West Virginia, USA. J. Environ. Qual., 36:654-663.

Rose, J., Flank, A.M., Masion, A., Bottero, J.Y., Elmerich, P. (1997) Nucleation and growth mechanisms of Fe oxyhydroxide in the presence of PO_4 ions. 2. P K-edge EXAFS study. Langmuir 13, 1827-1834.

Sherman, D.M. and Randall, S.R. (2003) Surface complexation of arsenic(V) to iron(III) (hydr)oxides: structural mechanism from ab initio molecular geometries and EXAFS spectroscopy. Geochim. Cosmochim. Acta 67, 4223-4230.

Sigg, L. and Stumm, W. (1981) The interactions of anions and weak acids with hydrous goethite (α-FeOOH) surface. Colloids and Surface 2, 101-117.

Slomp, C.P., Van der Gasst, S.J., and Van Raaphorst, W. (1996) Phosphorus binding by poorly crystalline iron oxides in North Sea sediments. Marine Chemistry 52, 55-73.

Smedley, P.L. and Kinniburgh, D.G. (2002) A review of the source, behaviour and distribution of arsenic in natural waters. Applied Geochemistry 17, 517-568.

Smil, V. (2000). Phosphorus in the environment: natural flows and human interferences. Annul. Rev. Energy Environment. 25, 53-88.

Smith R.M. and Martell A.E. (1976) Critical stability constants. IV. Inorganic complexes. Plenum Press, New York.

Snoeyink, V.L. and Jenkins, D. (1980) Water chemistry. John Willey & Sons, New York, 463 p.

Sparks, D.L. (1989) Kinetics of soil chemical processes. Academic Press, New York, 210 p.

Strauss, R., Brümmer, G.W., and Barrow, N.J. (1997) Effects of crystallinity of goethite: II. Rates of sorption and desorption of phosphate. Eur. J. Soil Sci. 48, 101-114.

Su, C. and Puls, R.W. (2001) Arsenate and arsenite removal by zerovalent iron: effects of phosphate, silicate, carbonate, borate, sulfate, chromate, molybdate, and nitrate, relative to chloride. Environ. Sci. Technol. 35, 4562-4568.

Sverjensky D.A., Shock E.L., and Helgeson H.C. (1997) Prediction of the thermodynamic properties of aqueous metal complexes to 1000 _C and 5 kb. Geochim. Cosmoschim. Acta 61(7), 1359–1412.

Tejedor-Tejedor, M.I. and Anderson, M.A. (1990) Protonation of phosphate on the surface of goethite as studied by CIR-FTIR and electrophoretic mobility. Langmuir 6, 602–611.

Violante, A. and Pigna, M. (2002) Competitive sorption of arsenate and phosphate on different clay minerals and soils. Soil Sci. Soc. Am. J. 66, 1788-1796.

Wagman, D.D., Evans, W.H., Parker, V.B., Schumm, R.H., Halow, I., Bailey, S.M., Churney, K.L., and Nuttall, R.L. (1982) The NBS tables of chemical thermodynamic properties. Selected values for inorganic and C_1, and C_2, organic substances in SI units. J. Phys. Chem. Ref. Data, Suppl. 11, No. 2.

Waychunas, G., Trainor T. , Eng, P., Catalano, J., Brown, G., Davis, J., Rogers, J. and Bargar, J. (2005) Surface complexation studied via combined grazing-incidence EXAFS and surface diffraction: arsenate on hematite (0001) and (10–12). Anal. Bioanal. Chem. 383, 12-27.

Waychunas, G.A., Rea, B.A., Fuller, C.C., and Davis, J.A. (1993) Surface chemistry of ferrihvdrite: Part 1. EXAFS studies of the geometry of coprecipitated and adsorbed arsenate. Geochim. Cosmochim. Acta 57, 2251-2269.

Withers, P.J.A., Clay, S.D., and Breeze, V.G. (1999) Phosphorus transfer in runoff following application of fertilizer, manure, and sewage sludge. J. Environ. Qual. 30, 180-188.

Yang, L. and Donahoe, R.J. (2007) The form, distribution and mobility of arsenic in soils contaminated by arsenic trioxide, at sites in southeast USA. Applied Geochemistry 22, 320-341.

Yang, L., Donahoe, R.J., Redwine, J.C. (2007) In situ chemical fixation of arsenic-contaminated soils: An experimental study. Sci. Total Environ. 387, 28-41.

Yates, D.E., Levine, S., and Healy, T.W. (1974) Site-binding model of the electrical double layer at the oxide/water interface. J. Chem. Soc. Farada y Trans. 170, 1807-1818.

Zabinsky, S.I., Rehr, J. J., Ankudinov, A., Albers, R.C., and Eller, M.J. (1995) Multiple-scattering calculations of x-ray-absorption spectra. Physical Review B, 52, 2995-3009.

Zeng, H., Fisher, N., and Giammar, D.E. (2008) Individual and competitive adsorption of arsenate and phosphate to a high-surface-area iron oxide-based sorbent. Environ. Sci. Technol. 42, 147-152.

Zhang, G., Dong, H., Jiang, H., Kukkadapu, R.K., Kim, J., Eberl, D., and Xu, Z. (2009) Biomineralization associated with microbial reduction of Fe3+ and oxidation of Fe2+ in solid minerals. Am. Min. 94, 1049-1058.

Zhang, P. and Sparks, D.L. (1990). Kinetics of selenate and selenite adsorption/desorption at the goethite/water interface. Environ. Sci. Technol. 24, 1848-1856.

Zhang, J. and Stanforth, R. (2005) Slow Adsorption Reaction between Arsenic Species and Goethite (r-FeOOH): Diffusion or Heterogeneous Surface Reaction Control. Langmuir 21, 2895-2901.

Zhao, H. and Stanforth, R. (2001) Competitive adsorption of phosphate and arsenate on goethite. Environ. Sci. Technol. 35, 4753-4757.

CHAPTER – 5

CALCIUM-PHOSPHATE TREATMENT OF CONTAMINATED SOIL FOR ARSENIC IMMOBILIZATION[a]

Abstract

The application of As-based herbicide at several industrial sites resulted in numerous localized areas of As-contaminated soil. In this study, an As contaminated soil (As = 278 mg/kg) collected from an industrial site located in the southeastern United States was subjected to phosphate (P_i) treatments. Although P_i treatments have been previously used for flushing As from contaminated soils, in this study, contaminated soil was amended with P_i to study the possible fixation and immobilization of As through co-precipitation. Specifically, the P_i amendment was aimed at simultaneous flushing of As from the soil with ortho-phosphoric acid and co-precipitating it as calcium-phosphate-arsenate phases. Bench-scale P_i treatment experiments were performed at different pH conditions with or without the addition of Ca. Sorption isotherms and envelopes of P_i on BH soil in the absence or presence of additional Ca were determined, along with the associated mobilities of As. A significant portion of the environmentally available As (up to 55% at pH 4, 10-15% at pH 8, and ~30% at pH 11) was released from the contaminated soil during P_i sorption experiments. This increased mobility of As after the addition of P_i resulted from the competitive desorption of As from the soil. Although

---

[a] This chapter has been submitted for the publication in *Applied Geochemistry*.

P_i sorption at high pH (>8) was largely controlled by precipitation, As did not co-precipitate with P_i-minerals. Aqueous geochemical modeling indicated that this lack of As co-precipitation during P_i-only treatment was primarily determined by the deficiency of Ca in the system. When additional Ca (16.9 mmol) was supplied along with P_i (3.38 mmol), the mobility of As was decreased significantly at near-neutral to high solution pH. Geochemical modeling suggested that the leachable As in the soil was potentially precipitated as As-bearing Ca-P_i phases. X-ray diffraction analysis of precipitates separated from the treated soil and from the synthetic leachate confirmed that the formation of a carbonate apatite-like phase occurred as a consequence of the treatment. The results of this study support the potential application of Ca-P_i treatment for remediation of As-contaminated soil at environmentally relevant pH values.

Key words: Arsenic, Phosphate, Soil contamination, Remediation, Immobilization

5.1. Introduction

Arsenic is a toxic element. An acute dose of 50 to 300 mg of As is considered to be lethal for humans due to gastrointestinal, respiratory, cardiovascular, neurological or other body system failures (ATSDR, 2000). Similarly, chronic ingestion of As, either through food or water, has been proven to be responsible for several different types of cancer (Jackson and Grainge, 1975; Bates et al., 1992; Karagas et al., 2002). Elevated concentrations of As in the environment can occur by natural processes as well as anthropogenic activities (Smedley and Kinniburgh, 2002). Groundwater As contamination from natural sources has adversely affected the health of millions of people in several areas around the world (Nordstrom, 2002; Hossain, 2006; Bundschuh et al.,

2012). Anthropogenic As contamination occurs through the use of As-based pesticides (Simcox et al., 1995; Robinson et al., 2007), herbicides (Yang and Donahoe, 2007), and wood preservatives (Morrell et al., 2003), and through mining and smelting activities (Carbonell-Barrachina et al., 2004).

In the US, As compounds were used in the past for different purposes such as for agricultural pesticide and herbicide applications, as wood preservatives, and in glass production (Welch et al., 2000). Although the widespread use of different arsenical compounds gradually declined after the 1960s when the adverse environmental effects of As were realized, their legacy environmental impact is still pronounced in many areas of the US (Welch et al., 2000). Several industrial sites in the southeastern U.S. which received heavy applications of arsenical herbicides during the 1950s continue to leach As into surface water and groundwater (Yang and Donahoe, 2007; Qi and Donahoe, 2008). Regulatory agencies such as the United States Environmental Protection Agency (USEPA) have developed and are enforcing more stringent standards for As in drinking water. For example, the USEPA lowered the maximum contaminant level (MCL) for arsenic in drinking water from 50 μg/L to 10 μg/L in 2006. This required development and implementation of As remediation strategies at several contaminated sites to avoid potential contamination of local potable water sources.

Several different techniques such as isolation and separation (Mulligan et al., 2001), solidification and stabilization (Yang et al., 2007), vitrification (Mulligan et al., 2001), soil flushing (Alam et al., 2001), electrokinetic treatment (Yuan and Chiang, 2007), and bioremediation (Ma et al., 2001) have been proposed for remediation of As-contaminated soils. Previous bench-scale As-remediation experiments performed in our laboratory (Yang et al., 2007; Bhattacharyya et al. 2009; Neupane et al., 2010) have successfully demonstrated the *in situ*

chemical fixation of As in contaminated soil and coal fly ash with ferrous sulfate solutions. Flushing of As from contaminated soil and soil constituents with solutions containing competing ligands such as P_i and OH^- has been studied extensively (Johnson and Barnard, 1979; Peryea and Kammereck, 1997; Wasay et al., 2000; Alam et al., 2001; Tokunaga and Hakuta, 2002; Kaplan and Knox, 2004). Because of its similar chemistry, P_i has a high potential to desorb $As_{(V)}$ from the soil through ion exchange reactions (Woolson et al., 1973; Jackson and Miller, 2000; Wasay et al., 2000; Alam et al., 2001; Kaplan and Knox, 2004). Phosphoric acid is very effective in rapidly displacing As from contaminated soil by providing P_i to compete with $As_{(V)}$ for adsorption sites and by dissolving As-harboring metal oxides present in the soil (Tokunaga and Hakuta, 2002). A few studies (e.g., Grisafe and Hummel, 1970; Twidwell et al., 1994) also demonstrated the co-precipitation of As along with P_i minerals. Arsenate was able to substitute for P_i to form continuous solid solutions of fluor- and chlor-apatites (Grisafe and Hummel, 1970). Mahapatra et al. (1987) successfully synthesized the arsenate hydroxyapatite. Similarly, Twidwell et al. (1994) and others at Montana Tech (Wilson, 1998; Orser, 2001) showed the removal of As from solution by the precipitation of Ca- P_i-$As_{(V)}$ minerals at pH 8-10. Their study indicated that P_i-$As_{(V)}$ hydroxyapatite with a P:As ratio ≥ 7 has a low solubility (<10 ppb) and greater stability against atmospheric CO_2 compared to other P_i-$As_{(V)}$ apatites .

In this study, an As-contaminated soil collected from an industrial site located in the southeastern United States was subjected to a Ca-P_i treatment. The objective of this study was to test the potential application of phosphate-based treatment for remediation of As-contaminated soils. The remediation method evaluated in this study was aimed at flushing arsenic from the contaminated soil with phosphoric acid and immobilizing it through precipitation as Ca-P_i-$As_{(V)}$ minerals.

5.2. Materials and methods

5.2.1. Contaminated site and soil sample collection

Arsenic-contaminated soil was collected from an industrial site (BH) located near the Gulf Coast in the southeastern United States. The soil at the sampling site was developed from Quaternary undifferentiated marine and fluvial sediments. With increasing depth, four subsurface units – an unconfined sandy aquifer, a silty peat semi-confining bed, a semi-confined sand aquifer, and a confining silt/clay layer–were reported to be present at the site (Yang and Donahoe, 2007). The regional climate of the contaminated area is humid and semitropical with an annual rainfall of about 162 cm (Yang and Donahoe, 2007). The rainy season at the sampling site begins in May and ends in November, accounting for about 60% of the annual rainfall (Black, 1993). Temperatures are moderate, with an average high of 28 ºC in summer and an average low of 10 ºC in winter (Yang and Donahoe, 2007).

The soil at this site was contaminated with As during the 1950s through the one-time application of an herbicide rich in arsenic trioxide (arsenolite) which had a trade name of Anaconda, produced at the Anaconda smelter in Montana (Yang and Donahoe, 2007). Originally, the arsenolite was applied as a one-inch thick layer on top of the natural soil surface and covered with a 5-10 cm thick layer of limestone gravel. During the last five decades, the arsenolite was weathered and dispersed into the soil, creating a potential risk of As exposure to the local population (Yang and Donahoe, 2007). Because earlier studies (e.g., Yang and Donahoe, 2007) indicated that the As was mostly confined to vadose zone soil above the surficial unconfined sand aquifer, the soil sample was collected at a single location from 10 to 60 cm below the surface and placed in two 5-gallon buckets. The soil was air dried, passed through a 2mm sieve, homogenized by thorough mixing, and stored at room temperature for chemical/mineralogical

characterizations and P_i treatments. Sub-samples taken from the homogenized soil sample were used for all treatment experiments.

5.2.2. Characterization of BH soil

The environmentally available As and other elements in BH soil were extracted by microwave-assisted partial acid digestion (USEPA, 2007) and the extractant solutions analyzed with a Perkin Elmer Optima 3000DV inductively coupled plasma-optical emission spectrometer (ICP-OES). The soil pH was measured according to USEPA Method 9045D for a 1:1 soil:reagent water (>18MΩ) mixture (USEPA, 2004). The single-point BET specific surface area of soil sample was determined with ASTM D4567-03 method (ASTM, 2003) using a device with flow of 30% N_2 in He using a Leybold-Inficon mass spectrometer to detect the gasses. Minerals present in the bulk soil, the soil clay fraction, and experimental precipitates were determined by X-ray diffraction (XRD) using a Brüker D8 Advance powder diffractometer. The bulk soil sample was powdered in an iron Shatterbox® mill for 2 min for XRD analysis. The clay-sized soil fraction was separated by flotation according to Stoke's Law. The XRD data were analyzed with DIFRACplus EVA version 11.0.03 (XRD data evaluation and presentation software provided by Bruker AXS), using the International Center for Diffraction Data, ICDD PDF-2 Release 2005 database.

5.2.3. Experiments

5.2.3.1. Mobilization of As from BH soil as a function of pH

Mobilization of As from BH soil as a function pH was studied in batch experiments. For each experimental setup, 3.0 g of soil were weighed in a 50 mL centrifuge tube and then 45 mL

of 0.1 mol NaCl solution was added. A series of similar experimental sets were prepared and agitated at 200 rpm on an orbital platform shaker for 24 hours. The pH of the soil mixture was set initially and adjusted periodically when needed in the range of 3 to 12 using 0.1 mol or 1.0 mol HCl and NaOH solutions. The supernatant solutions were filtered through 0.2µm nylon syringe filters after 20 minute centrifugation at 8,500 rpm, acidified to 2% HNO_3 with OPTIMA® ultrapure nitric acid, and stored at 4 ºC in a refrigerator until chemical analysis by ICP-OES.

5.2.3.2. P_i sorption and mobilization of As from BH soil

The sorption of P_i on BH soil was evaluated with sorption isotherms and envelopes. The term 'sorption' is used to encompass all processes (adsorption, absorption, and precipitation) that transfer aqueous sorbate (e.g., P_i) to the solid phase (Sposito, 1986). Each sorption experiment was performed at a 1:15 solid:liquid ratio by mixing 3.0 g soil with 45 mL of 0.1 mol NaCl electrolyte in a 50 mL centrifuge tube. All sorption experiments were performed in duplicate, but each was treated as an individual sample, rather than calculating an average value for the duplicate samples.

The phosphate stock solution was prepared from 85% H_3PO_4, and the P_i concentration was determined by ICP-OES analysis. Further dilutions of the P_i stock solution were performed with respect to its analyzed concentration. Isotherms for phosphate sorption on BH soil at pH 4, 8, and 11 were constructed using 0.15 to 13.24 mmol initial P_i concentrations. Whereas, sorption envelopes were determined for 0.57 mmol and 3.38 mmol initial P_i concentrations in the pH range from 3 to 12. The pH of the soil mixture was adjusted at the beginning of the experiment using HCl and NaOH solutions. Furthermore, pH was checked intermittently and adjusted, if

necessary. The pH values of the sorption envelope samples were recorded at the end of the experiments. The tubes were agitated for 24 hours and the samples centrifuged, filtered, acidified, and stored for chemical analysis with ICP-OES. During ICP-OES analyses, quality control check standards were run after analysis of each batch of 10 samples. The relative standard deviations of As, Ca, and P concentrations in the check standards were generally within ±5%, and never exceeded ±10%.

5.2.3.3. Ca-P_i treatment of BH soil

The contaminated soil was treated with Ca and P_i in batch experiments. For each experiment, 3.0 g of soil was weighed in a 50 mL centrifuge tube and 45 mL of a Ca-P_i treatment solution were added into it. The Ca treatment solutions were prepared from dry, analytical grade $CaCl_2$, and the Ca concentrations were determined by ICP-OES analysis. Two sets of batch treatment experiments were performed over the pH range from 3 to 12. The first sert of experiments was conducted with Ca and P_i concentrations of 5.63 mmol and 3.38 mmol, respectively, yielding a 1:67 initial Ca:P_i ratio in the soil mixture. The second set of experiments used the same concentration of P_i but a much higher concentration of Ca (16.90 mmol), producing an initial Ca:P_i ratio of 5:1. The pH of the soil mixture was adjusted with HCl and NaOH solutions and agitated for 24 hours. Finally, the tubes were centrifuged and the supernatant solutions were separated by filtration and stored in a refrigerator until chemical analysis. The mineralogy of precipitates in the treated soil was analyzed with XRD.

5.2.3.4. Precipitation of Ca-P_i-$As_{(V)}$ phases from synthetic leachate

Ca-P_i-$As_{(V)}$ solid phases were precipitated from synthetic leachate prepared by mixing Ca, P_i, and $As_{(V)}$ stock solutions in 0.1 mol NaCl electrolyte. The calculated amount of $Na_2HAsO_4 \bullet 7H_2O$, previously dried in a vacuum desiccator, was weighed on a Mettler Toledo Balance for preparation of the $As_{(V)}$ stock solution. In addition, the concentration of As in the stock solution was determined by ICP-OES analysis. The initial leachate with $As_{(V)}$ = 0.48 mmol, P_i = 3.38 mmol, and Ca = 6.44 mmol was stirred in contact with air for 24 hours at room temperature (ca. 21 ºC) to precipitate Ca-P_i-$As_{(V)}$ solid phases in a 250 mL beaker. The $As_{(V)}$:P_i ratio was selected to be 1:7, as suggested by Wilson (1998), while the Ca:($As_{(V)}$ + P_i) ratio was fixed at 1.67. The pH of the synthetic leachate was adjusted to 8 with NaOH and HCl solutions. At the end of the 24 hour period, the precipitate formed was separated by vacuum filtration and analyzed by XRD.

5.2.4. PHREEQC simulations and potential precipitation of Ca-P_i-$As_{(V)}$ minerals

The aqueous chemical data were used to calculate the saturation indices of several Ca, Ca-$As_{(V)}$, Ca-P_i, and Ca-P_i-$As_{(V)}$ minerals with the PHREEQC geochemical code (Parkhurst and Appelo, 1999), using the llnl.dat database. Thermodynamic data for several potential minerals and aqueous species (Tables 5.1 and 5.2) were collected from additional sources (Smith and Martell, 1976; Bothe and Brown, 1999; Wilson, 1998; Montastruc et al., 2003) and incorporated into the llnl.dat database. Most of the thermodynamic data for the different solid phases compiled for this study were determined/estimated at 20 to 25 ºC. Because the laboratory temperature during the experiments performed for this study was recorded in the range of 20 to 22 ºC, the thermodynamic data were used as obtained without any temperature correction. During the PHREEQC simulations, all solutions were allowed to equilibrate with atmospheric CO_2 and O_2.

Table 5.1. Aqueous reactions and equilibria

Aqueous Reactions	log K
$AsO_4^{3-} + H^+ \Leftrightarrow HAsO_4^{2-}$	11.60[a]
$HAsO_4^{2-} + H^+ \Leftrightarrow H_2AsO_4^-$	6.67[a]
$H_2AsO_4^- + H^+ \Leftrightarrow H_3AsO_4^0$	2.25[a]
$Ca^{2+} + AsO_4^{3-} \Leftrightarrow CaAsO_4^-$	4.36[a]
$Ca^{2+} + HAsO_4^{2-} \Leftrightarrow CaHAsO_4^0$	2.66[a]
$Ca^{2+} + H_2AsO_4^- \Leftrightarrow CaH_2AsO_4^+$	1.30[a]
$Ca^{2+} + OH^- \Leftrightarrow CaOH^+$	1.33[a]
$H^+ + OH^- \Leftrightarrow H_2O$	14.00[a]
$PO_4^{3-} + H^+ \Leftrightarrow HPO_4^{2-}$	12.38[b]
$HPO_4^{2-} + H^+ \Leftrightarrow H_2PO_4^-$	7.19[b]
$H_2PO_4^- + H^+ \Leftrightarrow H_3PO_4^0$	2.15[b]
$Ca^{2+} + HPO_4^{2-} \Leftrightarrow CaHPO_4^0$	2.74[c]
$Ca^{2+} + H^+ + HPO_4^{2-} \Leftrightarrow CaH_2PO_4^+$	1.4[c]
$Ca^{2+} + HPO_4^{2-} \Leftrightarrow CaPO_4^- + H^+$	-5.86[c]
$CO_3^{-2} + H^+ \Leftrightarrow HCO_3^-$	10.33[c]
$HCO_3^- + H^+ \Leftrightarrow CO_2 + H_2O$	6.34[c]
$Ca^{2+} + H_2O \Leftrightarrow CaOH^+ + H^+$	-12.85[c]

[a] Bothe and Brown (1999), [b] Smith and Martell (1976), [c] llnl.dat in Phreeqc

The precipitation potential of a mineral in a solution was determined by evaluating its state of saturation (undersaturation or oversaturation). The degree of undersaturation or oversaturation of an aqueous sample with respect to a particular mineral was determined in terms of the saturation index (SI), calculated using Eq. 5.1:

$$SI = \log(IAP/K_{sp}) \ldots (5.1)$$

where IAP is the ion activity product and K_{sp} is the solubility constant for a particular mineral (Drever, 1997). If the calculated SI for a mineral was greater than 0, then that aqueous solution was considered to be oversaturated with respect to that particular mineral and the solution likely to spontaneously precipitate that mineral, depending on kinetic constraints.

Table 5.2. Reaction equilibria for minerals

#	Aqueous-solid Reactions	log K
1	$3Ca^{+2} + 2H_2AsO_4^{-3} \Leftrightarrow Ca_3(AsO_4)_2 + 4H^+$	17.82[a]
2	$3Ca^{+2} + 2AsO_4^{-3} + 3.66\,H_2O \Leftrightarrow Ca_3(AsO_4)_2 : 3.66H_2O$	21.00[b]
3	$3Ca^{+2} + 2AsO_4^{-3} + 4.25\,H_2O \Leftrightarrow Ca_3(AsO_4)_2 : 4.25H_2O$	21.00[b]
4	$4Ca^{+2} + 2AsO_4^{-3} + 2OH^- + 4\,H_2O \Leftrightarrow Ca_4(OH)_2(AsO_4)_2 : 4H_2O$	29.20[b]
5	$5Ca^{+2} + 3AsO_4^{-3} + OH^- \Leftrightarrow Ca_5(AsO_4)_3OH$	38.04[b]
6	$Ca^{+2} + H^+ + AsO_4^{-3} + H_2O \Leftrightarrow CaHAsO_4 : H_2O$	4.79[b]
7	$Ca^{+2} + HCO_3^- \Leftrightarrow H^+ + CaCO_3(Calcite)$	7.00[a]
8	$5Ca^{+2} + 2H^+ + 4AsO_4^{-3} + 9H_2O \Leftrightarrow Ca_5H_2(AsO_4)_4 : 9H_2O(Ferrarsite)$	31.49[b]
9	$5Ca^{+2} + 2H^+ + 4AsO_4^{-3} + 9H_2O \Leftrightarrow Ca_5H_2(AsO_4)_4 : 9H_2O(Guerinite)$	30.69[b]
10	$Ca^{+2} + 2H_2O \Leftrightarrow H^+ + Ca(OH)_2$(Portlandite)	22.56[a]
11	$3Ca^{+2} + 2HPO_4^{-2} \Leftrightarrow 2H^+ + Ca_3(PO_4)_2$ (Amorphous calcium phosphate)	26.52[c]
12	$CaHPO_4 : 2H_2O$ (Brushite)$\Leftrightarrow Ca^{+2} + HPO_4^{-2} + 2H_2O$	6.55[a]
13	$10Ca^{+2} + 0.42\,HAsO_4^{-2} + 5.58\,HPO_4^{-2} + 2H_2O \Leftrightarrow Ca_{10}(AsO_4)_{0.42}(PO_4)_{5.58}(OH)_2 + 8H^+$	8.88[d]
14	$10Ca^{+2} + 0.66\,HAsO_4^{-2} + 5.34\,HPO_4^{-2} + 2H_2O \Leftrightarrow Ca_{10}(AsO_4)_{0.66}(PO_4)_{5.34}(OH)_2 + 8H^+$	9.23[d]
15	$10Ca^{+2} + 0.9\,HAsO_4^{-2} + 5.1\,HPO_4^{-2} + 2H_2O \Leftrightarrow Ca_{10}(AsO_4)_{0.9}(PO_4)_{5.1}(OH)_2 + 8H^+$	10.32[d]
16	$10Ca^{+2} + 2.04\,HAsO_4^{-2} + 3.96\,HPO_4^{-2} + 2H_2O \Leftrightarrow Ca_{10}(AsO_4)_{2.04}(PO_4)_{3.96}(OH)_2 + 8H^+$	8.16[d]
17	$10Ca^{+2} + 3.78\,HAsO_4^{-2} + 2.22\,HPO_4^{-2} + 2H_2O \Leftrightarrow Ca_{10}(AsO_4)_{3.78}(PO_4)_{2.22}(OH)_2 + 8H^+$	7.99[d]
18	$10Ca^{+2} + 5.64\,HAsO_4^{-2} + 0.36\,HPO_4^{-2} + 2H_2O \Leftrightarrow Ca_{10}(AsO_4)_{5.64}(PO_4)_{0.36}(OH)_2 + 8H^+$	20.23[d]
19	$10Ca^{+2} + 6\,HPO_4^{-2} + 2H_2O \Leftrightarrow 8H^+ + Ca_{10}(PO_4)_6(OH)_2$(Hydroxylapatite)	11.37[d]
20	$Ca^{+2} + HPO_4^{-2} \Leftrightarrow CaHPO_4$ (Dicalciumphosphate)	6.90[c]
21	$Ca^{+2} + HPO_4^{-2} + 2H_2O \Leftrightarrow CaHPO_4 : 2H_2O$ (Dicalciumphosphatedihydrate)	6.69[c]
22	$4Ca^{+2} + 3HPO_4^{-2} + 2.5H_2O \Leftrightarrow Ca_4H(PO_4)_3 : 2.5H_2O$ (Octocalcium phosphate)	49.6[c]
23	$3Ca^{+2} + 2HPO_4^{-2} \Leftrightarrow 2H^+ + Ca_3(PO_4)_2$ (Tricalcium phosphate)	26.00[c]
24	$3Ca^{+2} + 2HPO_4^{-2} \Leftrightarrow 2H^+ + Ca_3(PO_4)_2$ (Whitlockite)	4.22[a]

[a]llnl.dat in Phreeqc, [b]Bothe and Brown (1999), [c]Montastruc et al. (2003), [d]Wilson (1998)

Speciation modeling was performed by PHREEQC for different treatment scenarios. The chemical data obtained as a function of pH from the batch experiments without an external supply of P_i or Ca were used as a primary chemical data set. Initially, the amounts of As and Ca

mobilized as a function of pH were evaluated for any potential precipitation. Subsequently, the amounts of P_i and Ca supplied to the soil during treatments were added to the primary chemical data set and the potential for precipitation of different minerals from the augmented solutions was evaluated.

5.3. Results and discussion

5.3.1. Characterization of BH soil

The BH soil was classified as a basic (pH ~ 8.4), medium dark gray (N4), sandy-clay loam. This soil mostly consisted of quartz, calcite, and kaolinite with a minor amount of gehlenite, montmorillonite, and muscovite. The environmentally available concentration of As in BH soil, as determined by microwave-assisted partial acid digestion using USEPA Method 3051A (USEPA, 2007), is 278 mg/kg (3.71 mmol/kg). The background concentration of As in soil near the sampling site was reported to be less than 3 mg/kg (Yang and Donahoe, 2007). Similarly, BH soil had large concentrations of environmentally available Ca (23,723 mg/kg), Fe (1,356 mg/kg), Al (5,863 mg/kg), Mg (5,604 mg/kg), K (765 mg/kg), and Na (280 mg/kg). The organic carbon content (loss-on-ignition) of BH soil was reported to be 6.5 mg/g (Neupane et al., 2010), and the single point BET surface area of the bulk soil was determined to be 2.65 m^2/g.

The association and speciation of As in BH soil was studied in detail by Yang and Donahoe (2007), who used sequential extraction, electron microprobe analysis, scanning electron microscopy, μ-XRD, and X-ray absorption spectroscopy. Yang and Donahoe (2007) reported that most of the As in BH soil remained sorbed on amorphous Al- and Fe-hydroxides. However, trace amounts of some As-rich minerals (e.g., phaunouxite) were also present in the contaminated soil (Yang and Donahoe, 2007). Sequential chemical extraction and μ-XANES studies indicated that

the original $As_{(III)}$ arsenolite herbicide applied more than 5 decades ago was mostly oxidized to $As_{(V)}$ by weathering processes (Yang and Donahoe, 2007).

5.3.2. P_i sorption on BH soil

5.3.2.1. Sorption isotherms

Phosphate sorption isotherms on BH soil at pH 4, 8, and 11 were performed in batch experiments. The sorbed amount was calculated as the difference in initial and equilibrium concentrations of P_i in solution. Experimental sorption data were fitted with the Freundlich isotherm model (Eq. 5.2):

$$q_e = KC_e^n \ldots (5.2)$$

where q_e is the amount of sorbate (P_i) sorbed on BH soil (mmol/kg), C_e is the equilibrium sorbate concentration (mmol), K (L/kg) and n (dimensionless) are constants. Freundlich isotherm model parameters were obtained by converting Eq.1 into linear form Eq. (5.3):

$$\log q_e = \log K + n \log C_e \ldots (5.3)$$

where values of n and K can be determined from the slope and y-intercept of a graph obtained by plotting log C_e along the x-axis and log q_e along y-axis (Limousin et al., 2007). For each isotherm, the goodness of model fit was determined by calculating the coefficient of determination (R^2) with Eq. (5.4):

$$R^2 = \frac{\sum_{i=1}^{n} \left(q_m - \overline{q_e}\right)^2}{\sum_{i=1}^{n} \left(q_m - \overline{q_e}\right)^2 + \sum_{i=1}^{n} \left(q_m - q_e\right)^2} \ldots (5.4)$$

where q_e is defined in Eq. 1, q_m is the model-derived maximum adsorbed amount (mmol/kg), and $\overline{q_e}$ is the average experimental sorbed amount (mmol/kg). The closer the value of R^2 is to 1.0, the

better the model is in predicting sorption. The R^2 value for each isotherm was obtained by using the *n* values for the experimental and corresponding model datasets.

Experimental isotherms with Freundlich model fits for P_i (ad)sorption on BH soil at pH 4, 8, and 11 are shown in Fig. 5.1. As expected, all three isotherms showed a greater sorption of P_i at higher initial concentrations, and relatively greater proportions of P_i were sorbed at lower initial concentrations than at higher initial concentrations. The Freundlich isotherm model is able to describe the experimental data at pH 4 ($R^2 = 0.93$) and 11 ($R^2 = 0.93$). However, while fitting the experimental isotherm data for pH 8 with the Freundlich model, the data points with $C_e > 6.5$ mmol were not used due to an apparent change in sorption mechanism (i.e., precipitation). With that exclusion, the Freundlich model resulted in a very good fit for pH 8 experimental isotherm data ($R^2 = 0.97$).

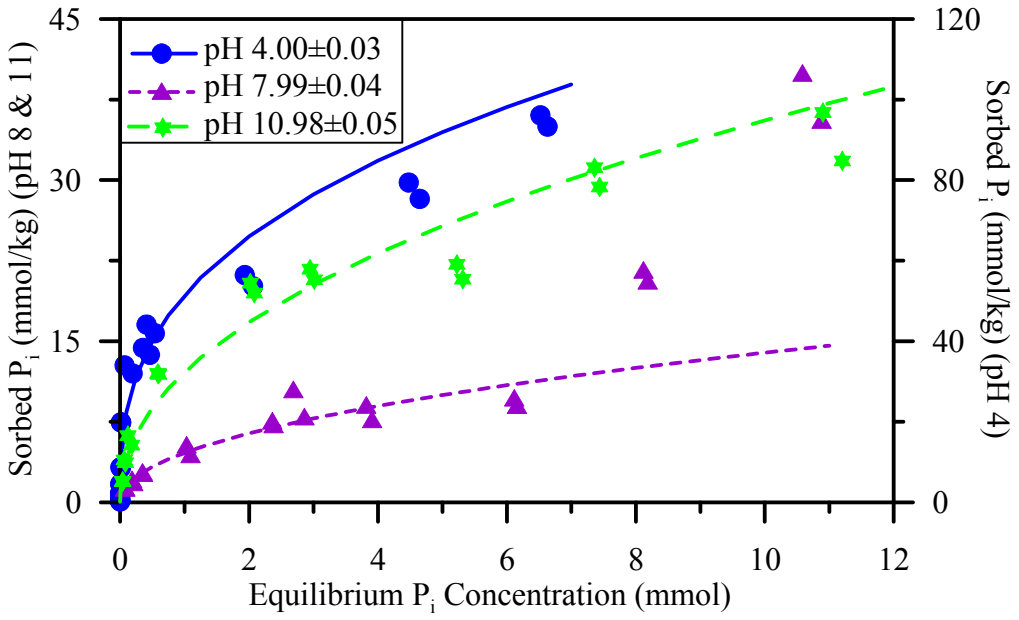

Fig. 5.1. Phosphate sorption on BH soil in 0.1 mol NaCl at pH 4, 8, and 11.. Lines represent Freundlich isotherm model fits to data.

The *n* values for P_i sorption on BH soil at pH 4, 8, and 11 are 0.36, 0.48, and 0.47, respectively. Fig. 5.1 shows that the sorption of P_i on BH soil was highest at pH 4. The large value of K (51.46 L/kg) for the isotherm fit also reflects the strong sorption of P_i at this pH. Relatively smaller K values are obtained for sorption of P_i on BH soil at pH 8 (4.62 L/kg) and pH 11 (12.15 L/kg). Although decreasing sorption of P_i at the sorbent-water interface with increasing pH has been consistently reported by several researchers (e.g., Violante and Pigna, 2002), greater sorption of P_i on BH soil was observed at pH 11 than at pH 8 (except at the highest P_i concentration). Sorption of P_i was higher at pH 11 than at pH 8 until the equilibrium concentration (C_e) of P_i was >6 mmol (Fig. 5.1). The greater sorption of P_i on BH soil at pH 11 compared to pH 8 was caused by precipitation. The sorption envelopes (section 5.3.2.2.) also indicate that the sorption of Pi on BH soil is high at low pH, but decreases with increasing pH to a minimum at near-neutral pH, and increases thereafter. With increasing concentration of P_i in the system, however, sorption of P_i at pH 8 also increased and approached the level of sorption at pH 11 once precipitation became the dominant mechanism of sorption at $C_e > 6$ mmol (Fig. 1). Similarly, the precipitation of P_i phases at pH 4 at high surface coverage could not be ruled out because some previous workers (e.g., Zhao and Stanforth, 2001; Ler and Stanforth, 2003) have suggested that surface precipitation of P_i and $As_{(V)}$ on the adsorbent phase occurs at high surface loadings and low pH.

3.2.2. Sorption envelopes

Phosphate sorption envelopes on BH soil for two initial P_i concentrations (0.57 mmol and 3.38 mmol) are shown in Fig. 5.2. The sorption of P_i on soil is presented as percentage sorbed. Sorption of P_i was high at acidic conditions, lowest at circum-neutral pH, and relatively high at

alkaline conditions. Although the absolute amount of sorption was greater with higher initial concentration (C_i), the proportionate sorption was greater at low C_i. Sorption of P_i was nearly 100% at pH < 5 for a C_i of 0.57 mmol. At very low pH (< 3.5), however, sorption of P_i was moderate (Fig. 5.2) because of the dissolution of Al-Fe-Mn oxyhydroxides. In general, the sorption of P_i decreased with increasing pH from 4 to 7 (Fig. 5.2), and is attributed to adsorption controlled by pH-dependent surface charge. At pH > 7, the sorption of P_i again increased with increasing pH. Goldberg and Glaubig (1988a, 1988b) reported similar observations for sorption of $As_{(V)}$ and $Se_{(IV)}$ on Ca-montmorillonite. Interestingly, Goldberg and Glaubig (1988b) found no increase in sorption with increasing pH for alkaline conditions after Ca was removed from the soil. Therefore, the increased sorption of P_i and other oxyanions at alkaline pH conditions in the presence of soil Ca is interpreted to have been caused by precipitation.

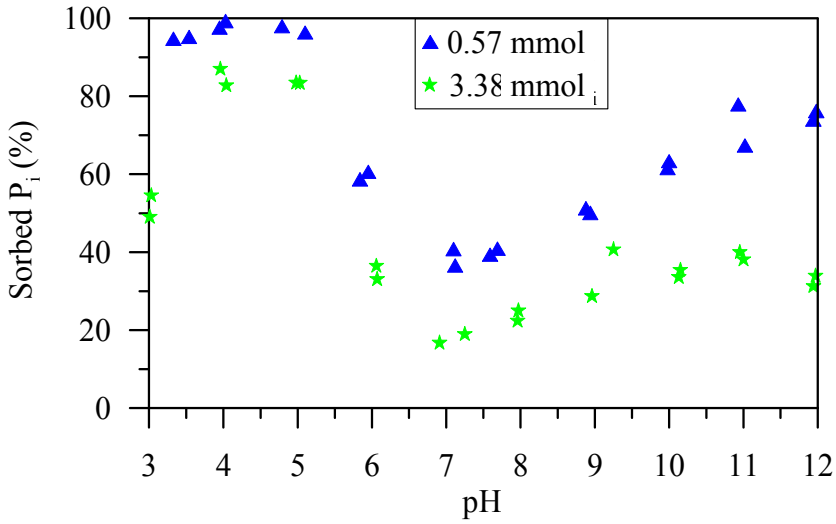

Fig. 5.2. Phosphate sorption on BH soil as a function of pH for 0.57 mmol or 3.38 mmol initial P_i concentrations in 0.1 mol NaCl.

3.3. Mobilization of As and Ca from BH soil

3.3.1. As and Ca mobilization as a function of pH

Data showing the mobilization of As and Ca from BH soil as a function of pH are presented in Fig. 5.3 in terms of mmol per kilogram of dry soil mass (Fig. 5.3a) and as the % mobilized (Fig. 5.3b). The percent mobilization for As and Ca was calculated with respect to the environmentally available amount of each element in the soil, as determined by microwave-assisted partial acid digestion, using Eq. 5.5:

$$\%\ \text{Mobilized} = \frac{\text{Amount leached to solution}}{\text{Environmentally available amount}} \times 100\% \quad \ldots (5.5)$$

Each set of duplicate batch experiments containing 3.0 g soil and 45 mL 0.1 mol NaCl was adjusted to a certain pH level with 0.1 mol or 1.0 mol solutions of NaOH and HCl. No other reagents were added. Figs. 5.3a and 5.3b indicate that solution pH had a strong control over the mobilities of As and Ca. However, these elements showed opposite trends in mobility as a function of pH, except at low pH (~3) where both elements displayed high mobility. The greater mobility of As at very low pH was caused by the dissolution of As-harboring materials such as Al- and Fe-oxyhydroxides, as indicated by greater concentrations of Al and Fe in solution. Mobilization of As increased with increasing pH from 4 to 12. The OH^- ligand was very effective in displacing oxyanion species such as $As_{(V)}$ from contaminated soil. Jackson and Miller (2000) found hydroxide to be the most effective anion for desorbing different forms of As, except $As_{(III)}$ from iron oxides. Johnston and Barnard (1979) reported that the chemical rich in OH^- ligand had the greatest effectiveness for removing As from soil.

In contrast to the observed higher release of As from soil with increasing pH, the mobility of Ca decreased with increasing pH (Fig. 5.3a-b). Calcium is a cationic species with low

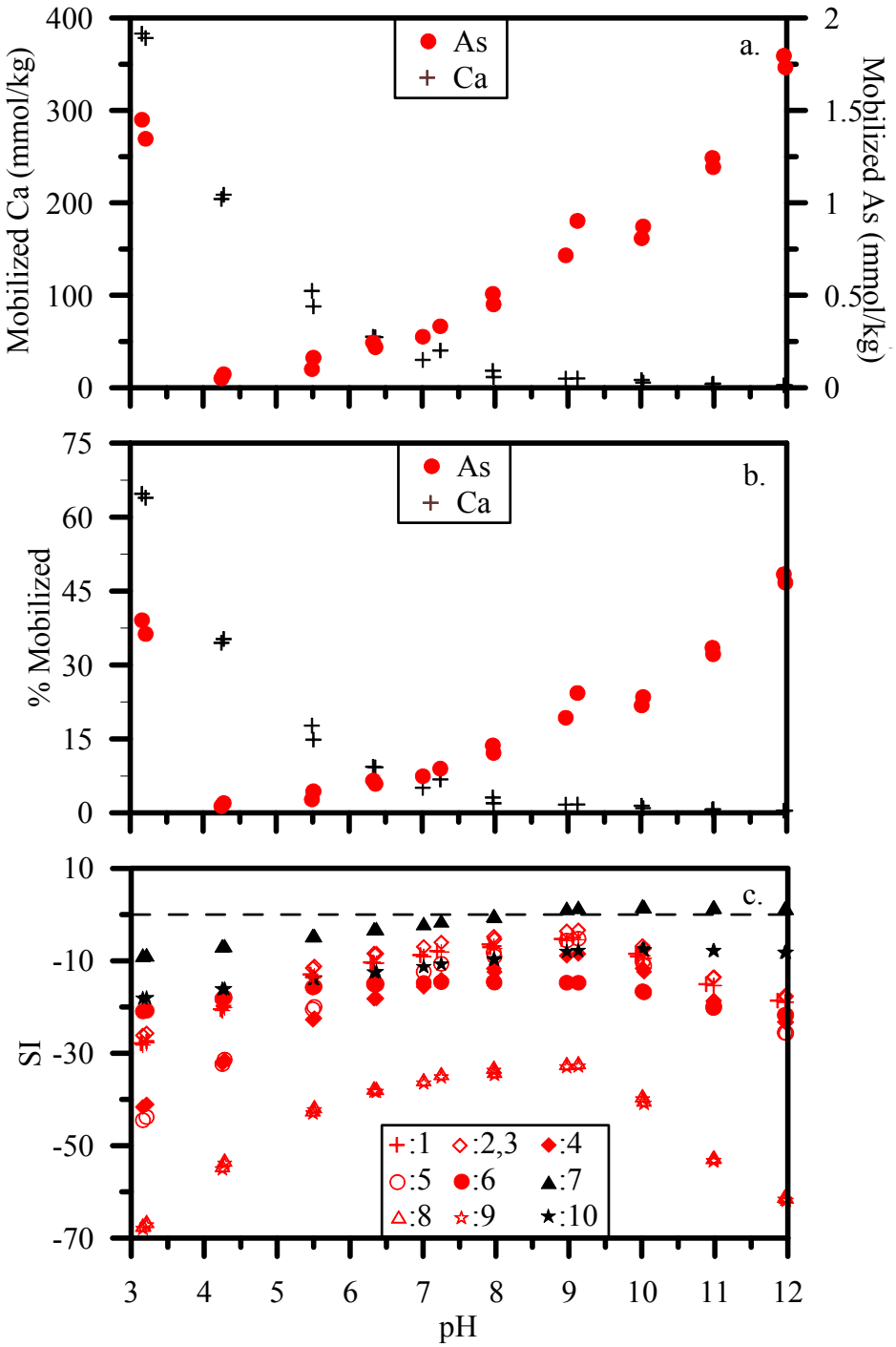

Fig. 5.3. Mobilized As and Ca as a function of pH during batch leaching of 3 g soil in 45 mL 0.1 mol NaCl. (a) Mobilized As and Ca given in mmol/kg dry soil; (b) % Mobilized calculated with respect to environmentally available soil concentrations (As = 3.71 mmol/kg; Ca = 592 mmol/kg); and (c) mineral saturation indices calculated using PHREEQC. In (c), Symbols/numbers correspond to minerals listed in Table 5.2. Red symbols (online version) represent minerals containing As.

adsorption on metal oxyhydroxides at low pH. Moreover, acidic conditions increase the dissolution of Ca-bearing phases in soil, such as carbonates. At higher pH, however, Ca shows a greater affinity for adsorption and precipitation. On the other hand, adsorption of oxyanions on soil oxyhydroxides decreases with increasing pH. Arsenic in BH soil mostly existed in the oxidized ($As_{(V)}$) form (Yang and Donahoe, 2007); therefore, greater mobility of As with increasing pH is consistent with its general aqueous geochemical behavior.

Because increased mobility of Ca under acidic conditions was not accompanied by the increased mobilization of As (except at pH 3), it is apparent that these elements are not associated with the same solid phase in BH soil. Using a 7-step sequential chemical extraction procedure, Qi and Donahoe (2008) reported that more than 60% of the As in BH soil is associated with amorphous Al-Fe oxyhydroxides, while another 20% was associated with crystalline Al-Fe oxides. The remaining 20% of the As in BH soil was reported to be associated with the water soluble, exchangeable, carbonate, Mn-oxide, and organic soil fractions (Qi and Donahoe, 2008).

The mobilized concentrations of As and Ca at each solution pH were used to calculate the saturation indices for several Ca-As minerals, as well as some Ca minerals (e.g., calcite and portlandite). The saturation indices for these minerals as a function of pH are shown in Fig. 3c. At all pH levels, the soil leachates were undersaturated with respect to Ca-As minerals. The solution was only marginally oversaturated with respect to calcite at pH >9. Between pH 6 to 9, the saturation indices of all As-Ca minerals were relatively higher due to the higher mobilities of both elements in this pH range. Therefore, the highly undersaturated state of the soil solution with respect to Ca-As minerals at low pH and high pH was controlled by low aqueous concentrations of As and Ca, respectively.

5.3.3.2. As and Ca mobilization as a function of P_i

During P_i sorption isotherm experiments (section 5.3.2.1), varying amounts of As and Ca were released from BH soil. Figs. 5.4a and 5.4b show the mobilization of As and Ca as a function of P_i at pH 4, 8, and 11. The mobilities of these elements are expressed as % Mobilized, calculated using Eq. 5.2. Both elements showed greater mobility at pH 4, compared to pH 8 and 11. Mobilization of Ca at pH 4 was two orders of magnitude greater than at pH 8 and 11. The mobility of Ca decreased with increasing pH (pH 4 > pH 8 > pH 11). The mobilities of As and Ca increased with increasing initial concentration of P_i at pH 4. The mobility of Ca leveled off at 42-45% Mobilized for C_i > 4 mmol P_i at pH 4, while the rate of increase in the mobility of As slowed for C_i > 6 mmol P_i. Although the mobilities of As and Ca are positively correlated at pH 4 for C_i < 4 mmol P_i, they lack such correlation at pH 8 and pH 11. At pH 8 and pH 11, As showed P_i-independent mobility while Ca mobility gradually decreased with increasing P_i in the system. The mobility of As at pH 11 in the presence of varying amounts P_i (Fig. 4a) was very similar to its mobility at that pH without P_i (Fig. 5.3). Therefore, the P_i-independent mobility of As at pH 11 can be attributed to pH-induced desorption of As associated with Al- and Fe-oxyhydroxides in the soil. However, the greater mobility of As at pH 4 is largely related to P_i-induced competitive desorption. Previously, several researchers (e.g., Peryea and Kammereck, 1997; Alam et al., 2001) also reported enhanced mobility of As after P_i amendments of contaminated soil. Tokunaga and Hakuta (2002) tested the effectiveness of several acids, including phosphoric acid, for leaching As from an artificially contaminated soil. They found phosphoric acid (9.4%) to be the most effective for extracting As from the soil.

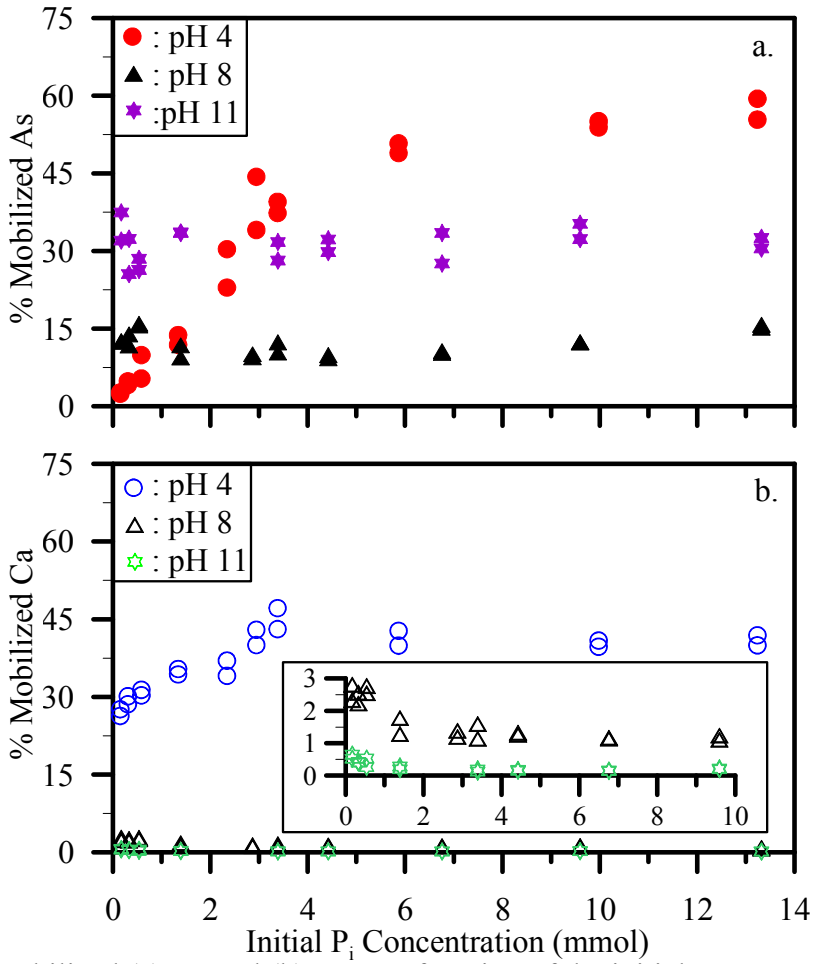

Fig. 5.4. Percent mobilized (a) As and (b) Ca as a function of the initial concentration of P_i and calculated with respect to the environmentally available concentrations of these elements in BH soil (As = 3.71 mmol/kg; Ca = 592 mmol/kg). The inset in (b) shows the expanded Y-axis for pH 8 and 11.

The saturation indices for several Ca-P_i-$As_{(V)}$ and Ca-P_i minerals were calculated for non-P_i soil leachates at pH 4, 8, 11, combined with the initial P_i concentrations used in the sorption experiments. The input solution compositions for these simulations consisted of concentrations of As and Ca from pH-specific non-P_i leachate, and the concentrations of P_i used in the sorption experiments. Therefore, the As and Ca concentrations at each pH were the same for all P_i concentrations used. Because P_i was not allowed to sorb on the soil during the PHREEQC

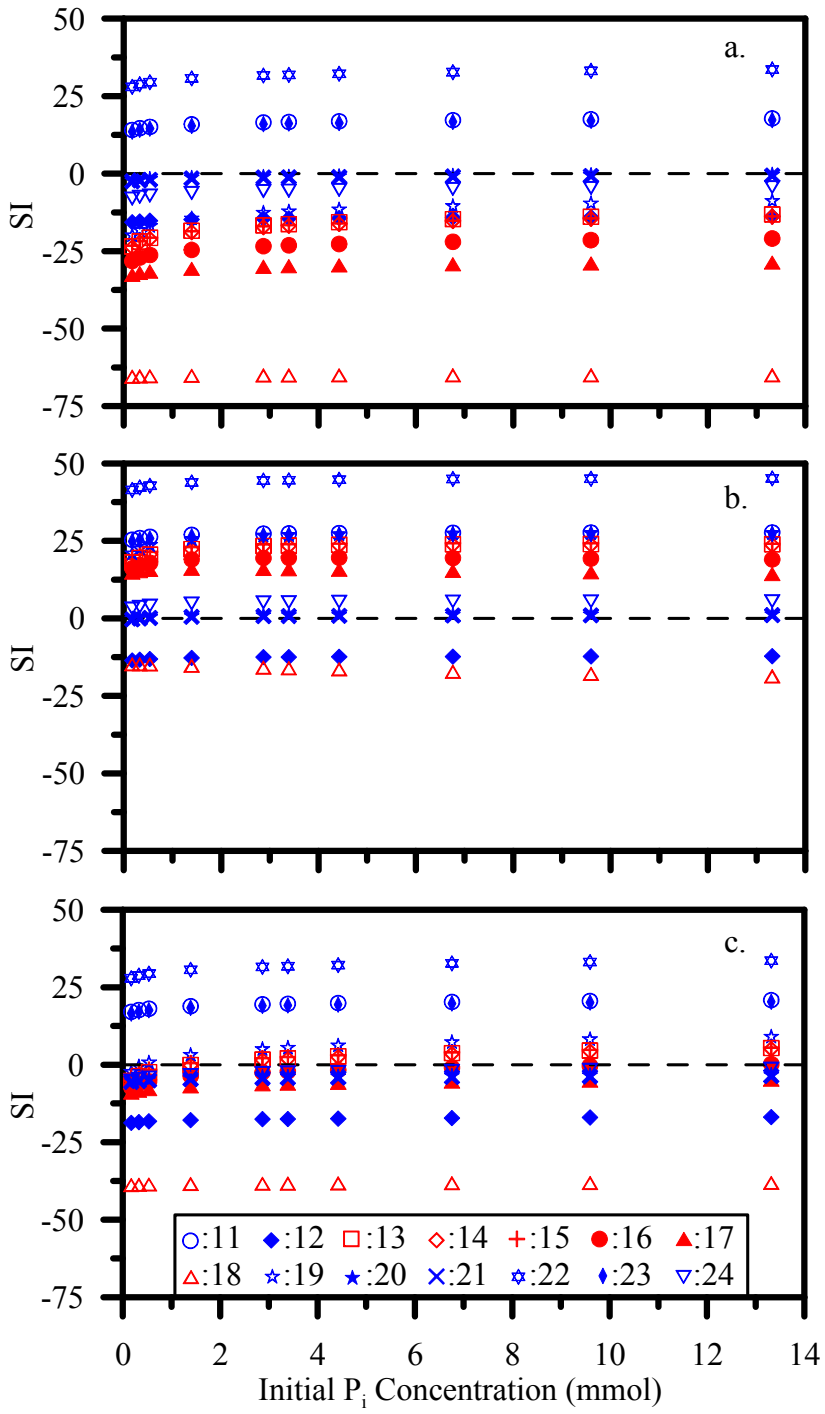

Fig. 5.5. Mineral saturation indices calculated using PHREEQC for (a) pH 4, (b) pH 8, and (c) pH 11. Concentrations of aqueous As and Ca at pH 4, 8, and 11 were taken from Fig. 5.3. Different initial concentrations of P_i were used during PHREEQC simulations. Symbols/numbers represent minerals listed in Table 5.2. Red symbols (online version) represent minerals containing As.

simulations, the total P_i in solution was considered to be freely available to interact with aqueous As and Ca. Fig. 5.5 shows the calculated saturation indices for several minerals as a function of P_i concentration. The saturation index of each mineral varied with pH, but for most minerals, the saturation indices at each pH did not change significantly with increasing P_i. At pH 4 (Fig. 5.5a), the solution was undersaturated with respect to all Ca-P_i-$As_{(V)}$ minerals considered. Similarly, the solution was undersaturated with respect to most of the Ca-P_i minerals (except #11: amorphous calcium phosphate, #19: hydroxyapatite, and #22: octocalcium phosphate). The calculated mineral saturation indices at pH 8 and 11 were significantly different than those at pH 4. In particular, the simulated solution at pH 8 was supersaturated with respect to several Ca-P_i-$As_{(V)}$ and Ca-P_i minerals (Fig. 5.5b), because the non-P_i leachate (Fig. 5.3) was slightly richer in Ca than the actual equilibrium solution for the pH 8 P_i sorption experiment (Fig. 5.4b). Therefore, the subsequent saturation indices calculated for the addition of P_i to the non-P_i leachate resulted in oversaturation of the solution with respect to several minerals at pH 8. At pH 11, the solution was approximately saturated with respect to most of the As-bearing minerals across the range of P_i concentrations used. At alkaline pH, the controlling factor for the degree of saturation was presumably the amount of aqueous Ca, rather than the amount of As or P_i in solution. It was therefore anticipated that the mobility of soil As potentially could be decreased by precipitation of Ca-P_i-$As_{(V)}$ minerals, if Ca were to be supplied along with P_i during soil treatment.

3.3.3. Mobilization of As and Ca as functions of pH and P_i

The mobilization of As and Ca with pH in the presence P_i was evaluated using chemical data obtained from experiments conducted for P_i sorption envelopes with initial concentrations of 0.57 mmol and 3.38 mmol. Fig. 5.6 shows the % mobilized As and Ca during P_i treatment

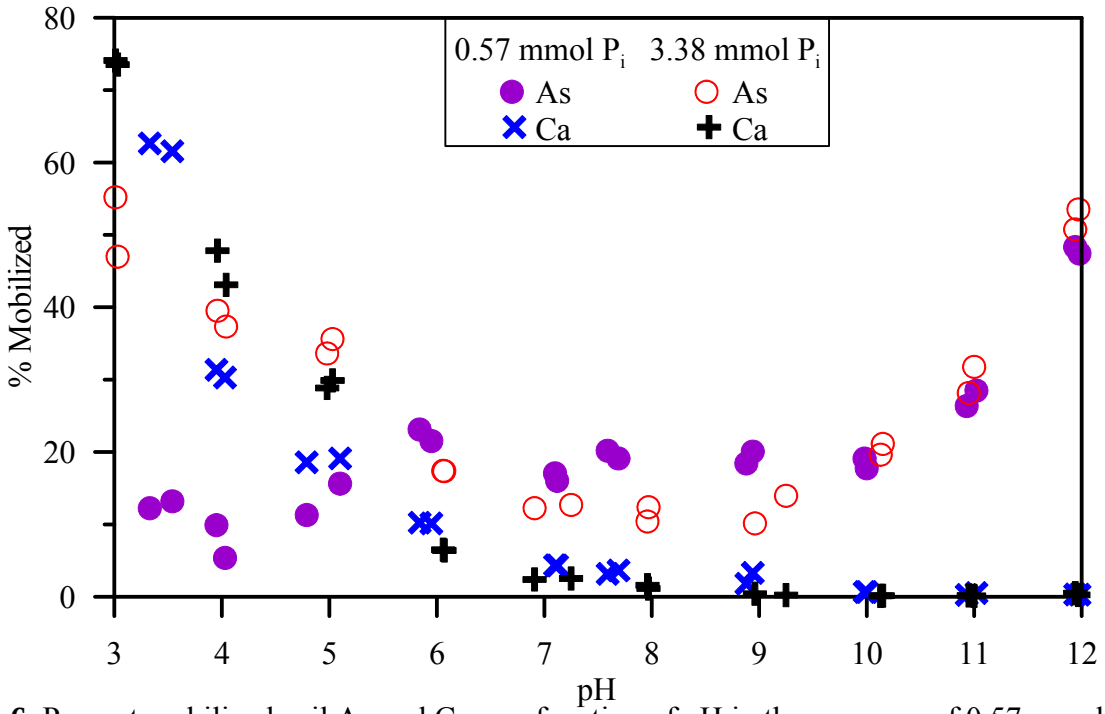

Fig. 5.6. Percent mobilized soil As and Ca as a function of pH in the presence of 0.57 mmol or 3.38 mmol P_i. The percent mobilization was calculated with respect to the environmentally available concentrations of these elements in BH soil (As = 3.71 mmol/kg; Ca = 592 mmol/kg).

of BH soil at several pH levels. Concentrations of mobilized Ca as a function of pH for 0.57 mmol and 3.38 mmol P_i were very similar, with the highest mobility observed at low pH. The mobility of Ca decreased rapidly with increasing pH and Ca essentially became immobile under circum-neutral to basic conditions. Arsenic also showed similar mobilization for both initial concentrations of P_i at pH > 6, but demonstrated significantly different mobilities for the two P_i concentrations at pH < 6. In acidic conditions, As mobility was significantly higher for 3.38 mmol P_i. The mobility of As was lowest at intermediate pH (6 to 9.5). At pH > 9.5, the mobility of As again increased with pH and almost 50% of the environmentally available As in BH soil was leached at pH 12. The increase in As concentrations without mobilization of Ca for basic conditions indicates that these two elements are not associated with a common phase in BH soil. The lower mobility of Ca, the higher mobility of As, and the reversal in sorption of P_i at pH >7

(Figs. 5.2, 5.3, and 5.6) indicates precipitation of a Ca-P_i phase without incorporation of As. Although sorption of P_i by BH soil at pH > 7 was presumably controlled by precipitation, only a portion of the total P_i added (up to 80% for 0.57 mmol and up to 40% for 3.38 mmol initial P_i concentration) was removed from the soil solution. The complete removal of P_i from solution by precipitation at high pH was primarily prevented by the system's Ca deficiency. Similarly, the As that was leached from BH soil was not precipitated due to the system's apparent Ca deficiency at pH >8. Supplying adequate Ca in the treatment solution along with P_i would eventually lead to co-precipitation of As with Ca-P_i phases and decrease its mobility.

PHREEQC modeling was also used to evaluate the potential precipitation of Ca-P_i-$As_{(V)}$ minerals as a function of pH from the non-P_i soil leachate (Fig. 5.3) with the addition of 0.57 mmol and 3.38 mmol of P_i. The calculated saturation indices of different minerals for the simulated solutions as a function of pH are shown in Fig. 5.7. Both concentrations of P_i resulted in similar variations in the calculated mineral saturation indices with pH. The saturation index of each mineral increased with increasing pH and peaked between pH 7 to 9, then slightly decreased at pH > 9. For pH 7 to 9, the simulated solution was oversaturated with respect to most of the Ca-P_i-$As_{(V)}$ minerals considered. The simulated solution was oversaturated across a broader range of pH with respect to the Ca-P_i minerals than the Ca-P_i-$As_{(V)}$ minerals. Particularly, the undersaturated state of the simulated solution with respect to Ca-P_i-$As_{(V)}$ minerals at lower pH levels was caused by low concentrations of As, while at higher pH levels such undersaturated conditions were caused by low concentrations of Ca in the non-P_i leachate.

As noted earlier, the greater mobility of As at low pH (except at pH ~ 3) in the presence of P_i was caused by the competitive desorption, rather than by dissolution. However, the increased mobility of As at intermediate and higher pH levels was related to pH-induced

desorption because As mobility at pHs 8 and 11 was observed to be independent of P_i. Therefore, at circum-neutral to basic pH, the supply of additional P_i would not have a significant effect on the mobility of As. However, addition of P_i was found to increase the mobility of soil As under acidic conditions.

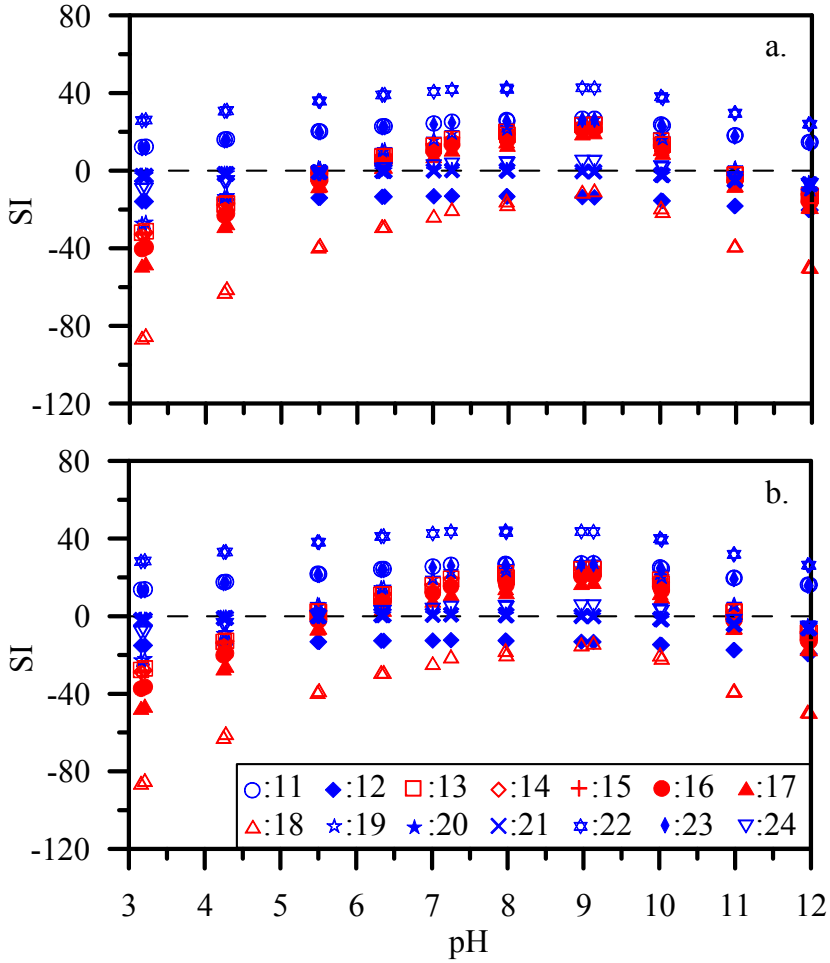

Fig. 5.7. Mineral saturation indices as a function of pH calculated using PHREEQC: (a) 0.57 mmol P_i was added to each sample; (b) 3.38 mmol P_i was added to each sample. Symbols/numbers represent minerals listed in Table 5.2. Red symbols (online version) represent minerals containing As. Concentrations of aqueous As and Ca were taken from Fig. 5.3.

3.4. Phosphate and Ca treatment of soil

3.4.1. Sorption of P_i during Ca-P_i treatment

Phosphate sorption envelopes on BH soil were determined using a C_i of 3.38 mmol P_i, but different amounts of Ca. For one set of experiments, 5.63 mmol Ca was supplied to yield a solution Ca:P_i ratio of 1.67:1. In another set of experiments, however, an excess amount of Ca (16.9 mmol) was supplied, producing a solution Ca:P_i ratio of 5:1. Both sorption envelopes for P_i on BH soil are given in Fig. 5.8, and show that the sorption of P_i at pH < 5 is similar to the sorption of P_i on BH soil in the absence of an external supply of Ca (Fig. 5.2). At pH < 5, the sorption of P_i increased with increasing pH. Interestingly, the presence of 16.9 mmol Ca slightly decreased the sorption of P_i for solution pH < 5. However, the addition of external Ca significantly increased P_i sorption by BH soil at pH 5-7 compared to P_i sorption in the same pH range without additional Ca. Moreover, the additional Ca resulted in a large increase in the removal of P_i from solution at pH > 8. The P_i sorption envelopes in the absence of external Ca (Fig. 5.2) showed an increasing, but incomplete, transfer of P_i to the solid phase at pH > 7. However, almost 100% of the P_i in the soil solution was transferred to the solid phase in basic conditions when Ca was externally supplied. This transfer of P_i to the solid phase at pH > 6 was attributed primarily to precipitation.

3.4.2. Mobilization of As and Ca during Ca-P_i treatments

The treatment of BH soil with P_i and an external supply of Ca was evaluated in batch experiments for its potential application in the chemical fixation of soil As. Fig. 5.9 shows the calculated mobilities of As and Ca as a function of pH when both Ca and P_i were supplied to the soil. The % mobilization of As was calculated using Eq. 5. However, Eq. 5.5 was modified to Eq. 5.6 so as to include the externally supplied Ca while calculating its % mobilization during treatment:

$$\%\,\text{Mobilized}_{Ca} = \frac{\text{Ca in equilibrium solution} - \text{externally supplied Ca}}{\text{Environmentally available Ca}} \times 100\% \quad \ldots(5.6)$$

According to Eq. 5.3, 0% mobilization indicates neither release of Ca from soil to solution nor transfer of Ca from solution to soil. Therefore, a soil solution with 0% mobilization of Ca contains only the externally supplied aqueous Ca. Positive % mobilization values indicate that the equilibrium solution was enriched in Ca due to the release of Ca from BH soil, while negative % mobilization values mean that some of the externally supplied Ca was transferred to the soil solid phase by sorption and/or precipitation. During Ca-P_i treatments, 45 mL of 5.63

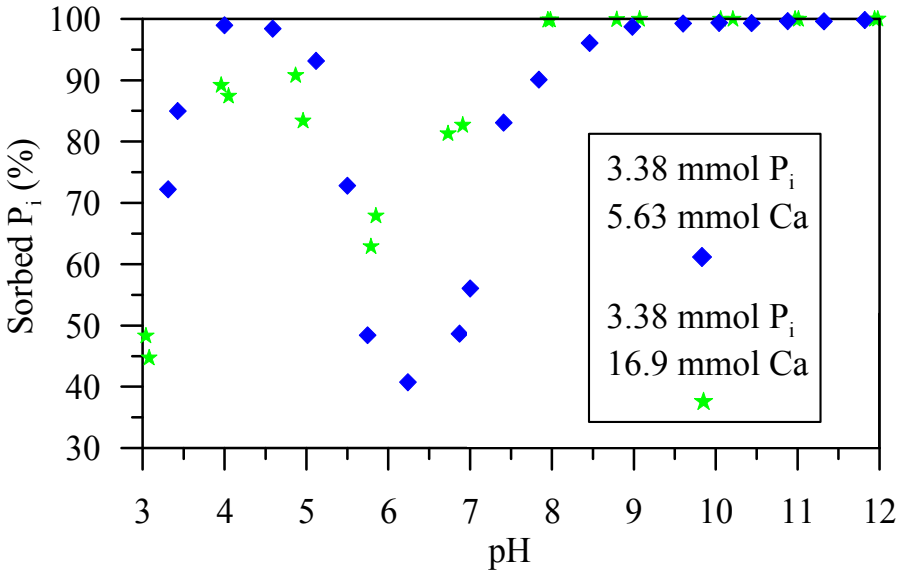

Fig. 5.8. Phosphate sorption on BH soil as a function of pH and initial Ca concentration. Initial P_i concentration was fixed at 3.38 mmol in all experiments, while the initial Ca concentration was 5.63 mmol for one sorption envelope and 16.9 mmol for the second sorption envelope.

mmol or 16.9 mmol Ca, along with 3.38 mmol P_i, were reacted with 3 g of BH soil. Therefore, complete transfer of Ca from the treatment solution to the solid phase would result in calculated Ca mobilities of about -14% (for 5.63 mmol added Ca) and -42% (for 16.9 mmol added Ca), with respect to the soil's 592 mmol/kg of environmentally available Ca. For As, however, the

calculated mobilization should be always ≥ 0 %. A 0% Mobilized value indicates that no As wasreleased from soil to solution during the Ca-P_i treatment.

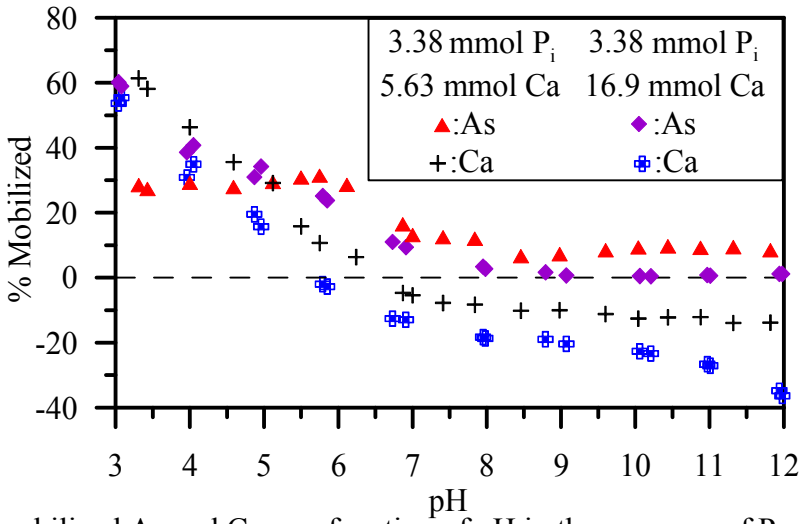

Fig. 5.9. Percent mobilized As and Ca as a function of pH in the presence of P_i and an additional supply of Ca. The percent mobilization was calculated with respect to the environmentally available concentrations of these elements in BH soil (As = 3.71 mmol/kg; Ca = 592 mmol/kg).

The amount of Ca mobilized from BH soil was slightly greater across the pH range when less external Ca was supplied during treatment. In general, Ca mobility decreased with increasing solution pH (Fig. 5.9). No Ca was transferred from solution to the solid phase at pH < 5.8 for 16.9 mmol external Ca, and at pH < 6.8 for 5.63 mmol external Ca.. But at pH > 5.8 and pH > 6.8, respectively, for high and low externally supplied Ca, net transfer of Ca from solution to soil occurred. At pH 8, nearly 45% and 60% of the externally supplied Ca was transferred to the soil, resulting in -20% and -9% calculated Ca mobilities, respectively, for 16.9 mmol and 5.63 mmol external Ca. With further increase in pH, a successively greater proportion of the externally supplied Ca was transferred to the solid phase. Almost 85% and 98% of the added Ca was transferred to the solid phase at pH 12 during Ca-P_i treatments with 16.9 mmol and 5.63 mmol Ca, respectively.

The mobility of As also decreased with increasing pH. At pH 8, about 3% and 10% of the environmentally available As was released from BH soil after P_i treatments with 16.9 mmol and 5.63 mmol Ca, respectively. The P_i treatment with 5.63 mmol Ca resulted in a 4-6% mobilization of As at pH > 8. However, the P_i treatment with 16.9 mmol Ca consistently decreased the mobility of As with increasing pH. At pH 9, the mobility of As decreased to < 1% of the environmentally available As in BH soil. This decrease in As mobility after Ca-P_i treatment of the soil was remarkable compared to the mobilization of As depicted in Figs. 5.3a-b, 5.4a, and 6 for P_i only treatments. The diminishing mobility of As along with a large transfer of externally supplied Ca and P_i to soil solid phase indicates the precipitation of As-bearing Ca-P_i mineral phases.

Figs. 5.10 and 5.11 show the calculated saturation indices for Ca-$As_{(V)}$ and Ca-P_i-$As_{(V)}$ minerals in PHREEQC simulations where externally supplied Ca and P_i are combined with the composition of the non-P_i leachate. Fig. 5.10 indicates that the addition of Ca alone is not adequate to trigger precipitation of Ca-$As_{(V)}$ minerals. The solution is only supersaturated with respect to calcite at higher pH. The simulated solution is undersaturated with respect to all Ca-$As_{(V)}$ minerals, even after the addition of 16.9 mmol Ca (Fig. 5.11b). However, the simulated solution is oversaturated with respect to most of the Ca-P_i and Ca-P_i-$As_{(V)}$ minerals at pH > 5.5. Although the addition of 5.63 mmol and 16.9 mmol Ca with 3.38 mmol P_i resulted in very similar mineral saturation indices as a function of pH (Figs. 5.10 and 5.11), the BH soil treatment experiments using the lower Ca concentration (5.63 mmol) failed to completely immobilize the As. Therefore, the addition of excess Ca along with P_i is required for complete immobilization of As in contaminated soil.

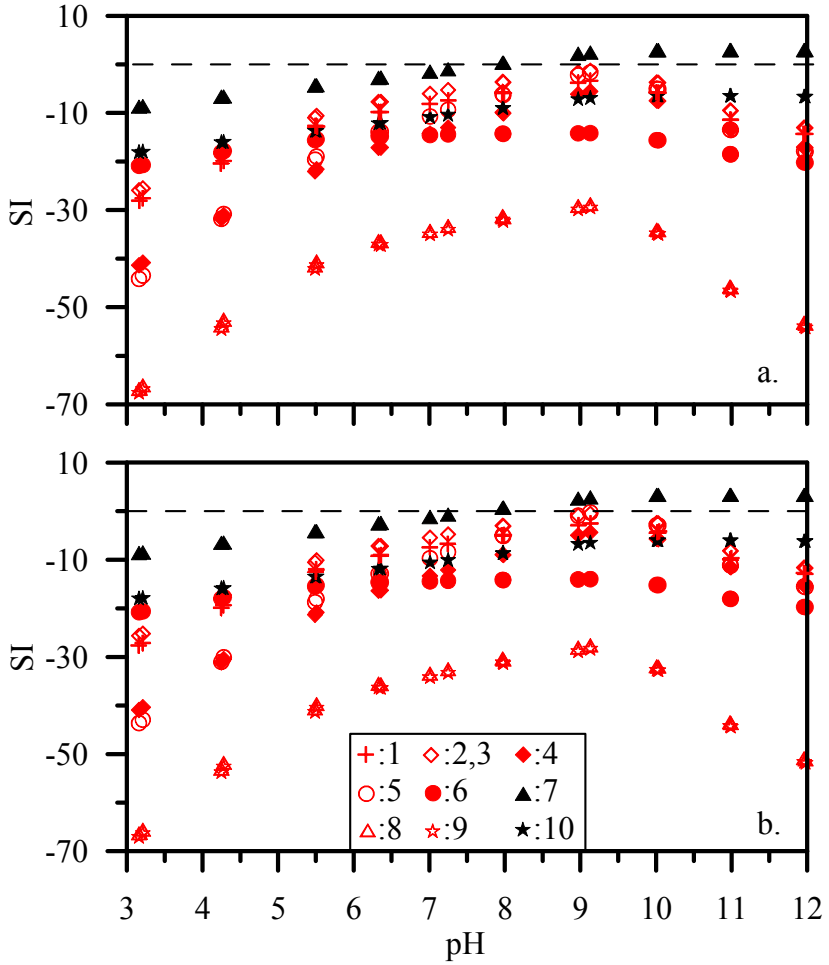

Fig. 5.10. Mineral saturation indices as a function of pH calculated using PHREEQC: (a) 3.38 mmol P_i and 5.64 mmol Ca were added to each sample; (b) 3.38 mmol P_i and 16.9 mmol Ca were added to each sample. Symbols/numbers represent minerals listed in Table 2. Red symbols (online version) represent minerals containing As. Concentrations of aqueous As and Ca were taken from Fig. 5.3.

3.4.3. Characterization of precipitates

The PHREEQC simulations described above indicated the potential precipitation of several Ca-P_i-$As_{(V)}$ minerals after Ca-P_i treatment of BH soil. Similarly, PHREEQC speciation modeling indicated that the synthetic leachate (As: 0.48 mmol, Ca: 6.44 mmol, P_i: 3.38 mmol, pH: 8) equilibrated with atmospheric CO_2 is oversaturated with all Ca-P_i-$As_{(V)}$ minerals included in Table 5.2, as well as calcite, dicalcium phosphate, apatite, octocalcium phosphate, tricalcium

phosphate, and whitlockite. Moreover, the synthetic leachate was undersaturated with respect to minerals containing Ca-$As_{(V)}$, as reported above for BH soil leachates after Ca-P_i treatments.

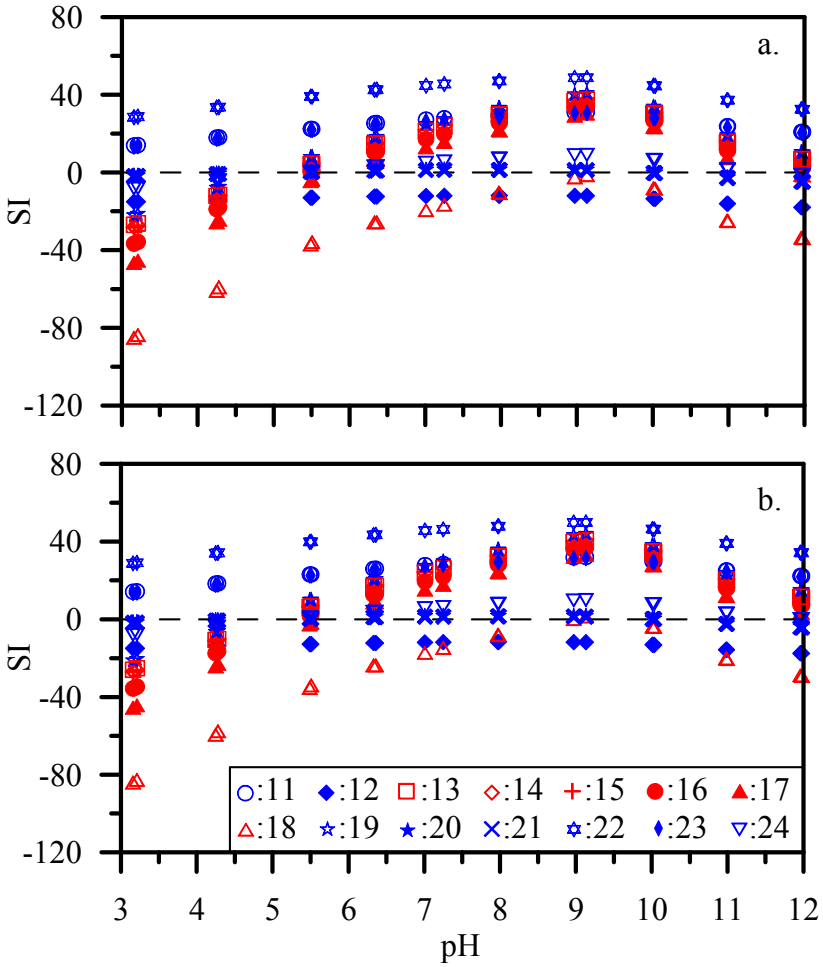

Fig. 5.11. Mineral saturation indices as a function of pH calculated using PHREEQC: (a) 3.38 mmol P_i and 5.64 mmol Ca were added to each sample; (b) 3.38 mmol P_i and 16.9 mmol Ca were added to each sample. Symbols/numbers represent minerals listed in Table 2. Red symbols (online version) represent minerals containing As. Concentrations of aqueous As and Ca were taken from Fig. 5.3.

Fig. 5.12 shows XRD patterns of precipitate separated after Ca-P_i treatment of BH soil at pH 8, and of material precipitated from the synthetic leachate. A reference XRD pattern for a carbonate apatite is also shown in Fig. 5.12. The XRD patterns for both precipitates closely match that of the carbonate apatite standard obtained from the ICDD database. Previous studies

by Twidwell et al. (1994) and others at Montana Tech (Wilson, 1998; Orser, 2001) reported removal of arsenic from solution by the precipitation of apatite-like minerals at pH 8-10. The Montana Tech studies (Twidwell et al., 1994; Wilson, 1998; and Orser, 2001) demonstrated that the exposure of the experimental system to air (i.e., CO_2) could potentially result in conversion of the precipitate into calcium carbonate with release of As back into the solution if the P_i:$As_{(V)}$ ratio was <7. However, these studies also indicated that at P_i:$As_{(V)}$ ratios ≥7 the Ca- P_i-$As_{(V)}$ precipitates were stable under atmospheric conditions. In the present study, the Ca- P_i-$As_{(V)}$ precipitate formed in BH soil after Ca-P_i treatment should have a P_i:$As_{(V)}$ ratio >>7, as determined by mass-balance calculations. The precipitation of the Ca- P_i-$As_{(V)}$ solid phase along with the low mobility of As, the negative mobility of Ca, and the nearly complete removal of P_i from solution at pH > 8 suggest that Ca-P_i treatment successfully immobilized As in BH soil.

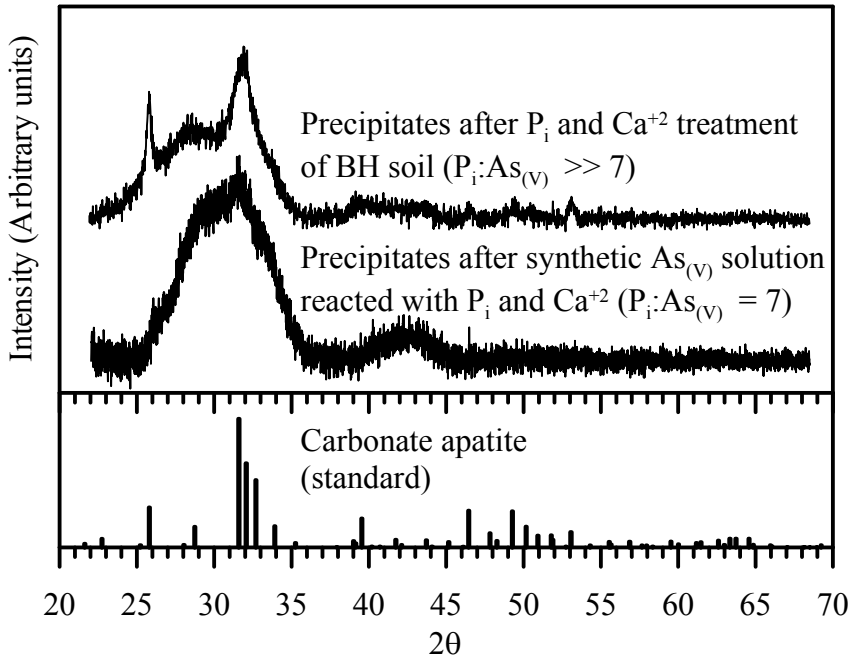

Fig. 5.12. Comparison of an XRD pattern of precipitates in Ca-P_i treated BH soil with an XRD pattern of material precipitated from synthetic P_i-$As_{(V)}$-Ca leachate. The bar diagram at the bottom is a reference pattern for carbonate apatite obtained from the ICDD database.

5.4. Conclusions

In this study, the applicability of P_i treatment with and without added Ca for immobilization of As in contaminated soil was tested through various batch experiments. An As-contaminated soil sample (BH: 278 mg/kg As) collected from an industrial site in the southeastern United States was subjected to bench-scale P_i and Ca-P_i treatments. Batch experiments showed that BH soil has a significant sorption capacity for P_i. The P_i sorption isotherms and envelopes indicated that the least sorption of P_i along with the lowest As mobility occur at near-neutral pH. The mobility of As increased with increasing initial concentration of P_i at pH 4, and at this pH, the highest concentration of P_i (>13 mmol) only removed about 60% of the environmentally available As from soil. On the otherhand, As mobility was independent of P_i concentration at pH 8 and 11. Therefore, the mobilization of As from BH soil at pH 4 was related to P_i-induced competitive desorption, while mobilization of As at higher pH levels is attributed to pH-induced desorption.

Treatment of BH soil with P_i and Ca resulted in decreased mobility of As. After Ca-P_i treatment, geochemical modeling indicated that soil solutions and synthetic leachate were oversaturated with respect to several Ca-P_i-$As_{(V)}$ phases. The externally supplied Ca and P_i were therefore likely removed from solution by precipitation of solid phases during soil treatment. XRD analysis indicated the existence of a poorly crystalline carbonate-apatite phase in the Ca-P_i treated soil. A similar phase was also identified in precipitate from synthetic Ca-P_i-$As_{(V)}$ leachate. Most importantly, treatment of BH soil with 3.38 mmol P_i and 16.9 mmol Ca almost completely immobilized soil As from near-neutral pH to higher pH levels. The large sorption of P_i without mobilization of Ca, the oversaturated state of soil leachates with respect to several Ca-P_i-$As_{(V)}$ minerals, and XRD evidence for the formation of phosphate mineral(s) in treated BH soil and in

the precipitate formed from the synthetic Ca-P_i-$As_{(V)}$ leachate indicate that the immobilization of As in BH soil after Ca-P_i treatment likely resulted from the precipitation of Ca-P_i-$As_{(V)}$ minerals.

The results of this study have demonstrated that Ca-P_i treatment has potential application for immobilization of As in contaminated soil. In particular, this method would work best for As remediation in Ca-rich soil, which does not respond as well to other chemical fixation treatment methods (Qi and Donahoe, 2008). Furthermore, Ca-P_i treatment could also be extended for remediation of As-contaminated wastewater.

The low solubilities of many of the Ca-P_i-$As_{(V)}$ minerals suggest that Ca-P_i treatment has promise as an effective, long-term method for in situ chemical fixation of As in contaminated soils and wastewaters.

Acknowledgements: We would like to thank Dr. Sidhartha Bhattacharyya, Elizabeth Y. Graham, and Ziming Yue for their help during laboratory experiments and chemical analyses. This research was partly funded by student research grants from the Geological Society of America, the Gulf Coast Association of Geological Societies, and the W.G. Hooks Fund (UA Department of Geological Sciences). Suggestions from three anonymous reviewers were helpful in revising the original manuscript.

REFERENCES

Alam, M.G.M., Tokunaga, S., and Maekawa, T., 2001. Extraction of arsenic in a synthetic arsenic-contaminated soil using phosphate. Chemosphere 43, 1035-1041.

ASTM, 2003. ASTM D4567– 03: Standard test method for single-point determination of specific surface area of catalysts and catalyst carriers using nitrogen adsorption by continuous flow method. ASTM International, 100 Barr Harbor Drive, PO Box C700, West Conshohocken, PA 19428-2959, United States, p. 4.

ATSDR, 2000. Case Studies in Environmental Medicine- Arsenic Toxicity. ATSDR Publication No.: ATSDR-HE-CS-2002-0003 U.S. Department of Health and Human Services, Agency for Toxic Substances and Disease Registry, Division of Toxicology and Environmental Medicine, p. 42.

Bates, M.N., Smith, A.H., and Hopenhayn-Rich, C., 1992. Arsenic ingestion and internal cancers: A Review. Am. J. Epidemiol. 135, 462-476.

Bhattacharyya, S., Donahoe, R.J., and Patel, D., 2009. Experimental study of chemical treatment of coal fly ash to reduce the mobility of priority trace elements. Fuel 88, 1173-1184.

Black, R.J., 1993. Florida climate data. Circular EES-5, Florida Cooperative Extension Service, Institute of Food and Agricultural Sciences, University of Florida, p. 4.

Bothe, J.V. and Brown, P.W., 1999. The stabilities of calcium arsenates at 23 ± 1ºC. J. Hazard. Mater. 69, 197-207.

Bundschuh, J., Litter, M.I., Parvez, F., Román-Ross, G., Nicolli, H.B., Jean, J., Liu, C., López, D., Armienta, M.A., Guilherme, L.R.G., Cuevas, A.G., Cornejo, L., Cumbal, L., and Toujaguez, R., 2012. One century of arsenic exposure in Latin America: A review of history and occurrence from 14 countries. Science of the Total Environment 429, 2-35.

Carbonell-Barrachina, A.A., Rocamora, A., García-Gomis, C., Martínez-Sánchez, F., and Burló, F., 2004. Arsenic and zinc biogeochemistry in pyrite mine waste from the Aznalcóllar environmental disaster. Geoderma 122, 195-203.

Drever, J.I., 1997. The geochemistry of natural waters: surface and groundwater environments. third ed. Prentice Hall, New Jersey.

Goldberg, S. and Glaubig, R.A., 1988a. Anion sorption on a calcareous, montmorillonitic soil-arsenic. Soil Sci. Soc. Am. J. 52, 1297-1300.

Goldberg, S. and Glaubig, R.A., 1988b. Anion sorption on a calcareous, montmorillonitic soil-selenium. Soil Sci. Soc. Am. J. 52, 954-958.

Grisafe, D.A. and Hummel, F.A., 1970. Pentavalent Ion substitutions in the apatite structure Part A. Crystal chemistry. Journal of Solid State Chemistry 2, 160-l66.

Hossain, M.F., 2006. Arsenic contamination in Bangladesh-An overview. Agriculture, Ecosystems and Environment 113, 1-16.

Jackson, R. and Grainge, J. W., 1975. Arsenic and cancer. Canadian Medical Association Journal 113 (5), 396-401. Soil Sci. Soc. Am. J. 64, 1616-1622.

Jackson, B.P. and Miller, W.P., 2000. Effectiveness of phosphate and hydroxide for desorption of arsenic and selenium species from iron oxides. Soil Sci. Soc. Am. J. 64, 1616-1622

Johnson, S.E. and Barnard, W.M., 1979. Comparative effectiveness of fourteen solutions for extracting arsenic from four western New York soils. Soil Sci. Soc. Am. J. 43, 304–308.

Kaplan, D.I. and Knox, A.S., 2004. Enhanced contaminant desorption induced by phosphate mineral additions to sediment. Environ. Sci. Technol. 38, 3153-3160.

Karagas, M.R., Stukel, T.A., Tosteson, T.D., 2002. Assessment of cancer risk and environmental levels of arsenic in New Hampshire. Int. J. Hyg. Environ. Health 205, 85-94.

Ler, A., and Stanforth, R., 2003. Evidence for surface precipitation of phosphate on goethite. Environ. Sci. Technol. 37, 2694-2700.

Limousin, G., Gaudet J.-P., Charlet, L., Szenknect, S., Barthès, V., Krimissa, M. (2007). Sorption isotherms: A review on physical bases, modeling and measurement. Appl. Geochem. 22, 249-275.

Ma, L.Q., Komar, K.M., Tu, C., Zhang, Z., Cai, Y., and Kennelley, E.D., 2001. A Fern that Hyperaccumulates Arsenic. Nature 409, 579.

Mahapatra, P.P., Mahapatra, L.M., and Mishra, B., 1987. Arsenate hydroxyapatite: a physico-chemical and thermodynamic investigation. Polyhedron 6, 1049-52.

Montastruc, L., Azzaro-Pantel, C., Biscans, B., Cabassud, M., Domenech, S. and Dibouleau, L., 2003. A general framework for pellet reactor modelling: Application to P-recovery. Trans. Inst. Chem. Eng. Part A: Chem. Eng. Res. Design 81, 1271-1278.

Morrell, J.J., Keefe, D., and Baileys, R.T., 2003. Copper, zinc, and arsenic in soil surrounding douglas-fir poles treated with ammoniacal copper zinc arsenate (ACZA). J. Environ. Qual. 32, 2095-2099.

Mulligan, C.N., Yong, R.N., and Gibbs, B.F., 2001. Remediation Technologies for Metal-Contaminated Soil and Groundwater: An Evaluation. Eng. Geol. 60, 193-207.

Neupane, G., Donahoe, R.J., and Qi, Y., 2010. Fate of arsenic, iron, and lanthanum in arsenic-contaminated soils treated with ferrous sulfate and ferrous sulfate-lanthanum chloride. G-073, in K.A. Fields and G.B. Wickramanayake (Chairs), Remediation of Chlorinated and Recalcitrant Compounds—2010. Seventh International Conference on Remediation of Chlorinated and Recalcitrant Compounds (Monterey, CA; May 2010). ISBN 978-0-9819730-2-9, Battelle Memorial Institute, Columbus, OH, www.battelle.org/chlorcon.

Nordstrom, D.K., 2002. Worldwide occurrences of arsenic in ground water. Science 296, 2143-2145.

Orser, T., 2001. Removal of arsenic from waste water solutions as storable stable precipitates. MS Thesis, Department of Metallurgical and Materials Engineering, Montana Tech of The University of Montana.

Parkhurst, D.L. and Appelo, C.A.J., 1999. User's guide to PHREEQC (Version 2)-A computer program for speciation, batch-reaction, one-dimensional transport, and inverse geochemical calculations. U.S. Geol. Survey, Water Resour. Invest. Rep. 99-4259, 326 p.

Peryea, F.J. and Kammereck, R., 1997. Phosphate-enhanced movement of arsenic out of lead arsenate-contaminated topsoil and through uncontaminated subsoil. Water, Air, Soil Pollut. 93, 243-254.

Qi, Y. and Donahoe, R.J., 2008. The environmental fate of arsenic in surface soil contaminated by historical herbicide application. Sci. Total Environ. 405, 246-254.

Robinson, G.R. Jr., Larkins, P., Boughton, C.J., Reed, B.W., and Sibrell, P.L., 2007. Assessment of contamination from arsenical pesticide use on orchards in the Great Valley region, Virginia and West Virginia, USA. J. Environ. Qual. 36, 654-663.

Simcox, N.J., Fenske, R.A., Wolz, S.A., Lee, I.C., Kalman, D.A., 1995. Pesticides in household dust and soil: exposure pathways for children of agricultural families. Environ. Health Perspect. 103, 1126-1134.

Smedley, P.L. and Kinniburgh, D.G., 2002. A review of the source, behaviour and distribution of arsenic in natural waters. Appl. Geochem. 17, 517-568.

Smith, R.M. and Martell, A.E., 1976. Critical Stability Constants. IV. Inorganic Complexes, Plenum Press, New York.

Sposito, G., 1986. On distinguishing adsorption from surface precipitation, in: Davis J.A., Hayes K.F. (Eds.), Geochemical Processes at Mineral Surfaces. ACS Symposium Ser. 323, Amer. Chem. Soc., Washington, D.C., 217-228.

Tokunaga, S. and Hakuta, T., 2002. Acid washing and stabilization of an artificial arsenic-contaminated soil. Chemosphere 46, 31-38.

Twidwell, L.G., Plessas, K.O., Comba, P.G. and Dahnke, D.R., 1994. Removal of arsenic from wastewaters and stabilization of arsenic bearing waste solids: Summary of experimental studies. J. Hazard. Mater. 36, 69-80.

USEPA, 2004. Method 9045D: Soil and waste pH. Revision 4, November 2004, US Environmental Protection Agency, USA, p. 5.

USEPA, 2007. Method 3051A: Microwave-assisted acid digestion of sediments, sludges, soils and oils. Revision 1, February 2007, US Environmental Protection Agency, USA, p. 30.

Violante, A. and Pigna, M., 2002. Competitive Sorption of Arsenate and Phosphate on Different Clay Minerals and Soils. Soil Sci. Soc. Am. J. 66, 1788-1796.

Wasay, S.A., Parker, W., Van Geel, P.J., Barrington, S., and Tokunaga, S., 2000. Arsenic pollution of a loam soil: Retention form and decontamination. Soil Sed. Contam. 9, 51-64.

Welch, A.H., Westjohn, D.B., Helsel, D.R., and Wanty, R.B., 2000. Arsenic in ground water of the United States: occurrence and geochemistry. Ground Water 38, 589-604.

Wilson, S.R., 1998. Removal of arsenic from ASARCO acid plant blowdown water as stable, storable precipitates. MS Thesis, Department of Metallurgical and Materials Engineering, Montana Tech of The University of Montana.

Woolson, E.A., Axley, J.H. and Kearney, P.C., 1973. Chemistry and phytotoxicity of arsenic in soils. II. Effects of time and phosphorus. Soil Sci. Soc. Am. J. 37, 254-259

Yang, L. and Donahoe, R.J., 2007. The form, distribution and mobility of arsenic in soils contaminated by arsenic trioxide, at sites in southeast USA. Appl. Geochem. 22, 320-341.

Yang, L., Donahoe, R.J., and Redwine, J.C., 2007. In situ chemical fixation of arsenic-contaminated soils: An experimental study. Sci. Total Environ. 387, 28-41.

Yuan, C. and Chiang, T.S., 2007. The mechanisms of arsenic removal from soil by electrokinetic process coupled with iron permeable reaction barrier. Chemosphere 67, 1533-1542.

Zhao, H., and Stanforth, R., 2001. Competitive adsorption of phosphate and arsenate on goethite. Environ. Sci. Technol. 35, 4753-4757.

CHAPTER – 6

OVERALL SUMMARY

Trace element contamination in the near-surface environment is a major concern because of the potential adverse effects on human health. Although trace elements can be sourced from natural processes, anthropogenic activities commonly result in harmful concentrations of arsenic and other priority trace elements in the environment. The research described in this dissertation is primarily focused on characterizing and remediating trace element contamination caused by coal fly ash disposal and arsenic trioxide herbicide. The first two papers describe studies aimed at determining the mobility of trace elements associated with four different coal fly ash samples and testing the potential effectiveness of a surfactant-modified zeolite permeable reactive barrier to attenuate trace element-contaminated leachate emanating from old un-lined fly ash disposal facilities. The third and fourth papers present research aimed at evaluating the competitive adsorption-desorption of $As_{(V)}$ and P_i at the ferric hydroxide-water interface, and evaluating a P_i-based remediation technique for arsenic-contaminated soil.

Overall, the dissertation was focused on the following research objectives:

1) To determine the leachability of trace elements in one Class C (alkaline) and three Class F (acidic) fly ash samples. This was accomplished by short-term and long-term batch leaching experiments and column leaching experiments using DDI water and synthetic acid rain.

2) To evaluate the effectiveness of SMZ as a permeable reactive barrier material to attenuate trace elements leached from fly ash disposal facilities. The ability of SMZ to remove trace elements from fly ash leachate was determined with batch and column experiments.

3) To study the competitive adsorption/desorption of $As_{(V)}$ and P_i at the ferric hydroxide-water interface. Competitive adsorption/desorption of $As_{(V)}$ and P_i on ferric hydroxide were investigated using equilibrium and kinetic batch experiments, geochemical modeling, and As K-edge X-ray absorption spectroscopy.

4) To evaluate the potential use of Pi-based treatment methods for fixation of arsenic in contaminated soil. The P_i-treatment was performed with phosphoric acid on a arsenic-contaminated soil in batch experiments along with an additional supply of Ca.

The major results of this research are summarized below:

1) The four fly ash samples studied contained priority pollutant elements in different proportions. Environmentally available trace elements were found in greater amounts in the acidic fly ash samples compared to the alkaline fly ash sample. Significant proportions of As, B, Cr, Mo, Sb, Se, Sr, and V were leached by water and synthetic acid rain during batch and column leaching experiments.

2) The SMZ treatment results showed the potential use of SMZ in permeable reactive barriers to control the dispersion of heavy metal and metalloid trace elements from ash disposal sites. The SMZ batch treatment with 10% SMZ removed up to 30% of As, Mo, and V; up to 80% of Cr; and up to 20% of Se and Sr from fly ash leachate. Similarly, in column experiments, SMZ treatment delayed and diminished the peak leaching concentrations of several priority pollutant elements. While SMZ was effective in attenuation of fly ash leachate for the first portion of the column experiments, its effectiveness decreased with time.

3) Ferric hydroxide has a large capacity for adsorption of both $As_{(V)}$ and P_i from aqueous solutions. Experimentally determined adsorption isotherms and envelopes for $As_{(V)}$ and P_i on ferric hydroxide showed that the adsorption of these oxyanions was strongly controlled by pH, with greater adsorption at lower pH levels. Freundlich and competitive Langmuir isotherm models were able to satisfactorily predict the empirical single element and competitive adsorption data. Similarly, the triple-layer model successfully described the single element as well as the competitive adsorption envelopes using bidentate surface complexes.

4) Both $As_{(V)}$ and P_i showed similar adsorption behavior on ferric hydroxide when loaded separately. Individual as well as competitive adsorption/desorption of $As_{(V)}$ and P_i at the ferric hydroxide-water interface rapidly increased initially and then slowed. The initial rapid adsorption/desorption kinetics were attributed to solute-surface interactions, while the later slow adsorption kinetics were regarded to be reactions controlled by the rate-limiting diffusion of oxyanions to/from the ferric hydroxide interior. The adsorption/desorption kinetic data showed good compliance with pseudo-second order, Elovich, and power-function rate equations. The As K-edge EXAFS analysis of $As_{(V)}$- and/or P_i-adsorbed ferric hydroxide indicated the presence of two types of inner-sphere complexes for $As_{(V)}$: bidentate mononuclear and bidentate binuclear complexes. In general, the coordination number for both complexes increased with increasing reaction time and slightly decreased with introduction of P_i into the system. The research findings also indicated that both $As_{(V)}$ and P_i compete for adsorption on ferric hydroxide and that each of these oxyanions shows a capacity to desorb the pre-sorbed co-oxyanion. Therefore, excessive input of P_i to contaminated soils and sediments due to the overuse of fertilizers could release As through competitive desorption.

5) P_i-treatment with an additional supply of Ca showed promise in batch experiments as a method to chemically fix As in contaminated soil. When the soil was treated only with P_i, the mobility of As was increased; however, when the P_i amendment of soil was performed along with added Ca, the mobility of As mobility was decreased to essentially zero in the environmentally relevant pH range. The fixation of As during the P_i-Ca treatment was attributed to the precipitation of $As_{(V)}$-bearing phosphate mineral phases. The XRD spectra of the material precipitated in the treated soil closely matched that of carbonate apatite.

This dissertation research showed the importance of diverse leaching tests to evaluate the environmental leachability of trace elements from fly ash samples. This study showed that both alkaline and acidic coal fly ash samples leach environmentally significant amount of trace elements and could potentially contaminate the potable water resources. This study also evaluated the effectiveness of surfactant-modified zeolite to contain trace elements within the fly ash disposal facility and restrict their dispersion into the surrounding environments. Similarly, this study also showed that the adsorption/desorption of $As_{(V)}$ and P_i on ferric hydroxide is depended on pH, presence/absence of competing co-oxyanion, and sequence of loadings. This study illustrated that $As_{(V)}$ was the preferred adsorption species in competitive experiments, and both oxyanions showed limited desorption capacity to the pre-equilibrated co-oxyanion. Therefore, excessive input of P_i to contaminated geomedia due to the overuse of fertilizers could mobilize As by competitive desorption. However, this study also illustrated that the addition of P_i along with Ca into the contaminated soil could help immobilize As in soil by co-precipitation of low solubility Ca-P_i-$As_{(V)}$ minerals. Therefore, the Ca-P_i treatment of contaminated soil has potential application for immobilization of As in contaminated soil. And this Ca-P_i treatment could also be extended for remediation of As-contaminated wastewater.